College of Engineering
Virginia Polytechnic Institute and State University
Blacksburg, Virginia 24061

May 1994

CCMS-94-04
VPI-E-94-04

Interlaminar Stress Analysis of Dropped-Ply Laminated Plates and Shells by a Mixed Method

Peter N. Harrison[1]
Eric R. Johnson[2]
James H. Starnes, Jr.[3]

Department of Aerospace and Ocean Engineering

NASA Grant NAG-1-343

Interim Report 96

The NASA-Virginia Tech Composites Program

Prepared for: Aircraft Structures Branch
National Aeronautics and Space Administration
Langley Research Center
Hampton, VA 23681-0001

---

[1]Graduate Research Assistant, Department of Aerospace and Ocean Engineering, Virginia Polytechnic Institute and State University

[2]Professor, Department of Aerospace and Ocean Engineering, Virginia Polytechnic Institute and State University

[3]Head, Aircraft Structures Branch, NASA Langley Research Center, Hampton, VA

Abstract

A mixed method of approximation based on Reissner's variational principle is developed for the linear analysis of interlaminar stresses in laminated composites, with special interest in laminates that contain terminated internal plies (dropped-ply laminates). Two models are derived, one for problems of generalized plane deformation and the other for the axisymmetric response of shells of revolution. A layerwise approach is taken in which the stress field is assumed with an explicit dependence on the thickness coordinate in each layer. The dependence of the stress field on the thickness coordinate is determined such that the three-dimensional equilibrium equations are satisfied by the approximation. The solution domain is reduced to one dimension by integration through the thickness. Continuity of tractions and displacements between layers is imposed.

The governing two-point boundary value problem is composed of a system of both differential and algebraic equations (DAEs) and their associated boundary conditions. Careful evaluation of the system of DAEs was required to arrive at a form that allowed application of a one-step finite difference approximation. A two-stage Gauss implicit Runge-Kutta finite difference scheme was used for the solution because of its relatively high degree of accuracy. Patch tests of the two models revealed problems with solution accuracy for the axisymmetric model of a cylindrical shell loaded by internal pressure.

Parametric studies of dropped-ply laminate characteristics and their influence on the interlaminar stresses were performed using the generalized plane deformation model. Eccentricity of the middle surface of the laminate through the ply drop-off was found to have a minimal effect on the interlaminar stresses under longitudinal compression, transverse tension, and in-plane shear. A second study found the stiffness change across the ply termination to have a much greater influence on the interlaminar stresses.

Correlations between the stiffness ratio of the thick to the thin sections of the laminates and the magnitude of a parameter based on a quadratic delamination criterion were found to be surprisingly good for longitudinal compression and in-plane shear loadings. For laminates with very stiff terminated plies loaded in longitudinal compression, inclusion of a short insert of softer composite material at the end of the dropped plies was found to significantly reduce the interlaminar stresses produced.

Acknowledgements

This research was supported under NASA Grant NAG1-343 and was monitored by Dr. James H. Starnes, Jr., Head of the Aircraft Structures Branch. The author wishes to thank Dr. Starnes for his continued support through the grant as well as through the encouragement gained from his passion for this work. The author also would like to thank Dr. Michael Hyer and Dr. Carl Herakovich for their administration of the NASA-Virginia Tech Composites Program and for their motivational support of all the students in the program.

Table of Contents

Chapter 1: Introduction 1
1.1 Literature Review 2
1.1.1 Classification and Overview of Parametric Effects 2
1.1.2 Approaches to Modeling and Analysis 6
1.1.3 Failure Analysis 8
1.1.4 Summary Comments 11
1.2 Objective 12

Chapter 2: Choice of Method of Approximation 14
2.1 Methods of Approximation 14
2.1.1 Approximate Solution to the Governing PDEs of Elasticity 14
2.1.2 Variational Methods 15
2.1.2.1 Conventional Finite Element Methods 16
2.1.2.2 Hybrid Finite Element Methods 17
2.1.3 Criteria for Interlaminar Stress Approximation 19
2.2 Approach 19
2.2.1 Variational Principle 20
2.2.2 Assumed Stresses 22
2.2.3 Governing Equations 23

Chapter 3: Generalized Plane Deformation Model 25
3.1 Displacement Field 25
3.2 Assumed Stress Field 27
3.3 Application of the Principle 31
3.4 Interlayer Traction and Displacement Continuity 36
3.5 Differential-Algebraic Equations Systems 39

3.6 Resolving the Order of the System and Number of Boundary Conditions.....40
3.7 Summary of Governing Equations.....42
3.7.1 Compatibility Equations.....42
3.7.2 Equilibrium Equations.....43
3.7.3 Interlayer Traction Continuity Equations.....43
3.7.4 Surface Conditions.....43
3.7.5 Boundary Conditions.....44
3.7.6 Continuity Between Longitudinal Segments.....46
3.7.7 Accounting of Variables and Equations.....47

Chapter 4: Axisymmetric Model.....50
4.1 Displacement Field.....50
4.2 Assumed Stress Field.....51
4.3 Application of the Principle.....56
4.4 Summary of Governing Equations.....61
4.4.1 Compatibility Equations.....61
4.4.2 Equilibrium Equations.....62
4.4.3 Interlayer Traction Continuity Equations.....63
4.4.4 Surface Conditions.....63
4.4.5 Boundary Conditions.....64
4.4.6 Continuity Between Longitudinal Segments.....65

Chapter 5: Numerical Solution and Verification of Accuracy.....67
5.1 Modeling of Dropped-Ply Laminates.....67
5.2 Incorporation of Material Properties.....68
5.2.1 Piecewise Integration.....69
5.2.2 Determination of Homogenized Compliance Coefficients.....69
5.2.3 Comparison of Approaches.....70
5.2.4 Material Properties for Curved Sublaminate Layers.....71
5.3 Two-Point Boundary Value Problem.....73
5.3.1 Solution Method.....74
5.3.2 Failure of the Trapezoidal Finite Difference Scheme.....77
5.4 Patch Tests.....82
5.4.1 Generalized Plane Deformation Model.....82
5.4.1.1 Examination of the Effect of the Magnitude of Rigid Body Displacements.....82
5.4.1.2 Examination of the Effect of the Slope of the Interface Between Layers.....84
5.4.1.3 Examination of the Effect of the Relative Thickness of Layers.....84

5.4.1.4 Examination of the Effect of Several Thin Layers....90
5.4.2 Axisymmetric Model....94
5.4.2.1 Examination of the Effect of the Magnitude of Rigid Body Displacements....94
5.4.2.2 Examination of the Effect of the Slope of the Interface Between Layers....95
5.4.2.3 Examination of the Effect of the Relative Thickness of Layers....96
5.4.2.4 Comparison of Condition Numbers to Pagano's Original Axisymmetric Formulation....98
5.4.2.5 Comments Regarding the Patch Test results for the Axisymmetric Model....99
5.5 Comparison with Other Solutions....100
5.5.1 Tensile Coupon Free Edge Problem....100
5.5.2 Dropped-Ply Laminate Under Uniaxial Compression....103

Chapter 6: Parametric Studies....109
6.1 Effect of Eccentricity of the Middle Surface....109
6.2 Effect of the Magnitude of the Stiffness Discontinuity....119
6.3 Effect of a Soft Insert....127

Chapter 7: Concluding Remarks....132
7.1 Discussion and Conclusions....132
7.2 Suggestions for Future Work....137

References....139

Appendix A: Homogenization Procedure....144
A.1 Equating Strain Energy....144
A.2 Voigt and Reuss Approximations....147
A.3 Homogenized Compliances....148
A.4 Homogenized Stiffnesses....152

Appendix B: Two-Stage Gauss Implicit Runge-Kutta Finite Difference Scheme....155
B.1 Implicit Runge-Kutta Schemes....155
B.2 Development of Finite Difference Scheme: Parameter Condensation....156
B.3 Gauss Schemes....157

List of Figures

Fig. 2.1 Section of a uniform thickness layer in $(\alpha_1, \alpha_2, \zeta)$ orthogonal coordinates 23
Fig. 3.1 Generalized plane deformation 26
Fig. 3.2 Schematic of a typical layer 28
Fig. 3.3 Displacement weighting functions for $z_1 = 1.1$ and $z_2 = 1.2$ 32
Fig. 3.4 Schematic of layer assemblage 33
Fig. 3.5 Enlargement of layer interface region at an end illustrating interdependence between traction B.C.s 45
Fig. 4.1 Axial dropped-ply cylinder 51
Fig. 4.2 Schematic of a typical layer 52
Fig. 5.1 Modeling of a dropped-ply laminate 68
Fig. 5.2 Strain distribution associated with a uniform axial stress distribution 71
Fig. 5.3 Rotation from ply x´, y´, z´ coordinates to structural x, y, z coordinates 72
Fig. 5.4 Rigid body displacement test problem 79
Fig. 5.5 Test problem results for $w = 0.5$ cm translation, solution by trapezoidal scheme solution with 40 intervals 79
Fig. 5.6 Test problem results for $w = 0.5$ cm translation, solution by trapezoidal scheme solution with 80 intervals 80
Fig. 5.7 Test problem results for $w = 0.5$ cm translation, solution by trapezoidal scheme solution with 320 intervals 81
Fig. 5.8 Test problem results for $w = 0.5$ cm translation, solution by two-stage Gauss scheme solution with 40 intervals 81
Fig. 5.9 Patch test problem for rigid body displacements 83
Fig. 5.10 Patch test problem for examining relative thickness of a layer 86

Fig. 5.11 Plot of errors in σ_{xx} for t = 0.0001 cm case of Table 5.7 90
Fig. 5.12 Patch test problem for examining several thin layers 91
Fig. 5.13 Plot of errors in σ_{xx} for $N = 6$ case of Table 5.8 93
Fig. 5.14 Plot of errors in σ_{zz} for $N = 6$ case of Table 5.8 93
Fig. 5.15 Patch test problem for rigid body displacements in the axisymmetric model 95
Fig. 5.16 Patch test problem for examining relative thickness of a layer 97
Fig. 5.17 Four ply laminate subject to uniform extension on ends y = constant 101
Fig. 5.18 Distribution of the interlaminar normal stress σ_z in the 0/90 interface 102
Fig. 5.19 Distribution of the interlaminar shear stress τ_{xz} in the 0/90 interface 103
Fig. 5.20 Finite element mesh for the dropped-ply laminate modeled in Ref. 21 104
Fig. 5.21 Ply drop-off as modeled using present analysis 105
Fig. 5.22 Comparison to finite element model of Ref. 21 for σ_{nn} along lower interface 106
Fig. 5.23 Comparison to finite element model of Ref. 21 for σ_{ns} along lower interface 107
Fig. 5.24 Comparison to finite element model of Ref. 21 for σ_{nn} along upper interface 107
Fig. 5.25 Comparison to finite element model of Ref. 21 for σ_{ns} along upper interface 108
Fig. 6.1 Laminates with and without eccentricity in the middle surface 110
Fig. 6.2 Delamination fraction along the lower interface for four 0° plies dropped loaded in longitudinal compression 114
Fig. 6.3 Delamination fraction along the upper interface for four 0° plies dropped loaded in longitudinal compression 115
Fig. 6.4 σ_{nn} along the upper interface for four 0° plies dropped loaded in longitudinal compression 115
Fig. 6.5 σ_{ns} along the upper interface for four 0° plies dropped loaded in longitudinal compression 116
Fig. 6.6 M_x distribution for four 0° plies dropped loaded in longitudinal compression, with eccentricity 117
Fig. 6.7 Laminate used to examine effect of the stiffness of the dropped plies on the interlaminar stresses 119
Fig. 6.8 Delamination fraction along the lower interface for different values of θ of the dropped sublaminate $[\pm\theta]_s$ (longitudinal compression loading) 121
Fig. 6.9 Delamination fraction along the upper interface for different values of θ of the dropped sublaminate $[\pm\theta]_s$ (longitudinal compression loading) 121

Fig. 6.10 Delamination fraction along the lower interface for different values of θ of the dropped sublaminate $[\pm\theta]_s$ (in-plane shear loading) 122
Fig. 6.11 Delamination fraction along the upper interface for different values of θ of the dropped sublaminate $[\pm\theta]_s$ (in-plane shear loading) 122
Fig. 6.12 Plot of the correlation between the stiffness ratio and the peak value of $\sqrt{F}$ (longitudinal compression loading) 125
Fig. 6.13 Plot of the correlation between the stiffness ratio and the peak value of $\sqrt{F}$ (in-plane shear loading) 126
Fig. 6.14 Schematic of dropped ply laminate with soft insert 128
Fig. 6.15 Interlaminar normal stress along upper interface 129
Fig. 6.16 Interlaminar shear stresses along upper interface 129
Fig. 6.17 Interlaminar normal stresses along lower interface 130
Fig. 6.18 Interlaminar shear stresses along lower interface 130
Fig. 6.19 Peak interlaminar stresses vs. length of 90° insert 131
Fig. A.1 Heterogeneous sub-laminate and equivalent homogeneous solid 145

List of Tables

Table 3.1 Summary of the mathematical model (N = number of mathematical layers) 48
Table 3.2 Summary of first order differential equations and boundary conditions (BCs). N = number of mathematical layers 49
Table 5.1 Comparison of methods of determining layer compliances 70
Table 5.2 Errors resulting from rigid body translations 83
Table 5.3 Errors resulting from steep interfacial slopes 84
Table 5.4 Condition numbers for A = 0 and $z_0 = 0$ 87
Table 5.5 Condition numbers for A = 0 and $z_0 = 100$ cm 88
Table 5.6 Condition numbers for increasing distance from the x-axis, A = 0 and $t = 0.1$ 89
Table 5.7 Condition numbers and maximum errors for varying center layer thickness 90
Table 5.8 Condition numbers and maximum errors for several thin layers of thickness $t = 0.001$ cm 92
Table 5.9 Errors resulting from rigid body displacements 95
Table 5.10 Errors resulting from steep interfacial slopes 96
Table 5.11 Condition numbers and maximum errors for varying center layer thickness and radius 98
Table 5.12 Condition numbers for Pagano's original formulation and the present formulation 99
Table 6.1 Boundary conditions and out of plane deformations for eccentricity study 112
Table 6.2 Results for eccentricity study (t_{thin} is the thickness of the thin section) 118

Table 6.3 Results for study of the effect of stiffness of the dropped plies $\pm\theta$ (t_{thin} is the thickness of the thin section) 123
Table 6.4 Ratios of the longitudinal stiffness of the thick section to the thin section for different values of θ of the dropped sublaminate $[\pm\theta]_s$ 124
Table 6.5 Ratios of the shear stiffness of the thick section to the thin section for different values of θ of the dropped sublaminate $[\pm\theta]_s$ 125

Chapter 1: Introduction

The application of advanced composites in aerospace structures has increased dramatically in the past decade. Their advantages in stiffness and strength to weight ratios over conventional metals allow lighter, more efficient aircraft. In addition, their anisotropic behavior allows the design of components with response characteristics that are not possible with isotropic materials. The most visible example of such an application is the forward swept wing of the X-29 technology demonstrator which has bending-twist coupling characteristics that prevent the aeroelastic divergence that had previously made such a design impractical.

When composite materials are used in aerospace structural components, it is usually desirable to tailor the material to match the localized strength and stiffness requirements in order to minimize the weight. For a fibrous composite laminate composed of unidirectional layers, this is often done by changing the number of plies. This abrupt change in thickness, which is referred to as a ply drop-off (other sources have used the terms tapered laminates and laminates with terminated plies), introduces a stress concentration which can lead to premature delamination failure of a laminate. It is this interlaminar stress concentration that is the subject of the present research.

A common application of the ply drop-off is a composite aircraft wing skin, or stabilizer skin, which requires much greater thickness at the root as compared to the tip. When fasteners are used to attach two components together, laminates must be built up to handle the concentrated bearing loads. The multi-segment composite solid rocket booster casing for the space shuttle currently under development is a highly visible example of this application.[1,2] Other applications of composites with dropped plies which have been mentioned in the literature include helicopter yokes,[3] helicopter rotor flexbeams,[4,5] and

flywheels.[6]

1.1 Literature Review

Most of the literature on the subject of ply drop-offs has been published in the past decade. Research has been done on the response, failure initiation, damage tolerance, failure modes and even beneficial effects on failure loads of ply termination in laminated composites. Longitudinal and transverse as well as internal and external ply drop-offs have been examined under various loading conditions and environmental influences. This literature review will concentrate on the static response of dropped-ply laminates without stability considerations and will therefore exclude studies dealing with fatigue or buckling.

1.1.1 Classification and Overview of Parametric Effects

There are several types of ply drop-offs which differ depending upon which plies through the thickness are dropped and the orientation of the termination with respect to the loading. An external ply drop-off is one in which the dropped plies are on a surface of the laminate while an internal ply drop, as its name implies, has plies terminated from the interior. Because of the large peeling stresses present in such a design, external ply drop-offs are relatively weak and are therefore avoided when possible. The most common instance where an external ply drop-off is used is for attachment of stiffeners.[7] Internal ply drop-offs, which require the remaining plies to contour around the ends of the dropped plies, while not without their own problems, are more common in stiffness tailoring.

A ply drop-off can be classified further depending upon the orientation of the load path with respect to the direction normal to the terminated edge. Excluding shear loadings, which have received little attention in the literature, a longitudinal ply drop-off is oriented such that the normal to the terminated edge is perpendicular to the load and a transverse drop has the normal parallel to the loading direction.

A ply drop-off can also be classified based on symmetry. Symmetric ply drop-offs are those where all plies that are dropped on one side of the middle surface have a counterpart of the same orientation dropped symmetrically with respect to this middle surface. In addition, the middle surface does not shift in the thickness direction through the ply drop-off region. A configuration not classified as such is asymmetric and couples extension and bending. Aircraft wing skins typically utilize asymmetric ply drop-offs in order to have the

surface exposed to the airflow as flat as possible.

External ply drops were examined by Daoust and Hoa,[3] Wu and Webber,[8] Wu,[9] and by Kubr.[7] Wu and Webber performed a finite element analysis of external ply drops under transverse tensile loading and found very high peak stresses in the corner of the drop. When a resin fillet was added to the analysis, the peak interlaminar stresses were reduced to about half their original values. The paper by Wu was a follow up of this analysis, in which nonlinear material behavior was included to account for the redistribution of stresses in the resin that would occur in the presence of the peak stresses. Without a fillet, resin nonlinearity also had the effect of reducing the peak interlaminar stresses by about half. No comparison was made to a uniform thickness laminate so the degree of strength degradation was not determined. Daoust and Hoa used finite elements to examine the effects of several parameters on the strength of transverse ply drop-offs including external versus internal configurations. Under tension, bending and torsion they found that internal ply drop-offs are typically twice as strong as external ply drop-offs. Kubr looked at external ply drop-offs in the context of co-cured stringer reinforced composite plates. He used a finite element analysis and examined the stress singularity at the reentrant corner using a highly refined mesh in this area.

A few papers examined **longitudinal ply drop-offs**. In each case, the purpose of introducing longitudinal drop-offs was to alter the stress field in the free edge region in an attempt to prevent delamination. Chan and Ochoa[10] used finite elements in analyzing laminates with 90° plies dropped symmetrically just inside of the free edge and found that under tensile loading, interlaminar normal stresses were reduced by 85% and interlaminar shear by 43%. In an accompanying experimental program, the tensile strength was found to be increased by 40% and premature delamination was eliminated. In a follow up study,[11] the authors also examined the longitudinal ply drop-off under bending and torsion loads. They found that under these loadings, the maximum interlaminar stresses were not altered significantly and in most cases were increased a small amount. Pogue and Vizzini[12] looked at four methods of edge alteration in tension specimens, including dropping plies, in a purely experimental study. Vizzini[13] later added a finite element analysis which agreed reasonably well with experiments in predicting the strain level at failure initiation. These studies reached a different conclusion than Chan and Ochoa regarding the merits of longitudinal ply drops. Working with symmetric delamination-critical laminates composed of ±15° and 0° layers, Vizzini found that dropping plies from these laminates usually caused failure to initiate internally at the end of the dropped layer. The delamination

initiation load was found to be lowered by as much as 10% or increased by as much as 16% relative to an unaltered specimen, depending on the configuration. This difference in conclusions between these two studies may be attributed to the fact that for the laminates studied by Chan and Ochoa, the mismatch in Poisson's ratio was critical while in those that Vizzini looked at, the mismatch in the coefficients of mutual influence was critical.

The remainder of this overview concentrates on **transverse internal ply drop-offs** as their application is more prevalent and of most interest to this study. Of these, a small group of sources[14,15,16] examined both geometrically symmetric and asymmetric ply drop-offs, allowing a comparison between the two configurations. Kemp and Johnson[14] performed a finite element analysis of two layups of T300/5208 and found that in tension, geometrically symmetric ply drops have a 8-21% higher strain to initial failure than asymmetric drops, depending on the layup and number of plies dropped. In compression they found the reverse, asymmetric ply drops stronger than symmetric by 7-26%. In addition to the change in failure strain, they also found that the location of the predicted failure initiation sometimes moved due to a change in symmetry conditions. Lagace and Cannon[15,16] used an analysis employing classical laminated plate theory in approximating the in-plane stress concentration of an idealized asymmetric step change in thickness, performed experiments, and concluded that the effect on fracture of bending induced by an asymmetric ply drop was insignificant. However, it is worth noting here that only tension was considered and the asymmetric laminate tested had only one ply out of six terminated. In addition, a comparison to a symmetric version of the same layup was not made.

In experimental and finite element analysis of a symmetric ply drop, Wisnom[17,18] investigated three factors influencing failure when internal plies are terminated in unidirectional glass-epoxy specimens subject to either tension or compression. (Unidirectional specimens were used to avoid failure by free edge delamination that is prevalent with many angle ply specimens.) The first factor was the stress concentration associated with terminating internal plies, the second was the interlaminar shear and normal stresses induced by the tapered geometry, and the third was the effect of the curved fibers adjacent to the ply drop. Straight specimens with cut central plies were subject to tension to assess the stress concentration associated with ply termination (no taper or curved plies). Straight specimens were also severely tapered, or waisted, through the thickness by machining with a diamond wheel (no internal ply terminations or curved plies) and subjected to tension. Finally, the effect of fiber curvature was investigated by means of inserting two plies of nylon film in the middle of eight ply tensile specimens, or two layers

of film adhesive in the middle of thirty-two ply compression specimens. The straight specimens with cut central plies failed by delamination between the discontinuous and continuous plies, the waisted specimens delaminated due to a stress concentration dominated by interlaminar shear stress, and specimens with inclusions failed due to fiber breakage in the grips. It was concluded that the critical parameter affecting delamination in tapered unidirectional composites is the strain energy release rate due to the terminating internal plies.

Papers by Botting, Vizzini, and Lee[19] and Fish and Vizzini[5] are similar in that they examined the effect of altering the sequence in which plies are dropped. Both papers analyzed glass/epoxy laminates with plies dropped symmetrically in three steps from 28 to 16 plies with a taper angle of 5.7°. The Fish and Vizzini paper was purely experimental and all of the plies were oriented at 0° in order to minimize free edge effects. In a multi-ply staggered drop, they altered two characteristics of the taper region. First, the sequence that the plies through the thickness were dropped was varied, giving either a staircase or overlapped appearance. Second, the particular plies through the thickness that were dropped was varied, or more specifically whether the dropped plies were adjacent to each other or not. The result was a four way comparison between laminates that were staircased or overlapped and grouped or dispersed. Bending stiffness was measured at the start and as damage progressed. They found that delamination onset loads varied by 38% and bending stiffness retention varied by 56% between configurations with a tendency for tradeoff between the two. The overlapped-dispersed configuration was found to provide the best overall performance. The work by Botting, Vizzini and Lee included a three dimensional finite element analysis as well as experiments in examining the effects of the longitudinal sequence of ply termination with all dropped plies interspersed between continuous sublaminates. The continuous sublaminates were either $[\pm 45_2/0_4]_s$ or $[0_4/\pm 45_2]_s$ and the dropped plies were ±45 pairs. For the $[0_4/\pm 45_2]_s$ laminates, the best configuration was one in which the second dropped ply from the mid-surface was overlapped over the first at the thin end of the drop region. This provided a 16% strength increase over the simple staircase configuration. Through visual inspection and x-ray photography, the $[\pm 45_2/0_4]_s$ laminates were found to delaminate due to free edge effects and therefore no conclusions could be made regarding the effect of the configuration of the drop.

In an analysis incorporating finite elements as well as experiments, Curry et al.[20,21] found that strength reduction due to asymmetric ply drop-offs was greater in compression than in tension and that the strength reduction was proportional to the stiffness change

across the drop. This finding was corroborated by Trethewey et al.[22] In their finite element study, Daoust and Hoa[3] found that internal ply drop-offs lose very little strength in torsion. They also found that increasing the distance between the end of the terminated plies and the joining of the continuous plies, thereby reducing the taper angle, lowers the magnitude of the interlaminar stresses generated. Kemp and Johnson[14] corroborated this finding by predicting increased failure strains under those circumstances in their finite element based analysis.

1.1.2 Approaches to Modeling and Analysis

The methods of analysis employed in the literature varied depending upon the objectives of the studies and the resources available. Because of their relative ease of application to geometrically complex problems, by far the most prevalent method was finite elements. In fact the only studies found that did not employ finite elements were the previously mentioned work by Lagace and Cannon,[15,16] Trethewey, Gillespie and Wilkins,[22] and a few which were purely experimental.[1,5,23,12] Lagace and Cannon determined the bending deflections of dropped ply laminates modeled essentially as two asymmetrically end-butted beams and then determined the in-plane stresses from the stress-strain relations based on classical laminated plate theory. The work done by Trethewey et al. divided a dropped-ply laminate into six subregions and employed shear deformation plate theory to these subregions. A damage tolerance analysis was then performed using linear elastic fracture mechanics. The choice of shear deformation plate theory over continuum finite elements was made in order to streamline the analysis for use as a preliminary design tool.

Three-Dimensional Finite Element Analyses

Some of the studies employed fully three-dimensional finite element analyses. One of the earliest was by Adams, Ramkumar and Walrath[24] and included the effects of nonlinear material response and thermal residual stresses. However, although the model was three-dimensional, the lateral surfaces were constrained to remain planar, essentially imposing generalized plane strain conditions and not accounting for free-edge effects. In addition, each layer was modeled by one element through the thickness except for the dropped layer which had two. Also, no longitudinal mesh refinement was made at the actual ply drop location. Hoa, Daoust, Du and Vu-Khanh[25] refined their three-dimensional mesh at the ply drop by a submodeling (or zooming) technique. This approach involved successive

reduction and refinement of the mesh in the region of interest while retaining the results of the previous iteration as boundary conditions for the reduced mesh. The purpose of this method was to have a refined mesh in the region of large stress gradients while keeping the number of degrees of freedom of the solution required for each pass of the finite element solver within the capability of the computer that was available. In an extension of this work, Daoust and Hoa[3] once again used three-dimensional finite elements; however rather than using submodeling, they developed a more efficient computer routine. Finally, Fish and Lee[4,26,27] and Botting, Vizzini and Lee[19] used a three-dimensional assumed stress hybrid finite element approach in order to obtain more accurate stress predictions than conventional displacement based elements, which are used in the previously mentioned studies. Extensive mesh refinement at the end of the ply drop-off was incorporated into their analyses. However, each element spanned the half-width of the quarter symmetry model and therefore the benefits of a three-dimensional model were not fully utilized.

Plane Stress and Strain Finite Element Analyses

Because of the computationally intensive nature of three-dimensional finite element models, most of the authors reduced the domain of the problem to two dimensions. Wisnom[17] was the only author who used plane stress finite elements in his study of unidirectional glass/epoxy laminates, which do not suffer from free edge effects. This approach predicts the stresses along the edge of a specimen, where a state of plane stress exists. Salpekar, Raju and O'Brien[28] employed the plane strain assumption in their two-dimensional analysis.

Quasi Three-Dimensional Finite Element Analyses

Kemp and Johnson,[14] Curry et al.,[20,21] Wu and Webber,[8] Wu,[9] Kubr,[7] and Messick et al.[2] all reduced the domain to a cross-sectional plane parallel to the load axis for transverse ply drops through the elimination of the dependence of the strains on one coordinate. Kemp and Johnson and also Kubr assumed a displacement field independent of the coordinate normal to the plane of analysis. Curry et al., Wu, and Wu Webber assumed the strains to be independent of the coordinate normal to the plane of the analysis, which restricts but does not preclude dependence of the displacements on that coordinate. Finally, Messick et al. used the assumption of axisymmetry in their analysis of the shuttle solid rocket booster casing. In each of these models, although the domain was reduced to two dimensions, the displacement normal to the plane of the model was still included and

therefore these models have five or six nonzero components of strain. This type of finite element analysis will be referred to as quasi three-dimensional in this literature review.

There are several features of these quasi three-dimensional analyses that are worth mentioning. In order to arrive at a solution that took into account the out of plane boundary conditions imposed by an actual test fixture with simply supported edges, Curry et al. first used a plate finite element routine with a two step change in thickness to obtain boundary conditions for their quasi three-dimensional model of the ply drop-off region. In their analysis of external ply drop-offs, Wu and Webber included a thin resin layer between the continuous and dropped layers and then in his follow-up paper, Wu added nonlinear material response for the resin layer. Messick et al. used submodeling in their analysis of the composite shuttle solid rocket casing because of the large number of plies involved. Salpekar et al. as well as Wisnom refined their mesh extensively at the tips of the dropped plies in order to allow for accurate strain energy release rate calculations in their fracture analysis. Fish and Lee[4] used an assumed stress hybrid element approach to examine the free edge effects in a dropped ply specimen.

The remainder of the studies incorporating quasi three-dimensional finite element analyses examined longitudinal ply drops. Because of the orientation of the ply drop in these cases, the plane of the finite element mesh was oriented transverse to the principle loading direction. Chan and Ochoa[10,11] used displacement assumptions similar to Curry et al., allowing for extension in the direction of, and torsion about, the out-of-plane normal (the specimen longitudinal axis), as well as bending about the transverse axis (the specimen width-wise axis). Vizzini[13] performed a similar analysis in tension using assumed stress hybrid elements.

1.1.3 Failure Analysis

In order to predict the performance of the various laminates studied, some kind of failure analysis was applied and often more than one was used. Frequently, different criteria were used for prediction of in-plane and out-of-plane failure of the plies as well as for out-of-plane failure between plies (delamination). Most studies used some type of strength-of-materials approach which compares the local stress or strain state to material strength allowables. Others used criteria based on fracture mechanics where the strain energy release rate is compared to some toughness parameter to determine whether a flaw will grow and lead to failure.

Strength-of-Materials Approach

Starting with the strength of materials approaches, several authors used some form of the maximum stress criterion. Daoust and Hoa[3] used it to predict the location of both in-plane and out-of-plane failure although no experiments were performed to verify the results. Fish and Lee[26,27] applied it in instances where one stress component was dominant. For a case where the interlaminar shear stress was dominant in the interply resin surrounding the ply drop-off, the criterion was applied in combination with interlaminar stress averaging. In comparison to experiments, Fish and Lee found that with a stress averaging distance of one ply thickness along the interface, consistently accurate delamination initiation predictions were obtained. Curry et al.[20,21] used the maximum stress criterion in the resin rich region ahead of the ply drop, but failure initiation was both predicted and experimentally found to occur at the interface between the dropped and continuous plies. In their purely analytical paper, Kemp and Johnson[14] used the maximum stress criterion in terms of the principal stresses in the resin rich region and applied it to the interply resin surrounding the dropped plies as well. Lagace and Cannon[15,16] applied the maximum stress criterion in their analysis; however, only in-plane stresses were considered, and as mentioned previously, the laminates they chose tended to be unaffected by the ply drop-off. In their analysis of the shuttle solid rocket booster casings, Messick et al.[2] found a good correlation between the magnitude of the peak value of the axial stress, which did not change location under minor design changes, and the failure load of the specimen.

While they used the maximum stress failure criterion for resin failure, Kemp and Johnson used the Tsai-Wu criterion for intralaminar failure prediction. Curry et al. also used Tsai-Wu for intralaminar failure prediction but with a refinement developed by Hashin that eliminates the influence of a tensile strength parameter on a compressive failure mode and vice versa. In addition, Curry et al. used an interlaminar criterion based on matrix failure modes, also developed by Hashin. In combination with their quasi three-dimensional finite element analysis, these criteria underestimated experimentally determined failure loads by more than 30%. In addition to applying maximum shear stress to the interply resin, Fish and Lee also used a form of the Tsai-Wu criterion that considered only interlaminar stresses for out-of-plane failure of the plies as well as the interply resin. This criterion did not give good correlation with experiments for out-of-plane ply failure, but gave good results when applied to the interply resin with a longitudinal stress averaging distance of one ply thickness. Vizzini[13] used a combination of Tsai-Wu and von-Mises

criteria in his analysis of longitudinal discontinuities, including ply drops. The Tsai-Wu criterion was applied to the case of alteration of the ply orientation near the free-edge in a model without a resin zone at the discontinuity. The von-Mises criterion, which is an isotropic criterion, was applied within a resin zone for a modified model of the edge alteration as well as to the resin zone of the ply drop-off, and provided better strength prediction when compared to experiments.

Wu[9] was the only author to use the maximum strain failure criterion in his study of external ply drop-offs. Coupled with his finite element analysis employing nonlinear material behavior, he obtained reasonable delamination prediction compared to experiments.

Fracture Mechanics Approach

Salpekar et al.[28] and Trethewey et al.[22] applied linear elastic fracture mechanics to predict failure. In both cases, their analyses were used to calculate the strain energy release rates for modes I and II which were compared to the corresponding fracture toughness of the matrix. However, neither of these papers included an experimental investigation and therefore the accuracy of these methods has not been verified.

Wisnom[17,18] concludes the strain energy release rate is the critical parameter affecting delamination in dropped-ply unidirectional glass-epoxy specimens. In his experiments the onset of delamination was more difficult to measure objectively than the delamination propagation. The finite element analysis required considerable effort to compute initial strain energy release rate, and it was found that the initial strain energy release rate for the specimens with cut central plies was higher than the propagation value, while the opposite was true for the dropped ply specimens. (The propagation value corresponds to the uniform value of the strain energy release rate attained with increasing delamination crack length.) Moreover, a simple formula was derived to compute the applied stress for the delamination propagation which does not require a finite element analysis, but was confirmed by finite element analysis to be accurate. The experimental results for dropped-ply specimens correlated reasonably well using the simple formula to predict the applied stress for delamination propagation when the critical value of the strain energy release rate was measured from the straight specimens with cut central plies. For tension loading, the simple formula gave conservative predictions that were within 27% of measured values in Ref. 17, and within –20% to 3.9% in Ref. 18. For compression[18], the simple formula gave conservative predictions that were within –5.5% to 1.9%. However, it was observed

that the critical strain energy release rate was not a material parameter since it increased as the thickness of the straight specimen with cut central plies increased. Also, tests on scaled specimens, in which the ratio of the number of cut central plies to continuous plies is constant, showed a scale effect since the delamination strength decreased with increasing thickness. (This phenomenon was also noted by Brewer and Lagace[29] in their study of delamination at straight free-edges.) Wisnom[18] investigated the use of the point stress criterion and the average stress criterion applied to the straight specimens with cut central plies, and found that the distance parameters in these criteria are not material constants either, but vary significantly with the specimen geometry.

1.1.4 Summary Comments

For studies in which results from analyses are compared to experimental results, deductions can be made regarding the merits of various approaches to analysis and failure prediction. A few features were common to two of the studies that obtained a good correlation to experiments. Fish and Lee[26,27] and Vizzini[13] used hybrid finite element analyses and applied their strength-of-materials failure criteria within interply resin zones. Fish and Lee found that better prediction of delamination was made when they applied their Tsai-Wu based criterion to an interply resin zone that was 10% the thickness of a lamina than when applied within a lamina. They also incorporated a stress averaging distance of one lamina thickness. Vizzini applied the von-Mises criterion to the resin rich zone bordered by the ends of the dropped plies and the two continuous layers and did not use stress averaging. However, his analysis produced stresses at only one point for each element which probably had the effect of averaging. Both of these analyses also employed finite element meshes that contain step changes in slope of the lamina which is not consistent with the actual geometry of a ply drop-off. In a follow up of his master's thesis[20], which had abrupt slope changes, Curry[21] found that smoothing the changes in slope did have a fairly large effect on the stress state. The interlaminar shear stress was reduced by about 30% through this smoothing in some cases.

Wisnom[17] also was able to closely match his analysis with experimental results. His use of a strain energy release rate approach proved very accurate for laminates that were the same thickness as the one he used to measure the fracture toughness. However, he found a dependence of that toughness parameter on the thickness of the laminate.

Other studies that attempted to predict failure with a comparison to experiments were

those by Curry,[20,21] Wu,[9] and Cannon.[15,16] Curry et al. underestimated the experimental failure load by 30%. Including a stress averaging distance or a characteristic distance would probably have improved on this result. Wu's analytical prediction was off by about 25% of the failure load which he attributed to not including a fillet in the corner of the external ply drop-off. The analysis by Cannon did not attempt to model the geometry in the ply drop-off region accurately, and therefore the poor correlation with experiment in predicting failure is understandable.

This review of the literature indicates that delamination is the predominant mode when dropped-ply laminates fail prematurely. Much has been written about delamination in laminated composite materials, mostly dealing with the free-edge problem. In their paper presenting a quadratic stress criterion for predicting delamination initiation, Brewer and Lagace[29] described delamination as an initiation and growth process. After initiation, the delamination can undergo stable or unstable growth eventually leading to in-plane and final failure. While delamination initiation may not be the ultimate failure of a laminate, it is nevertheless important to predict.

While the strain energy release rate approach has shown the ability to predict initiation and growth characteristics of delamination, there are major drawbacks to the method. In predicting initiation, for instance, the location of the delamination must be assumed in order to determine the strain energy release rate for a crack located there. Also, as mentioned previously, the critical strain energy release rate appears to be a function of laminate thickness. Finally, O'Brien[30] found that the critical strain energy release rate is a function of the percentage of Mode I present which requires a detailed analysis such as finite elements to determine.

The main advantage of the strength of materials approaches is their ease of application, thus allowing the application of the failure criteria to more of the laminate at minimal expense. This advantage makes locating the point of delamination initiation more efficient than with the strain energy release rate approach. However, as stated previously, delaminations can undergo stable growth and mechanics of materials approaches cannot discern this characteristic of a delamination. Therefore, both of these approaches have their uses in failure prediction.

1.2 Objective

The objective of this research is to study the use of an assumed stress, or stress-based,

method of approximation to predict interlaminar stress distributions in the vicinity of the ply termination. The aim is to develop a model accurately reflecting the geometry and material discontinuity of the dropped ply laminate such that distributions of the interlaminar stresses may be used with confidence in a point stress criterion or an average stress criterion. Stress based methods are discussed in Chapter 2, and Chapters 3 and 4 present specific models based on the method of analysis chosen in Chapter 2. The accuracy of the numerical methods used to solve the models is discussed in Chapter 5. Parametric studies are given in Chapter 6, and concluding remarks are given in Chapter 7.

Chapter 2: Choice of Method of Approximation

This chapter begins by presenting a discussion of various approaches that were considered and the reasons for the choice of analysis that was made. Then, a general outline of the approach is presented. Following that, specific formulations are detailed that are of interest for the analysis of dropped-ply laminates.

2.1 Methods of Approximation

The most accurate way of solving for the static linear response of a solid body is to develop an exact analytical solution to the governing partial differential equations of three-dimensional linear elasticity satisfying the specified boundary conditions. However, for most problems, including laminates containing ply drop-offs, exact solutions are intractable and some form of approximation must be used. There are two general types of methods for approximating the continuous response of structures that are too complicated for an exact solution. The first involves developing an approximate solution to the governing differential equations of elasticity. The second uses the variational principles of solid mechanics and assumptions regarding the stress and or displacement fields to either derive the corresponding governing Euler equations or to arrive at the approximate solution directly.

2.1.1 Approximate Solution to the Governing PDEs of Elasticity

The primary approach to solving the governing equations of elasticity that is suitable for

complicated geometries such as ply drop-offs is the finite difference method. The finite difference method approximates the field variables on a mesh of points distributed throughout the domain. Approximations of the partial derivatives in terms of the field variables at the grid points, known as difference quotients, are substituted into the PDEs giving the difference form of the PDEs. These difference equations, applied over the domain, along with discretized forms of the boundary conditions, give a system of algebraic equations that can be solved for the grid point values of the field variables.

There are several drawbacks to the finite difference method including inaccuracy of the derivatives of the approximated solution, difficulty in imposing boundary conditions on curved boundaries, and the inability to employ nonuniform and nonrectangular meshes.[31]

2.1.2 Variational Methods

Variational methods are much more common in dealing with complex structures than methods that operate directly on the governing equations of elasticity. Based on the variational principles of solid mechanics, variational methods can be applied in many ways and can be tailored to the problem at hand and the results desired.

One way in which the variational principles may be applied is to develop a structural theory based on some type of assumption regarding the field variables. An example of this approach is the development of classical beam theory through application of the principle of minimum potential energy. In this instance, the displacement field is restricted to a form explicit in the cross-sectional coordinates and substituted into the principle, which is then integrated with respect to the cross-sectional coordinates, giving the governing equation of classical beam theory as the Euler equation. A solution to a problem can then be obtained through solution of the boundary value problem consisting of the governing equations and the associated boundary conditions of the structural theory.

Another class of variational methods, which obtain approximate solutions directly from the variational statement, are known as direct methods. They include the Ritz method and also the weighted residual methods of Galerkin, Kantorovich and Trefftz. It should be noted that the weighted residual methods can also be applied in instances where a variational statement does not exist and are therefore not exclusively direct methods. Because the Ritz method is applicable to any problem for which a variational statement exists and gives results that are in general superior to the weighted residual methods[32], it is far more common in structural mechanics. The most popular use of Ritz type methods is in

the development of finite element approximations.

In the finite element approach, the domain is divided into subdomains or elements with the form of the solution assumed within each element in terms of discrete values and polynomial interpolation functions. Application of the Ritz method to the appropriate variational principle in a piecewise manner results in a linear system of equations that is then solved for the discrete unknowns. While they may at first seem similar, these methods are generally recognized as being superior to finite differences.

2.1.2.1 Conventional Finite Element Methods

Within the field of finite elements as applied to solid mechanics there are several types of models which differ in the form of variational principle employed and the field variables that are assumed.[33,34] Using the terminology of Pian and Tong,[33] those based on the conventional variational principles of minimum potential energy, minimum complementary energy and the Hellinger-Reissner principle are the compatible, equilibrium and mixed models respectively.

In the compatible models, the assumed field variables are the displacements which are required to be continuous within and between elements and therefore compatible (or kinematically admissible). They are the most commonly used of the finite element models because of their inherent ease of development for most applications and efficiency of computation. Their ease of development is due to the relatively loose restriction of continuity on the assumed displacement field. However, this simplicity does not come without a cost, namely a loss of accuracy in predicting stresses. This loss of accuracy is due to the fact that equilibrium of the stresses within the elements is satisfied only in an integral sense as is traction continuity between elements.

The equilibrium models are derived from an assumed equilibrating stress field that must also satisfy interelement traction equilibrium, i.e., a statically admissible stress field. These models tend to have improved accuracy for stress prediction as compared to compatible models. However, satisfying the differential equations of equilibrium within an element and traction continuity between adjacent elements is very difficult for elements of varying shapes. Another drawback is that displacement continuity between adjacent elements is satisfied only in an integral sense.

The mixed models assume both the stress and displacement fields with no a priori equilibrium requirement for the stresses nor compatibility requirements for the displacements. Conditions on the stresses and displacements between adjacent elements,

which are developed from the condition that the functional must be uniquely integrable, are also more flexible. Eight possible combinations result from the requirement that either the displacement or traction must be continuous in the normal and two tangential directions relative to the interface.[33] This feature makes the mixed finite element models useful for the analysis of plates and shells where difficulties in developing interpolation functions that meet continuity requirements on the derivatives of the out-of-plane displacement can be avoided. Moreover, it also provides benefits in stress analysis by allowing assumption of stresses, which according to Pian and Tong[33] can improve their accuracy, without the complication of having to satisfy equilibrium a priori.

2.1.2.2 Hybrid Finite Element Methods

Beyond the conventional variational principles are the modified variational principles which allow for relaxed continuity requirements between elements. The models based on these principles are the hybrid models and are distinguished by the independent assumption of field variables within the elements and along the element boundaries which are allowed by the modified principles.[35,36] Derived from the conventional variational principles through the use of Lagrange multiplier terms that apply the conditions on the tractions and displacements between elements as constraints, the modified principles of potential energy and complementary energy lead to the hybrid-displacement and hybrid-stress models[33] while the modified Hellinger-Reissner principle leads to the hybrid-mixed models.[34,37] In the hybrid-displacement models, the displacement field is assumed within the elements while the tractions and also possibly a separate form of the displacements are assumed on the element boundaries. The hybrid-stress model assumes interior stresses and boundary displacements. The hybrid-mixed models use assumed element stresses and displacements with separate boundary displacements and possibly tractions.

The hybrid-displacement models take three basic forms, two based on the assumption of element displacements and boundary tractions and one that assumes element displacements and both boundary tractions and displacements.[34,38] The difference between the first two forms is that one bases its displacement assumptions on nodal displacements which guarantees compatibility with neighboring elements while the other uses general displacement parameters. The third form is a combination of the first two in that it assumes the element displacements in terms of general displacement parameters while the boundary displacements are in terms of nodal displacements. These models offer flexibility in dealing with interelement displacements and like the conventional mixed models, are typically

applied to plate and shell problems.

First introduced in 1964 by Pian[39], hybrid-stress models are typically applied where more accurate stresses are desired. As in the equilibrium model, this hybrid model uses an assumed equilibrating stress field within the elements which enhances stress accuracy. However, it avoids the problem of meeting interelement traction equilibrium through the modification of the variational principle. Instead, the boundary displacements are assumed in terms of nodal values such that they satisfy interelement continuity. Of the hybrid models, these have been applied to the broadest range of problems, from multilayer plates and shells to fracture mechanics.

The hybrid-mixed models, like the hybrid-displacement models, have been applied to a relatively small number of problems as compared to the hybrid-stress models. In fact, it is considered to be impractical in the field of linear solid mechanics to assume all of the variables allowed by this approach, i.e. separate internal and boundary values of the stresses and displacements.[34,36] Instead, this approach is recommended for dynamic problems and incremental analysis of finite deformation problems.

Application of these finite element models to the analysis of laminates can be achieved in two ways. The first is to simply apply elements developed for the analysis of continuous media, i.e. continuum elements, to the laminate. In this approach, the individual plies can be modeled by one or more elements through the thickness, or groups of plies can be modeled by one element through their collective thickness using some type of smearing scheme to arrive at an approximation of their constitutive behavior. The second approach is to develop a laminate finite element that takes into account the multilayer nature when developing the element approximation of the field variables.

A few studies have been done regarding hybrid-stress or mixed finite element analysis of laminated plates that use the second approach rather than simply discretizing the layers with ordinary continuum elements. Spilker[40,41] formulated hybrid-stress laminate elements that are isoparametric in the transverse coordinates with stress fields that equilibrate within each layer and satisfy traction continuity between adjacent layers. However, this approach does not allow for tapered layers as is required in analyzing dropped-ply laminates. Cook[42] also developed hybrid-stress elements, but they were based on plate theory and also cannot account for taper. Most recently, Shi and Chen[43] developed a global-local model that uses compatible elements in the global portion and hybrid-stress elements in the local region. Once again, however, taper cannot be accounted for in their model.

The difficulty in formulating a hybrid-stress model of a tapered laminate using this type

of approach lies in satisfying both the equilibrium equations on the interior of each layer and traction continuity at interfaces for layers with curved boundaries. For a finite element approach, one of the two must be relaxed, which is essentially the same as going back to treating the laminate like any other domain and using standard continuum elements.

2.1.3 Criteria for Interlaminar Stress Approximation

For accurate prediction of interlaminar stresses from an approximate continuum model, the method of approximation should meet certain requirements. Specifically, the stress field should satisfy equilibrium within the layers of the laminate as well as equilibrium of tractions, also referred to as traction continuity, between layers. In addition, it would be desirable to satisfy displacement continuity between layers.

Of the finite element methods presented, those that come closest to meeting these goals are the stress based methods of equilibrium and hybrid-stress and also the mixed methods. While the equilibrium models meet the requirements regarding the stress assumptions, development of such elements is difficult and displacement continuity between layers is not met. The hybrid-stress models do not enforce traction continuity and developing a mixed model that meets these requirements runs into the same difficulties as the equilibrium models. Therefore, it is felt that a different approach is necessary, which is the subject of this dissertation.

2.2 Approach

The approach chosen is based on work by Pagano[44,45] and develops a structural theory in a similar manner to the development of classical beam theory using the principle of minimum potential energy. However, instead of assumptions on the displacements, the present theory makes assumptions on the stresses. In addition, the Hellinger-Reissner stationary variational principle will be used instead of the principle of minimum potential energy

Development of the theory begins with division of the domain into layers with the stress field assumed within each layer. The dependence of the stresses on the thickness coordinate is expressed explicitly with considerations for the satisfaction of equilibrium and traction continuity between layers. The Euler equations are obtained from the stationarity condition with traction and displacement continuity imposed. Solution of the governing

equations is by a one step finite difference scheme. Pagano's presentation of this type of approach was first developed for analyzing flat laminates.[44] Later, he modified the approach to handle layers defined by curved meridians in axisymmetric bodies.[45]

2.2.1 Variational Principle

The starting point for the derivation of this analysis is the Hellinger-Reissner functional for a domain composed of N subvolumes and no body forces. In cartesian coordinates,

$$\Pi_R = \sum_{k=1}^{N} \int_{V_k} \left[\sigma_{ij}\varepsilon_{ij}(u_i) - W(\sigma_{ij}) \right]^{(k)} dV_k - \int_{S_\sigma} \tilde{\tau}_i u_i dS - \int_{S_u} \tau_i (u_i - \tilde{u}_i) dS \tag{2-1}$$

in which the displacements are denoted u_i, the strains ε_{ij}, the stresses σ_{ij}, the surface tractions τ_i, and the complementary strain energy density W. Repeated indices are summed from one to three in the usual indicial notation and the tilde symbol ($\tilde{}$) indicates a prescribed value. The portion of the surface with tractions prescribed is denoted by S_σ, while S_u represents the portion with displacements prescribed. In this form, the functional assumes that the displacements are continuous between subvolumes, i.e., the strains in the first term of the volume integral can be represented without the use of the delta function. Without this condition, an additional integral along the border between subvolumes must be included in order to account for the presence of the delta function in the strain field.[33] In addition, the tractions would have to be continuous for the functional to exist if the displacements are not continuous.

Stationarity of the functional with respect to all possible variations in the displacements and stresses gives the governing equations of elasticity as its Euler equations. The vanishing of the first variation is given by

$$\begin{aligned} \delta\Pi_R = \sum_{k=1}^{N} \int_{V_k} \left[\delta\sigma_{ij}\varepsilon_{ij} + \sigma_{ij}\delta\varepsilon_{ij} - \frac{\partial W}{\partial \sigma_{ij}} \delta\sigma_{ij} \right]^{(k)} dV_k - \int_{S_\sigma} \tilde{\tau}_i \delta u_i dS \\ - \int_{S_u} \delta\tau_i (u_i - \tilde{u}_i) dS = 0 \end{aligned} \tag{2-2}$$

for all admissible $\delta\sigma_{ij}$ and δu_i. Beyond symmetry of the stress tensor which is required in order to arrive at the governing equations of elasticity from the principle, admissibility of the stresses and displacements is governed by the boundary conditions and the unique definability of the functional of Eq. (2-1). As mentioned previously, for the functional to be uniquely defined, the $\sigma_{ij}\varepsilon_{ij}$ term must be integrable throughout the domain. Continuity of

displacements throughout the domain ensures this without the need for additional terms in the functional. Therefore, admissible variations in the displacements are to be continuous within subvolumes and at interfaces and vanish on S_u. As stated in the objective, it is desired to develop a theory in which tractions are continuous between layers. Therefore, admissible stress variations are to be symmetric ($\delta\sigma_{ij} = \delta\sigma_{ji}$), continuous in subvolumes, satisfy traction continuity at interfaces and vanish on S_σ.

In the cartesian reference, the variation of the strains written in terms of the displacements is

$$\delta\varepsilon_{ij} = \tfrac{1}{2}\left(\delta u_{i,j} + \delta u_{j,i}\right) \tag{2-3}$$

where the comma convention is used to indicate partial differentiation. Therefore, by substituting (2-3) and incorporating symmetry of the stress tensor:

$$\int_{V_k} \sigma_{ij}\delta\varepsilon_{ij} dV_k = \int_{V_k} \sigma_{ij}\delta u_{i,j} dV_k \tag{2-4}$$

Applying a rearranged version of the product rule of differentiation and then using Gauss' divergence theorem and Cauchy's relation for surface tractions in terms of stresses leads to the result:

$$\int_{V_k} \sigma_{ij}\delta\varepsilon_{ij} dV_k = \int_{S_k} \tau_i \delta u_i dS_k - \int_{V_k} \sigma_{ij,j}\delta u_i dV_k \tag{2-5}$$

where S_k represents the surface of each subvolume V_k and $\tau_i = \sigma_{ij}n_j$.

Substituting (2-5) back into (2-2) yields

$$\begin{aligned} \sum_{k=1}^{N} \int_{V_k} \left[\left(\varepsilon_{ij} - \frac{\partial W}{\partial \sigma_{ij}} \right) \delta\sigma_{ij} - \sigma_{ij,j}\delta u_i \right]^{(k)} dV_k + \int_{S_\sigma} \left(\tau_i - \tilde{\tau}_i\right)\delta u_i dS \\ - \int_{S_u} \delta\tau_i \left(u_i - \tilde{u}_i\right) dS + \sum_{l=1}^{M} \int_{I_l} \left[\tau_i^- \delta u_i^- + \tau_i^+ \delta u_i^+ \right] dI_l = 0 \end{aligned} \tag{2-6}$$

The new summation term results from the part of the surface integral in Eq. (2-5) taken over the portion of S_k, which is denoted by I_l, that borders another subvolume where neither tractions nor displacements are prescribed. In this term the value of M will depend on the geometry of the domain chosen and the + and – superscripts denote the two sides of the interface.

From the previously stated condition that the displacement field is continuous between

subvolumes, the interface displacement variations are no longer independent, i.e. $\delta u_i^+ = \delta u_i^-$, and the internal interface term becomes the condition of traction continuity. For a domain composed of layers, there will be one less interface than there are layers. Numbering these layers sequentially such that layer k is adjacent to layer $k+1$ for all k and denoting the interface between these adjacent layers by I_k, the principle takes the final form for application to laminates. Thus,

$$\sum_{k=1}^{N}\int_{V_k}\left[\left(\varepsilon_{ij}-\frac{\partial W}{\partial\sigma_{ij}}\right)\delta\sigma_{ij}-\sigma_{ij,j}\delta u_i\right]^{(k)}dV_k+\int_{S_\sigma}(\tau_i-\tilde{\tau}_i)\delta u_i dS \qquad (2\text{-}7)$$
$$-\int_{S_u}\delta\tau_i(u_i-\tilde{u}_i)dS+\sum_{k=1}^{N-1}\int_{I_k}\left[\left(\tau_i^{(k)}+\tau_i^{(k+1)}\right)\delta u_i^{(k)}\right]dI_k=0\,.$$

2.2.2 Assumed Stresses

Development of the assumed stress field is outlined for the general case of an orthogonal coordinate system with dependence of the stresses on all three coordinates. It should be noted here that while this procedure is applicable to all such coordinate systems, it becomes very involved for most cases. Use of this more general form is simply for illustrative purposes and the models developed subsequently are for specific applications of the procedure in simple coordinate systems.

For the general orthogonal coordinate system $(\alpha_1,\alpha_2,\zeta)$, it is required that the surfaces that define the boundaries of the layers be expressed as $\zeta = g(\alpha_1,\alpha_2)$ where g is a smooth function. The lateral boundaries would be defined by constant values of either α_1 or α_2 (see Fig. 2.1). A multilayered domain could therefore be defined by a family of surfaces in the thickness direction and by constant values of α_1 or α_2 at the lateral edges.

Considering a single layer bounded by $\zeta = \zeta_1(\alpha_1,\alpha_2)$ and $\zeta = \zeta_2(\alpha_1,\alpha_2)$ with $\zeta_2 > \zeta_1$ for all α_1 and α_2 within the domain, the stress field within that layer is assumed in the form

$$\sigma_i(\alpha_1,\alpha_2,\zeta)=\sigma_{ij}(\alpha_1,\alpha_2)f_j^{(i)}(\alpha_1,\alpha_2,\zeta)\,,\quad\text{no sum on } i \qquad (2\text{-}8)$$

where σ_i are the six stress components in contracted notation, σ_{ij} are functions only of α_1 and α_2 to be determined through application of the principle, and $f_j^{(i)}$ are shape functions with explicit dependence on ζ and known implicit dependence on α_1 and α_2 through functions ζ_1 and ζ_2. The requirements that

$$\sigma_i(\alpha_1,\alpha_2,\zeta_1) = \sigma_{i1}(\alpha_1,\alpha_2)$$
$$\sigma_i(\alpha_1,\alpha_2,\zeta_2) = \sigma_{i2}(\alpha_1,\alpha_2) \tag{2-9}$$

are imposed on the stress assumptions in order to facilitate interlayer traction continuity.

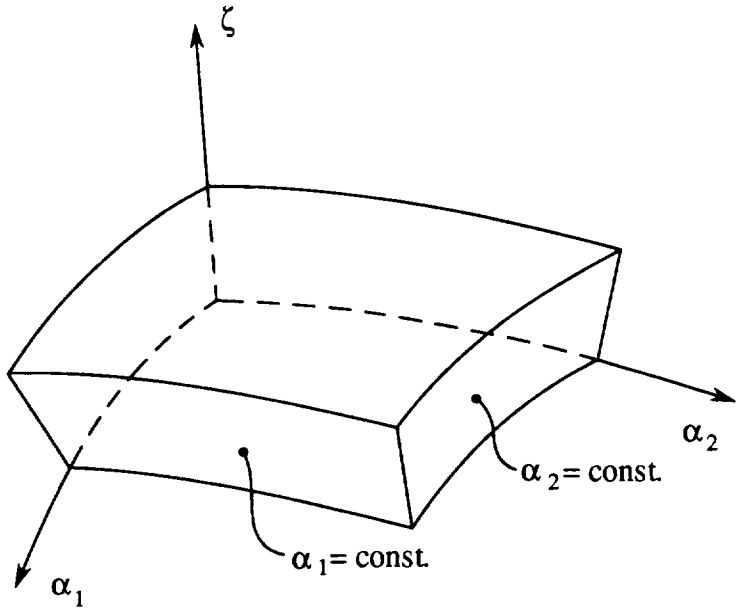

Fig. 2.1 Section of a uniform thickness layer in $(\alpha_1,\alpha_2,\zeta)$ orthogonal coordinates.

In arriving at the specific form of the shape functions, the "in-plane" stresses σ_{11}, σ_{22} and σ_{12} are assumed to have a specific dependence on ζ. Based on the elasticity equilibrium equations, the through the thickness distribution of the remaining stress components are determined. This procedure involves substitution of σ_{11}, σ_{22} and σ_{12} and integrating with respect to ζ in order to determine the dependence on ζ that the remaining stresses must have if non-trivial values of the stress variables σ_{ij} are to satisfy equilibrium.

2.2.3 Governing Equations

The form of the complementary strain energy density W for linear-elastic materials in terms of the stresses in contracted notation is

$$W = \tfrac{1}{2} S_{ij}\sigma_i\sigma_j \tag{2-10}$$

where S_{ij} are the compliance coefficients. This expression is substituted into Eq. (2-7) along with the assumed stress field (2-8) and its variation,

$$\delta\sigma_i(\alpha_1,\alpha_2,\zeta) = \delta\sigma_{ij}(\alpha_1,\alpha_2) f_j^{(i)}(\alpha_1,\alpha_2,\zeta) \tag{2-11}$$

and Cauchy's relation for the surface tractions in terms of the stresses. Integration with respect to ζ is then carried out. Because the displacements have unknown dependence on ζ, integrals through a layer of the displacements weighted by functions of ζ are defined as new unknowns in the model.

The Euler equations of the resulting form of the principle are one of two types. Those associated with the variation in σ_{ij} are the compatibility/constitutive equations, which may contain derivatives of the weighted displacements. Those associated with the variations in the weighted displacements are the equilibrium equations, which may contain derivatives of the stress variables. It should be noted that, while satisfaction of the equilibrium Euler equations implies satisfaction of the elasticity equilibrium equations within the layers, satisfaction of the Euler compatibility/constitutive equations only implies satisfaction of the corresponding elasticity equations in an integral sense within the layers. The system of Euler equations contains both first order linear ordinary differential equations and linear algebraic equations. A system containing both differential and algebraic equations is referred to in the literature as a system of DAEs. The solution of the systems will be detailed following the development of specific models using this approach.

Chapter 3: Generalized Plane Deformation Model

The first version of the model is developed for problems of generalized plane deformation in cartesian coordinates. Therefore, $(\alpha_1, \alpha_2, \zeta) = (x, y, z)$ for this formulation. In this class of problems, the loading, geometric and material properties, and hence stresses and strains are independent of y. The solution domain is thus reduced to the x-z plane where the x-axis is the longitudinal direction and the z-axis is the thickness direction. These problems differ from generalized plane strain in that bending about the x- and z-axes and torsion about the y-axis are allowed. A generic dropped ply laminate represented in a generalized plane deformation model is shown in Fig. 3.1. In this figure P denotes the extensional force along the y-axis, M_x is the bending moment along the x-axis, M_z is the bending moment along the z-axis, and T denotes the torque along the y-axis. Actions P, M_x, M_z, and T are independent of the y-coordinate, and they lead to displacements that depend on coordinate y in an explicit manner.

3.1 Displacement Field

For this class of problems, the most general form of the displacement field (see page 104 of Ref. 46) is

$$\begin{aligned} u(x,y,z) &= -1/2\,Ay^2 + \theta yz + U(x,z) + u' \\ v(x,y,z) &= y(Ax + Bz + C) + V(x,z) + v' \\ w(x,y,z) &= -1/2\,By^2 - \theta xy + W(x,z) + w' \end{aligned} \tag{3-1}$$

where A and B are the negative bending curvatures in the x-y and y-z planes respectively, C is the normal strain ε_y at $x = 0$ and $z = 0$, and the product θy is the rotation of a cross section about the y-axis. A, B, C, and θ are all constant over the domain and are the prescribed out-of-plane deformation quantities. Quantities A, B, C, and θ can be related through Hooke's law and static equivalence to actions P, M_x, M_z, and T of Fig. 3.1. The functions U, V and W are the unknown portions of the displacements which are functions only of x and z, and u', v', and w' are the rigid body displacements composed of three translation and three rotation modes.

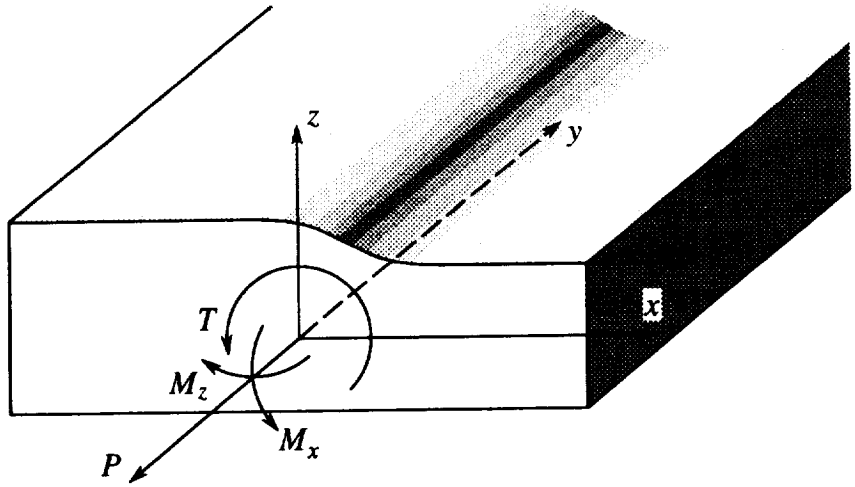

Fig. 3.1 Generalized plane deformation.

It is worth noting that this displacement field does not include all possible out-of-plane deformations (those whose displacements involve dependence on y) which have strains that are independent of y. For instance, a uniform state of simple shear that would correspond to a term consisting of the product of a constant times y in either the u or w displacement is not included. Because the tractions on the edges parallel to the y axis are arbitrary at this point, such a deformation is precluded by the fact that it would produce a stress field that varies with y.

Based on the displacement field in Eqs. (3-1), the engineering strains, which appear in the first term in the volume integral of Eq. (2-7) when the summation over i and j is carried out, have the following forms:

$$
\begin{aligned}
\varepsilon_x &= u_{,x} = U_{,x} \\
\varepsilon_y &= v_{,y} = Ax + Bz + C \\
\varepsilon_z &= w_{,z} = W_{,z} \\
\gamma_{yz} &= v_{,z} + w_{,y} = V_{,z} - \theta x \\
\gamma_{xz} &= u_{,z} + w_{,x} = U_{,z} + W_{,x} \\
\gamma_{xy} &= u_{,y} + v_{,x} = V_{,x} + \theta z
\end{aligned}
\tag{3-2}
$$

Note that these representations of the strains are independent of y as required.

3.2 Assumed Stress Field

A generic layer for the generalized plane deformation model is shown in Fig. 3.2. Eq. (2-8) for this problem has the form

$$
\sigma_i(x,z) = \sigma_{ij}(x) f_j^{(i)}(x,z) \ , \quad \text{no sum on } i \tag{3-3}
$$

As outlined in Sec. 2.2.2, the in-plane stresses σ_{xx}, σ_{yy} and σ_{xy} (σ_1, σ_2 and σ_6 in contracted notation) are assumed to have linear dependence on z. Based on the y-independent form of the elasticity equations of equilibrium without body forces,

$$
\begin{aligned}
\sigma_{xx,x} + \sigma_{xz,z} &= 0 \\
\sigma_{xy,x} + \sigma_{yz,z} &= 0 \\
\sigma_{xz,x} + \sigma_{zz,z} &= 0
\end{aligned}
\tag{3-4}
$$

the through the thickness distribution of the remaining stress components are determined. The through-the-thickness shear stresses σ_{yz} and σ_{xz} (σ_4 and σ_5) are found to have quadratic dependence on z and the thickness normal stress σ_{zz} (σ_3) has a cubic distribution.

In their most general form, the stresses can be expressed as

$$
\begin{aligned}
\sigma_1(x,z) &= a_1(x) + b_1(x) z \\
\sigma_2(x,z) &= a_2(x) + b_2(x) z \\
\sigma_3(x,z) &= a_3(x) + b_3(x) z + c_3(x) z^2 + d_3(x) z^3 \\
\sigma_4(x,z) &= a_4(x) + b_4(x) z + c_4(x) z^2 \\
\sigma_5(x,z) &= a_5(x) + b_5(x) z + c_5(x) z^2 \\
\sigma_6(x,z) &= a_6(x) + b_6(x) z
\end{aligned}
\tag{3-5}
$$

To arrive at stress assumptions of the form given in Eq. (3-3), the conditions of Eqs. (2-9) are used in the form

$$\begin{aligned} \sigma_i(x,z_1) &= \sigma_{i1}(x) \\ \sigma_i(x,z_2) &= \sigma_{i2}(x) \end{aligned} \tag{3-6}$$

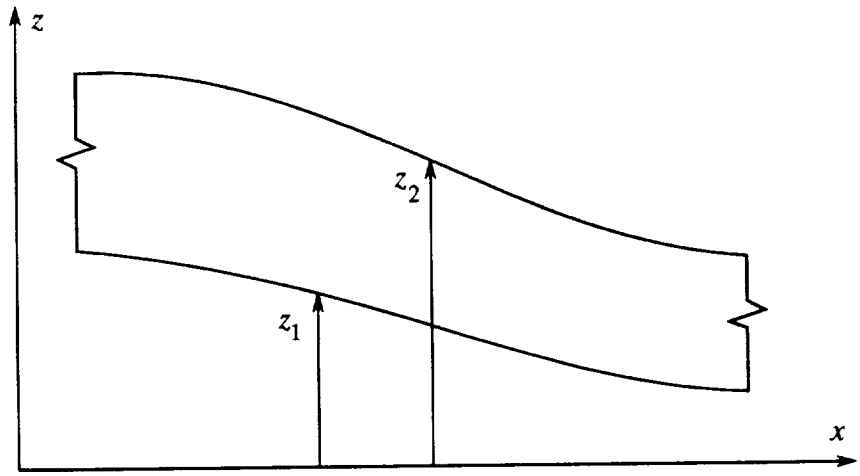

Fig. 3.2 Schematic of a typical layer.

For the in-plane stresses σ_1, σ_2 and σ_6, these conditions lead in a straightforward manner to the following expressions:

$$\begin{aligned} \sigma_1 &= \sigma_{11}\left(\frac{z_2 - z}{z_2 - z_1}\right) + \sigma_{12}\left(\frac{z - z_1}{z_2 - z_1}\right) \\ \sigma_2 &= \sigma_{21}\left(\frac{z_2 - z}{z_2 - z_1}\right) + \sigma_{22}\left(\frac{z - z_1}{z_2 - z_1}\right) \\ \sigma_6 &= \sigma_{61}\left(\frac{z_2 - z}{z_2 - z_1}\right) + \sigma_{62}\left(\frac{z - z_1}{z_2 - z_1}\right) \end{aligned} \tag{3-7}$$

The out-of-plane stresses, on the other hand, are not uniquely determined by the two conditions of Eq. (3-6). In fact, there are an infinite number of possible choices for them. A simple method for determining a form for these stresses is to eliminate two of the coefficient functions from the general form for the stresses of Eq. (3-5) using the conditions of Eq. (3-6). Using this approach, the resulting form of the assumed stresses depend on which of the coefficient functions a_i, b_i etc. are eliminated through imposing Eqs. (3-6). By eliminating a_4 and b_4 from the σ_4 expression of Eq. (3-5), the result for σ_4

is

$$\sigma_4 = \sigma_{41}\left(\frac{z_2 - z}{z_2 - z_1}\right) + \sigma_{42}\left(\frac{z - z_1}{z_2 - z_1}\right) + c_4\left(z^2 - z(z_1 + z_2) + z_1 z_2\right) \tag{3-8}$$

The other two possibilities, elimination of a_4 and c_4 or b_4 and c_4, result in quadratic polynomials in z as the shape functions multiplying σ_{41} and σ_{42}. The form given in Eq. (3-8) will be used because it contains the same linear shape functions as the in-plane stresses of Eq. (3-7). At this point, c_4 could simply be replaced by σ_{43} and Eq. (3-8) would have the desired form given in Eq. (3-3). However, that would leave σ_{43} without the dimensions of stress. In addition, the extremum value of $\left(z^2 - z(z_1 + z_2) + z_1 z_2\right)$ within the layer is $-(z_2 - z_1)^2/4$ which, for thin layers ($z_1 \approx z_2$), approaches zero. Both of these situations are avoided by replacing c_4 by $\sigma_{43}/(z_2 - z_1)^2$ which is also a function only of x. The same approach is used for σ_5, leading to

$$\begin{aligned}
\sigma_4 &= \sigma_{41}\left(\frac{z_2 - z}{z_2 - z_1}\right) + \sigma_{42}\left(\frac{z - z_1}{z_2 - z_1}\right) + \sigma_{43}\frac{\left(z^2 - z(z_1 + z_2) + z_1 z_2\right)}{(z_2 - z_1)^2} \\
\sigma_5 &= \sigma_{51}\left(\frac{z_2 - z}{z_2 - z_1}\right) + \sigma_{52}\left(\frac{z - z_1}{z_2 - z_1}\right) + \sigma_{53}\frac{\left(z^2 - z(z_1 + z_2) + z_1 z_2\right)}{(z_2 - z_1)^2}
\end{aligned} \tag{3-9}$$

The shape functions associated with σ_{43} and σ_{53} are referred to as bubble functions because they are zero at $z = z_1$ and $z = z_2$ and therefore do not contribute to the surface values of the stresses. This designation is borrowed from finite element methods where a bubble function is one that vanishes on the boundary of the element.

Using the same procedure on σ_3 that led to Eq. (3-8) gives the following expression:

$$\begin{aligned}
\sigma_3 = \sigma_{31}\left(\frac{z_2 - z}{z_2 - z_1}\right) + \sigma_{32}\left(\frac{z - z_1}{z_2 - z_1}\right) + c_3\left(z^2 - z(z_1 + z_2) + z_1 z_2\right) \\
+ d_3\left(z^3 - z\left(z_1^2 + z_1 z_2 + z_2^2\right) + z_1 z_2 (z_1 + z_2)\right)
\end{aligned} \tag{3-10}$$

Once again, this expression has the form of Eq. (3-3) by replacing c_3 by σ_{33} and d_3 by σ_{34}. However, the cubic shape function in Eq. (3-10), which is also a bubble function, has its third root at $z = -(z_1 + z_2)$. In order to separate its contribution to the distribution of σ_3 within a layer from the quadratic term as much as possible, the cubic bubble function is modified to locate its third root at $(z_1 + z_2)/2$. This change also makes the cubic bubble function orthogonal to the quadratic one within the layer, that is, the inner product of the

two over the interval $z_1 \le z \le z_2$ equals zero. The scaling factor for this modified cubic bubble function that keeps the extremum value within the layer from approaching zero for thin layers is $(z_2 - z_1)^3$. Therefore, c_3 and d_3 are given by the following:

$$c_3 = \frac{\sigma_{33}}{(z_2 - z_1)^2} - \frac{3(z_1 + z_2)\sigma_{34}}{(z_2 - z_1)^3}$$
$$d_3 = \frac{2\sigma_{34}}{(z_2 - z_1)^3} \tag{3-11}$$

The resulting expression for σ_3 is

$$\sigma_3 = \sigma_{31}\left(\frac{z_2 - z}{z_2 - z_1}\right) + \sigma_{32}\left(\frac{z - z_1}{z_2 - z_1}\right) + \sigma_{33}\frac{\left(z^2 - z(z_1 + z_2) + z_1 z_2\right)}{(z_2 - z_1)^2}$$
$$+\sigma_{34}\frac{\left(2z^3 - 3z^2(z_1 + z_2) + z(z_1^2 + 4z_1 z_2 + z_2^2) - z_1 z_2(z_1 + z_2)\right)}{(z_2 - z_1)^3} \tag{3-12}$$

Therefore, the shape functions of Eq. (3-3) are given by

$$f_1^{(1)} = f_1^{(2)} = f_1^{(3)} = f_1^{(4)} = f_1^{(5)} = f_1^{(6)} = \frac{z_2 - z}{z_2 - z_1}$$
$$f_2^{(1)} = f_2^{(2)} = f_2^{(3)} = f_2^{(4)} = f_2^{(5)} = f_2^{(6)} = \frac{z - z_1}{z_2 - z_1}$$
$$f_3^{(3)} = f_3^{(4)} = f_3^{(5)} = \frac{z^2 - z(z_1 + z_2) + z_1 z_2}{(z_2 - z_1)^2} \tag{3-13}$$
$$f_4^{(3)} = \frac{2z^3 - 3z^2(z_1 + z_2) + z(z_1^2 + 4z_1 z_2 + z_2^2) - z_1 z_2(z_1 + z_2)}{(z_2 - z_1)^3}$$

These shape functions are used to define the assumed stress field for each layer of the domain with z_1 and z_2 representing the lower and upper surfaces of a particular layer. It should be noted that the dependence of $f_j^{(i)}$ on x expressed in Eq. (3-3) is implicit through the presence of z_1 and z_2. More specific notation regarding the description of these surfaces is introduced in the following section.

3.3 Application of the Principle

The governing equations for this model are developed through the procedure outlined in Sec. 2.2.3. Taking advantage of the independence of the integrands on y in Eq. (2-7) for generalized plane deformation, integration through a unit depth in y is carried out. This simply reduces the volume integral to an area integral in the x-z plane and the surface integrals to contour integrals in the same plane. Integration with respect to z is then carried out, reducing the solution domain to one dimension. Because of the dependence of z_1 and z_2 on x, Leibnitz's theorem must be used on terms involving derivatives in x.

At this point, the displacement terms U, V and W are the only remaining unknowns in the area integrals that are functions of z. In order to complete the integration with respect to z, the following definitions for weighted integrals are made within each layer:

$$\left(\bar{g}(x),\breve{g}(x),\hat{g}(x)\right)=\int_{z_1}^{z_2}\left[h_1,h_2,h_3\right]g(x,z)\,dz \tag{3-14a}$$

where

$$\begin{aligned} h_1 &= \frac{z_2-z}{\left(z_2-z_1\right)^2} \\ h_2 &= \frac{z-z_1}{\left(z_2-z_1\right)^2} \\ h_3 &= \frac{z^2-z\left(z_1+z_2\right)+z_1z_2}{\left(z_2-z_1\right)^3} \end{aligned} \tag{3-14b}$$

and g represents a displacement component. The weighting functions h_1, h_2 and h_3 are simply the first three shape functions of Eq. (3-13) divided by the layer thickness (z_2-z_1). This scaling is done in order to retain the dimensions of length for the weighted displacements and to keep the integral of the weighting functions from approaching zero for thin layers.

The weighting functions for the displacements in Eqs. (3-14b) are different from Pagano's[44,45], which are simple powers of the thickness coordinate. This change was made to overcome problems with matrix conditioning encountered when numerically solving the governing equations for thin layers or layers located at moderately large values of z relative to the layer thickness. The reason for this change is illustrated in Fig. 3.3 which shows plots of h_1, h_2 and h_3 within a layer compared to Pagano's 1, z, and z^2. As

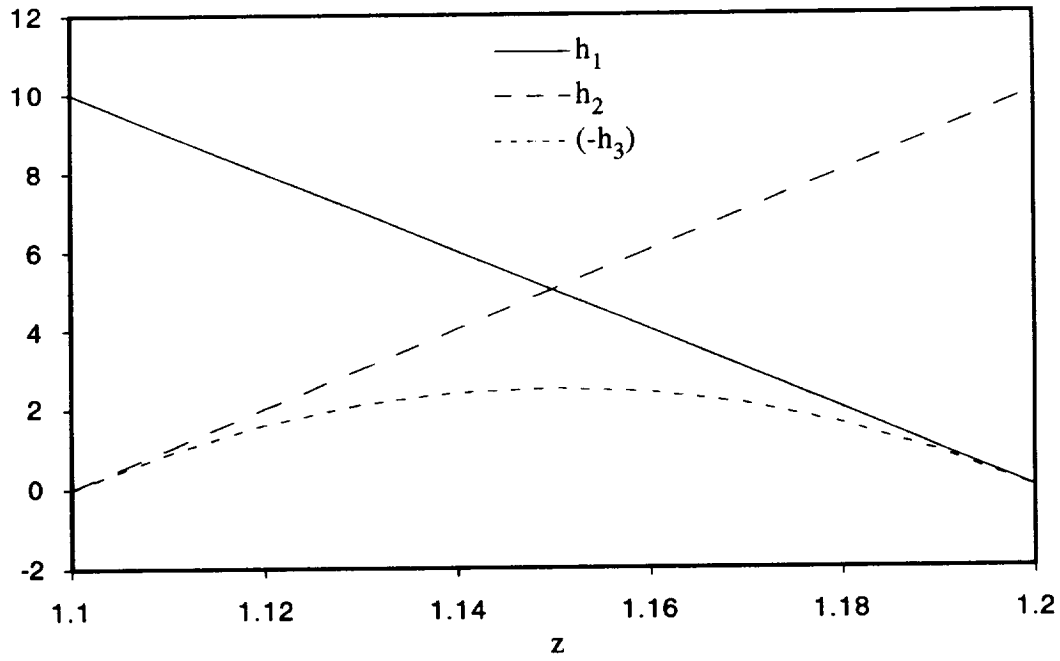

(a) Weighting functions of Eqs. (3-14b).

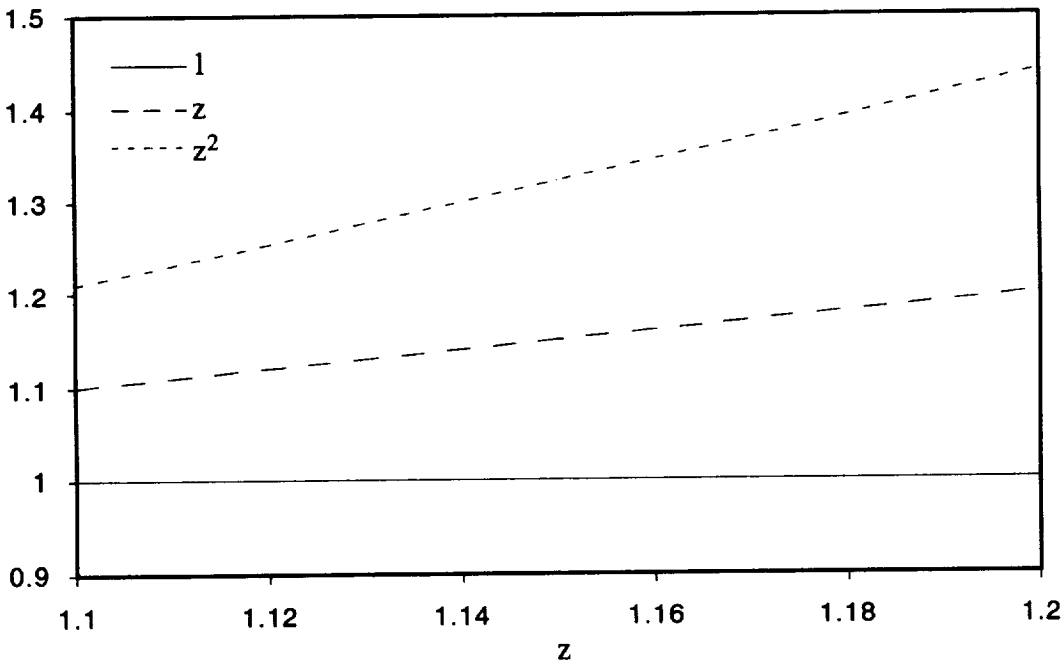

(b) Pagano's simple powers of z.

Fig. 3.3 Displacement weighting functions for z_1=1.1 and z_2=1.2.

layer thicknesses become smaller relative to their distance from the origin, of which Fig. 3.3 is not an extreme case, z^2 approaches a straight line within the layer. Therefore, a linear combination of 1 and z can closely approximate z^2 within the layer. The choice of weighting functions given in Eqs. (3-14b) clearly avoids this.

To this point, the derivation of the governing equations has centered on a single layer. However, the final model is composed of several layers and requires a slight modification of the notation as well as the definition of a few additional terms. A schematic of an assembly of N layers is shown in Fig. 3.4 along with some new notation. The z-coordinate of the kth interface at the top of layer k is designated $z_k(x)$ and the angle between the horizontal and the tangent to interface k is γ_k. From the geometry, $z_k'(x) = \tan \gamma_k(x)$, where a prime denotes an ordinary derivative with respect to x. The bottom of layer 1 and the top of layer N are part C^s of the edge curve C, and ends $x = x_1$ and $x = x_2$ $(x_2 > x_1)$ are part C^e of C $(C = C^s + C^e)$.

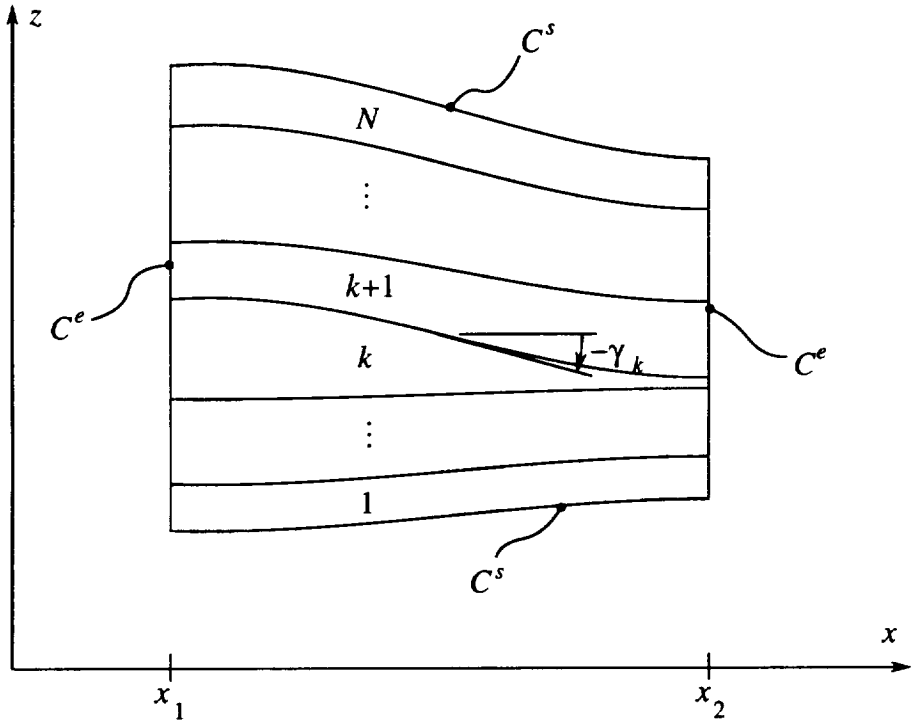

Fig. 3.4 Schematic of layer assemblage.

Layer variables are denoted by the layer number in parentheses as a superscript. Additional subscripts 1 and 2 are used to denote dependent variables evaluated at the bottom and top, respectively, of a layer; e.g., $u^{(k)}(x, z_{k-1}(x)) = u_1^{(k)}(x)$ and

$u^{(k)}(x,z_k(x)) = u_2^{(k)}(x)$. The resulting form of the variational principle for the structural approximation is

$$
\begin{aligned}
&\int_{x_1}^{x_2}\Bigg\{\sum_{k=1}^{N}\Big[\left(\mu_{iJ}+\chi_{iJ}\right)^{(k)}\delta\sigma_{iJ}^{(k)}-\left(G_1\delta\overline{U}+G_2\delta\breve{U}+G_3\delta\overline{V}+G_4\delta\breve{V}+G_5\delta\overline{W}+G_6\delta\breve{W}\right.\\
&\left.+G_7\delta\hat{W}\right)^{(k)}\Big]+\Big\langle\Big[\left(\tau_{x1}-\tilde{\tau}_{x1}\right)^{(1)}\delta u_1^{(1)}+\left(\tau_{y1}-\tilde{\tau}_{y1}\right)^{(1)}\delta v_1^{(1)}+\left(\tau_{z1}-\tilde{\tau}_{z1}\right)^{(1)}\delta w_1^{(1)}\Big]\sec\gamma_0\\
&+\Big[\left(\tau_{x2}-\tilde{\tau}_{x2}\right)^{(N)}\delta u_2^{(N)}+\left(\tau_{y2}-\tilde{\tau}_{y2}\right)^{(N)}\delta v_2^{(N)}+\left(\tau_{z2}-\tilde{\tau}_{z2}\right)^{(N)}\delta w_2^{(N)}\Big]\sec\gamma_N\Big\rangle_{C_\sigma^s}\\
&-\Big\langle\Big[\left(u_1-\tilde{u}_1\right)^{(1)}\delta\tau_{x1}^{(1)}+\left(v_1-\tilde{v}_1\right)^{(1)}\delta\tau_{y1}^{(1)}+\left(w_1-\tilde{w}_1\right)^{(1)}\delta\tau_{z1}^{(1)}\Big]\sec\gamma_0\\
&+\Big[\left(u_2-\tilde{u}_2\right)^{(N)}\delta\tau_{x2}^{(N)}+\left(v_2-\tilde{v}_2\right)^{(N)}\delta\tau_{y2}^{(N)}+\left(w_2-\tilde{w}_2\right)^{(N)}\delta\tau_{z2}^{(N)}\Big]\sec\gamma_N\Big\rangle_{C_u^s}\\
&+\sum_{k=1}^{N-1}\Big[\left(\sigma_{52}^{(k)}-\sigma_{12}^{(k)}z_k'-\sigma_{51}^{(k+1)}+\sigma_{11}^{(k+1)}z_k'\right)\delta u_2^{(k)}+\left(\sigma_{42}^{(k)}-\sigma_{62}^{(k)}z_k'-\sigma_{41}^{(k+1)}+\sigma_{61}^{(k+1)}z_k'\right)\delta v_2^{(k)}\\
&+\left(\sigma_{32}^{(k)}-\sigma_{52}^{(k)}z_k'-\sigma_{31}^{(k+1)}+\sigma_{51}^{(k+1)}z_k'\right)\delta w_2^{(k)}\Big]\Bigg\}dx\\
&+\sum_{k=1}^{N}\Bigg\{\Big\langle\Big[\left(\sigma_{11}-\tilde{\sigma}_{11}\right)^{(k)}\delta\overline{U}^{(k)}+\left(\sigma_{12}-\tilde{\sigma}_{12}\right)^{(k)}\delta\breve{U}^{(k)}+\left(\sigma_{61}-\tilde{\sigma}_{61}\right)^{(k)}\delta\overline{V}^{(k)}\\
&+\left(\sigma_{62}-\tilde{\sigma}_{62}\right)^{(k)}\delta\breve{V}^{(k)}+\left(\sigma_{51}-\tilde{\sigma}_{51}\right)^{(k)}\delta\overline{W}^{(k)}+\left(\sigma_{52}-\tilde{\sigma}_{52}\right)^{(k)}\delta\breve{W}^{(k)}\\
&+\left(\sigma_{53}-\tilde{\sigma}_{53}\right)^{(k)}\delta\hat{W}^{(k)}\Big]\left(z_k-z_{k-1}\right)\Big\rangle_{C_\sigma^e}-\Big\langle\Big[\left(\overline{U}-\tilde{\overline{U}}\right)^{(k)}\delta\sigma_{11}^{(k)}+\left(\breve{U}-\tilde{\breve{U}}\right)^{(k)}\delta\sigma_{12}^{(k)}\\
&+\left(\overline{V}-\tilde{\overline{V}}\right)^{(k)}\delta\sigma_{61}^{(k)}+\left(\breve{V}-\tilde{\breve{V}}\right)^{(k)}\delta\sigma_{62}^{(k)}+\left(\overline{W}-\tilde{\overline{W}}\right)^{(k)}\delta\sigma_{51}^{(k)}+\left(\breve{W}-\tilde{\breve{W}}\right)^{(k)}\delta\sigma_{52}^{(k)}\\
&+\left(\hat{W}-\tilde{\hat{W}}\right)^{(k)}\delta\sigma_{53}^{(k)}\Big]\left(z_k-z_{k-1}\right)\Big\rangle_{C_u^e}\Bigg\}_{x_1}^{x_2}=0
\end{aligned}
\tag{3-15}
$$

Before describing the contents of Eq. (3-15), some comments on the terminology is needed. In the form presented here, the principle does not provide all of the Euler equations because of interdependence among some of the varied quantities. In the context of the variational principle, the word "term" will refer to quantities that may require additional consideration in that regard. The word "equation" will be reserved for the Euler equations, that is those associated with independent variations.

The integral on x from x_1 to x_2 in Eq. (3-15) contains compatibility terms associated

with the sixteen variations $\delta\sigma_{ij}$, equilibrium equations associated with the seven variations in weighted displacements, traction or displacement prescribed terms on C^s, and internal interface condition equations in which Cauchy's formula was used for the surface tractions. The remaining terms are boundary terms evaluated on C^e of C.

The compatibility terms in the variational principle of Eq. (3-15) contain the quantities μ_{ij}, which in turn contain displacements evaluated at the interfaces, and χ_{ij}, which relate the weighted displacement quantities to the stresses. The nonzero μ_{ij} are

$$\begin{aligned}
\mu_{11}^{(k)} &= z'_{k-1}\, u_1^{(k)} & \mu_{12}^{(k)} &= -z'_k\, u_2^{(k)} \\
\mu_{31}^{(k)} &= -w_1^{(k)} & \mu_{32}^{(k)} &= w_2^{(k)} \\
\mu_{41}^{(k)} &= -v_1^{(k)} & \mu_{42}^{(k)} &= v_2^{(k)} \\
\mu_{51}^{(k)} &= -u_1^{(k)} + z'_{k-1} w_1^{(k)} & \mu_{52}^{(k)} &= u_2^{(k)} - z'_k w_2^{(k)} \\
\mu_{61}^{(k)} &= z'_{k-1} v_1^{(k)} & \mu_{62}^{(k)} &= -z'_k v_2^{(k)}
\end{aligned} \tag{3-16}$$

The χ_{ij} are

$$\chi_{ij}^{(k)} = \Gamma_{ij}^{(k)} + \eta_{ij}^{(k)} - \hat{S}_{ijKJ}^{(k)} \sigma_{jK}^{(k)} \tag{3-17}$$

in which weighted integrals of the compliances are defined by

$$\hat{S}_{ijKJ}^{(k)} = \int_{z_{k-1}}^{z_k} S_{ij}\, f_K^{(j)} f_J^{(i)}\, dz \tag{3-18}$$

and the out-of-plane prescribed strains are contained in the quantities

$$\begin{aligned}
\Gamma_{21}^{(k)} &= 1/6\left(z_k - z_{k-1}\right)\left[3(Ax + C) + B\left(2z_{k-1} + z_k\right)\right] \\
\Gamma_{22}^{(k)} &= 1/6\left(z_k - z_{k-1}\right)\left[3(Ax + C) + B\left(z_{k-1} + 2z_k\right)\right] \\
\Gamma_{41}^{(k)} &= -1/2\left(z_k - z_{k-1}\right)\theta x \\
\Gamma_{42}^{(k)} &= -1/2\left(z_k - z_{k-1}\right)\theta x \\
\Gamma_{43}^{(k)} &= 1/6\left(z_k - z_{k-1}\right)\theta x \\
\Gamma_{61}^{(k)} &= 1/6\left(z_k - z_{k-1}\right)\left(2z_{k-1} + z_k\right)\theta \\
\Gamma_{62}^{(k)} &= 1/6\left(z_k - z_{k-1}\right)\left(z_{k-1} + 2z_k\right)\theta
\end{aligned} \tag{3-19}$$

Finally, the nonzero strain measures in terms of the weighted displacement quantities are

$$
\begin{aligned}
\eta_{11}^{(k)} &= (z_k - z_{k-1})\overline{U}^{(k)\prime} + (z_k' - 2z_{k-1}')\overline{U}^{(k)} - z_k'\breve{U}^{(k)} \\
\eta_{12}^{(k)} &= (z_k - z_{k-1})\breve{U}^{(k)\prime} + z_{k-1}'\overline{U}^{(k)} + (2z_k' - z_{k-1}')\breve{U}^{(k)} \\
\eta_{31}^{(k)} &= \overline{W}^{(k)} + \breve{W}^{(k)} \qquad \eta_{32}^{(k)} = -\overline{W}^{(k)} - \breve{W}^{(k)} \\
\eta_{33}^{(k)} &= \overline{W}^{(k)} - \breve{W}^{(k)} \qquad \eta_{34}^{(k)} = -\overline{W}^{(k)} - \breve{W}^{(k)} - 6\hat{W}^{(k)} \\
\eta_{41}^{(k)} &= \overline{V}^{(k)} + \breve{V}^{(k)} \qquad \eta_{42}^{(k)} = -\overline{V}^{(k)} - \breve{V}^{(k)} \\
\eta_{43}^{(k)} &= \overline{V}^{(k)} - \breve{V}^{(k)} \\
\eta_{51}^{(k)} &= (z_k - z_{k-1})\overline{W}^{(k)\prime} + (z_k' - 2z_{k-1}')\overline{W}^{(k)} - z_k'\breve{W}^{(k)} + \overline{U}^{(k)} + \breve{U}^{(k)} \\
\eta_{52}^{(k)} &= (z_k - z_{k-1})\breve{W}^{(k)\prime} + z_{k-1}'\overline{W}^{(k)} + (2z_k' - z_{k-1}')\breve{W}^{(k)} - \overline{U}^{(k)} - \breve{U}^{(k)} \\
\eta_{53}^{(k)} &= (z_k - z_{k-1})\hat{W}^{(k)\prime} - z_{k-1}'\overline{W}^{(k)} + z_k'\breve{W}^{(k)} + 3(z_k' - z_{k-1}')\hat{W}^{(k)} + \overline{U}^{(k)} - \breve{U}^{(k)} \\
\eta_{61}^{(k)} &= (z_k - z_{k-1})\overline{V}^{(k)\prime} + (z_k' - 2z_{k-1}')\overline{V}^{(k)} - z_k'\breve{V}^{(k)} \\
\eta_{62}^{(k)} &= (z_k - z_{k-1})\breve{V}^{(k)\prime} + z_{k-1}'\overline{V}^{(k)} + (2z_k' - z_{k-1}')\breve{V}^{(k)}
\end{aligned}
\tag{3-20}
$$

The equilibrium equations are simply $G_i^{(k)} = 0$ where

$$
\begin{aligned}
G_1^{(k)} &= (z_k - z_{k-1})\sigma_{11}^{(k)\prime} + z_{k-1}'(\sigma_{11}^{(k)} - \sigma_{12}^{(k)}) - \sigma_{51}^{(k)} + \sigma_{52}^{(k)} - \sigma_{53}^{(k)} \\
G_2^{(k)} &= (z_k - z_{k-1})\sigma_{12}^{(k)\prime} + z_k'(\sigma_{11}^{(k)} - \sigma_{12}^{(k)}) - \sigma_{51}^{(k)} + \sigma_{52}^{(k)} + \sigma_{53}^{(k)} \\
G_3^{(k)} &= (z_k - z_{k-1})\sigma_{61}^{(k)\prime} - \sigma_{41}^{(k)} + \sigma_{42}^{(k)} - \sigma_{43}^{(k)} + z_{k-1}'(\sigma_{61}^{(k)} - \sigma_{62}^{(k)}) \\
G_4^{(k)} &= (z_k - z_{k-1})\sigma_{62}^{(k)\prime} - \sigma_{41}^{(k)} + \sigma_{42}^{(k)} + \sigma_{43}^{(k)} + z_k'(\sigma_{61}^{(k)} - \sigma_{62}^{(k)}) \\
G_5^{(k)} &= (z_k - z_{k-1})\sigma_{51}^{(k)\prime} - \sigma_{31}^{(k)} + \sigma_{32}^{(k)} - \sigma_{33}^{(k)} + \sigma_{34}^{(k)} + z_{k-1}'(\sigma_{51}^{(k)} - \sigma_{52}^{(k)} + \sigma_{53}^{(k)}) \\
G_6^{(k)} &= (z_k - z_{k-1})\sigma_{52}^{(k)\prime} - \sigma_{31}^{(k)} + \sigma_{32}^{(k)} + \sigma_{33}^{(k)} + \sigma_{34}^{(k)} + z_k'(\sigma_{51}^{(k)} - \sigma_{52}^{(k)} - \sigma_{53}^{(k)}) \\
G_7^{(k)} &= (z_k - z_{k-1})\sigma_{53}^{(k)\prime} + 6\sigma_{34}^{(k)} - 2(z_k' - z_{k-1}')\sigma_{53}^{(k)}
\end{aligned}
\tag{3-21}
$$

3.4 Interlayer Traction and Displacement Continuity

As mentioned previously, before the Euler equations of the principle can be determined, the interdependence among the variations of the unknowns must be accounted for.

Therefore, the conditions of admissibility stated in Sec. 2.2.1 on the stresses and displacements and their variations across subvolume (layer) interfaces are now imposed. Interlayer continuity of displacements is stated as

$$\begin{aligned} u_2^{(k)} &= u_1^{(k+1)} \\ v_2^{(k)} &= v_1^{(k+1)} \\ w_2^{(k)} &= w_1^{(k+1)} \end{aligned} \tag{3-22}$$

with the same conditions on their variations, which have already been accounted for. Traction continuity at interface z_k is

$$\begin{aligned} x-\text{direction:}\quad & \left(\sigma_{52}^{(k)} - z_k'\sigma_{12}^{(k)}\right) = \left(\sigma_{51}^{(k+1)} - z_k'\sigma_{11}^{(k+1)}\right) \\ y-\text{direction:}\quad & \left(\sigma_{42}^{(k)} - z_k'\sigma_{62}^{(k)}\right) = \left(\sigma_{41}^{(k+1)} - z_k'\sigma_{61}^{(k+1)}\right) \\ z-\text{direction:}\quad & \left(\sigma_{32}^{(k)} - z_k'\sigma_{52}^{(k)}\right) = \left(\sigma_{31}^{(k+1)} - z_k'\sigma_{51}^{(k+1)}\right) \end{aligned} \tag{3-23}$$

It is assumed that the variations of the stresses satisfy traction continuity at the interfaces. Substitution of the variations of Eqs. (3-23) into the principle combines some of the compatibility terms, reducing their number by $3(N-1)$. Applying the continuity of displacements cancels the μ_{ij} terms for the internal interfaces, eliminating the internal interface displacements from the formulation. The resulting interface compatibility equations are

$$\left.\begin{aligned} &\chi_{i2}^{(k)} + \chi_{i1}^{(k+1)} = 0; \quad i = 1,3,4,5,6 \\ &\chi_{12}^{(k)} + z_k'\chi_{52}^{(k)} + \left(z_k'\right)^2\chi_{32}^{(k)} = 0 \\ &\chi_{62}^{(k)} + z_k'\chi_{42}^{(k)} = 0 \end{aligned}\right\} \qquad k = 1 \rightarrow N-1 \tag{3-24}$$

As an example of the procedure used to arrive at the surface condition equations, the y-direction conditions on the upper surface are developed. The two possible cases are $v_2^{(N)} = \tilde{v}_2^{(N)}$ or $\tau_{y2}^{(N)} = \tilde{\tau}_{y2}^{(N)}$. For the first case, $\delta\sigma_{62}^{(N)}$ and $\delta\sigma_{42}^{(N)}$ are independent giving the conditions

$$\begin{aligned} v_2^{(N)} &= \tilde{v}_2^{(N)} \\ \chi_{62}^{(N)} - z_N' v_2^{(N)} &= 0 \\ \chi_{42}^{(N)} + v_2^{(N)} &= 0 \end{aligned} \tag{3-25}$$

from which $v_2^{(N)}$ can be eliminated and with minor manipulation leaves

$$\begin{aligned} \chi_{62}^{(N)} + z_N' \chi_{42}^{(N)} &= 0 \\ \chi_{42}^{(N)} + \tilde{v}_2^{(N)} &= 0 \end{aligned} \tag{3-26}$$

For the traction prescription case where $\tau_{y2}^{(N)} = \tilde{\tau}_{y2}^{(N)}$, then $\delta\sigma_{42}^{(N)} - z_N'\delta\sigma_{62}^{(N)} = 0$ $(\cos\gamma_N \neq 0)$ and the surface conditions are

$$\begin{aligned} \chi_{62}^{(N)} + z_N' \chi_{42}^{(N)} &= 0 \\ \sigma_{42}^{(N)} \cos\gamma_N - \sigma_{62}^{(N)} \sin\gamma_N &= \tilde{\tau}_{y2}^{(N)} \end{aligned} \tag{3-27}$$

The first equation of Eqs. (3-26) and (3-27) are the same and therefore hold for either case while the second changes depending on the prescribed surface quantity. A similar procedure is used to arrive at the conditions in the x and z directions, however they are complicated somewhat by coupling introduced by the appearance of $\sigma_{52}^{(N)}$ and its variation in both directions for $z_N' \neq 0$. The resulting conditions for the upper surface are

$$\begin{aligned} \chi_{12}^{(N)} + z_N' \chi_{52}^{(N)} + \left(z_N'\right)^2 \chi_{32}^{(N)} &= 0 \\ \chi_{62}^{(N)} + z_N' \chi_{42}^{(N)} &= 0 \end{aligned} \tag{3-28}$$

$$\chi_{52}^{(N)} + z_N' \chi_{32}^{(N)} + \tilde{u}_2^{(N)} = 0 \tag{3-29a}$$

or

$$\sigma_{52}^{(N)} \cos\gamma_N - \sigma_{12}^{(N)} \sin\gamma_N = \tilde{\tau}_{x2}^{(N)} \tag{3-29b}$$

$$\chi_{42}^{(N)} + \tilde{v}_2^{(N)} = 0 \tag{3-30a}$$

or

$$\sigma_{42}^{(N)} \cos\gamma_N - \sigma_{62}^{(N)} \sin\gamma_N = \tilde{\tau}_{y2}^{(N)} \tag{3-30b}$$

$$\chi_{32}^{(N)} + \tilde{w}_2^{(N)} = 0 \tag{3-31a}$$

or

$$\sigma_{32}^{(N)} \cos\gamma_N - \sigma_{52}^{(N)} \sin\gamma_N = \tilde{\tau}_{z2}^{(N)} \tag{3-31b}$$

The conditions on the lower surface are similar and are presented later.

The remaining compatibility terms are unaffected by the interdependence among the stress variables between layers. These terms lead to the layer compatibility equations which are defined for all N layers:

$$\chi_{21}^{(k)} = \chi_{22}^{(k)} = \chi_{33}^{(k)} = \chi_{34}^{(k)} = \chi_{43}^{(k)} = \chi_{53}^{(k)} = 0 \tag{3-32}$$

This completes the development of the Euler equations.

3.5 Differential-Algebraic Equations Systems

At this point, it is necessary to discuss the nature of this system of equations. While some of the equations contain derivatives of the unknowns and are therefore differential, others do not and are algebraic. Among the designations for this type of system are singular, constrained or descriptor. It will be referred to it as a system of DAEs (differential-algebraic equations) in the present work as that is most widely used in the contemporary literature on their solution.

Solution of a system of DAEs may be thought of as integration of the differential equations and determination of the integration constants through application of the boundary condition equations. For a system of first order linear ODEs in which all unknowns appear as a differential, the number of these integration constants introduced corresponds to the order of the system. However, other factors come into play when dealing with DAEs and definition of an order for such a system becomes considerably more complicated. For instance, referring back to the above mentioned system of ODEs, which may be written in matrix form as

$$\mathbf{A}\mathbf{y}' + \mathbf{B}\mathbf{y} = \mathbf{f}, \tag{3-33}$$

consider the case for which some unknowns are present only as algebraic variables. Logically, if there are more differential equations than differential unknowns, **A** will have columns of zeros associated with the algebraic unknowns and will therefore be singular. Through elementary row operations on **A**, some of the rows can be driven to all zeros leaving either an equal number or fewer of differential equations as compared to the number of unknowns appearing as differentials. Therefore, while it did not appear to be so at first, a system in which some unknowns are present only as algebraic variables is actually a system of DAEs, and the number of boundary conditions required is fewer than first appeared.

Systems that are obviously DAEs from the start also are not straightforward in determining the number of boundary conditions required. For instance, suppose the first order system of Eq. (3-33) has been manipulated to a form such that the number of rows of

A is equal to the rank of **A**. This case would appear to require as many boundary conditions as the rank of **A**. However, it is possible that the algebraic equations introduce an interdependence among the differential variables that reduces the rank of **A**. These examples are given simply to present the complexity that is involved in evaluating a system of DAEs in preparation for their solution.

3.6 Resolving the Order of the System and Number of Boundary Conditions

For the present case, that of the Euler equations resulting from the stationarity of the Hellinger-Reissner variational principle, the system of field equations and boundary conditions should be a consistent boundary value problem. However, at first inspection this is not obvious, and some manipulations of the system are necessary to arrive at a form that makes this apparent.

As presented in Eq. (3-15), the principle contains 29 variables per layer (sixteen stress quantities, seven weighted displacements and three displacements at the bottom and top of the layer) for $29N$ total. The condition that displacements be continuous between layers reduces this number by $3(N-1)$, leaving $26N+3$. There are also $26N+3$ terms in the integral composed of a varied quantity and its coefficient. Of these coefficients $14N$ are differential, composed of all $7N$ of the equilibrium and $7N$ of the compatibility terms. There are also $7N$ boundary terms at each end. Substitution of the variations of the traction reciprocity conditions and continuity of displacements between layers reduces the number of variables by another $3(N-1)$ with the elimination of internal interface displacements. At the same time, the number of terms in the principle is reduced by another $3(N-1)$ from the combination of the layer compatibility terms into the interface compatibility equations (Eqs. (3-24)). In this procedure, two differential compatibility terms combine to produce one differential compatibility equations at each interface ($N-1$ interfaces). Also, prescription of the x-direction traction on a surface combines two differential terms into one as is evident in Eq. (3-29).

Thus, after invoking interfacial continuity and surface conditions the system has $23N$ equations and unknowns with $7N$ differential equations of equilibrium, either $6N-1$, $6N$ or $6N+1$ differential equations of compatibility (depending on the surface conditions), and the remaining equations are algebraic. In this form, difficulties arise in solving the system having to do with the number of differential equations and boundary conditions. Because

the number of differential compatibility equations are reduced without a like reduction in the number of differential equilibrium equations, it is possible to have a system with an odd number of differential equations. Application of the same boundary conditions at each end, giving an even number of boundary conditions, appears to be in conflict with this. This inconsistency was remedied by Pagano by using an involved interpretation of what he calls end conditions. He arrived at these end conditions by assuming the integrand of the functional vanishes at the ends. These conditions were then incorporated into his central difference approximation using three-point forward and backward differences at the ends.

As an alternative to Pagano's interpretation, a simple manipulation of the differential equilibrium equations is used to reduce their number by the same amount as the differential compatibility. This was done by differentiating the first of Eqs. (3-23), eliminating $\sigma_{12}^{(k)\prime}$, $\sigma_{51}^{(k+1)\prime}$ and $\sigma_{11}^{(k+1)\prime}$ by substituting from $G_2^{(k)}$, $G_5^{(k+1)}$ and $G_1^{(k+1)}$ and then substituting the result into $G_6^{(k)}$. It is worth noting that the traction continuity equation that is differentiated here is the same one that combined two of the differential compatibility terms when its variation was substituted into the principle. It is also the only algebraic equation that contains only differential unknowns (i.e., they appear as differential terms in other equations). The new form of the equation is labeled $\hat{G}_6^{(k)}$ and is given by

$$\begin{aligned}\hat{G}_6^{(k)} = &-\left(z_k'\right)^2\sigma_{11}^{(k)} + \left[\left(z_k - z_{k-1}\right)z_k'' + \left(z_k'\right)^2\right]\sigma_{12}^{(k)} - \sigma_{31}^{(k)} + \sigma_{32}^{(k)} + \sigma_{33}^{(k)} + \sigma_{34}^{(k)} \\ &+2z_k'\left(\sigma_{51}^{(k)} - \sigma_{52}^{(k)} - \sigma_{53}^{(k)}\right) + \frac{\left(z_k - z_{k-1}\right)}{\left(z_{k+1} - z_k\right)}\left\{\left[\left(z_k'\right)^2 - \left(z_{k+1} - z_k\right)z_k''\right]\sigma_{11}^{(k+1)}\right. \\ &-\left(z_k'\right)^2\sigma_{12}^{(k+1)} + \sigma_{31}^{(k+1)} - \sigma_{32}^{(k+1)} + \sigma_{33}^{(k+1)} - \sigma_{34}^{(k+1)} \\ &\left.+2z_k'\left(-\sigma_{51}^{(k+1)} + \sigma_{52}^{(k+1)} - \sigma_{53}^{(k+1)}\right)\right\}\end{aligned} \tag{3-34}$$

This equation is defined for $k = 1 \rightarrow N-1$.

The x-direction surface conditions require a similar treatment in order to avoid an odd number of differential equations. For $u_2^{(N)}$ prescribed, a differential compatibility equation applies while for $\tau_{x2}^{(N)}$ prescribed, the applicable equation is algebraic:

$$\sigma_{52}^{(N)}\cos\gamma_N - \sigma_{12}^{(N)}\sin\gamma_N = \tilde{\tau}_{x2}^{(N)} \tag{3-35}$$

In a similar treatment to that used previously, Eq. (3-35) is differentiated, $\sigma_{12}^{(N)\prime}$ is eliminated by substituting from $G_2^{(N)}$ and the result is substituted into $G_6^{(N)}$. This gives an algebraic form of $G_6^{(N)}$, labeled $\overline{G}_6^{(N)}$, and given by

$$\begin{aligned}\overline{G}_6^{(N)} = &-\left(z_N'\right)^2\sigma_{11}^{(N)} + \left[\gamma_N'\left(z_N - z_{N-1}\right) + \left(z_N'\right)^2\right]\sigma_{12}^{(N)} - \sigma_{31}^{(N)} + \sigma_{32}^{(N)} + \sigma_{33}^{(N)} + \sigma_{34}^{(N)} \\ &+2z_N'\left(\sigma_{51}^{(N)} - \sigma_{53}^{(N)}\right) + z_N'\left[\gamma_N'\left(z_N - z_{N-1}\right) - 2\right]\sigma_{52}^{(N)} \\ &+\left(z_N - z_{N-1}\right)\sec\gamma_N\,\tilde{\tau}_{x2}^{(N)\prime}\end{aligned} \tag{3-36}$$

Therefore, $\overline{G}_6^{(N)} = 0$ is applicable when $\tau_{x2}^{(N)}$ is prescribed while $G_6^{(N)} = 0$ is applicable when $u_2^{(N)}$ is prescribed. Following a similar procedure for layer 1 and $G_5^{(1)}$ gives

$$\begin{aligned}\overline{G}_5^{(1)} = &\left[\gamma_0'\left(z_1 - z_0\right) - \left(z_0'\right)^2\right]\sigma_{11}^{(1)} + \left(z_0'\right)^2\sigma_{12}^{(1)} - \sigma_{31}^{(1)} + \sigma_{32}^{(1)} - \sigma_{33}^{(1)} + \sigma_{34}^{(1)} \\ &+z_0'\left[2 + \gamma_0'\left(z_1 - z_0\right)\right]\sigma_{51}^{(1)} + 2z_0'\left(-\sigma_{52}^{(1)} + \sigma_{53}^{(1)}\right) - \left(z_1 - z_0\right)\sec\gamma_0\,\tilde{\tau}_{x1}^{(1)\prime}\end{aligned} \tag{3-37}$$

3.7 Summary of Governing Equations

The governing equations are summarized below with the differential equations underscored and the algebraic equations not underscored.

3.7.1 Compatibility Equations

$$\chi_{21}^{(k)} = \chi_{22}^{(k)} = \chi_{33}^{(k)} = \chi_{34}^{(k)} = \chi_{43}^{(k)} = \underline{\chi_{53}^{(k)}} = 0 \qquad k = 1 \to N \tag{3-38}$$

$$\left.\begin{aligned}&\chi_{i2}^{(k)} + \chi_{i1}^{(k+1)} = 0; \qquad i = \underline{1},3,4,\underline{5},\underline{6} \\ &\underline{\chi_{12}^{(k)} + z_k'\chi_{52}^{(k)} + \left(z_k'\right)^2\chi_{32}^{(k)}} = 0 \\ &\underline{\chi_{62}^{(k)} + z_k'\chi_{42}^{(k)}} = 0\end{aligned}\right\} \qquad k = 1 \to N-1 \tag{3-39}$$

$$\begin{aligned}&\underline{\chi_{11}^{(1)} + z_0'\chi_{51}^{(1)} + \left(z_0'\right)^2\chi_{31}^{(1)}} = 0 \\ &\underline{\chi_{61}^{(1)} + z_0'\chi_{41}^{(1)}} = 0 \\ &\underline{\chi_{12}^{(N)} + z_N'\chi_{52}^{(N)} + \left(z_N'\right)^2\chi_{32}^{(N)}} = 0 \\ &\underline{\chi_{62}^{(N)} + z_N'\chi_{42}^{(N)}} = 0\end{aligned} \tag{3-40}$$

3.7.2 Equilibrium Equations

$$\underline{G_1^{(k)}} = \underline{G_2^{(k)}} = \underline{G_3^{(k)}} = \underline{G_4^{(k)}} = \underline{G_7^{(k)}} = 0 \qquad k = 1 \rightarrow N \qquad (3\text{-}41)$$

$$\left.\begin{aligned} \widehat{G}_6^{(k)} &= 0 \\ \underline{G_5^{(k+1)}} &= 0 \end{aligned}\right\} \qquad k = 1 \rightarrow N-1 \qquad (3\text{-}42)$$

with either, for $u_1^{(1)}$ prescribed,

$$\underline{G_5^{(1)}} = 0 \qquad (3\text{-}43a)$$

or, for $\tau_{x1}^{(1)}$ prescribed,

$$\overline{G}_5^{(1)} = 0 \qquad (3\text{-}43b)$$

as well as either, for $u_2^{(N)}$ prescribed,

$$\underline{G_6^{(N)}} = 0 \qquad (3\text{-}44a)$$

or, for $\tau_{x2}^{(N)}$ prescribed,

$$\overline{G}_6^{(N)} = 0 \qquad (3\text{-}44b)$$

3.7.3 Interlayer Traction Continuity Equations

$$\left.\begin{aligned} \left(\sigma_{52}^{(k)} - z_k'\sigma_{12}^{(k)}\right) &= \left(\sigma_{51}^{(k+1)} - z_k'\sigma_{11}^{(k+1)}\right) \\ \left(\sigma_{42}^{(k)} - z_k'\sigma_{62}^{(k)}\right) &= \left(\sigma_{41}^{(k+1)} - z_k'\sigma_{61}^{(k+1)}\right) \\ \left(\sigma_{32}^{(k)} - z_k'\sigma_{52}^{(k)}\right) &= \left(\sigma_{31}^{(k+1)} - z_k'\sigma_{51}^{(k+1)}\right) \end{aligned}\right\} \qquad k = 1 \rightarrow N-1 \qquad (3\text{-}45)$$

3.7.4 Surface Conditions

For layer 1,

$$\underline{\chi_{51}^{(1)} + z_0'\chi_{31}^{(1)} - \tilde{u}_1^{(1)}} = 0 \qquad (3\text{-}46a)$$

or

$$\sigma_{11}^{(1)}\sin\gamma_0 - \sigma_{51}^{(1)}\cos\gamma_0 = \tilde{\tau}_{x1}^{(1)} \qquad (3\text{-}46b)$$

$$\chi_{41}^{(1)} - \tilde{v}_1^{(1)} = 0 \tag{3-47a}$$

or

$$\sigma_{61}^{(1)} \sin\gamma_0 - \sigma_{41}^{(1)} \cos\gamma_0 = \tilde{\tau}_{y1}^{(1)} \tag{3-47b}$$

$$\chi_{31}^{(1)} - \tilde{w}_1^{(1)} = 0 \tag{3-48a}$$

or

$$\sigma_{51}^{(1)} \sin\gamma_0 - \sigma_{31}^{(1)} \cos\gamma_0 = \tilde{\tau}_{z1}^{(1)} \tag{3-48b}$$

and for layer N.

$$\underline{\chi_{52}^{(N)} + z'_N \chi_{32}^{(N)} + \tilde{u}_2^{(N)}} = 0 \tag{3-49a}$$

or

$$\sigma_{52}^{(N)} \cos\gamma_N - \sigma_{12}^{(N)} \sin\gamma_N = \tilde{\tau}_{x2}^{(N)} \tag{3-49b}$$

$$\chi_{42}^{(N)} + \tilde{v}_2^{(N)} = 0 \tag{3-50a}$$

or

$$\sigma_{42}^{(N)} \cos\gamma_N - \sigma_{62}^{(N)} \sin\gamma_N = \tilde{\tau}_{y2}^{(N)} \tag{3-50b}$$

$$\chi_{32}^{(N)} + \tilde{w}_2^{(N)} = 0 \tag{3-51a}$$

or

$$\sigma_{32}^{(N)} \cos\gamma_N - \sigma_{52}^{(N)} \sin\gamma_N = \tilde{\tau}_{z2}^{(N)} \tag{3-51b}$$

3.7.5 Boundary Conditions

The boundary conditions are affected by the imposition of traction continuity and the surface conditions as well. In Eq. (3-15), there are $14N$ boundary terms at the x = constant edges (C^*) of which $7N$ apply for a particular set of conditions. Substitution of the variational form of the first of Eqs. (3-23) reduces the number of displacement prescription equations by N–1. Applying the unvaried form of the same equation reduces the number of independently specifiable stress variables in the traction prescription terms by N–1. In a similar manner, for each x-direction surface traction prescribed, the number of boundary conditions is reduced by one, thus retaining a consistent number of differential equations and boundary conditions.

A further point needs to be made regarding the development of the boundary

conditions. In order to allow the three tractions to be applied independently, restrictions must be placed on the geometry of the domain at the ends. Specifically, the slope of all layer interfaces are restricted to zero at the ends. The reasoning behind this restriction is illustrated in Fig. 3.5 where it can be seen that the x-direction traction continuity equation imposes an interdependence between τ_x and τ_z if $z_k' \neq 0$.

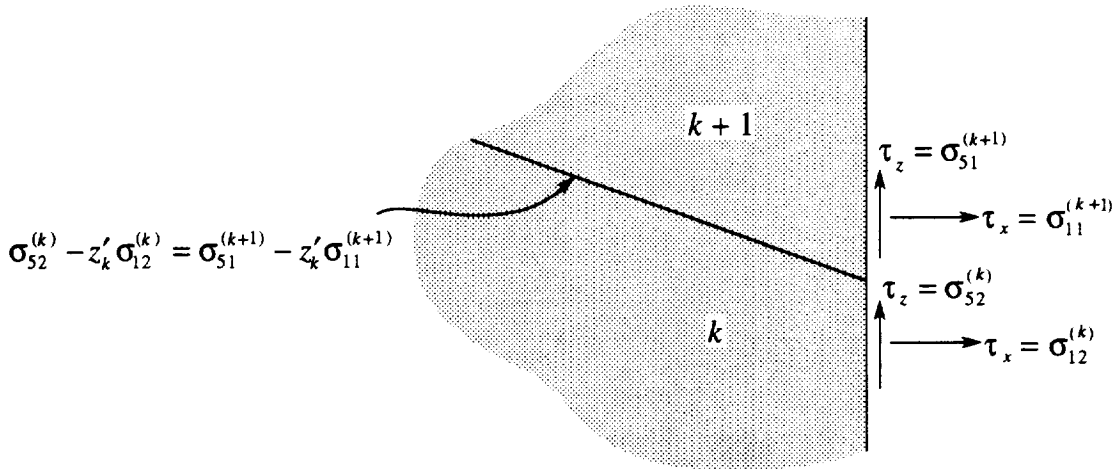

Fig. 3.5 Enlargement of layer interface region at an end illustrating interdependence between traction B.C.s.

The resulting boundary conditions are

$$\overline{U}^{(k)} = \tilde{\overline{U}}^{(k)} \quad \text{and} \quad \breve{U}^{(k)} = \tilde{\breve{U}}^{(k)} \qquad k = 1 \rightarrow N \tag{3-52a}$$

or

$$\sigma_{11}^{(k)} = \tilde{\sigma}_{11}^{(k)} \quad \text{and} \quad \sigma_{12}^{(k)} = \tilde{\sigma}_{12}^{(k)} \qquad k = 1 \rightarrow N \tag{3-52b}$$

$$\overline{V}^{(k)} = \tilde{\overline{V}}^{(k)} \quad \text{and} \quad \breve{V}^{(k)} = \tilde{\breve{V}}^{(k)} \qquad k = 1 \rightarrow N \tag{3-53a}$$

or

$$\sigma_{61}^{(k)} = \tilde{\sigma}_{61}^{(k)} \quad \text{and} \quad \sigma_{62}^{(k)} = \tilde{\sigma}_{62}^{(k)} \qquad k = 1 \rightarrow N \tag{3-53b}$$

$$\begin{cases} (z_k - z_{k-1})\breve{W}^{(k)} + (z_{k+1} - z_k)\overline{W}^{(k+1)} \\ = (z_k - z_{k-1})\tilde{\breve{W}}^{(k)} + (z_{k+1} - z_k)\tilde{\overline{W}}^{(k+1)} & k = 1 \rightarrow N-1 \\ \quad \text{and} & \\ \hat{W}^{(k)} = \tilde{\hat{W}}^{(k)} & k = 1 \rightarrow N \end{cases} \tag{3-54a}$$

or

$$\begin{cases} \sigma_{51}^{(k+1)} = \tilde{\sigma}_{51}^{(k+1)} & k = 1 \rightarrow N-1 \\ \quad \text{and} & \\ \sigma_{53}^{(k)} = \tilde{\sigma}_{53}^{(k)} & k = 1 \rightarrow N \end{cases} \tag{3-54b}$$

With, for $u_1^{(1)}$ prescribed,

$$\overline{W}^{(1)} = \tilde{\overline{W}}^{(1)} \tag{3-55a}$$

or

$$\sigma_{51}^{(1)} = \tilde{\sigma}_{51}^{(1)} \tag{3-55b}$$

and for $u_2^{(N)}$ prescribed,

$$\breve{W}^{(N)} = \tilde{\breve{W}}^{(N)} \tag{3-56a}$$

or

$$\sigma_{52}^{(N)} = \tilde{\sigma}_{52}^{(N)} \tag{3-56b}$$

3.7.6 Continuity Between Longitudinal Segments

In order to analyze a dropped-ply laminate, the formulation must also allow step changes in material properties in the longitudinal direction. To accomplish this, the domain is divided into segments, each having its own properties. The solutions for the different segments are joined through inter-segment continuity conditions. In deriving these conditions, restrictions on the geometry of the adjoining segments are imposed. Specifically, the layer boundaries must be continuous and the slope of the layer boundaries are required to be continuous. The first restriction is required to preserve consistency of definition of the weighted displacements between segments and to allow pointwise traction continuity. The second restriction is imposed because without it, σ_1, σ_3 and σ_5 would all have to be equal across both the layer and segment interfaces at the junction. The resulting conditions between segments designated *a* and *b* are

$$
\left.
\begin{aligned}
&\overline{V}_a^{(k)} = \overline{V}_b^{(k)} \\
&\breve{V}_a^{(k)} = \breve{V}_b^{(k)} \\
&\hat{W}_a^{(k)} = \hat{W}_a^{(k)} \\
&\overline{U}_a^{(k)} + z'_{k-1}\overline{W}_a^{(k)} = \overline{U}_b^{(k)} + z'_{k-1}\overline{W}_b^{(k)} \\
&\breve{U}_a^{(k)} + z'_k\breve{W}_a^{(k)} = \breve{U}_b^{(k)} + z'_k\breve{W}_b^{(k)} \\
&\sigma_{61a}^{(k)} = \sigma_{61b}^{(k)} \\
&\sigma_{62a}^{(k)} = \sigma_{62b}^{(k)} \\
&\sigma_{53a}^{(k)} = \sigma_{53b}^{(k)} \\
&\sigma_{11a}^{(k)} = \sigma_{11b}^{(k)} \\
&\sigma_{12a}^{(k)} = \sigma_{12b}^{(k)}
\end{aligned}
\right\} \qquad k = 1 \rightarrow N \qquad (3\text{-}57)
$$

$$
\left.
\begin{aligned}
&(z_{k+1} - z_k)\overline{W}_a^{(k+1)} + (z_k - z_{k-1})\breve{W}_a^{(k)} \\
&\quad = (z_{k+1} - z_k)\overline{W}_b^{(k+1)} + (z_k - z_{k-1})\breve{W}_b^{(k)} \\
&\sigma_{51a}^{(k+1)} = \sigma_{51b}^{(k+1)}
\end{aligned}
\right\} \qquad k = 1 \rightarrow N-1 \qquad (3\text{-}58)
$$

With, for $u_1^{(1)}$ prescribed,

$$\overline{W}_a^{(1)} = \overline{W}_b^{(1)} \qquad \text{and} \qquad \sigma_{51a}^{(1)} = \sigma_{51b}^{(1)} \qquad (3\text{-}59)$$

and for $u_2^{(N)}$ prescribed,

$$\breve{W}_a^{(N)} = \breve{W}_b^{(N)} \qquad \text{and} \qquad \sigma_{52a}^{(N)} = \sigma_{52b}^{(N)} \qquad (3\text{-}60)$$

3.7.7 Accounting of Variables and Equations

This completes the presentation of the equations associated with the model. The model is summarized in Table 3.1 by listing the unknowns and the equations used to solve for them. The number of first order ordinary differential equations, and the associated boundary conditions, are summarized in Table 3.2. Note that the order of the system is dependent on whether the x-direction displacements on the top and bottom external surfaces are prescribed or not prescribed.

Table 3.1 Summary of the mathematical model (N = number of mathematical layers).

Unknowns	Type	Number
$\sigma_{11},\sigma_{12},\sigma_{21},\sigma_{22},\sigma_{31},\sigma_{32},\sigma_{33},\sigma_{34},$ $\sigma_{41},\sigma_{42},\sigma_{43},\sigma_{51},\sigma_{52},\sigma_{53},\sigma_{61},\sigma_{62}$	*stress variables*	$16N$
$\overline{U},\breve{U},\overline{V},\breve{V},\overline{W},\breve{W},\hat{W}$	*weighted displacements*	$7N$
	Total	$23N$

Equations	Type	Number
(3-38)	*layer compatibility*	$6N$
(3-39)	*interface compatibility*	$7(N-1)$
(3-40)	*surface compatibility*	4
(3-41)	*layer equilibrium*	$5N$
(3-42)	*interface equilibrium*	$2(N-1)$
(3-43),(3-44)	*surface equilibrium*	2
(3-45)	*traction continuity*	$3(N-1)$
(3-46) through (3-51)	*surface conditions*	6
	Total	$23N$

Table 3.2 Summary of first order differential equations and boundary conditions (BCs). N = number of mathematical layers.

prescribed surface displacements; $x_1 \le x \le x_2$		Differential Equations		BCs at x_1 and x_2	
$u_1^{(1)}(x)$	$u_2^{(N)}(x)$	Equations	Number	Equations	Number
no	no	(3-38)	N	(3-52a) or (3-52b)	$4N$
		(3-39)	$5N-5$	(3-53a) or (3-53b)	$4N$
		(3-40)	4	(3-54a) or (3-54b)	$4N-2$
		(3-41)	$5N$		
		(3-42)	$N-1$		
		Total	$12N-2$	Total	$12N-2$
yes	no	(3-38)	N	(3-52a) or (3-52b)	$4N$
		(3-39)	$5N-5$	(3-53a) or (3-53b)	$4N$
		(3-40)	4	(3-54a) or (3-54b)	$4N-2$
		(3-41)	$5N$	(3-55a) or (3-55b)	2
		(3-42)	$N-1$		
		(3-43a)	1		
		(3-46a)	1		
		Total	$12N$	Total	$12N$
no	yes	(3-38)	N	(3-52a) or (3-52b)	$4N$
		(3-39)	$5N-5$	(3-53a) or (3-53b)	$4N$
		(3-40)	4	(3-54a) or (3-54b)	$4N-2$
		(3-41)	$5N$	(3-56a) or (3-56b)	2
		(3-42)	$N-1$		
		(3-44a)	1		
		(3-49a)	1		
		Total	$12N$	Total	$12N$
yes	yes	(3-38)	N	(3-52a) or (3-52b)	$4N$
		(3-39)	$5N-5$	(3-53a) or (3-53b)	$4N$
		(3-40)	4	(3-54a) or (3-54b)	$4N-2$
		(3-41)	$5N$	(3-55a) or (3-55b)	2
		(3-42)	$N-1$	(3-56a) or (3-56b)	2
		(3-43a) & (3-44a)	2		
		(3-46a) & (3-49a)	2		
		Total	$12N+2$	Total	$12N+2$

Chapter 4: Axisymmetric Model

The next version of the model which will be developed is for the axisymmetric response of a shell of revolution. This is a reformulation of Pagano's[45] theory for this class of problems with the incorporation of the changes applied in the generalized plane deformation model discussed in Chapter 3. In addition, a further modification was made to the development of the stress assumptions which reduces the number of dependent unknowns per layer by two from Pagano's original derivation.

The coordinates chosen for this derivation are slightly different from those used in most cylindrical coordinate systems. Specifically, the axial coordinate will be x rather than z, while the radial and circumferential coordinates will be the conventional r and θ, respectively. This change was made in order to have x as the independent variable as in the generalized plane deformation model and also to avoid confusion that may result from another z coordinate at a different orientation.

In the present class of problems, the loading, geometric and material properties, and hence stresses and strains are independent of θ. The solution domain is thus reduced to the x-r plane. The stress field will be assumed explicitly in terms of r and implicitly in terms of x with independence of θ. Therefore, curvilinear coordinates $(\alpha_1, \alpha_2, \zeta)$ used in Sec. 2.2.2 are identified as (x, θ, r) for this formulation. This model is applicable to the analysis of laminated cylinders with axially dropped plies as illustrated in Fig. 4.1.

4.1 Displacement Field

Unlike generalized plane deformation which allows for dependence of the displacements on the y coordinate, axisymmetry does not permit dependence of the

displacements on θ. In addition, there is no rigid body translation in the radial and circumferential directions. Therefore, neglecting rigid body displacements, the axisymmetric form of the displacement field is

$$\begin{aligned} u(x,\theta,r) &= U(x,r) \\ v(x,\theta,r) &= V(x,r) \\ w(x,\theta,r) &= W(x,r) \end{aligned} \tag{4-1}$$

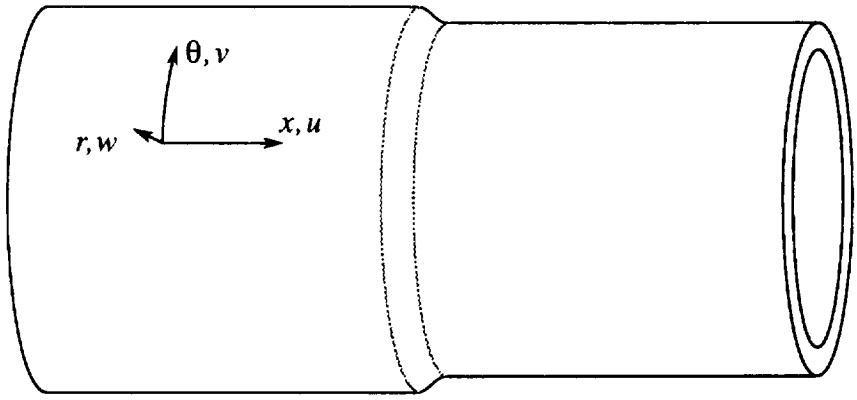

Fig. 4.1 Axial dropped-ply cylinder.

The engineering strain field for the displacements given by Eqs. (4-1) has the following form:

$$\begin{aligned} \varepsilon_x &= u_{,x} = U_{,x} \\ \varepsilon_\theta &= \frac{1}{r}v_{,\theta} + \frac{w}{r} = \frac{W}{r} \\ \varepsilon_r &= w_{,r} = W_{,r} \\ \gamma_{\theta r} &= v_{,r} - \frac{v}{r} + \frac{1}{r}w_{,\theta} = V_{,r} - \frac{V}{r} \\ \gamma_{xr} &= u_{,r} + w_{,x} = U_{,r} + W_{,x} \\ \gamma_{x\theta} &= \frac{1}{r}u_{,\theta} + v_{,x} = V_{,x} \end{aligned} \tag{4-2}$$

4.2 Assumed Stress Field

A generic layer for the axisymmetric model is shown in Fig. 4.2. The assumed stress field within such a layer for this model is taken in the form

$$\sigma_i(x,r) = \sigma_{ij}(x) f_j^{(i)}(x,r), \quad \text{no sum on } i \tag{4-3}$$

where contracted notation is employed once again.

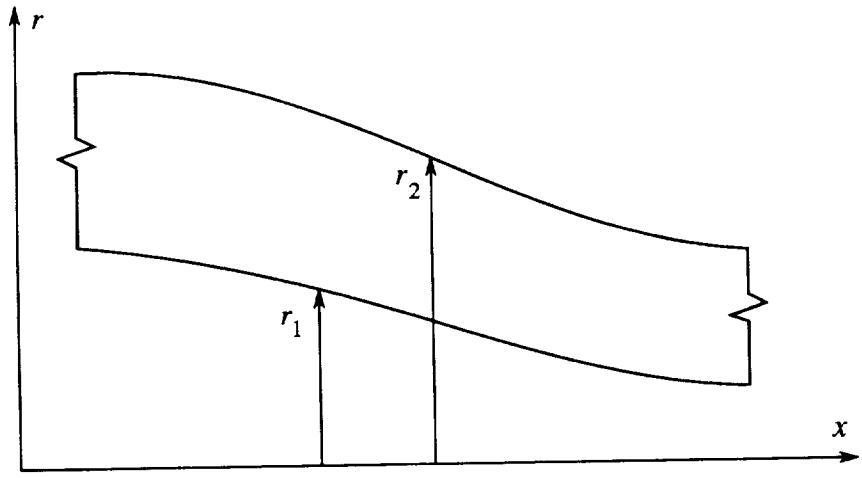

Fig. 4.2 Schematic of a typical layer.

As mentioned previously, the stress assumptions for this model were changed from those used by Pagano. These changes include those utilized in the generalized plane deformation model as well as an additional modification that reduces the number of dependent unknowns. Specifically, this additional change involves the assumption of the *r*-surface stresses σ_{xx}, $\sigma_{\theta\theta}$ and $\sigma_{x\theta}$ (σ_1, σ_2 and σ_6 in contracted notation). In both the generalized plane deformation model and Pagano's version of this model, the *r*-surface stresses were assumed to have a linear dependence on the thickness coordinate within each layer. This approach works well for the generalized plane deformation model giving the dependences of the other stresses shown in Eqs. (3-5). These expressions for the stresses have the characteristic of containing the minimum number of coefficient functions of x introduced through integration of the equilibrium equations. By contrast, if linear distributions of the *r*-surface stresses are substituted into the axisymmetric equations of equilibrium, given by

$$\frac{1}{r}(r\sigma_{xr})_{,r} + \sigma_{xx,x} = 0$$
$$\frac{1}{r^2}(r^2\sigma_{r\theta})_{,r} + \sigma_{x\theta,x} = 0 \qquad (4\text{-}4)$$
$$\frac{1}{r}(r\sigma_{rr})_{,r} + \sigma_{xr,x} - \frac{\sigma_{\theta\theta}}{r} = 0$$

in which body force terms are neglected, the resulting expressions for the transverse stresses are

$$\sigma_{rr}(x,r) = a_3(x)\frac{1}{r} + b_3(x) + c_3(x)r + d_3(x)r^2 + e_3(x)r^3$$
$$\sigma_{\theta r}(x,r) = a_4(x)\frac{1}{r^2} + b_4(x)r + c_4(x)r^2 \qquad (4\text{-}5)$$
$$\sigma_{xr}(x,r) = a_5(x)\frac{1}{r} + b_5(x)r + c_5(x)r^2$$

Note that the expression for σ_{rr} contains five terms rather than the four terms present in the generalized plane deformation model for σ_{zz} (see σ_3 in Eqs.(3-5)).

Examination of the axisymmetric equations of equilibrium revealed that an alternative choice for the r-surface stresses would result in a form for σ_{rr} that contains only four terms. Division of the linear functions assumed for σ_{xx} and $\sigma_{x\theta}$ by r resulting in rational functions was found to achieve the desired result. This was not done with the third r-surface stress component, $\sigma_{\theta\theta}$, because the $1/r$ term would produce a logarithmic term in σ_{rr}. Summarizing the general form for the assumed stress field in contracted notation:

$$\sigma_1(x,r) = \sigma_{xx}(x,r) = a_1(x)\frac{1}{r} + b_1(x)$$
$$\sigma_2(x,r) = \sigma_{\theta\theta}(x,r) = a_2(x) + b_2(x)r$$
$$\sigma_3(x,r) = \sigma_{rr}(x,r) = a_3(x)\frac{1}{r} + b_3(x) + c_3(x)r + d_3(x)r^2$$
$$\sigma_4(x,r) = \sigma_{\theta r}(x,r) = a_4(x)\frac{1}{r^2} + b_4(x) + c_4(x)r \qquad (4\text{-}6)$$
$$\sigma_5(x,r) = \sigma_{xr}(x,r) = a_5(x)\frac{1}{r} + b_5(x) + c_5(x)r$$
$$\sigma_6(x,r) = \sigma_{x\theta}(x,r) = a_6(x)\frac{1}{r} + b_6(x)$$

Once again, the final forms of the stress assumptions given by Eq. (4-3) are arrived at

through application of the conditions on the stresses at the surfaces of the layers given by

$$\begin{aligned} \sigma_i(x,r_1) &= \sigma_{i1}(x) \\ \sigma_i(x,r_2) &= \sigma_{i2}(x) \end{aligned} \tag{4-7}$$

Also, conditions similar to those used in the derivation of the bubble functions for the generalized plane deformation model will be applied.

The r-surface stresses are uniquely determined by the conditions of Eq. (4-7) and are given by

$$\begin{aligned} \sigma_1 &= \sigma_{11}\left(\frac{r_1(r_2-r)}{r(r_2-r_1)}\right)+\sigma_{12}\left(\frac{r_2(r-r_1)}{r(r_2-r_1)}\right) \\ \sigma_2 &= \sigma_{21}\left(\frac{r_2-r}{r_2-r_1}\right)+\sigma_{22}\left(\frac{r-r_1}{r_2-r_1}\right) \\ \sigma_6 &= \sigma_{61}\left(\frac{r_1(r_2-r)}{r(r_2-r_1)}\right)+\sigma_{62}\left(\frac{r_2(r-r_1)}{r(r_2-r_1)}\right) \end{aligned} \tag{4-8}$$

The transverse shear stresses σ_4 and σ_5 are developed through elimination of the coefficients b_i and c_i, i = 4, 5, by application of Eqs. (4-7) and subsequent use of the following expressions for a_4 and a_5, which are chosen to scale and nondimensionalize the shape functions.

$$\begin{aligned} a_4 &= -\frac{r_1^2 r_2^2}{(r_2-r_1)^2}\sigma_{43} \\ a_5 &= -\frac{r_1 r_2 (r_1+r_2)}{(r_2-r_1)^2}\sigma_{53} \end{aligned} \tag{4-9}$$

This leads to the following assumed forms for σ_4 and σ_5.

$$\begin{aligned} \sigma_4 &= \sigma_{41}\left(\frac{r_2-r}{r_2-r_1}\right)+\sigma_{42}\left(\frac{r-r_1}{r_2-r_1}\right)+\sigma_{43}\left(\frac{-r^3(r_1+r_2)+r^2\left(r_1^2+r_1r_2+r_2^2\right)-r_1^2r_2^2}{r^2(r_2-r_1)^2}\right) \\ \sigma_5 &= \sigma_{51}\left(\frac{r_2-r}{r_2-r_1}\right)+\sigma_{52}\left(\frac{r-r_1}{r_2-r_1}\right)+\sigma_{53}\left(\frac{-(r_1+r_2)\left[r^2-r(r_1+r_2)+r_1r_2\right]}{r(r_2-r_1)^2}\right) \end{aligned} \tag{4-10}$$

The development of the assumption for σ_3 is obtained in a different manner for the axisymmetric model than for the generalized plane deformation model. Instead of eliminating a couple of the coefficient functions through application of Eqs. (4-7), a desired

form for the stress assumption will be chosen and verified as having the form of σ_3 in Eq. (4-6) through the definition of all four of the coefficient functions. This change was made because the second bubble function obtained using the previous approach did not have all three of its zeros in the range $r_1 \le r \le r_2$ as is desirable to accentuate the difference in its contribution to the stress distribution from the first bubble function.

The first two shape functions will simply be the familiar linear functions used in σ_2. The first of the two bubble functions is a scaled rational function arrived at by dividing the quadratic that passes through zero at r_1 and r_2 by r. The second bubble function is a scaled rational function composed of the cubic that has zeros at r_1, $(r_1+r_2)/2$, and r_2, divided by r. In each case, the scaling factor is chosen such that the peak value of the bubble function within the layer does not vary with r_1 and r_2. This desired form for σ_3 results from the following definitions for the coefficient functions:

$$\begin{aligned}
a_3 &= -\frac{r_1 r_2 (r_1 + r_2)}{(r_2 - r_1)^2}\sigma_{33} - \frac{r_1 r_2 (r_1 + r_2)^2}{(r_2 - r_1)^3}\sigma_{34} \\
b_3 &= \frac{r_2\sigma_{31} - r_1\sigma_{32}}{(r_2 - r_1)} + \frac{(r_1 + r_2)^2}{(r_2 - r_1)^2}\sigma_{33} + \frac{(r_1 + r_2)\left(r_1^2 + r_1 r_2 + r_2^2\right)}{(r_2 - r_1)^3}\sigma_{34} \\
c_3 &= \frac{\sigma_{32} - \sigma_{31}}{(r_2 - r_1)} - \frac{(r_1 + r_2)}{(r_2 - r_1)^2}\sigma_{33} - \frac{3(r_1 + r_2)^2}{(r_2 - r_1)^3}\sigma_{34} \\
d_3 &= \frac{2(r_1 + r_2)}{(r_2 - r_1)^3}\sigma_{34}
\end{aligned} \tag{4-11}$$

and is given by

$$\begin{aligned}
\sigma_3 = \sigma_{31}\left(\frac{r_2 - r}{r_2 - r_1}\right) + \sigma_{32}\left(\frac{r - r_1}{r_2 - r_1}\right) + \sigma_{33}\left(\frac{-(r_1 + r_2)\left[r^2 - r(r_1 + r_2) + r_1 r_2\right]}{r(r_2 - r_1)^2}\right) \\
+\sigma_{34}\left(\frac{(r_1 + r_2)\left[2r^3 - 3r^2(r_1 + r_2) + r\left(r_1^2 + r_1 r_2 + r_2^2\right) - r_1 r_2 (r_1 + r_2)\right]}{r(r_2 - r_1)^3}\right)
\end{aligned} \tag{4-12}$$

The shape functions of Eq. (4-3) are therefore given by

$$\begin{aligned}
f_1^{(1)} &= f_1^{(6)} = \frac{r_1(r_2 - r)}{r(r_2 - r_1)} \\
f_2^{(1)} &= f_2^{(6)} = \frac{r_2(r - r_1)}{r(r_2 - r_1)}
\end{aligned} \tag{4-13}$$

$$f_1^{(2)} = f_1^{(3)} = f_1^{(4)} = f_1^{(5)} = \frac{r_2 - r}{r_2 - r_1}$$

$$f_2^{(2)} = f_2^{(3)} = f_2^{(4)} = f_2^{(5)} = \frac{r - r_1}{r_2 - r_1}$$

$$f_3^{(3)} = f_3^{(5)} = -\frac{(r_1 + r_2)\left[r^2 - r(r_1 + r_2) + r_1 r_2\right]}{r(r_2 - r_1)^2} \qquad \text{(4-13) (cont.)}$$

$$f_4^{(3)} = \frac{(r_1 + r_2)\left[2r^3 - 3r^2(r_1 + r_2) + r\left(r_1^2 + r_1 r_2 + r_2^2\right) - r_1 r_2 (r_1 + r_2)\right]}{r(r_2 - r_1)^3}$$

$$f_3^{(4)} = \frac{-r^3(r_1 + r_2) + r^2\left(r_1^2 + r_1 r_2 + r_2^2\right) - r_1^2 r_2^2}{r^2(r_2 - r_1)^2}$$

While this formulation produces an increase in the number of different shape functions from four in the generalized plane deformation model to seven here, it still represents a reduction from the nine in Pagano's formulation. More significant is the reduction in the number of stress variables from seventeen in Pagano's formulation to sixteen in the present one.

4.3 Application of the Principle

Because of the independence of the integrands of Eq. (2-7) from θ, integration with respect to θ for any axisymmetric volume simply introduces a factor of 2π, which can be canceled, and reduces the volume and surface integrals to area and contour integrals in the x-r plane. Integration with respect to the thickness coordinate, r for the present model, again requires the application of Leibnitz's theorem for terms involving derivatives in x and also the definition of weighted integrals for the displacements.

The definitions of the weighted displacements for this model were chosen in a similar manner to those of the generalized plane deformation model in that they are based on the shape functions used in the stress assumptions. However, in this case, the shape functions are multiplied by r from the volume integration in cylindrical coordinates. Once again they are scaled by division by the layer thickness $(r_2 - r_1)$. Additionally, because of multiplication by r from the volume integration, they are also divided by either r_1, r_2 or $(r_1 + r_2)$, based on which of these factors simplify the particular shape function. Finally, because of the changes in the stress assumptions, the same diacritical notation for two

displacement components does not necessarily mean that they are weighted by the same function. The weighted displacements are defined by

$$\left(\overline{U},\breve{U},\overline{V},\breve{V},\overline{W},\breve{W},\hat{W}\right)=\int_{r_1}^{r_2}\left(h_1U,h_2U,h_1V,h_2V,h_3W,h_4W,h_5W\right)dr \tag{4-14a}$$

where the weighting functions are

$$\begin{aligned}
h_1 &= \frac{r_2-r}{(r_2-r_1)^2}\\
h_2 &= \frac{r-r_1}{(r_2-r_1)^2}\\
h_3 &= \frac{r(r_2-r)}{r_1(r_2-r_1)^2}\\
h_4 &= \frac{r(r-r_1)}{r_2(r_2-r_1)^2}\\
h_5 &= -\frac{\left(r^2-r(r_1+r_2)+r_1r_2\right)}{(r_2-r_1)^3}
\end{aligned} \tag{4-14b}$$

It is worth noting here that there is one fewer weighted *W*-displacement unknown than is required by Pagano's formulation. This is due to the changes in the stress assumptions which eliminate the need for an r^3 term in σ_3.

Using the same notation for denoting layers and interfaces as was used in the generalized plane deformation model with the exception that *r* replaces *z* as the thickness coordinate, the variational principle for this approximation is

$$\begin{aligned}
&\int_{x_1}^{x_2}\left\{\sum_{k=1}^{N}\left[\left(\mu_{ij}+\chi_{ij}\right)^{(k)}\delta\sigma_{ij}^{(k)}-\left(G_1\delta\overline{U}+G_2\delta\breve{U}+G_3\delta\overline{V}+G_4\delta\breve{V}+G_5\delta\overline{W}+G_6\delta\breve{W}\right.\right.\right.\\
&\left.\left.\left.+G_7\delta\hat{W}\right)^{(k)}\right]+\left\langle\left[\left(\tau_{x1}-\tilde{\tau}_{x1}\right)^{(1)}\delta u_1^{(1)}+\left(\tau_{\theta1}-\tilde{\tau}_{\theta1}\right)^{(1)}\delta v_1^{(1)}+\left(\tau_{r1}-\tilde{\tau}_{r1}\right)^{(1)}\delta w_1^{(1)}\right]r_0\sec\gamma_0\right.\right.\\
&\left.\left.+\left[\left(\tau_{x2}-\tilde{\tau}_{x2}\right)^{(N)}\delta u_2^{(N)}+\left(\tau_{\theta2}-\tilde{\tau}_{\theta2}\right)^{(N)}\delta v_2^{(N)}+\left(\tau_{r2}-\tilde{\tau}_{r2}\right)^{(N)}\delta w_2^{(N)}\right]r_N\sec\gamma_N\right\rangle_{C_\sigma^s}\right.\\
&\left.-\left\langle\left[\left(u_1-\tilde{u}_1\right)^{(1)}\delta\tau_{x1}^{(1)}+\left(v_1-\tilde{v}_1\right)^{(1)}\delta\tau_{\theta1}^{(1)}+\left(w_1-\tilde{w}_1\right)^{(1)}\delta\tau_{r1}^{(1)}\right]r_0\sec\gamma_0\right.\right.\\
&\left.\left.+\left[\left(u_2-\tilde{u}_2\right)^{(N)}\delta\tau_{x2}^{(N)}+\left(v_2-\tilde{v}_2\right)^{(N)}\delta\tau_{\theta2}^{(N)}+\left(w_2-\tilde{w}_2\right)^{(N)}\delta\tau_{r2}^{(N)}\right]r_N\sec\gamma_N\right\rangle_{C_u^s}\right.
\end{aligned} \tag{4-15}$$

$$+\sum_{k=1}^{N-1}\Big[\Big(\sigma_{52}^{(k)}-\sigma_{12}^{(k)}r_k'-\sigma_{51}^{(k+1)}+\sigma_{11}^{(k+1)}r_k'\Big)\delta u_2^{(k)}+\Big(\sigma_{42}^{(k)}-\sigma_{62}^{(k)}r_k'-\sigma_{41}^{(k+1)}+\sigma_{61}^{(k+1)}r_k'\Big)\delta v_2^{(k)}$$

$$+\Big(\sigma_{32}^{(k)}-\sigma_{52}^{(k)}r_k'-\sigma_{31}^{(k+1)}+\sigma_{51}^{(k+1)}r_k'\Big)\delta w_2^{(k)}\Big]r_k\Big\}dx$$

$$+\sum_{k=1}^{N}\Big\{\Big\langle\Big[r_{k-1}\big(\sigma_{11}-\tilde{\sigma}_{11}\big)^{(k)}\delta\overline{U}^{(k)}+r_k\big(\sigma_{12}-\tilde{\sigma}_{12}\big)^{(k)}\delta\breve{U}^{(k)}+r_{k-1}\big(\sigma_{61}-\tilde{\sigma}_{61}\big)^{(k)}\delta\overline{V}^{(k)}$$

$$+r_k\big(\sigma_{62}-\tilde{\sigma}_{62}\big)^{(k)}\delta\breve{V}^{(k)}+r_{k-1}\big(\sigma_{51}-\tilde{\sigma}_{51}\big)^{(k)}\delta\overline{W}^{(k)}+r_k\big(\sigma_{52}-\tilde{\sigma}_{52}\big)^{(k)}\delta\breve{W}^{(k)} \qquad \text{(4-15)}$$

$$+\big(r_{k-1}+r_k\big)\big(\sigma_{53}-\tilde{\sigma}_{53}\big)^{(k)}\delta\hat{W}^{(k)}\Big]\big(r_k-r_{k-1}\big)\Big\rangle_{C_\sigma^e}-\Big\langle\Big[r_{k-1}\Big(\overline{U}-\tilde{\overline{U}}\Big)^{(k)}\delta\sigma_{11}^{(k)} \qquad \text{(cont.)}$$

$$+r_k\Big(\breve{U}-\tilde{\breve{U}}\Big)^{(k)}\delta\sigma_{12}^{(k)}+r_{k-1}\Big(\overline{V}-\tilde{\overline{V}}\Big)^{(k)}\delta\sigma_{61}^{(k)}+r_k\Big(\breve{V}-\tilde{\breve{V}}\Big)^{(k)}\delta\sigma_{62}^{(k)}+r_{k-1}\Big(\overline{W}-\tilde{\overline{W}}\Big)^{(k)}\delta\sigma_{51}^{(k)}$$

$$+r_k\Big(\breve{W}-\tilde{\breve{W}}\Big)^{(k)}\delta\sigma_{52}^{(k)}+\big(r_{k-1}+r_k\big)\Big(\hat{W}-\tilde{\hat{W}}\Big)^{(k)}\delta\sigma_{53}^{(k)}\Big]\big(r_k-r_{k-1}\big)\Big\rangle_{C_u^e}\Big\}_{x_1}^{x_2}=0$$

It is worth noting that, except for the appearance of the radial location of layer interfaces multiplied by some of the terms, Eq. (4-15) is the same as Eq. (3-15) for the generalized plane deformation model. Therefore, the terms will not be described again here and the quantities appearing in the principle will be presented.

The surface displacements are contained in μ_{iJ} which are

$$\begin{aligned}
\mu_{11}^{(k)}&=r_{k-1}r_{k-1}'u_1^{(k)} & \mu_{12}^{(k)}&=-r_kr_k'u_2^{(k)}\\
\mu_{31}^{(k)}&=-r_{k-1}w_1^{(k)} & \mu_{32}^{(k)}&=r_kw_2^{(k)}\\
\mu_{41}^{(k)}&=-r_{k-1}v_1^{(k)} & \mu_{42}^{(k)}&=r_kv_2^{(k)}\\
\mu_{51}^{(k)}&=r_{k-1}\big(-u_1^{(k)}+r_{k-1}'w_1^{(k)}\big) & \mu_{52}^{(k)}&=r_k\big(u_2^{(k)}-r_k'w_2^{(k)}\big)\\
\mu_{61}^{(k)}&=r_{k-1}r_{k-1}'v_1^{(k)} & \mu_{62}^{(k)}&=-r_kr_k'v_2^{(k)}
\end{aligned} \qquad \text{(4-16)}$$

The χ_{iJ} are defined similarly to the generalized plane deformation case with the exception that the out-of-plane prescribed strain terms do not appear in the present model:

$$\chi_{iJ}^{(k)}=\eta_{iJ}^{(k)}-\hat{S}_{ijKJ}^{(k)}\sigma_{jK}^{(k)} \qquad \text{(4-17)}$$

The weighted compliances are defined by

$$\hat{S}_{ijKJ}^{(k)}=\int_{r_{k-1}}^{r_k}S_{ij}\,f_K^{(j)}f_J^{(i)}r\,dr \qquad \text{(4-18)}$$

and the strain weighted displacement quantities are

$$\eta_{11}^{(k)} = r_{k-1}(r_k - r_{k-1})\overline{U}^{(k)\prime} + r_{k-1}(r_k' - 2r_{k-1}')\overline{U}^{(k)} - r_{k-1}r_k'\breve{U}^{(k)}$$

$$\eta_{12}^{(k)} = r_k(r_k - r_{k-1})\breve{U}^{(k)\prime} + r_k r_{k-1}'\overline{U}^{(k)} + r_k(2r_k' - r_{k-1}')\breve{U}^{(k)}$$

$$\eta_{21}^{(k)} = (r_k - r_{k-1})\overline{W}^{(k)} - \left[(r_k - r_{k-1})^2 / r_{k-1}\right]\hat{W}^{(k)}$$

$$\eta_{22}^{(k)} = (r_k - r_{k-1})\breve{W}^{(k)} + \left[(r_k - r_{k-1})^2 / r_k\right]\hat{W}^{(k)}$$

$$\eta_{31}^{(k)} = (2r_{k-1} - r_k)\overline{W}^{(k)} + r_k\breve{W}^{(k)} + \left[(r_k - r_{k-1})^2 / r_{k-1}\right]\hat{W}^{(k)}$$

$$\eta_{32}^{(k)} = -r_{k-1}\overline{W}^{(k)} + (r_{k-1} - 2r_k)\breve{W}^{(k)} - \left[(r_k - r_{k-1})^2 / r_k\right]\hat{W}^{(k)}$$

$$\eta_{33}^{(k)} = -(r_{k-1} + r_k)\overline{W}^{(k)} + (r_{k-1} + r_k)\breve{W}^{(k)} + \frac{(r_{k-1} + r_k)^2(r_k - r_{k-1})}{r_{k-1}r_k}\hat{W}^{(k)}$$

$$\eta_{34}^{(k)} = -(r_{k-1} + r_k)\overline{W}^{(k)} - (r_{k-1} + r_k)\breve{W}^{(k)} + \frac{(r_{k-1} + r_k)(r_{k-1}^2 + 4r_{k-1}r_k + r_k^2)}{r_{k-1}r_k}\hat{W}^{(k)}$$

$$\eta_{41}^{(k)} = (3r_{k-1} - 2r_k)\overline{V}^{(k)} + r_k\breve{V}^{(k)} \qquad \eta_{42}^{(k)} = -r_{k-1}\overline{V}^{(k)} + (2r_{k-1} - 3r_k)\breve{V}^{(k)}$$

$$\eta_{43}^{(k)} = -(r_{k-1} + 2r_k)\overline{V}^{(k)} + (2r_{k-1} + r_k)\breve{V}^{(k)} \tag{4-19}$$

$$\eta_{51}^{(k)} = r_{k-1}(r_k - r_{k-1})\overline{W}^{(k)\prime} + (2r_{k-1} - r_k)\overline{U}^{(k)} + r_k\breve{U}^{(k)}$$
$$+\left[r_{k-1}(r_k' - 3r_{k-1}') + r_k r_{k-1}'\right]\overline{W}^{(k)} - r_k r_k'\breve{W}^{(k)}$$

$$\eta_{52}^{(k)} = r_k(r_k - r_{k-1})\breve{W}^{(k)\prime} - r_{k-1}\overline{U}^{(k)} + (r_{k-1} - 2r_k)\breve{U}^{(k)}$$
$$+r_{k-1}r_{k-1}'\overline{W}^{(k)} + \left[r_k(3r_k' - r_{k-1}') - r_{k-1}r_k'\right]\breve{W}^{(k)}$$

$$\eta_{53}^{(k)} = (r_{k-1} + r_k)\left[(r_k - r_{k-1})\hat{W}^{(k)\prime} - \overline{U}^{(k)} + \breve{U}^{(k)} + r_{k-1}'\overline{W}^{(k)} - r_k'\breve{W}^{(k)}\right]$$
$$+\frac{r_{k-1}r_k'(2r_k^2 + 3r_{k-1}r_k + r_{k-1}^2) - r_k r_{k-1}'(r_k^2 + 3r_{k-1}r_k + 2r_{k-1}^2)}{r_{k-1}r_k}\hat{W}^{(k)}$$

$$\eta_{61}^{(k)} = r_{k-1}(r_k - r_{k-1})\overline{V}^{(k)\prime} + r_{k-1}(r_k' - 2r_{k-1}')\overline{V}^{(k)} - r_{k-1}r_k'\breve{V}^{(k)}$$

$$\eta_{62}^{(k)} = r_k(r_k - r_{k-1})\breve{V}^{(k)\prime} + r_k r_{k-1}'\overline{V}^{(k)} + r_k(2r_k' - r_{k-1}')\breve{V}^{(k)}$$

The equilibrium equations are

$$
\begin{aligned}
G_1^{(k)} &= r_{k-1}(r_k - r_{k-1})\sigma_{11}^{(k)\prime} + r_k r'_{k-1}\left(\sigma_{11}^{(k)} - \sigma_{12}^{(k)}\right) + (r_k - 2r_{k-1})\sigma_{51}^{(k)} + r_{k-1}\sigma_{52}^{(k)} \\
&\quad + (r_{k-1} + r_k)\sigma_{53}^{(k)} \\
G_2^{(k)} &= r_k(r_k - r_{k-1})\sigma_{12}^{(k)\prime} + r_{k-1}r'_k\left(\sigma_{11}^{(k)} - \sigma_{12}^{(k)}\right) - r_k\sigma_{51}^{(k)} + (2r_k - r_{k-1})\sigma_{52}^{(k)} \\
&\quad - (r_{k-1} + r_k)\sigma_{53}^{(k)} \\
G_3^{(k)} &= r_{k-1}(r_k - r_{k-1})\sigma_{61}^{(k)\prime} + (2r_k - 3r_{k-1})\sigma_{41}^{(k)} + r_{k-1}\sigma_{42}^{(k)} + (r_{k-1} + 2r_k)\sigma_{43}^{(k)} \\
&\quad + r_k r'_{k-1}\left(\sigma_{61}^{(k)} - \sigma_{62}^{(k)}\right) \\
G_4^{(k)} &= r_k(r_k - r_{k-1})\sigma_{62}^{(k)\prime} - r_k\sigma_{41}^{(k)} + (3r_k - 2r_{k-1})\sigma_{42}^{(k)} - (2r_{k-1} + r_k)\sigma_{43}^{(k)} \\
&\quad + r_{k-1}r'_k\left(\sigma_{61}^{(k)} - \sigma_{62}^{(k)}\right) \\
G_5^{(k)} &= r_{k-1}(r_k - r_{k-1})\sigma_{51}^{(k)\prime} - (r_k - r_{k-1})\sigma_{21}^{(k)} + (r_k - 2r_{k-1})\sigma_{31}^{(k)} + r_{k-1}\sigma_{32}^{(k)} \\
&\quad + (r_{k-1} + r_k)\left(\sigma_{33}^{(k)} + \sigma_{34}^{(k)}\right) + r_{k-1}r'_{k-1}\left(\sigma_{51}^{(k)} - \sigma_{52}^{(k)}\right) - r'_{k-1}(r_{k-1} + r_k)\sigma_{53}^{(k)} \\
G_6^{(k)} &= r_k(r_k - r_{k-1})\sigma_{52}^{(k)\prime} - (r_k - r_{k-1})\sigma_{22}^{(k)} - r_k\sigma_{31}^{(k)} + (2r_k - r_{k-1})\sigma_{32}^{(k)} \\
&\quad - (r_{k-1} + r_k)\left(\sigma_{33}^{(k)} - \sigma_{34}^{(k)}\right) + r_k r'_k\left(\sigma_{51}^{(k)} - \sigma_{52}^{(k)}\right) + r'_k(r_{k-1} + r_k)\sigma_{53}^{(k)} \\
G_7^{(k)} &= (r_k^2 - r_{k-1}^2)\sigma_{53}^{(k)\prime} + \frac{(r_k - r_{k-1})^2}{r_{k-1}r_k}\left(r_k\sigma_{21}^{(k)} - r_{k-1}\sigma_{22}^{(k)} - r_k\sigma_{31}^{(k)} + r_{k-1}\sigma_{32}^{(k)}\right) \\
&\quad - \frac{(r_{k-1} + r_k)}{r_{k-1}r_k}\left[(r_k^2 - r_{k-1}^2)\sigma_{33}^{(k)} + (r_k^2 + 4r_k r_{k-1} + r_{k-1}^2)\sigma_{34}^{(k)}\right] \\
&\quad + \frac{r_k^2 r'_{k-1}(3r_{k-1} + r_k) - r_{k-1}^2 r'_k(r_{k-1} + 3r_k)}{r_{k-1}r_k}\sigma_{53}^{(k)}
\end{aligned}
\tag{4-20}
$$

Due to the changes made in the stress assumptions from those that Pagano used, the present axisymmetric model has the same form as the generalized plane deformation. That is, there are an equal number of terms in the variational statement and the same terms contain the same differentiated variables. Therefore, the manipulations of Sec. 3.4 are the same as those used in the present model and will not be reiterated here.

The equilibrium equations resulting from the manipulations are as follows:

$$
\begin{aligned}
\bar{G}_6^{(k)} = & -r_{k-1}\left(r_k'\right)^2\sigma_{11}^{(k)} + \left[r_k\left(r_k - r_{k-1}\right)r_k'' + r_{k-1}\left(r_k'\right)^2\right]\sigma_{12}^{(k)} - \left(r_k - r_{k-1}\right)\sigma_{22}^{(k)} \\
& - r_k\sigma_{31}^{(k)} + \left(2r_k - r_{k-1}\right)\sigma_{32}^{(k)} - \left(r_{k-1} + r_k\right)\left(\sigma_{33}^{(k)} - \sigma_{34}^{(k)}\right) \\
& + r_k'\left[2r_k\sigma_{51}^{(k)} - \left(3r_k - r_{k-1}\right)\sigma_{52}^{(k)} + 2\left(r_{k-1} + r_k\right)\sigma_{53}^{(k)}\right] \\
& + \frac{\left(r_k - r_{k-1}\right)}{\left(r_{k+1} - r_k\right)}\left\{\left[r_{k+1}\left(r_k'\right)^2 - r_k\left(r_{k+1} - r_k\right)r_k''\right]\sigma_{11}^{(k+1)}\right. \\
& - r_{k+1}\left(r_k'\right)^2\sigma_{12}^{(k+1)} + \left(r_{k+1} - r_k\right)\sigma_{21}^{(k)} - \left(r_{k+1} - 2r_k\right)\sigma_{31}^{(k+1)} \\
& - r_k\sigma_{32}^{(k+1)} - \left(r_k + r_{k+1}\right)\left(\sigma_{33}^{(k+1)} + \sigma_{34}^{(k+1)}\right) \\
& \left. + r_k'\left[\left(r_{k+1} - 3r_k\right)\sigma_{51}^{(k+1)} + 2r_k\sigma_{52}^{(k+1)} + 2\left(r_k + r_{k+1}\right)\sigma_{53}^{(k+1)}\right]\right\}
\end{aligned}
\tag{4-21}
$$

which is defined for $k = 1 \rightarrow N-1$.

$$
\begin{aligned}
\bar{G}_5^{(1)} = & \left[\gamma_0' r_0\left(r_1 - r_0\right) - r_1\left(r_0'\right)^2\right]\sigma_{11}^{(1)} + r_1\left(r_0'\right)^2\sigma_{12}^{(1)} - \left(r_1 - r_0\right)\sigma_{21}^{(1)} + \left(r_1 - 2r_0\right)\sigma_{31}^{(1)} \\
& + r_0\sigma_{32}^{(1)} + \left(r_0 + r_1\right)\left(\sigma_{33}^{(1)} + \sigma_{34}^{(1)}\right) + r_0'\left[\gamma_0' r_0\left(r_1 - r_0\right) + 3r_0 - r_1\right]\sigma_{51}^{(1)} \\
& - 2r_0'\left[r_0\sigma_{52}^{(1)} + \left(r_0 + r_1\right)\sigma_{53}^{(1)}\right] - r_0\left(r_1 - r_0\right)\sec\gamma_0\,\tilde{\tau}_{x1}^{(1)\prime}
\end{aligned}
\tag{4-22}
$$

and

$$
\begin{aligned}
\bar{G}_6^{(N)} = & -r_{N-1}\left(r_N'\right)^2\sigma_{11}^{(N)} + \left[\gamma_N' r_N\left(r_N - r_{N-1}\right) + r_{N-1}\left(r_N'\right)^2\right]\sigma_{12}^{(N)} - \left(r_N - r_{N-1}\right)\sigma_{22}^{(N)} \\
& - r_N\sigma_{31}^{(N)} + \left(2r_N - r_{N-1}\right)\sigma_{32}^{(N)} - \left(r_{N-1} + r_N\right)\left(\sigma_{33}^{(N)} - \sigma_{34}^{(N)}\right) \\
& + 2r_N'\left[r_N\sigma_{51}^{(N)} + \left(r_{N-1} + r_N\right)\sigma_{53}^{(N)}\right] + r_N'\left[\gamma_N' r_N\left(r_N - r_{N-1}\right) + r_{N-1} - 3r_N\right]\sigma_{52}^{(N)} \\
& + r_N\left(r_N - r_{N-1}\right)\sec\gamma_N\,\tilde{\tau}_{x2}^{(N)\prime}
\end{aligned}
\tag{4-23}
$$

4.4 Summary of Governing Equations

The governing equations for the axisymmetric model are summarized below. Once again, the differential equations are underscored and the algebraic equations are not.

4.4.1 Compatibility Equations

$$
\chi_{21}^{(k)} = \chi_{22}^{(k)} = \chi_{33}^{(k)} = \chi_{34}^{(k)} = \chi_{43}^{(k)} = \underline{\chi_{53}^{(k)}} = 0 \qquad\qquad k = 1 \rightarrow N \tag{4-24}
$$

$$\left.\begin{aligned} &\chi_{i2}^{(k)} + \chi_{i1}^{(k+1)} = 0; \qquad i = \underline{1},3,4,\underline{5},\underline{6} \\ &\underline{\chi_{12}^{(k)} + r_k'\chi_{52}^{(k)} + \left(r_k'\right)^2 \chi_{32}^{(k)} = 0} \\ &\underline{\chi_{62}^{(k)} + r_k'\chi_{42}^{(k)} = 0} \end{aligned}\right\} \qquad k = 1 \rightarrow N-1 \qquad (4\text{-}25)$$

$$\begin{aligned} &\underline{\chi_{11}^{(1)} + r_0'\chi_{51}^{(1)} + \left(r_0'\right)^2 \chi_{31}^{(1)} = 0} \\ &\underline{\chi_{61}^{(1)} + r_0'\chi_{41}^{(1)} = 0} \\ &\underline{\chi_{12}^{(N)} + r_N'\chi_{52}^{(N)} + \left(r_N'\right)^2 \chi_{32}^{(N)} = 0} \\ &\underline{\chi_{62}^{(N)} + r_N'\chi_{42}^{(N)} = 0} \end{aligned} \qquad (4\text{-}26)$$

4.4.2 Equilibrium Equations

$$\underline{G_1^{(k)} = G_2^{(k)} = G_3^{(k)} = G_4^{(k)} = G_7^{(k)} = 0} \qquad k = 1 \rightarrow N \qquad (4\text{-}27)$$

$$\left.\begin{aligned} &\widehat{G}_6^{(k)} = 0 \\ &\underline{G_5^{(k+1)} = 0} \end{aligned}\right\} \qquad k = 1 \rightarrow N-1 \qquad (4\text{-}28)$$

with either, for $u_1^{(1)}$ prescribed,

$$\underline{G_5^{(1)} = 0} \qquad (4\text{-}29a)$$

or, for $\tau_{x1}^{(1)}$ prescribed,

$$\overline{G}_5^{(1)} = 0 \qquad (4\text{-}29b)$$

as well as either, for $u_2^{(N)}$ prescribed,

$$\underline{G_6^{(N)} = 0} \qquad (4\text{-}30a)$$

or, for $\tau_{x2}^{(N)}$ prescribed,

$$\overline{G}_6^{(N)} = 0 \qquad (4\text{-}30b)$$

4.4.3 Interlayer Traction Continuity Equations

$$\left.\begin{aligned}
\left(\sigma_{52}^{(k)} - r_k'\sigma_{12}^{(k)}\right) &= \left(\sigma_{51}^{(k+1)} - r_k'\sigma_{11}^{(k+1)}\right) \\
\left(\sigma_{42}^{(k)} - r_k'\sigma_{62}^{(k)}\right) &= \left(\sigma_{41}^{(k+1)} - r_k'\sigma_{61}^{(k+1)}\right) \\
\left(\sigma_{32}^{(k)} - r_k'\sigma_{52}^{(k)}\right) &= \left(\sigma_{31}^{(k+1)} - r_k'\sigma_{51}^{(k+1)}\right)
\end{aligned}\right\} \quad k = 1 \rightarrow N-1 \qquad (4\text{-}31)$$

4.4.4 Surface Conditions

For layer 1,

$$\underline{\chi_{51}^{(1)} + r_0'\chi_{31}^{(1)} - \tilde{u}_1^{(1)} = 0} \qquad (4\text{-}32a)$$

or

$$\sigma_{11}^{(1)}\sin\gamma_0 - \sigma_{51}^{(1)}\cos\gamma_0 = \tilde{\tau}_{x1}^{(1)} \qquad (4\text{-}32b)$$

$$\chi_{41}^{(1)} - \tilde{v}_1^{(1)} = 0 \qquad (4\text{-}33a)$$

or

$$\sigma_{61}^{(1)}\sin\gamma_0 - \sigma_{41}^{(1)}\cos\gamma_0 = \tilde{\tau}_{\theta 1}^{(1)} \qquad (4\text{-}33b)$$

$$\chi_{31}^{(1)} - \tilde{w}_1^{(1)} = 0 \qquad (4\text{-}34a)$$

or

$$\sigma_{51}^{(1)}\sin\gamma_0 - \sigma_{31}^{(1)}\cos\gamma_0 = \tilde{\tau}_{r1}^{(1)} \qquad (4\text{-}34b)$$

and for layer N.

$$\underline{\chi_{52}^{(N)} + r_N'\chi_{32}^{(N)} + \tilde{u}_2^{(N)} = 0} \qquad (4\text{-}35a)$$

or

$$\sigma_{52}^{(N)}\cos\gamma_N - \sigma_{12}^{(N)}\sin\gamma_N = \tilde{\tau}_{x2}^{(N)} \qquad (4\text{-}35b)$$

$$\chi_{42}^{(N)} + \tilde{v}_2^{(N)} = 0 \qquad (4\text{-}36a)$$

or

$$\sigma_{42}^{(N)}\cos\gamma_N - \sigma_{62}^{(N)}\sin\gamma_N = \tilde{\tau}_{\theta 2}^{(N)} \qquad (4\text{-}36b)$$

$$\chi_{32}^{(N)} + \tilde{w}_2^{(N)} = 0 \tag{4-37a}$$

or

$$\sigma_{32}^{(N)} \cos\gamma_N - \sigma_{52}^{(N)} \sin\gamma_N = \tilde{\tau}_{r2}^{(N)} \tag{4-37b}$$

4.4.5 Boundary Conditions

The boundary conditions are derived in the same manner as for the generalized plane deformation model. The conditions on the stress variables and their variations required by the x-direction traction continuity equation reduce the number of independently specifiable boundary conditions by $2N-1$. In addition, the interface between layers is restricted to having $r' = 0$ at the ends of the domain as before in order to eliminate interdependence among the three prescribed end tractions.

The boundary conditions are

$$\overline{U}^{(k)} = \tilde{\overline{U}}^{(k)} \quad \text{and} \quad \breve{U}^{(k)} = \tilde{\breve{U}}^{(k)} \qquad k = 1 \rightarrow N \tag{4-38a}$$

or

$$\sigma_{11}^{(k)} = \tilde{\sigma}_{11}^{(k)} \quad \text{and} \quad \sigma_{12}^{(k)} = \tilde{\sigma}_{12}^{(k)} \qquad k = 1 \rightarrow N \tag{4-38b}$$

$$\overline{V}^{(k)} = \tilde{\overline{V}}^{(k)} \quad \text{and} \quad \breve{V}^{(k)} = \tilde{\breve{V}}^{(k)} \qquad k = 1 \rightarrow N \tag{4-39a}$$

or

$$\sigma_{61}^{(k)} = \tilde{\sigma}_{61}^{(k)} \quad \text{and} \quad \sigma_{62}^{(k)} = \tilde{\sigma}_{62}^{(k)} \qquad k = 1 \rightarrow N \tag{4-39b}$$

$$\begin{cases} (r_k - r_{k-1})\breve{W}^{(k)} + (r_{k+1} - r_k)\overline{W}^{(k+1)} \\ = (r_k - r_{k-1})\tilde{\breve{W}}^{(k)} + (r_{k+1} - r_k)\tilde{\overline{W}}^{(k+1)} & k = 1 \rightarrow N-1 \\ \quad \text{and} & \\ \hat{W}^{(k)} = \tilde{\hat{W}}^{(k)} & k = 1 \rightarrow N \end{cases} \tag{4-40a}$$

or

$$\begin{cases} \sigma_{51}^{(k+1)} = \tilde{\sigma}_{51}^{(k+1)} & k = 1 \rightarrow N-1 \\ \quad \text{and} & \\ \sigma_{53}^{(k)} = \tilde{\sigma}_{53}^{(k)} & k = 1 \rightarrow N \end{cases} \tag{4-40b}$$

With, for $u_1^{(1)}$ prescribed,

$$\overline{W}^{(1)} = \tilde{\overline{W}}^{(1)} \tag{4-41a}$$

or

$$\sigma_{51}^{(1)} = \tilde{\sigma}_{51}^{(1)} \tag{4-41b}$$

and for $u_2^{(N)}$ prescribed,

$$\breve{W}^{(N)} = \tilde{\breve{W}}^{(N)} \tag{4-42a}$$

or

$$\sigma_{52}^{(N)} = \tilde{\sigma}_{52}^{(N)} \tag{4-42b}$$

4.4.6 Continuity Between Longitudinal Segments

The conditions between segments of the domain also parallel those of the generalized plane deformation model. Once again, the layer boundaries and their slopes are required to be continuous. The conditions between segments a and b are

$$\left.\begin{aligned}
&\overline{V}_a^{(k)} = \overline{V}_b^{(k)} \\
&\breve{V}_a^{(k)} = \breve{V}_b^{(k)} \\
&\hat{W}_a^{(k)} = \hat{W}_b^{(k)} \\
&\overline{U}_a^{(k)} + r'_{k-1}\overline{W}_a^{(k)} = \overline{U}_b^{(k)} + r'_{k-1}\overline{W}_b^{(k)} \\
&\breve{U}_a^{(k)} + r'_k\breve{W}_a^{(k)} = \breve{U}_b^{(k)} + r'_k\breve{W}_b^{(k)} \\
&\sigma_{61a}^{(k)} = \sigma_{61b}^{(k)} \\
&\sigma_{62a}^{(k)} = \sigma_{62b}^{(k)} \\
&\sigma_{53a}^{(k)} = \sigma_{53b}^{(k)} \\
&\sigma_{11a}^{(k)} = \sigma_{11b}^{(k)} \\
&\sigma_{12a}^{(k)} = \sigma_{12b}^{(k)}
\end{aligned}\right\} \quad k = 1 \rightarrow N \tag{4-43}$$

$$\left.\begin{aligned}
&(r_{k+1} - r_k)\overline{W}_a^{(k+1)} + (r_k - r_{k-1})\breve{W}_a^{(k)} \\
&\quad = (r_{k+1} - r_k)\overline{W}_b^{(k+1)} + (r_k - r_{k-1})\breve{W}_b^{(k)} \\
&\sigma_{51a}^{(k+1)} = \sigma_{51b}^{(k+1)}
\end{aligned}\right\} \quad k = 1 \rightarrow N-1 \tag{4-44}$$

With, for $u_1^{(1)}$ prescribed,

$$\overline{W}_a^{(1)} = \overline{W}_b^{(1)} \qquad \text{and} \qquad \sigma_{51a}^{(1)} = \sigma_{51b}^{(1)} \tag{4-45}$$

and for $u_2^{(N)}$ prescribed,

$$\tilde{W}_a^{(N)} = \tilde{W}_b^{(N)} \qquad \text{and} \qquad \sigma_{52a}^{(N)} = \sigma_{52b}^{(N)} \tag{4-46}$$

This completes the presentation of the axisymmetric model.

Chapter 5: Numerical Solution and Verification of Accuracy

Application of the models presented in the previous two chapters to laminates requires the definition of the geometric and material properties and the solution of a two-point boundary value problem. This chapter presents the methods that were chosen to accomplish these tasks as well as some that were found to be less suitable. In addition, the limits of the applicability and the accuracy of these structural models are examined.

5.1 Modeling of Dropped-Ply Laminates

The cross section of a dropped-ply laminate is modeled as shown in Fig. 5.1 consistent with the developments presented in Chapters 3 and 4. Because of the relatively large number of dependent unknowns per mathematically modeled layer, efficient implementation requires minimizing the number of layers used. This is accomplished by including multiple plies (or sublaminates) in each mathematical layer and by using thicker layers to model larger groups of plies located away from the stress concentration. Therefore, a method of determining sublaminate material properties consistent with the assumed stress fields is required.

Another feature of dropped-ply laminates that must be accounted for is the material discontinuity at the end of the terminated plies. As mentioned previously, this is modeled by longitudinal segmentation of the model with different material properties in adjacent segments. The continuity conditions developed in Secs. 3.7.6 and 4.4.6 are then applied between these segments.

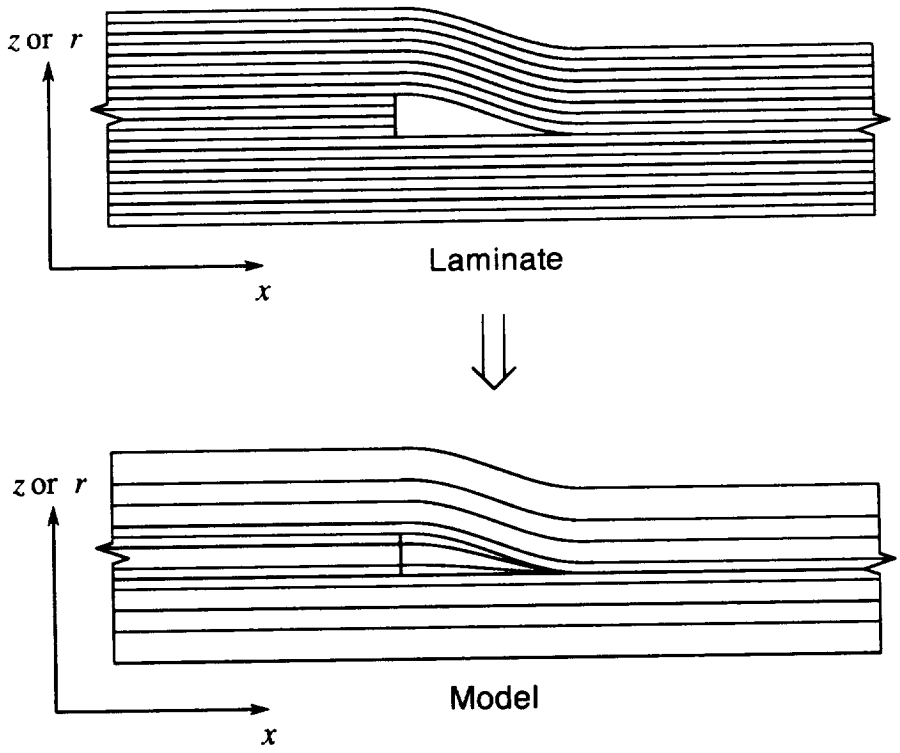

Fig. 5.1 Modeling of a dropped-ply laminate.

A final note that should be made regarding the model of the dropped-ply laminate shown in Fig. 5.1 involves the layers used to model the terminated plies. Because these models are developed for bodies with continuous mathematical layers, those layers that constitute the dropped plies cannot simply be terminated with the plies. Therefore, they are continued through the triangularly shaped resin region and also through the thin portion of the laminate as very thin layers between the lower and upper continuous sublaminates.

5.2 Incorporation of Material Properties

The material properties of the mathematical layers are introduced into the models through the weighted integrals of the compliance coefficients $\widehat{S}_{ijKJ}^{(k)}$ defined in Eqs. (3-18) and (4-18). For layers composed of more than one ply, these integrals can basically be determined in two different ways. The first is to integrate piecewise within a layer such that each individual integral is bounded by ply interfaces, and assume that the compliance coefficients are constant within each ply that comprises the layer. This allows the compliances, S_{ij}, to be moved outside of the individual integrals that sum to the layer value

of $\widehat{S}_{ijKJ}^{(k)}$.

The other option is to determine some approximation to the effective compliances for the layer and to then carry out the integration in one step through the entire layer. This approach allows for varying the complexity of the approximation, and therefore, the accuracy attained. The simplest form of this type of approach would be to determine the compliances for an "equivalent" homogeneous layer through some form of approximation. This homogenization approach was chosen to compare to the piecewise integration of the weighted integrals of the compliances.

5.2.1 Piecewise Integration

Consider first the option of breaking the integral up into a sum of ply-by-ply integrals. This appears to be a desirable option as compared to homogenization because it accounts for the location of the individual plies through the thickness of the layer due to the multiplication by the shape functions. For instance, since the first two shape functions for σ_α have their peak values at the layer surfaces, longitudinally stiffer plies being located there would be reflected in less compliant $\widehat{S}_{ijKJ}^{(k)}$ terms that represent bending. Using this approach, the integral of Eq. (3-18) would be broken up as follows:

$$\widehat{S}_{ijKJ}^{(k)} = \sum_{l=1}^{M} S_{ij}^{(l)} \int_{a_{l-1}}^{a_l} f_K^{(j)} f_J^{(i)} \, dz \tag{5-1}$$

where M is the number of plies within the layer, $S_{ij}^{(l)}$ are the compliances for layer l, and

$$\begin{aligned} a_0 &= z_{k-1} \\ a_l &= z_{k-1} + \sum_{\alpha=1}^{l} t_\alpha \qquad l = 1 \rightarrow M \end{aligned} \tag{5-2}$$

with $a_M = z_k$.

5.2.2 Determination of Homogenized Compliance Coefficients

A simple homogenization scheme was chosen to compare to the piecewise integration approach. The method is presented in Appendix A and is based on a combination of the Voigt and Reuss approximations.[47] The Voigt approximation is applied to the in-plane strains and serves to impose interply continuity of the in-plane displacements. The Reuss approximation is applied to the out-of-plane stresses and serves to impose interply traction reciprocity.

The result of this procedure is a set of effective compliance coefficients for a homogeneous layer that is, in a strain energy sense, "equivalent" to the sublaminate. Because these compliance coefficients are constant throughout the layer, the weighted integrals of the compliance coefficients for the generalized plane deformation model can be written as

$$\bar{S}_{ijKJ}^{(k)} = S_{ij}^{(k)} \int_{z_{k-1}}^{z_k} f_K^{(j)} f_J^{(i)} \, dz \tag{5-3}$$

with a similar result for the axisymmetric model.

5.2.3 Comparison of Approaches

A comparison between these two approaches can be made by a simple analysis of a uniform laminate loaded in uniaxial tension. A uniform thickness $[\pm 45/0/90]_s$ quasi-isotropic laminate under uniform extension ($\varepsilon_{xx} = 0.1\%$), with transverse distortion restrained ($\varepsilon_{yy} = 0.0$), and unrestrained to z-direction contraction, was analyzed. The thickness of the laminate is 2.54 mm and the material properties of the orthotropic layer are

$$E_{11} = 128 \text{ GPa} \quad (18.5 \text{ Msi}), \qquad E_{22} = E_{33} = 11.3 \text{ GPa} \quad (1.64 \text{ Msi})$$
$$G_{12} = G_{13} = 6.0 \text{ GPa} \quad (0.87 \text{ Msi}), \qquad G_{23} = 3.38 \text{ GPa} \quad (0.49 \text{ Msi})$$
$$\nu_{12} = \nu_{13} = 0.3, \quad \nu_{23} = 0.35$$

This problem was analyzed with the generalized plane deformation model using both approaches to determining the weighted integrals of the compliances. The results are presented in Table 5.1 along with results from analysis of the same problem using classical lamination theory.

Table 5.1 Comparison of methods of determining layer compliances.

	Piecewise Integration	Homogenization Scheme	CLT
N_x	46.8 kN/m	143.1 kN/m	143.1 kN/m
N_y	8.76 kN/m	43.2 kN/m	43.2 kN/m

These results illustrate a clear discrepancy between the two approaches in analyzing this simple problem. This difference, as well as the similarity of the results for the homogenization routine and classical lamination theory, can be traced to the way in which

these approaches model the interaction between layers in the sublaminate.

The homogenization scheme assumes uniform in-plane strains throughout in arriving at the average laminate properties. CLT, in general, does allow for non-uniform in-plane strains through the thickness. However, for this case of no bending, they are constant throughout the laminate and therefore the response would be expected to be very close to the homogenization results.

The use of piecewise integration of the weighted integrals of the compliance coefficients, on the other hand, makes no assumption regarding the in-plane strains directly. Instead, this approach assumes that the stresses have a continuous distribution through the thickness represented by the assumed stress field used in the theory. The in-plane strains are related to the stresses through the constitutive relation for each ply and are therefore, in general, discontinuous between plies as illustrated in Fig. 5.2. Thus, the piecewise integration method is more closely analogous to a Reuss-type assumption for the in-plane stresses, which for a bonded laminate, is clearly a poor approximation. The homogenization approach was therefore chosen for determining the layer material properties for the remainder of the present analysis.

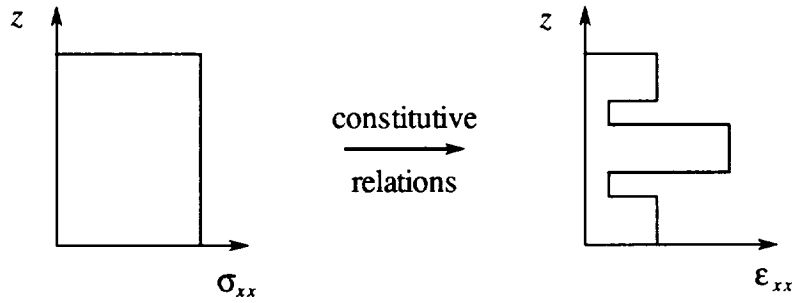

Fig. 5.2 Strain distribution associated with a uniform axial stress distribution.

5.2.4 Material Properties for Curved Sublaminate Layers

Since the theories presented in this research are able to analyze laminates with curved plies, the material properties for layers of curved sublaminates must be determined. The method used is very straightforward and is described here for the sake of completeness.

The procedure determines the sublaminate compliance coefficients through the homogenization procedure as if it were flat, then rotates these compliances about either the y or θ coordinate, depending on the model. Referring to Fig. 3.4, the angle of rotation used is an average of the angle of the lower and upper surfaces of the layer,

$-(\gamma_{k-1} + \gamma_k)/2$, which will be referred to as φ. The present application of these models does not account for the effect of variation in thickness of a ply on the material properties through changing fiber volume fraction.

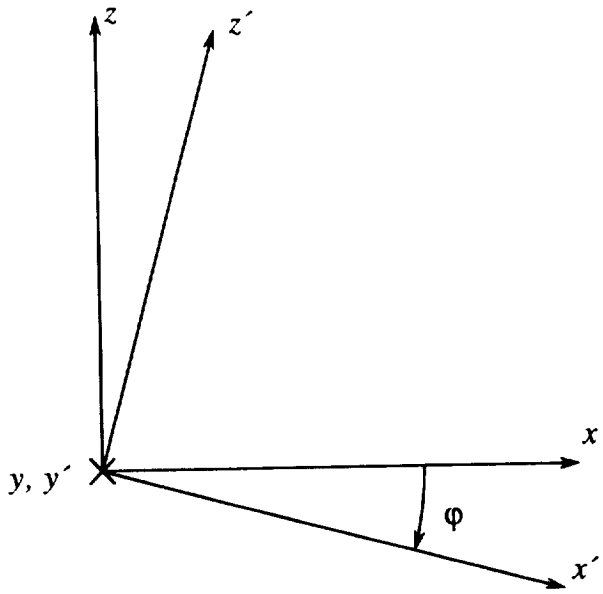

Fig. 5.3 Rotation from ply x', y', z' coordinates to structural x, y, z coordinates.

Fig. 5.3 shows the structural coordinates x, y, z and the rotation φ about y to arrive at the ply coordinates x', y', z'. For such a rotation, the stresses and strains transform according to the tensor transformation relations:

$$\sigma'_{ij} = a_{ik}a_{jl}\sigma_{kl} \quad \text{and} \quad \varepsilon'_{ij} = a_{ik}a_{jl}\varepsilon_{kl} \tag{5-4}$$

where $\boldsymbol{a}$ is the direction cosine matrix given by

$$\begin{bmatrix} \cos\varphi & 0 & -\sin\varphi \\ 0 & 1 & 0 \\ \sin\varphi & 0 & \cos\varphi \end{bmatrix} \tag{5-5}$$

Taking into account the symmetry of the stress and strain tensors, switching to engineering strains, and applying contracted notation leads to the transformation relations given by

$$\boldsymbol{\sigma}' = \mathbf{T}_\sigma \boldsymbol{\sigma}$$
$$\text{and} \tag{5-6}$$
$$\boldsymbol{\varepsilon}' = \mathbf{T}_\varepsilon \boldsymbol{\varepsilon}$$

where

$$\mathbf{T}_\sigma = \begin{bmatrix} \cos^2\varphi & 0 & \sin^2\varphi & 0 & -2\sin\varphi\cos\varphi & 0 \\ 0 & 1 & 0 & 0 & 0 & 0 \\ \sin^2\varphi & 0 & \cos^2\varphi & 0 & 2\sin\varphi\cos\varphi & 0 \\ 0 & 0 & 0 & \cos\varphi & 0 & \sin\varphi \\ \sin\varphi\cos\varphi & 0 & -\sin\varphi\cos\varphi & 0 & (\cos^2\varphi - \sin^2\varphi) & 0 \\ 0 & 0 & 0 & -\sin\varphi & 0 & \cos\varphi \end{bmatrix} \tag{5-7a}$$

and

$$\mathbf{T}_\varepsilon = \begin{bmatrix} \cos^2\varphi & 0 & \sin^2\varphi & 0 & -\sin\varphi\cos\varphi & 0 \\ 0 & 1 & 0 & 0 & 0 & 0 \\ \sin^2\varphi & 0 & \cos^2\varphi & 0 & \sin\varphi\cos\varphi & 0 \\ 0 & 0 & 0 & \cos\varphi & 0 & \sin\varphi \\ 2\sin\varphi\cos\varphi & 0 & -2\sin\varphi\cos\varphi & 0 & (\cos^2\varphi - \sin^2\varphi) & 0 \\ 0 & 0 & 0 & -\sin\varphi & 0 & \cos\varphi \end{bmatrix} \tag{5-7b}$$

Therefore, starting with the Hooke's law relation in ply coordinates,

$$\boldsymbol{\varepsilon}' = \mathbf{S}'\boldsymbol{\sigma}' \tag{5-8}$$

substitution of Eqs. (5-6) leads to the following expression for the compliances in the structural coordinate system

$$\mathbf{S} = \mathbf{T}_\varepsilon^{-1}\mathbf{S}'\mathbf{T}_\sigma \tag{5-9}$$

in which $\mathbf{T}_\varepsilon^{-1}(\varphi) = \mathbf{T}_\varepsilon(-\varphi)$.

5.3 Two-Point Boundary Value Problem

Application of these models requires the solution of a two-point boundary value problem composed of a system of first order linear DAEs and their associated boundary conditions. This section presents the problem in general form and the solution method

chosen for the present work.

In matrix form, the most general form of the system of DAEs to be solved can be written as

$$\mathbf{A}(x)\mathbf{y}'(x) + \mathbf{B}(x)\mathbf{y}(x) = \mathbf{f}(x) \tag{5-10}$$

where **A**(x) is singular due to the presence of the algebraic equations for which the associated row in **A**(x) is all zeros. The coefficient matrices **A**(x) and **B**(x) contain the geometric and material properties of the particular problem being analyzed. Due to the curved geometry at the ply drop-off, the system that the current work is concerned with has variable coefficient matrices as in Eq. (5-10). The solution vector **y** for an *N*-layer problem has the form

$$\mathbf{y}^T = \left[\mathbf{y}^{(1)^T}, \mathbf{y}^{(2)^T}, \ldots \mathbf{y}^{(N)^T}\right] \tag{5-11}$$

where each $\mathbf{y}^{(k)}$ contains 23 unknowns composed of the 16 stress variables and 7 weighted displacements,

$$\begin{aligned}\mathbf{y}^{(k)^T} = \big[&\sigma_{11}, \sigma_{12}, \sigma_{21}, \sigma_{22}, \sigma_{31}, \sigma_{32}, \sigma_{33}, \sigma_{34}, \sigma_{41}, \sigma_{42}, \sigma_{43}, \\ &\sigma_{51}, \sigma_{52}, \sigma_{53}, \sigma_{61}, \sigma_{62}, \overline{U}, \breve{U}, \overline{V}, \breve{V}, \overline{W}, \breve{W}, \hat{W}\big]^{(k)}\end{aligned} \tag{5-12}$$

It is worth noting that the **A**(x) and **B**(x) matrices have a block diagonal structure. This is due to the fact that each of the equations contain unknowns for, at most, two adjacent layers. While the present work does not take advantage of this fact, it could prove useful for improving the efficiency of the solution of the models.

5.3.1 Solution Method

The solution method chosen for this system is a one-step finite difference approximation. One-step differences were chosen over two-step schemes such as the central, forward, and backward differences used by Pagano[48,49] because of their flexibility in handling non-uniform mesh spacing as well as their lack of the need for special treatment at the boundaries for first order systems.

The application of a finite element approximation in x was also considered. This approach was developed for Pagano's original laminate theory[44] by Sandhu et al.[50] This theory applies to flat laminates and results in a system of partial differential equations in the plane of the laminate. The procedure Sandhu et al. followed was to develop a self-adjoint

version of Pagano's governing equations, which were not self-adjoint as published, from which they derived a new variational formulation. Using the Euler equations from this new variational formulation, the layer stress resultants were then solved for in terms of the displacement variables and the interfacial tractions through the constitutive/compatibility equations, thus guaranteeing their satisfaction. Finally, the displacement variables and interfacial tractions for all of the layers were approximated in terms of nodal values and interpolation functions in the 2-D domain of the laminate in an application of the finite element method. However, this solution method was very involved even for the flat laminate, constant coefficient case treated by Sandhu et al. Verification of self-adjointness of the equations for the generalized plane deformation and axisymmetric models is complicated somewhat by the fact that they have variable coefficients in contrast to the flat laminate formulation of Sandhu. If the governing equations are determined to be self-adjoint, they still are not formulated in terms of stress resultants, and because the layer interfaces are not required to be straight and parallel to the x-axis in general, five components of stress can contribute to the surface tractions as opposed to just three for the flat laminate case. This would make selection of interpolation functions for the interface stress variables such that they satisfy interlayer traction continuity much more difficult than in the flat laminate case. It is not clear what changes to Sandhu's approach would resolve these issues and therefore, such a finite element approach was not considered practical at this stage of the development of the present models.

In applying one-step finite differences to a first order system of ordinary differential equations, the approximate solution is represented by values of the dependent variables at discrete mesh points throughout the domain. Consider a finite difference mesh of ϕ points distributed along the x-axis. The location of each mesh point is x_α, $\alpha = 1,2,\ldots,\phi$, and the solution vector at x_α is $\mathbf{y}_\alpha$. Solution by finite differences simply replaces the differential equations by a set of algebraic equations in terms of the mesh values of the dependent variables. One-step finite differences are a sub-class for which each algebraic equation involves the values of the dependent variables only at two adjacent mesh points, i.e. one-step. Examples of one-step difference schemes are the trapezoidal and midpoint schemes.

In matrix form, the finite difference equations for a one-step scheme approximation to a system of p first order ODEs can be written as

$$\mathbf{Q}_\alpha \mathbf{y}_\alpha + \mathbf{R}_{\alpha+1} \mathbf{y}_{\alpha+1} = \mathbf{s}_\alpha \qquad \alpha = 1,2,\ldots,\phi - 1 \tag{5-13}$$

where $\mathbf{Q}$ and $\mathbf{R}$ are $p \times p$ matrices and $\mathbf{s}_\alpha$ is a $p \times 1$ vector, all of which are determined for

the interval from x_α to $x_{\alpha+1}$. This, along with the p boundary conditions at x_1 and x_ϕ,

$$\mathbf{D}_1\mathbf{y}_1 + \mathbf{D}_\phi\mathbf{y}_\phi = \mathbf{e} \tag{5-14}$$

where $\mathbf{D}_1$ and $\mathbf{D}_\phi$ are $p \times p$ matrices and $\mathbf{e}$ is a $p \times 1$ vector, gives $p\phi$ equations for the $p\phi$ unknown values of the dependent variables at the mesh points. The matrix equation used to solve for the approximation is

$$\begin{bmatrix} \mathbf{Q}_1 & \mathbf{R}_2 & & & & \\ & \mathbf{Q}_2 & \mathbf{R}_3 & & & \\ & & \ddots & \ddots & & \\ & & & \mathbf{Q}_{\phi-1} & \mathbf{R}_\phi & \\ \mathbf{D}_1 & & & & \mathbf{D}_\phi & \end{bmatrix} \begin{Bmatrix} \mathbf{y}_1 \\ \mathbf{y}_2 \\ \vdots \\ \mathbf{y}_{\phi-1} \\ \mathbf{y}_\phi \end{Bmatrix} = \begin{Bmatrix} \mathbf{s}_1 \\ \mathbf{s}_2 \\ \vdots \\ \mathbf{s}_{\phi-1} \\ \mathbf{e} \end{Bmatrix} \tag{5-15}$$

In contrast, solution of the same system by two-step finite differences, which are usually applied to second order differential equations, is less definite. Application of central differences to a system of first order differential equations, as done by Pagano, results in the matrix equations

$$\mathbf{P}_{\alpha-1}\mathbf{y}_{\alpha-1} + \mathbf{Q}_\alpha\mathbf{y}_\alpha + \mathbf{R}_{\alpha+1}\mathbf{y}_{\alpha+1} = \mathbf{s}_\alpha \qquad \alpha = 2,3,\ldots,\phi-1 \tag{5-16}$$

which apply at each internal mesh point for $p(\phi-2)$ equations. Boundary conditions such as those of Eq. (5-14) provide another p equations leaving a shortage of p equations for a complete system. As mentioned previously, Pagano used a combination of two-step central, forward, and backward differences with the forward and backward differences applied at the first and last mesh points respectively. For a system of ODEs, this approach would apparently leave no room for incorporation of the boundary conditions. However, for a system of DAEs, manipulations can be made that, in a sense, incorporate the boundary conditions into the conditions at the end mesh points. Pagano accomplished this by assuming that the integrand of the variational principle vanishes at the ends of the domain and derived "end conditions" which were a combination of the boundary conditions and some of the field equations. Experimentation with this approach presented by Pagano led to difficulties due to a step change in the governing equations between the end mesh points (the end conditions) and the interior points adjacent to them (field equations) for certain displacement prescribed boundary conditions. Having resolved the number of differential equations and boundary conditions as described in Sec. 3.6, the decision was made to switch to a more straightforward one-step difference scheme.

Solution of a system of linear DAEs by one-step finite differences is similar to the handling of ordinary differential equations. In fact, the differential equations of the system are replaced by difference equations in the same manner as for the ODEs. However, for a system of DAEs, there are fewer differential equations than there are unknowns. The additional equations required are simply the algebraic equations evaluated at each of the mesh points, including the end points.

For the two structural models presented here, there are $23N$ equations and unknowns. Depending upon whether the x-direction surface tractions or displacements are prescribed, there are either $12N$–2, $12N$, or $12N$+2 differential equations, the remaining algebraic (see Table 3.2). Correspondingly, there are either $6N$–1, $6N$, or $6N$+1 boundary conditions at each end of the domain. For problems that require segmentation because of discontinuous material properties, two mesh points are placed at the junction between adjacent segments, one associated with each segment. The additional $23N$ equations needed for these additional $23N$ values of the dependent unknowns are a combination of the segment continuity conditions of Eqs. (3-57) through (3-60) for the generalized plane deformation model or (4-43) through (4-46) for the axisymmetric model, and the algebraic equations applied at the additional mesh point.

5.3.2 Failure of the Trapezoidal Finite Difference Scheme

The trapezoidal finite difference scheme was attempted first on the DAE system from the generalized plane deformation model. This scheme gets its name from the fact that it can be derived by approximately integrating the differential equations from x_α to $x_{\alpha+1}$ using a single step of the trapezoidal rule for numerical integration. It has an accuracy of order 2, meaning the error is $O(h^2)$, h being the mesh spacing. However, as will be demonstrated, this scheme lacks the accuracy necessary to solve problems that contain rigid body displacements (or problems with large domains for which local displacements may be large relative to the local strains).

The implementation of the trapezoidal scheme used here is for a first order system with non-constant coefficients. For the system of Eq. (5-10), the finite difference equations for the interval from x_α to $x_{\alpha+1}$ are derived by approximating the integral of the system from x_α to $x_{\alpha+1}$ using a single trapezoid. Starting with the integration,

$$\int_{x_\alpha}^{x_{\alpha+1}} \mathbf{A}\mathbf{y}'\,dx + \int_{x_\alpha}^{x_{\alpha+1}} \mathbf{B}\mathbf{y}\,dx = \int_{x_\alpha}^{x_{\alpha+1}} \mathbf{f}\,dx \tag{5-17}$$

which can be rewritten as

$$\int_{x_\alpha}^{x_{\alpha+1}} [(\mathbf{Ay})' - \mathbf{A}'\mathbf{y}]dx + \int_{x_\alpha}^{x_{\alpha+1}} \mathbf{By}\,dx = \int_{x_\alpha}^{x_{\alpha+1}} \mathbf{f}\,dx \tag{5-18}$$

giving

$$[\mathbf{Ay}]_{x_\alpha}^{x_{\alpha+1}} + \int_{x_\alpha}^{x_{\alpha+1}} (\mathbf{B} - \mathbf{A}')\mathbf{y}\,dx = \int_{x_\alpha}^{x_{\alpha+1}} \mathbf{f}\,dx \tag{5-19}$$

Approximating the integrals by a trapezoid leads to the finite difference formula

$$\left[\frac{(\mathbf{B}_\alpha - \mathbf{A}'_\alpha)}{2} - \frac{\mathbf{A}_\alpha}{(x_{\alpha+1} - x_\alpha)}\right]\mathbf{y}_\alpha + \left[\frac{(\mathbf{B}_{\alpha+1} - \mathbf{A}'_{\alpha+1})}{2} + \frac{\mathbf{A}_{\alpha+1}}{(x_{\alpha+1} - x_\alpha)}\right]\mathbf{y}_{\alpha+1} = \frac{\mathbf{f}_\alpha + \mathbf{f}_{\alpha+1}}{2} \tag{5-20}$$

which is used in the following example.

A simple problem used to test the trapezoidal scheme is shown in Fig. 5.4. The problem consists of a rectangular plate of uniform isotropic material subjected to a rigid body translation. While this choice of a rigid body translation may seem peculiar, the reasoning behind it is to simulate the situation a large distance from a fixed point where displacements can be large relative to the strains. The plate is 1 cm thick and 10 cm long and is made of aluminum alloy with $E = 68.95$ GPa and $\nu = 0.31$. The rigid body displacement is a uniaxial translation in the z direction of $w = 0.5$ cm and is imposed at the ends. The plate is modeled by two layers separated by a curved interface, which is antisymmetric with respect to $x = 5$, as shown in Fig. 5.4. As required by the model in Chapter 3, the slopes of the surfaces and internal layer interface are zero at the ends.

The results of this test of the trapezoidal scheme as applied to the generalized plane deformation model is shown in Figs. 5.5–5.7 for three levels of mesh refinement. Fig. 5.5 shows the axial stress σ_{xx} along the internal interface at both sides of that interface for a mesh composed of 40 equally spaces points. It is clear that these results are unacceptable considering this problem should produce no stress while the erroneous values produced are a significant percentage of the tensile strength of this material, which is 90 MPa. Fig. 5.6 shows results for the same problem with an increase in the number of intervals to 80. The $O(h^2)$ accuracy of this scheme is evident in the reduction of the value of the erroneous stresses by a factor of four resulting from a halving of the mesh spacing.

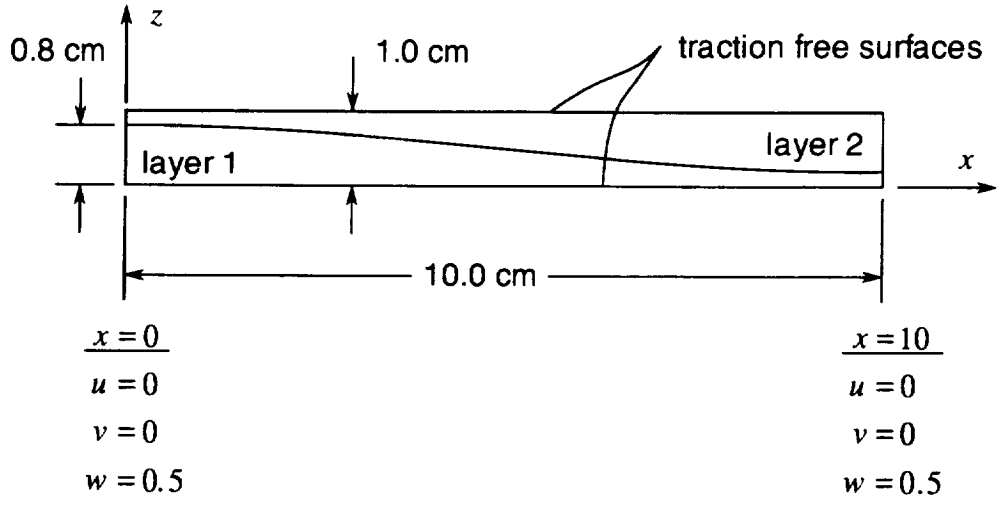

Fig. 5.4 Rigid body displacement test problem.

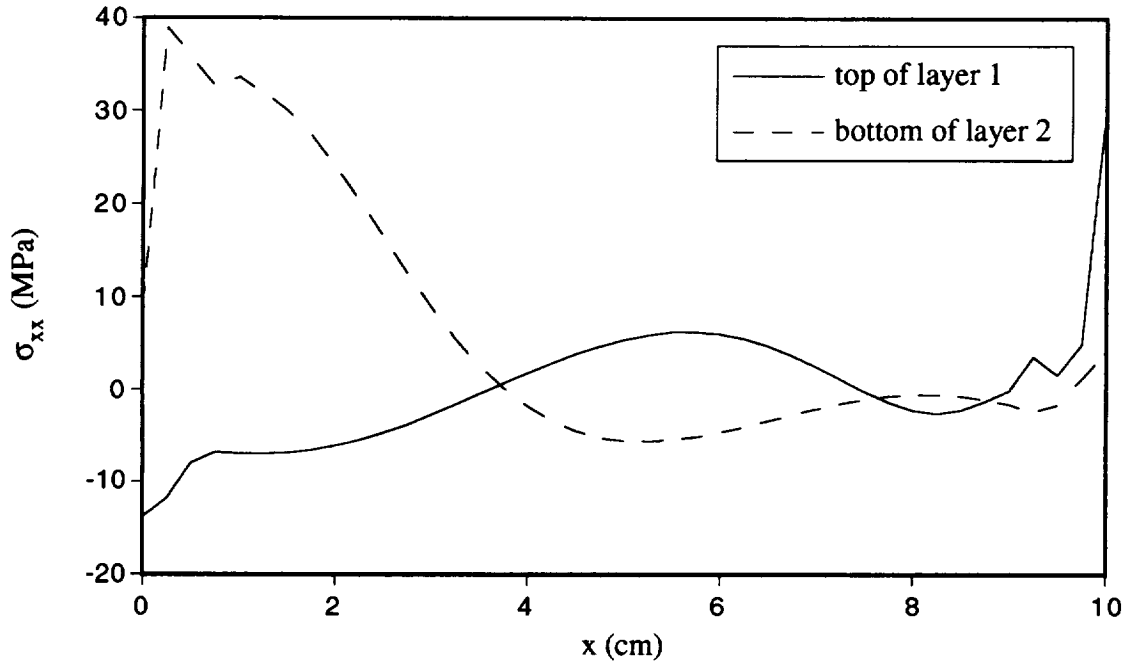

Fig. 5.5 Test problem results for $w = 0.5$ cm translation, solution by trapezoidal scheme solution with 40 intervals.

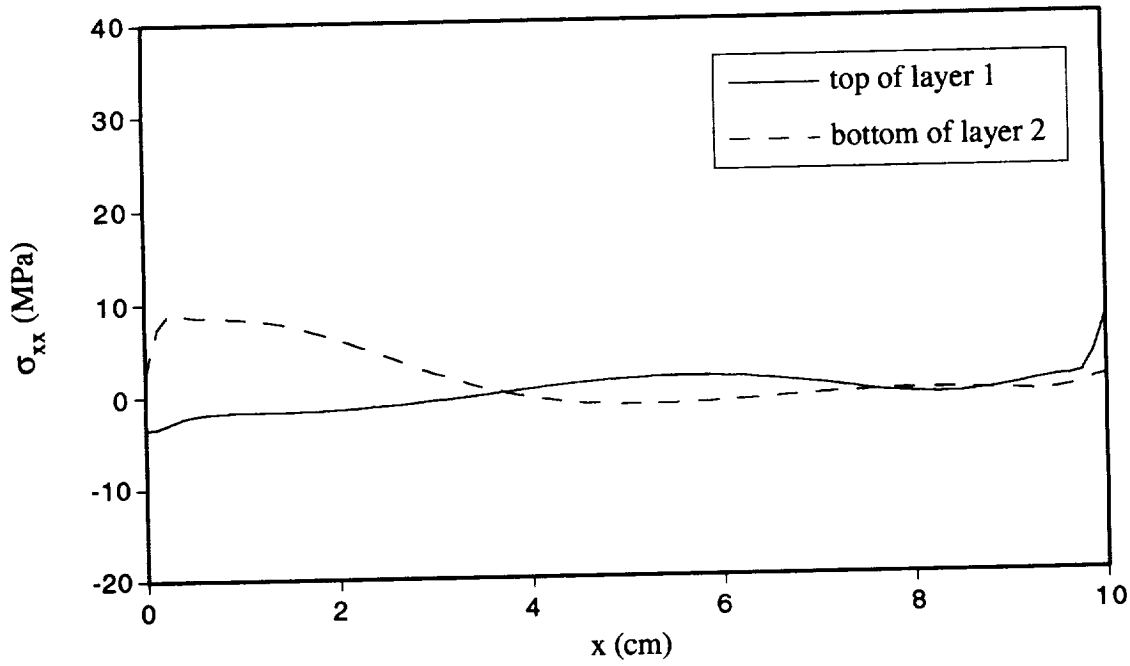

Fig. 5.6 Test problem results for $w = 0.5$ cm translation, solution by trapezoidal scheme solution with 80 intervals.

It appears from these results that simply increasing the number of mesh points will eventually produce acceptable results. However, increasing the number of mesh points to 320 produces the results shown in Fig. 5.7. While the magnitude of the discretization error from the trapezoidal scheme has been significantly reduced, an additional error has appeared in the form of oscillations. Therefore, it was concluded that the trapezoidal scheme is not suitable for the solution of the governing equations resulting from these theories.

The results shown in Fig. 5.8 are for the solution of the same test problem using a two-stage Gauss implicit Runge-Kutta finite difference scheme. This one-step scheme has an accuracy of order four and clearly provides a dramatic improvement for this test problem. In addition to superior accuracy as compared to the trapezoidal scheme, the Gauss scheme also offers improved stability for stiff ODEs due to its implicitness. This characteristic is desirable because DAEs are known to behave numerically similar to stiff differential equations.[51]

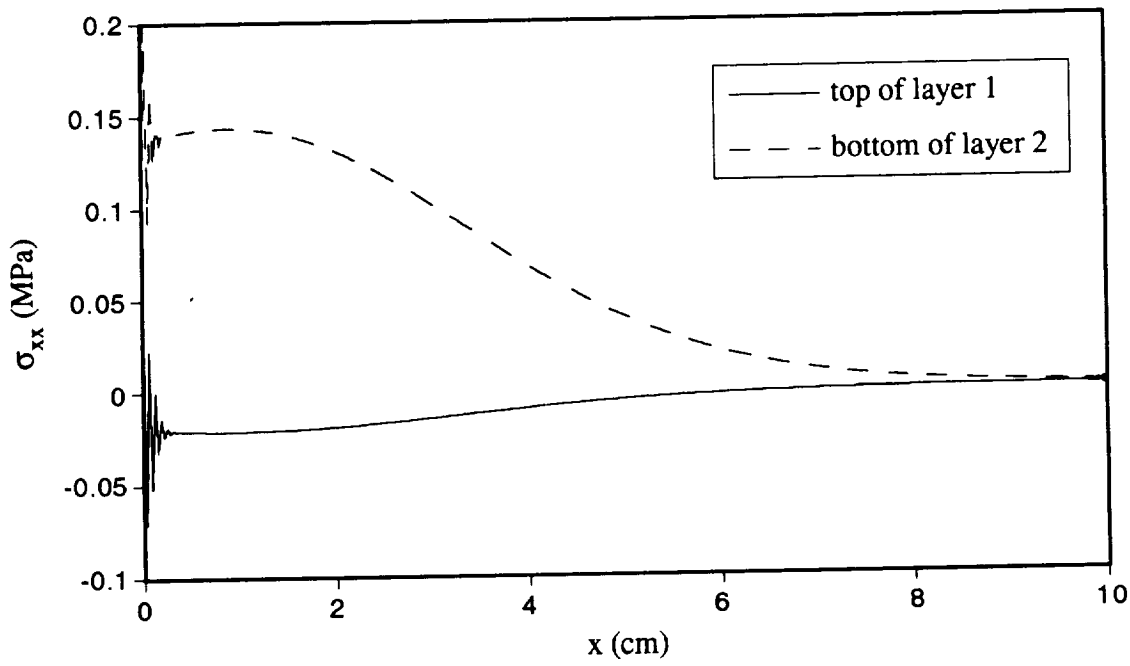

Fig. 5.7 Test problem results for w = 0.5 cm translation, solution by trapezoidal scheme solution with 320 intervals.

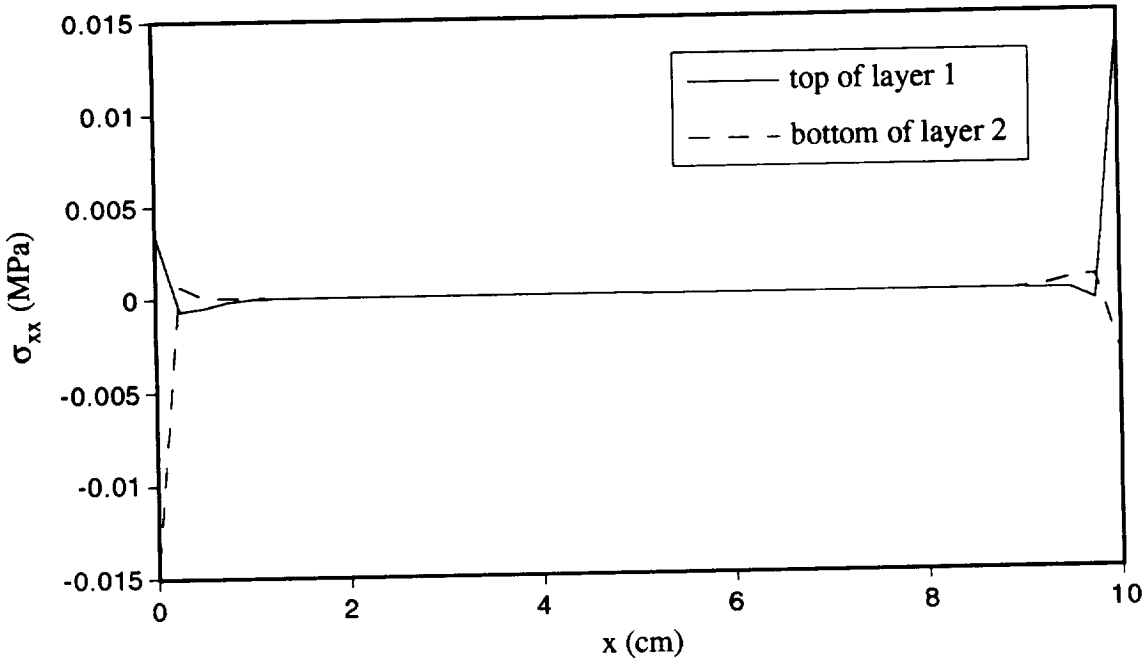

Fig. 5.8 Test problem results for w = 0.5 cm translation, solution by two-stage Gauss scheme solution with 40 intervals.

This scheme is presented on pp. 210–216 of Ref. 52 and is summarized in Appendix B. In that form, this scheme is applicable to systems of first order linear ODEs. Therefore, the DAEs of the present theories were converted to ODEs by differentiating the algebraic equations, making them ODEs, and applying them in their original algebraic form as boundary (in our case initial) conditions. While this is unlikely to be an optimal method for the solution of these systems from the aspect of efficiency, it is sufficient for the verification and evaluation of the theories and is used in the remainder of this work for both the generalized plane deformation and axisymmetric models unless otherwise noted.

5.4 Patch Tests

Various test problems were solved by the structural models in order to verify their accuracy and to examine their applicability and limitations. The test problems examined are what will be referred to as patch tests because of their similarity to tests of that name used to verify the accuracy finite elements. The concept of a patch test is very simple: choose a problem for which the exact elasticity solution is known, divide it into layers of varying geometries, and compare the results obtained to the exact solution. Usually the exact solution is one with uniform strain and stress states. Using this approach, the effect of such factors as the layer distortion and thickness on the accuracy of the solution were examined.

5.4.1 Generalized Plane Deformation Model

Patch tests were used to evaluate the effect of the magnitude of rigid body displacements, steepness of the slope of interfaces between layers, the thickness of individual layers, and the number of layers in the model on the accuracy and reliability of solutions using the generalized plane deformation model. In each of these patch tests, the material was the same isotropic aluminum alloy used in the example of Sec. 5.3.2. In each case, the uniform thickness plate was subjected to a uniaxial strain of $\varepsilon_{xx} = 0.1\%$, was constrained to $\varepsilon_{yy} = 0$, and was free to contract in the z-direction. This loading was chosen because it is characteristic of the type of loading applied to plates. The exact solution for this loading is $\tilde{\sigma}_{xx} = 76.281$ MPa, $\tilde{\sigma}_{yy} = 23.647$ MPa, and all other stresses zero.

5.4.1.1 Examination of the Effect of the Magnitude of Rigid Body Displacements

The test problem used in examining the effect of the magnitude of the rigid body

displacements is shown in Fig. 5.9. The geometry is the same as that used in Sec. 5.3.2 with only the boundary conditions different. The displacement in each coordinate direction is given the same amount of rigid body translation, A. The finite difference mesh in each case contained 20 equal sized intervals.

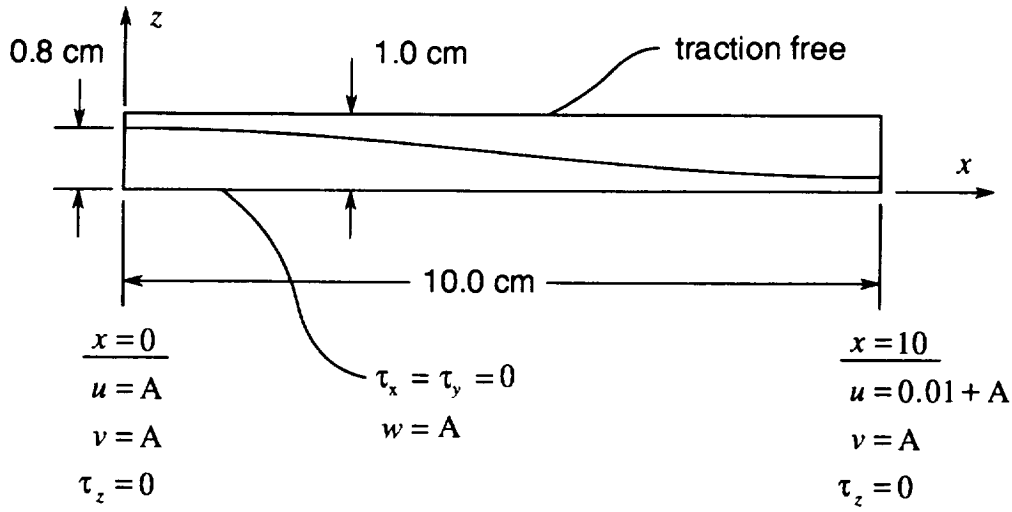

Fig. 5.9 Patch test problem for rigid body displacements.

The absolute value of the maximum error for each value of A was determined for the nonzero stresses σ_{xx} and σ_{yy} as was the magnitude of the other stress components relative to the exact σ_{xx}, since their exact values are zero. These results are presented in Table 5.2. It is clear that the finite difference solution by the two-stage Gauss implicit Runge-Kutta scheme does not suffer from difficulty in handling solutions with large amounts of rigid body translation as did the trapezoidal scheme. Even for the extreme case of A = 1000 cm, the errors all six stress components are, for all practical purposes, insignificant.

Table 5.2 Errors resulting from rigid body translations.

A (cm)	σ_{xx} (%)	σ_{yy} (%)	$\lvert\sigma_{zz}/\tilde{\sigma}_{xx}\rvert$	$\lvert\sigma_{yz}/\tilde{\sigma}_{xx}\rvert$	$\lvert\sigma_{xz}/\tilde{\sigma}_{xx}\rvert$	$\lvert\sigma_{xy}/\tilde{\sigma}_{xx}\rvert$
1.0	0.0	0.0	$O(10^{-6})$	$O(10^{-11})$	$O(10^{-7})$	$O(10^{-11})$
10.0	0.0	0.0	$O(10^{-6})$	$O(10^{-10})$	$O(10^{-7})$	$O(10^{-10})$
100.0	0.0013	0.0	$O(10^{-6})$	$O(10^{-9})$	$O(10^{-6})$	$O(10^{-9})$
1000.0	0.0315	0.055	1.6×10^{-4}	$O(10^{-8})$	$O(10^{-5})$	$O(10^{-8})$

5.4.1.2 Examination of the Effect of the Slope of the Interface Between Layers

Due to the assumption that $\cos\gamma \neq 0$ for these models, a vertical layer interface ($\gamma = 90°$) cannot be modeled. In this section the ability of the generalized plane deformation version to provide accurate solutions for very steep layer interfaces is determined. The test problem used for this is the same as that of Fig. 5.9 with one exception, the length of the plate will not be 10 cm. In order to increase the slope (dz_k/dx) of the internal interface, the length of the plate ℓ is reduced, compressing the curvature of the internal interface into a shorter horizontal distance and therefore increasing the slope. The loading will remain at $\varepsilon_{xx} = 0.1\%$ and A will be retained at 10 cm in order to examine the combined effect of rigid body displacements and a steep interfacial slope. Once again, the finite difference mesh will contain 20 intervals.

The maximum errors in σ_{xx} and σ_{yy} as well as the relative values of the other components were again calculated and are presented in Table 5.3. The maximum slope occurs at the mid-length of the plate and is also presented in the table. These results clearly show that this theory has the ability to model problems with very steep internal interfaces, likely beyond those required for the analysis of composite laminates.

Table 5.3 Errors resulting from steep interfacial slopes.

Max. $\lvert dz_k/dx \rvert$	σ_{xx} (%)	σ_{yy} (%)	$\lvert\sigma_{zz}/\tilde{\sigma}_{xx}\rvert$	$\lvert\sigma_{yz}/\tilde{\sigma}_{xx}\rvert$	$\lvert\sigma_{xz}/\tilde{\sigma}_{xx}\rvert$	$\lvert\sigma_{xy}/\tilde{\sigma}_{xx}\rvert$
1.125	0.0	0.0	$O(10^{-6})$	$O(10^{-10})$	$O(10^{-7})$	$O(10^{-10})$
11.25	0.0	0.0	$O(10^{-6})$	$O(10^{-10})$	$O(10^{-6})$	$O(10^{-10})$
112.5	0.0	0.0	$O(10^{-6})$	$O(10^{-10})$	$O(10^{-7})$	$O(10^{-10})$
1125	1.37	1.43	7.5×10^{-4}	$O(10^{-10})$	$O(10^{-6})$	$O(10^{-8})$

5.4.1.3 Examination of the Effect of the Relative Thickness of Layers

As mentioned in Sec. 3.3, the choice of displacement weighting functions in the two models presented in this work differ from those used by Pagano[44,45] in his original development of these types of theories. The reasons for the change centered on difficulties with numerical conditioning for problems with thin layers and for layers located at moderately large values of z relative to their thickness. Therefore, the first part of this section examines the degree to which the changes made were successful in overcoming

these difficulties. In the remainder of this section the accuracy of solutions using the higher order two-stage Gauss finite difference scheme for the same patch tests is examined.

Two versions of the generalized plane deformation model will be compared in their reliability in solving problems with thin layers. The first was derived using the same approach as Pagano used for derivation of his model for involute bodies of revolution and will be referred to as Pagano's approach. The second incorporates a series of modifications to the stress assumptions as well as the aforementioned change to the displacement weighting functions and will be referred to as the present approach.

In his original development of the stress assumptions, Pagano did not scale the bubble shape functions by powers of the thickness. He also did not choose his cubic shape functions such that they had their inflection points within the layer. These changes to the stress shape functions were made in the present approach prior to the changes in the displacement weighting functions as an attempt to overcome the numerical conditioning problem encountered when solving the system, but were found to be insufficient. However, they did provide a side benefit in that they simplified the equilibrium equations and the expressions resulting from evaluation of the weighted compliance integral of Eq. (5-3). The changes made to the displacement weighting functions, on the other hand, were found to provide significant improvement in numerical conditioning as will be demonstrated.

Both of these generalized plane deformation models were solved in their original DAE form using the trapezoidal one-step finite difference scheme. While this may not seem appropriate considering the inability of this solution approach to handle the test problem of Sec. 5.3.2, it is able to handle the present problem due to the absence of large displacements. For reasons that will become apparent later in this section, large displacements have little to no effect on the conditioning. Therefore, it was felt that the additional work involved in converting Pagano's approach to a fully differential system to be solved by the higher order scheme is unnecessary for present purposes.

The problem used to demonstrate the improvement in conditioning is shown in Fig. 5.10. It differs from the previous patch test problems by the introduction of a third layer of thickness t whose mid-surface is defined by the same contour as the internal interface in the previous patch tests. Two geometric parameters are changed to examine their effect on the solutions by the two models. They are the thickness of the middle layer, which is varied by movement of the layer interfaces without moving the layer mid-surface, and the distance from the bottom of the plate to the x axis. This second parameter will be referred to as z_0 in

keeping with the notation used in presenting the model in Chapter 3 and is used to examine the effect of varying the magnitude of z within the layers relative to the thickness of the layers (Δz).

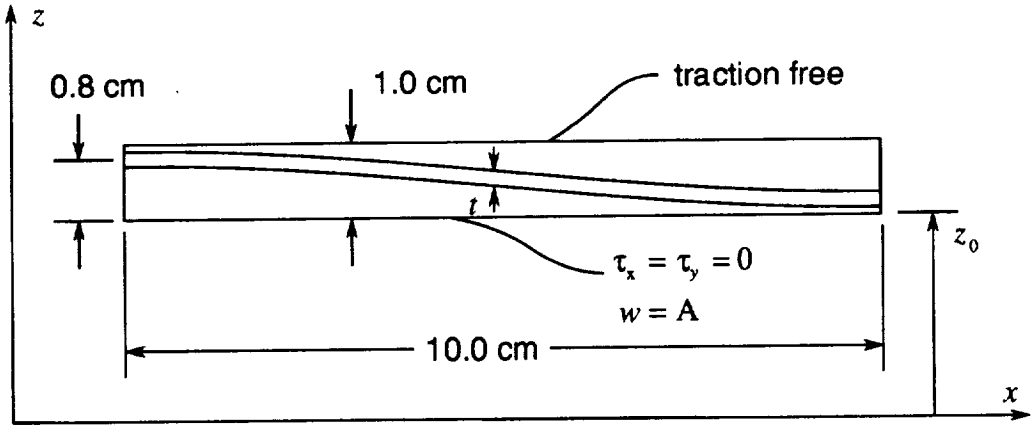

$x = 0$	$x = 10$
$u = A$	$u = 0.01 + A$
$v = A$	$v = A$
$\tau_z = 0$	$\tau_z = 0$

Fig. 5.10 Patch test problem for examining relative thickness of a layer.

The numerical conditioning of each case being referred to in this section is a measure of the reliability of the solutions obtained. The condition numbers that are presented are for the global finite difference matrix containing both the difference equation for each interval in the domain and the boundary conditions (see Eq. (5-15)). For the present class of problems, the boundary conditions are separated, leaving a banded matrix. The condition numbers presented here are the l_1 condition numbers estimated by the IMSL library routine named DLFCRB[53]. This routine uses an algorithm developed by Cline et al.[54] for estimating the condition number of a matrix with minimal computational expense.

The significance of the condition number in determining the reliability of the solution **x** to the general linear system

$$\mathbf{Hx} = \mathbf{b} \tag{5-21}$$

can be expressed in terms of the sensitivity of the solution to perturbations in **H** and **b**. The condition number for **H** will be represented by $\kappa(\mathbf{H})$. In essence, the relative error in **x** can be $\kappa(\mathbf{H})$ times the relative errors in **H** and **b** (see pp. 24–28 of Ref. 55). Therefore, a

matrix is considered to be ill-conditioned when the order of magnitude of the condition number approaches the number of significant digits used in the computations. For single precision fortran real numbers this is about seven and for double precision, which is used in the present study, it is about fifteen. Therefore, a condition number on the order of 10^{15} would indicate a poorly conditioned matrix and therefore an unreliable solution. It should be noted that while a poorly conditioned global finite difference matrix may produce reliable results for some right-hand-side vectors, this cannot be expected for all possible right-hand-side vectors as would occur with a well conditioned matrix.

Having described how the numerical conditioning of a particular problem was examined, it becomes clear why the presence of large displacements does not affect the conditioning significantly. The only factor in the prescription of boundary conditions that affects the condition of the matrix **H** of Eq. (5-21) is the type of condition, i.e. traction or displacement. The magnitude of the prescribed quantities enters the equation through the vector **b** and therefore has no effect on the condition of **H**.

The first set of results presented in Table 5.4 are for the case of A = 0 and $z_0 = 0$ while the thickness of the center layer is varied. The solution is approximated by a uniform mesh of 41 grid points, giving 40 intervals. This choice of mesh refinement is somewhat arbitrary in this demonstration as it has been found to have little effect on the condition of the solution matrix.

Table 5.4 Condition numbers for A = 0 and $z_0 = 0$.

t (cm)	Pagano's Formulation	Present Formulation
0.1	3.5×10^{13}	3.7×10^{6}
0.01	2.1×10^{20}	2.2×10^{8}
0.001	7.1×10^{23}	1.4×10^{11}
0.0001	3.4×10^{33}	2.0×10^{14}

From these results, it is clear that reducing the thickness of the center layer, at least relative to the other layers, causes a degradation in the condition of the finite difference solution matrix. It is also clear that the changes made to Pagano's formulation in arriving at the present formulation significantly improve the conditioning. While Pagano's formulation is on the verge of producing unreliable results for $t = 0.1$ cm, or 10% of the overall thickness of the plate, the present analysis is reliable past $t = 0.001$ cm or 0.1% of the

overall thickness.

The next set of results is for the case where $z_0 = 100$ cm, A = 0, and t is varied. For this case, the value of z within a layer has a very small range of values. Once again, a uniform mesh of 40 intervals was used in the approximation. The resulting condition numbers for this case with varying center layer thickness are presented in Table 5.5 for the two models.

Table 5.5 Condition numbers for A = 0 and $z_0 = 100$ cm.

t (cm)	Pagano's Formulation	Present Formulation
0.1	1.0×10^{17}	5.0×10^{6}
0.01	5.3×10^{21}	2.6×10^{8}
0.001	2.6×10^{20}	1.4×10^{11}
0.0001	9.1×10^{29}	2.0×10^{14}

Compared to Table 5.4, these condition numbers reveal three noteworthy characteristics of these two models. First, the condition number for Pagano's formulation with $t = 0.1$ cm deteriorates by three orders of magnitude to the point of producing unreliable solutions. Second, the present formulation of the model shows no degradation in the condition number relative to those shown in Table 5.4. Third, the trend of increasing condition number with decreasing t is reversed in going from $t = 0.01$ to $t = 0.001$ using Pagano's formulation. A re-examination of the two condition numbers in Table 5.4 associated with the same two thicknesses shows that the rate of increase in the condition numbers with thickness decrease is lower in that range for $z_0 = 0$ as well. This may be caused by a secondary influence on the condition numbers or possibly errors in the estimate of the condition numbers. However, because this anomaly occurs well into the range of condition numbers associated with ill-conditioned matrices, the matter was not examined further.

The next set of results is for the case where $t = 0.1$ cm, A = 0, and z_0 is varied. Once again, a uniform mesh of 40 intervals was used in the approximation. The resulting condition numbers for this case are presented in Table 5.6 for the two formulations of the model.

Table 5.6 Condition numbers for increasing distance from the x-axis, A = 0 and $t = 0.1$.

z_0(cm)	Pagano's Formulation	Present Formulation
0	2.8×10^{13}	3.7×10^{6}
1	2.4×10^{14}	5.3×10^{6}
10	8.3×10^{16}	4.4×10^{6}
100	1.0×10^{17}	5.0×10^{6}
1,000	5.9×10^{18}	4.2×10^{6}
10,000	5.3×10^{22}	4.4×10^{6}

These results reinforce the advantage of the present formulation over Pagano's approach. It is clear that the present formulation's condition number for the solution matrix is basically constant with respect to the z location of the domain. Pagano's formulation, on the other hand, shows a degradation in conditioning with increasing z_0.

The remainder of this section will focus on the effect of the relative thickness of layers on the accuracy of the solutions obtained. The same patch tests used in examining the reliability of the method are solved using the higher order two-stage Gauss implicit Runge-Kutta finite difference scheme. As in Secs. 5.4.1.1 and 5.4.1.2, 20 finite difference intervals will be used and the maximum relative errors in σ_{xx} and σ_{yy} are presented.

Table 5.7 presents the condition numbers and the accuracy of the stresses predicted by the model. Results for σ_{yz} and σ_{xy} are omitted because the analysis gave values of zero for them, which is exact. Comparison of the condition numbers from the second column of Table 5.7 with those from the third column of Table 5.4 reveals a degradation in conditioning. This is due to a combination of two factors; the conversion of the system of DAEs to ODEs, and the use of the higher order Gauss finite difference scheme. A test application of the trapezoidal scheme to the fully differential system used with the Gauss scheme showed that the majority of the degradation was caused by the conversion to the fully differential system. The accuracy results show good agreement down to a thickness of the internal layer of $t = 0.001$ cm, or 0.1% of the total thickness of the plate.

Table 5.7 Condition numbers and maximum errors for varying center layer thickness.

t (cm)	Condition #	σ_{xx} (%)	σ_{yy} (%)	$\lvert\sigma_{zz}/\tilde{\sigma}_{xx}\rvert$	$\lvert\sigma_{xz}/\tilde{\sigma}_{xx}\rvert$
0.1	2.0×10^{10}	0.0	0.0	$O(10^{-6})$	$O(10^{-7})$
0.01	2.9×10^{11}	0.0092	0.013	$O(10^{-5})$	$O(10^{-5})$
0.001	2.1×10^{13}	0.84	0.79	5.4×10^{-4}	7.9×10^{-4}
0.0001	2.7×10^{18}	18	17	5.6×10^{-3}	9.0×10^{-3}

An additional note should be made about the accuracy results presented in Table 5.7. Although the errors presented are large for the case of $t = 0.0001$ cm, these are maximum errors and are far from uniform over the domain. Fig. 5.11 is a plot of the errors in σ_{xx} along a series of parallel contours of constant x. From this plot, it is clear that the errors are mostly confined to the thin central layer and that the solution is quite good everywhere else.

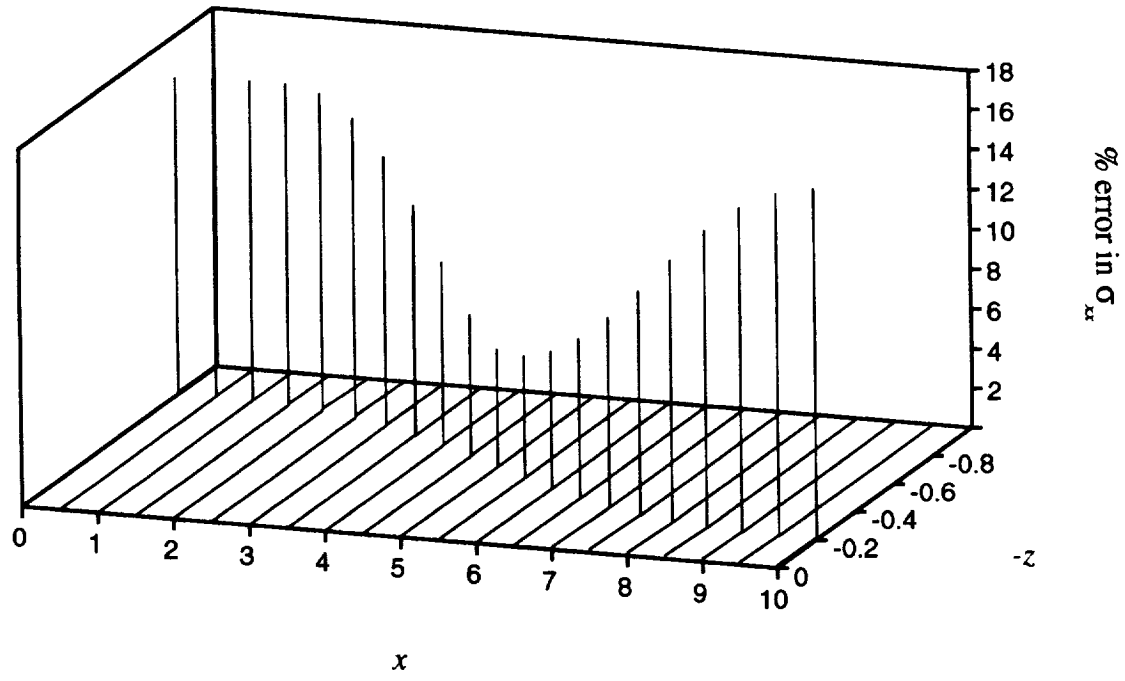

Fig. 5.11 Plot of errors in σ_{xx} for $t = 0.0001$ cm case of Table 5.7.

5.4.1.4 Examination of the Effect of Several Thin Layers

The geometry of the modeled dropped-ply laminate of Fig. 5.1 demonstrates the need for this model to handle a group of very thin layers. Those layers used to model the

dropped plies cannot be discontinued and therefore are treated as a thin resin layer between the continuous sublaminates. This section includes such a feature in a patch test to examine its effect on the accuracy of the model.

The problem used is an extension of the previous patch tests and is shown in Fig. 5.12. The geometry differs from that of the previous section only in that it includes additional internal thin layers. Each of these internal layers has thickness 0.001 cm, or 0.1% of the thickness of the entire plate. As a group, these layers are centered within the plate, that is the layer geometry is again antisymmetric with respect to $x = 5$. The material and boundary conditions are the same as the previous section, i.e. aluminum subjected to 0.1% axial strain and constrained from contracting in the y-direction.

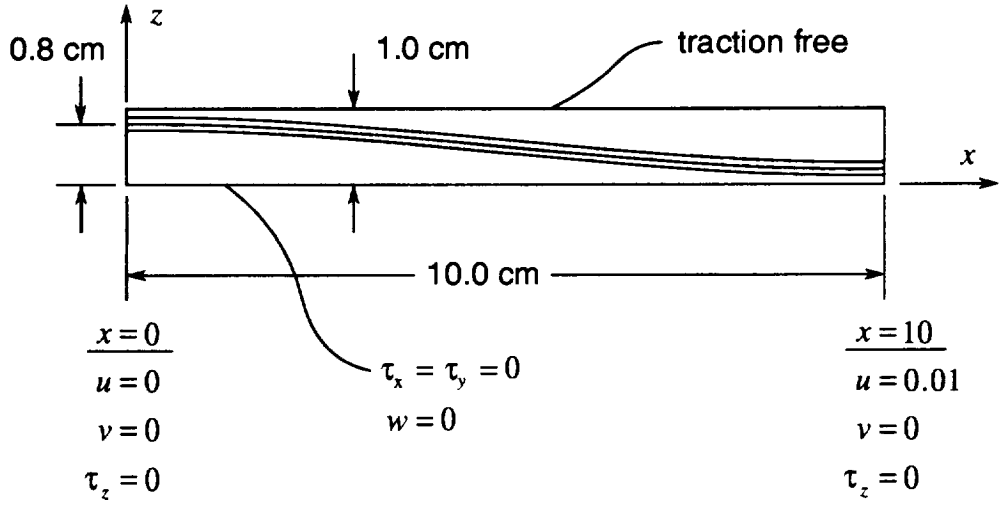

Fig. 5.12 Patch test problem for examining several thin layers.

Condition number and accuracy results for this patch test are presented in Table 5.8. These results were obtained using a finite difference mesh of 20 evenly spaced points. Once again, results for σ_{yz} and σ_{xy} are not presented because the theory correlated with the exact solution perfectly. The parameter N tabulated in the first column refers to the total number of layers in the model and therefore is two more than the number of interior layers. The case of $N = 3$ corresponds to the configuration in the previous section with $t = 0.001$ cm.

Table 5.8 Condition numbers and maximum errors for several thin layers of thickness $t = 0.001$ cm.

N	Condition #	σ_{xx} (%)	σ_{yy} (%)	$\lvert\sigma_{zz}/\tilde{\sigma}_{xx}\rvert$	$\lvert\sigma_{xz}/\tilde{\sigma}_{xx}\rvert$
3	2.1×10^{13}	0.84	0.79	5.4×10^{-4}	7.9×10^{-4}
4	2.9×10^{14}	0.75	6.0	0.050	8.6×10^{-4}
5	6.7×10^{14}	0.25	15	0.014	6.0×10^{-4}
6	1.1×10^{15}	0.27	16	0.051	4.0×10^{-4}

The results shown in table 5.8 reveal a potential drawback to this model in the form of deteriorating condition numbers for increasing numbers of thin layers. In addition, the accuracy of the transverse and through the thickness stresses σ_{yy} and σ_{zz} degrades with the number of thin layers. However, as noted previously, an ill conditioned matrix does not mean the solution will be poor, only more likely so. Therefore, care must be taken when evaluating solutions obtained with this model.

As far as the accuracy of results for the stresses, all but σ_{yy} and σ_{zz} agree well with the exact solution. Figs. 5.13 and 5.14 are plots of these two stress components for the case $N = 6$ revealing once again that the errors in predicted stresses tend to be isolated within the extremely thin layers. While it would be desirable to obtain a solution that is uniformly good, knowing where stresses are likely to be in error allows values obtained there to be scrutinized more carefully.

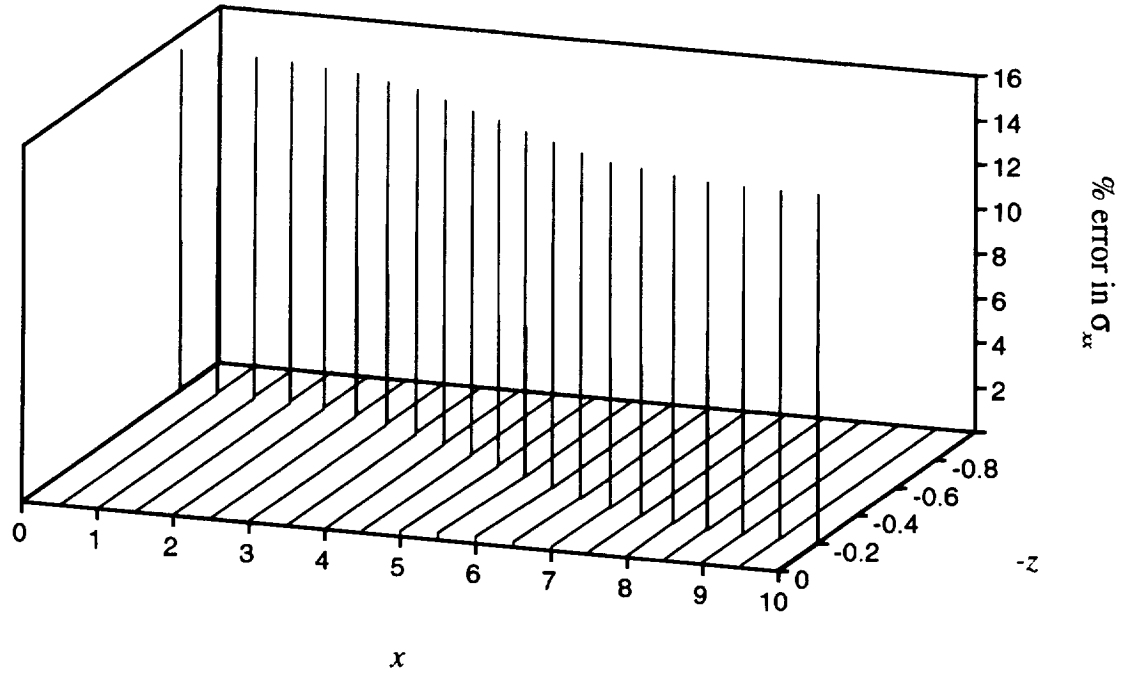

Fig. 5.13 Plot of errors in σ_{xx} for $N = 6$ case of Table 5.8.

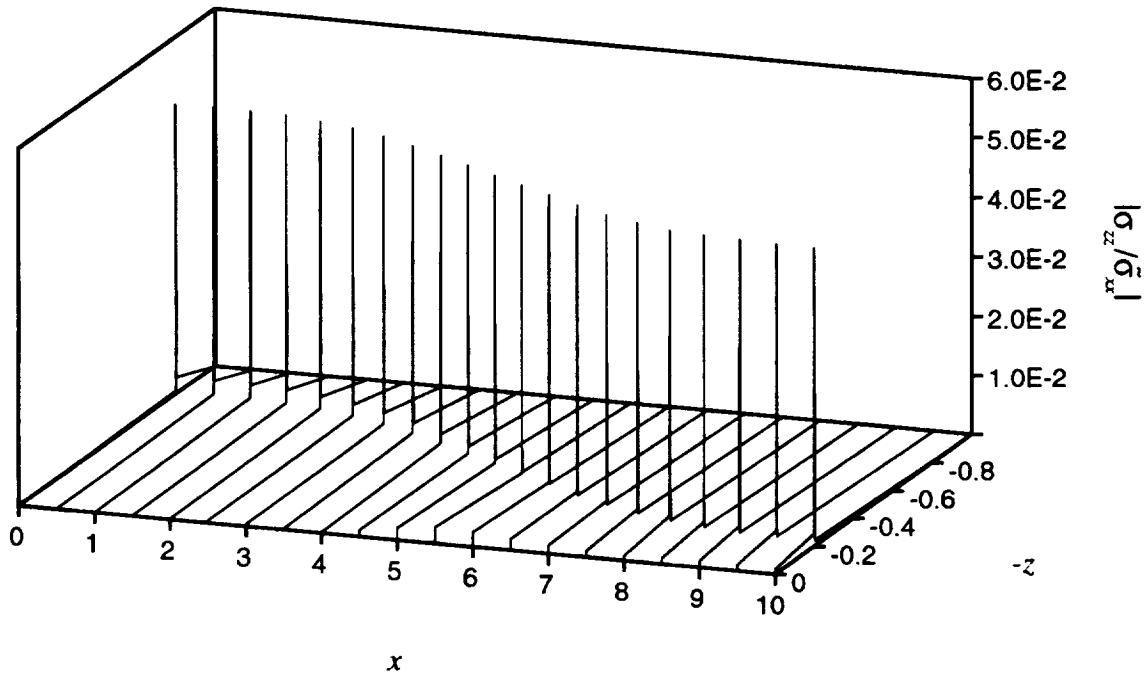

Fig. 5.14 Plot of errors in σ_{zz} for $N = 6$ case of Table 5.8.

5.4.2 Axisymmetric Model

Patch tests were also used to examine the stability and accuracy of the axisymmetric model. The effects of the magnitude of rigid body displacements, the slope of interfaces between layers, and the thickness of individual layers in the model on the results obtained and their reliability were examined. Once again the material chosen was isotropic, with material properties of an aluminum alloy, $E = 68.95$ GPa and $\nu = 0.31$. The structure chosen for the tests was a uniform thickness cylinder of constant radius subjected to a uniform end extension of $\varepsilon_{xx} = 0.1\%$ and an internal pressure of $p = 10$ kPa. The cylinder was free to expand or contract radially along its entire length, including the ends. The exact elasticity solution for this loading is given by the expressions[56]

$$\tilde{\sigma}_{xx} = E\varepsilon_x + \nu\left(\frac{2r_0^2 p}{r_N^2 - r_0^2}\right), \quad \tilde{\sigma}_{\theta\theta} = \frac{r_0^2 p}{r_N^2 - r_0^2}\left(1 + \frac{r_N^2}{r^2}\right), \quad \tilde{\sigma}_{rr} = \frac{r_0^2 p}{r_N^2 - r_0^2}\left(1 - \frac{r_N^2}{r^2}\right) \qquad (5\text{-}22)$$

where r_0 and r_N are the inside and outside radii respectively.

5.4.2.1 Examination of the Effect of the Magnitude of Rigid Body Displacements

The test problem used in examining the effect of the magnitude of the rigid body displacements on solutions from the axisymmetric model is shown in Fig. 5.15. The geometry of the cross section is the same as that used in Sec. 5.4.1.1 except that it now represents the cross section of a shell of revolution. The inside radius of the cylinder r_0 is 200 cm, giving a radius to thickness ratio R/T of about 200, which was chosen because it represents a typical value for the unstiffened shells that are of interest. The amount of rigid body displacements in the x and θ coordinate directions is denoted by A. For the θ direction, A is the circumferential displacement of the inner surface. There is no rigid body mode in the r coordinate direction because of the assumption of axisymmetry. The finite difference mesh in each case contained 20 equal sized intervals.

The absolute value of the maximum error for each value of A was determined for the nonzero stresses σ_{xx}, $\sigma_{\theta\theta}$, and σ_{rr}. For the other three stress components, their magnitude relative to the exact σ_{xx} was determined, since their exact values are zero. These results are presented in Table 5.9. As in the generalized plane deformation model, the results are virtually unaffected by the presence of the rigid body displacements. The only components to show a degradation in accuracy as A was increased were $\sigma_{\theta r}$ and $\sigma_{x\theta}$, but these errors were very small except for extremely large values of A. The errors appearing in the σ_{xx} and

$\sigma_{\theta\theta}$ stress components were due to the fact that only five significant digits of the stress variables were written to the output files from the analysis, which is why they do not change with increasing A. The error in σ_{rr} is probably due to the approximate nature of this model and its numerical solution and is well within acceptable limits.

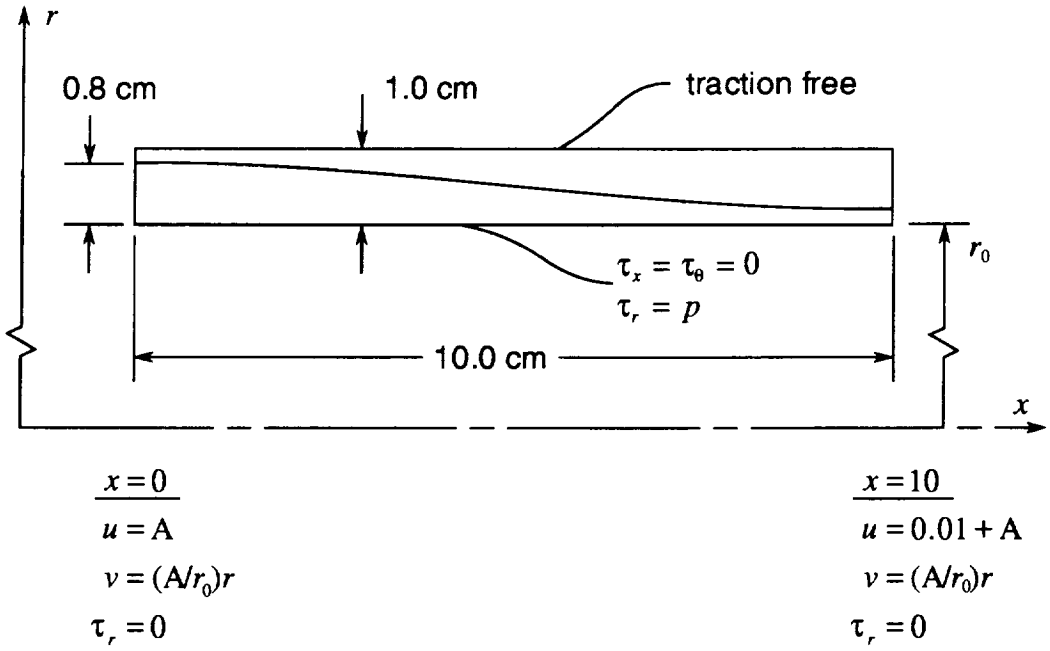

Fig. 5.15 Patch test problem for rigid body displacements in the axisymmetric model.

Table 5.9 Errors resulting from rigid body displacements.

A (cm)	σ_{xx} (%)	$\sigma_{\theta\theta}$ (%)	σ_{rr} (%)	$\lvert\sigma_{\theta r}/\tilde{\sigma}_{xx}\rvert$	$\lvert\sigma_{xr}/\tilde{\sigma}_{xx}\rvert$	$\lvert\sigma_{x\theta}/\tilde{\sigma}_{xx}\rvert$
1.0	7.8×10^{-4}	3.8×10^{-3}	9.0×10^{-2}	4.9×10^{-5}	$O(10^{-7})$	9.5×10^{-5}
10.0	7.8×10^{-4}	3.8×10^{-3}	9.0×10^{-2}	4.9×10^{-4}	$O(10^{-7})$	9.5×10^{-4}
100.0	7.8×10^{-4}	3.8×10^{-3}	9.0×10^{-2}	4.9×10^{-3}	$O(10^{-7})$	9.5×10^{-3}
1000.0	7.8×10^{-4}	3.8×10^{-3}	9.0×10^{-2}	4.9×10^{-2}	$O(10^{-7})$	9.5×10^{-2}

5.4.2.2 Examination of the Effect of the Slope of the Interface Between Layers

In the same manner as was used to test the generalized plane deformation model, the effect of steepness in slope of layer interfaces was examined. The test problem used for this

is the same as that of Fig. 5.15 with A = 0 and with the length of the plate ℓ successively reduced, thereby increasing the slope. The loading will remain the same as that applied in the previous patch test, end extension with $\varepsilon_{xx} = 0.1\%$ and internal pressure $p = 10$ kPa. Once again, the finite difference mesh will contain 20 intervals.

The absolute value of the maximum errors in σ_{xx}, $\sigma_{\theta\theta}$, and σ_{rr} were determined for each length ℓ based on the exact elasticity solution and are presented in Table 5.10. The maximum slope occurs at the mid-length of the plate and is also presented in the table. The errors in the shear stresses were negligible and are therefore not presented. Clearly these results indicate that the axisymmetric model does not handle the presence of steep interfacial slopes very well for this loading case. It was found, however, that removal of the internal pressure loading leaving uniform axial extension virtually eliminated these errors.

Table 5.10 Errors resulting from steep interfacial slopes.

Max. $\lvert dr_k/dx \rvert$	σ_{xx} (%)	$\sigma_{\theta\theta}$ (%)	σ_{rr} (%)
0.1125	7.5×10^{-4}	3.8×10^{-3}	9.0×10^{-2}
1.125	2.1×10^{-3}	2.4×10^{-2}	25.1
11.25	6.5×10^{-4}	6.5×10^{-2}	80.9
112.5	6.4×10^{-3}	9.3×10^{-1}	263

5.4.2.3 Examination of the Effect of the Relative Thickness of Layers

Having established that the changes made to the displacement weighting functions for the generalized plane deformation model were successful in overcoming the difficulties in numerical conditioning associated with layers that are thin relative to their coordinate location, this section presents results for similar tests of the axisymmetric model. The problem used to examine the accuracy and reliability of the solutions is shown in Fig. 5.16. As in the generalized plane deformation model patch tests, a third layer of thickness t was introduced whose mid-surface is defined by the same contour (antisymmetric with respect to $x = 5$) as the internal interface in the previous patch tests.

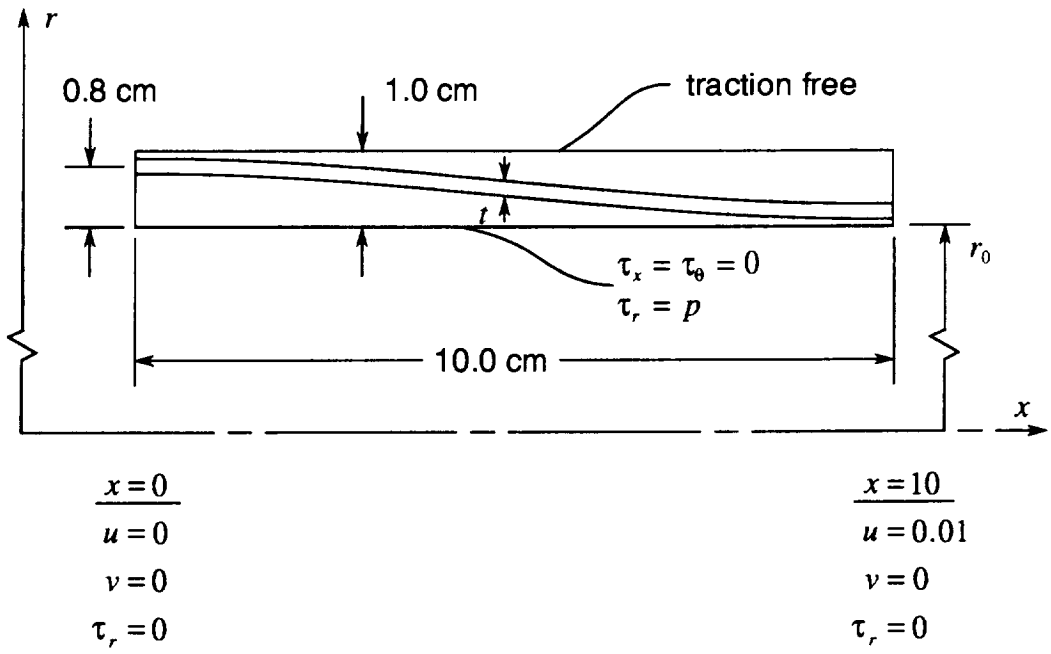

Fig. 5.16 Patch test problem for examining relative thickness of a layer.

The intent of this patch test was to verify that the axisymmetric model solved by the two-stage Gauss finite difference scheme produces results that are accurate and reliable for problems containing very thin layers in cylindrical shells with ratios of the radius to the thickness *R/T* of about 200. That is, geometries for which the thickness t is very small relative to the shell thickness $T = 1.0$ cm, and $r_0 = 200$ cm. However, in the first case examined, where $t = 0.1$ cm, unacceptable results were obtained. Presented in Table 5.11, these results show that while errors in σ_{xx} and $\sigma_{\theta\theta}$ were less than 3%, the maximum errors in σ_{rr} exceeded 1000% and the condition number of the finite difference solution matrix exceeded 10^{17}. As in the interface slope patch test, the three shear stress components were approximately zero, which is their exact value, and were therefore left out of this table.

In order to establish the effect of reducing the thickness of the internal layer, a second case with the same *R/T* was examined with t reduced to 0.01 cm. The results are presented in the second row of Table 5.11 and, as expected based on the results from the generalized plane deformation model, they were worse than for the larger value of t. Both the condition number and the accuracy of the stresses deteriorated significantly.

To determine the effect of varying the shell *R/T* ratio, the value of r_0 was reduced to 20 cm and t was returned to 0.1 cm while all other dimensions were left unchanged, giving an *R/T* of about 20. The results for this case are given on the third row of Table 5.11.

Compared to the first row of the table, the solution matrix remained poorly conditioned and the accuracy of the solution improved somewhat. While the errors in σ_{xx} and $\sigma_{\theta\theta}$ were acceptable at less than 1%, the error in σ_{rr} was again much larger at 27%.

Table 5.11 Condition numbers and maximum errors for varying center layer thickness and radius.

t (cm)	r_0(cm)	Condition #	σ_{xx} (%)	$\sigma_{\theta\theta}$ (%)	σ_{rr} (%)
0.1	200.0	2.0×10^{17}	0.093	2.59	1480
0.01	200.0	1.3×10^{20}	232	2560	2.20×10^{5}
0.1	20.0	1.7×10^{16}	$O(10^{-4})$	0.146	27.2
1.0	200.0	3.2×10^{14}	$O(10^{-5})$	3.11	78.4

Finally, all of the radial dimensions were scaled by a factor of ten from the previous case, leaving a cylinder of inside radius $r_0 = 200$ cm, total thickness $T = 10$ cm with a 1 cm thick inner layer. These results are given in the last line of Table 5.11 and actually show a deterioration in accuracy despite an improvement in the condition number. This increase in the errors may be due to the increase in interfacial slopes that this scaling produces, which was shown previously to affect the accuracy in the presence of an internal pressure loading. Removal of the internal pressure, as before, virtually eliminated these errors.

5.4.2.4 Comparison of Condition Numbers to Pagano's Original Axisymmetric Formulation

Although this reformulation of Pagano's original axisymmetric model still suffers from poorly conditioned finite difference solution matrices for the types of geometry necessary to analyze laminated cylindrical shells with dropped plies, it was successful in significantly improving the situation. This section presents a comparison of finite difference solution matrix condition numbers between the present axisymmetric formulation and Pagano's original model. The reader is referred to Sec. 5.4.1.3 for a brief explanation of the changes made to Pagano's approach or to Chapter 4 for a more thorough treatment.

As in Sec. 5.4.1.3, the comparison of conditions numbers was done using the one-step trapezoidal finite difference scheme as applied to the original DAE form of the governing equations. The problem used to demonstrate the effect of the reformulation on the numerical solution conditioning has the same two-layer geometry as the patch test problem used for examination of the effect of rigid body displacements and is shown in Fig. 5.15.

However, the total cylinder thickness is not 1 cm for all of these cases. The finite difference mesh contained 80 intervals in each case.

The condition number results for this comparison are presented in Table 5.12. As the accuracy of the results were bad for all cases due to the use of the trapezoidal scheme, they are not presented. The first and second cases differ only in that the radius of the cylinder is reduced from 200 to 20 cm. The third case is a radially scaled version of the second by a factor of 10. In a similar fashion to the results presented in Sec. 5.4.1.3 for the generalized plane deformation model, the condition numbers for the present version of the model are much lower than those for Pagano's formulation. They also tend to be influenced much less by the thickness of the cylinder and its radius. Another similarity between the condition number results from the axisymmetric model and the generalized plane deformation model is that the change in solution method from the trapezoidal scheme applied to the DAEs to the more accurate Gauss finite difference scheme applied to a fully differential system causes a significant degradation in the condition number. For example, the condition numbers for the rigid body displacement patch test were on the order of 10^{14} while the same geometry solved by the trapezoidal scheme, the first row of Table 5.12, had a condition number in the 10^{9} range.

Table 5.12 Condition numbers for Pagano's original formulation and the present formulation.

T(cm)	r_0(cm)	Pagano's Formulation	Present Formulation
1.0	200.0	7.6×10^{26}	3.6×10^{9}
1.0	20.0	3.6×10^{29}	2.2×10^{9}
10.0	200.0	1.4×10^{23}	1.7×10^{9}

5.4.2.5 Comments Regarding the Patch Test results for the Axisymmetric Model

As the results for the case where the thinnest layer was 10% of the total thickness with an R/T of 20 or 200 were unsatisfactory, modeling of resin layers on the order of 10% the thickness of a single ply in a composite laminate with a similar R/T does not appear to be feasible for an internal pressure loading. Despite the improvement in the conditioning of the numerical approximation attained through the modifications found to be successful in the generalized plane deformation, solution stability and accuracy are still deficient in the

present formulation and its solution by finite differences. The cause for this difference in the level of success likely lies in the inherent differences between plates and shells.

Variation of r_0, while somewhat similar to the variation of z_0 for the flat plate of the generalized plane deformation model, affects more than the numerical representation of the problem and its solution, it also affects the solution itself. That is, varying r_0 while keeping everything else the same changes the curvature of the shell and therefore, in general, the stress and displacement fields. This effect is magnified by the presence of an internal pressure loading. On the other hand, varying z_0 only changed the way the generalized plane deformation model represented the solution to what was essentially the same problem. The modifications to Pagano's approach simply minimized the degree to which varying z_0 changed that representation.

The main purpose of developing the axisymmetric model was for the analysis of laminated shells of revolution with dropped plies subjected to internal pressure. While the present formulation produces much better patch test results without internal pressure than with, the errors occurring with internal pressure are disconcerting. Therefore it was decided further application of this model, even to problems without internal pressure, should not be trusted without a better understanding of the cause of these errors.

5.5 Comparison with Other Solutions

While the patch tests of the previous section are useful for establishing some confidence in the generalized plane deformation model, they do not go far enough. Because their premise requires an exact solution to compare their results to, they are limited to very simple geometries. Problems involving multiple constituents for which exact elasticity solutions are available do not exist. Therefore, in order to verify the ability of these models to predict the stresses in composite laminates, comparisons must be made with established approximate solutions. This section presents results for the tensile coupon free edge problem and also for the problem of a dropped-ply laminate under compression, both of which are solved using the generalized plane deformation model.

5.5.1 Tensile Coupon Free Edge Problem

The first verification of the structural model as applied to laminates was a comparison to the benchmark problem of the interlaminar stress response near the straight free edge of a

tensile coupon. This was chosen as a baseline case because of the simple geometry and the availability of solutions. A four ply, symmetric laminate with $[0/90]_s$ layup is the test case selected (A 0°-ply is parallel to the y-axis). Each ply has uniform thickness h, the width of the laminate is $2b$, and $b = 8h$. See Fig. 5.17. The load is a prescribed normal strain ε in the y-direction, so $C = \varepsilon$ in Eqs. (3-1) and (3-2). All four lateral surfaces are traction free. We compare our results to those published by Pagano[44] for the interlaminar stress distributions along the x-axis in the 0/90 interface ($z = h$). Ply material properties are

$$E_{11} = 138\,\text{GPa} \quad (20\,\text{Msi}), \quad E_{22} = E_{33} = 14.5\,\text{GPa} \quad (2.1\,\text{Msi})$$
$$G_{12} = G_{13} = G_{23} = 5.86\,\text{GPa} \quad (0.85\,\text{Msi})$$
$$\nu_{12} = \nu_{13} = \nu_{23} = 0.21$$

Because of problem symmetry about the x-y and y-z planes, the solution domain is reduced to the quadrant $0 \le x \le b$ and $0 \le z \le 2h$ in the $y = 0$ plane. Each ply is divided into three mathematical layers, so $N = 6$.

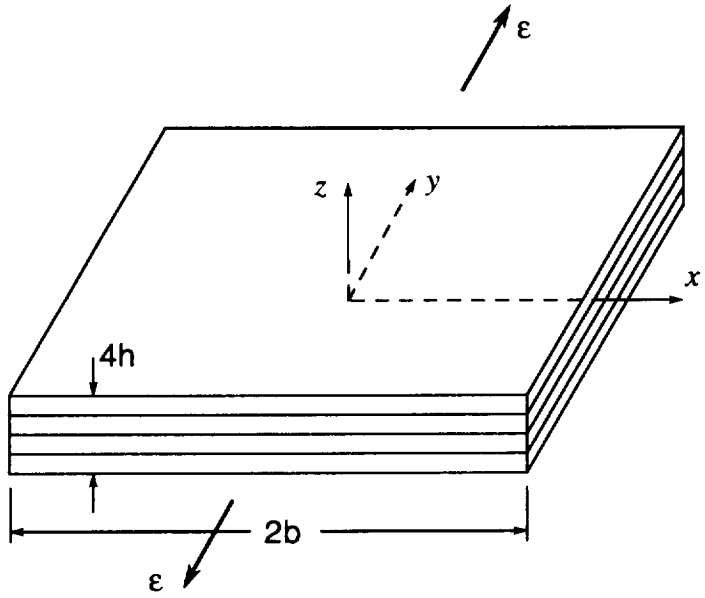

Fig. 5.17 Four ply laminate subject to uniform extension on ends y = constant.

The interlaminar normal stress distribution is shown in Fig. 5.18 and the distribution of the interlaminar shear stress, τ_{xz}, is shown in Fig. 5.19. It is clear from these plots that results of the present model compare very well to those presented by Pagano. A good comparison was expected for this problem since the stress assumptions in our structural model for straight and uniform thickness layers essentially reduce to those utilized by

Pagano in Ref. 44. It is worth noting that Pagano compared his results to those of Wang and Crossman[57] and found excellent agreement.

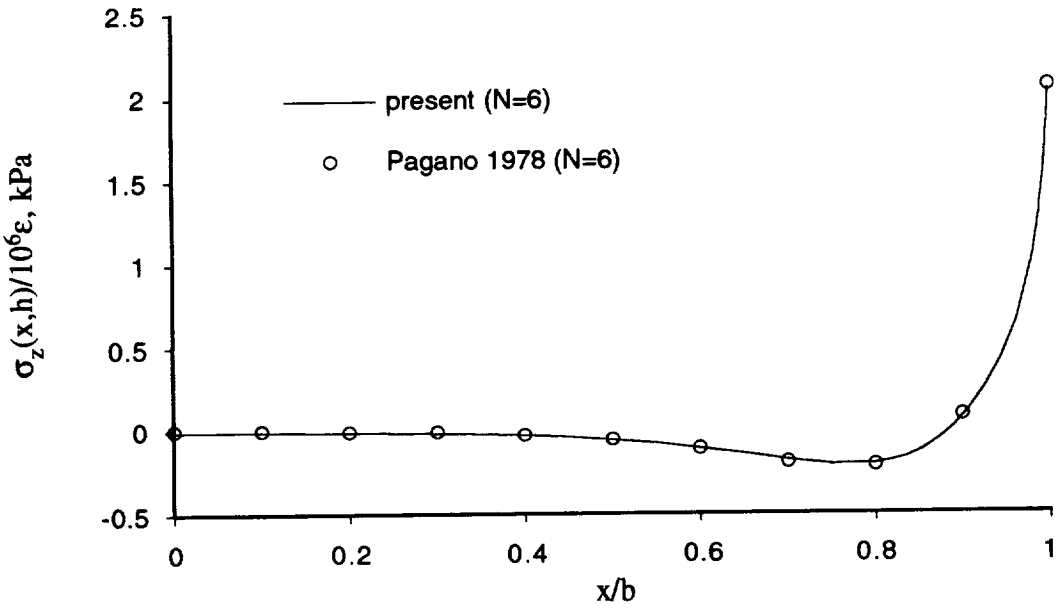

Fig. 5.18 Distribution of the interlaminar normal stress σ_z in the 0/90 interface.

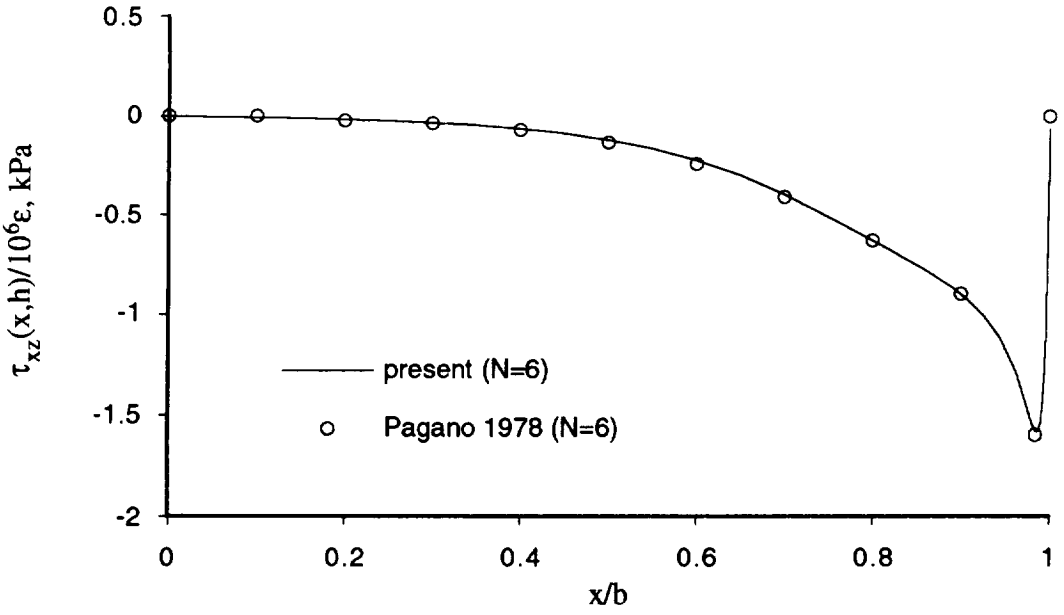

Fig. 5.19 Distribution of the interlaminar shear stress τ_{xz} in the 0/90 interface.

5.5.2 Dropped-Ply Laminate Under Uniaxial Compression

The second test case selected for the structural model as applied to laminates is a comparison to the results of Curry et al.[21] for the interlaminar stress response of a dropped-ply laminate subjected to axial compression. This problem was solved by a displacement-based finite element analysis in Ref. 21, and the finite element analysis was a part of an effort to correlate the prediction of delamination initiation with test results. Thus, the problem definition (laminate configuration, boundary conditions, etc.) were dictated by test conditions.

The laminate analyzed had a 20-ply thick section with the layup $[(\pm 45/0/90)_s/0_2]_s$ from which the center four 0° plies were dropped leaving a 16-ply quasi-isotropic $[\pm 45/0/90]_{2s}$ layup in the thin section. The thick portion is 2.79 mm (0.11 in.) thick and the thin portion is 2.24 mm (0.088 in.) thick. Each ply was modeled with one element through the thickness with the exception of the two adjacent 90° plies which were modeled together by a single element through the thickness. The portion of the mesh used to model the transition region is shown in Fig. 5.20.

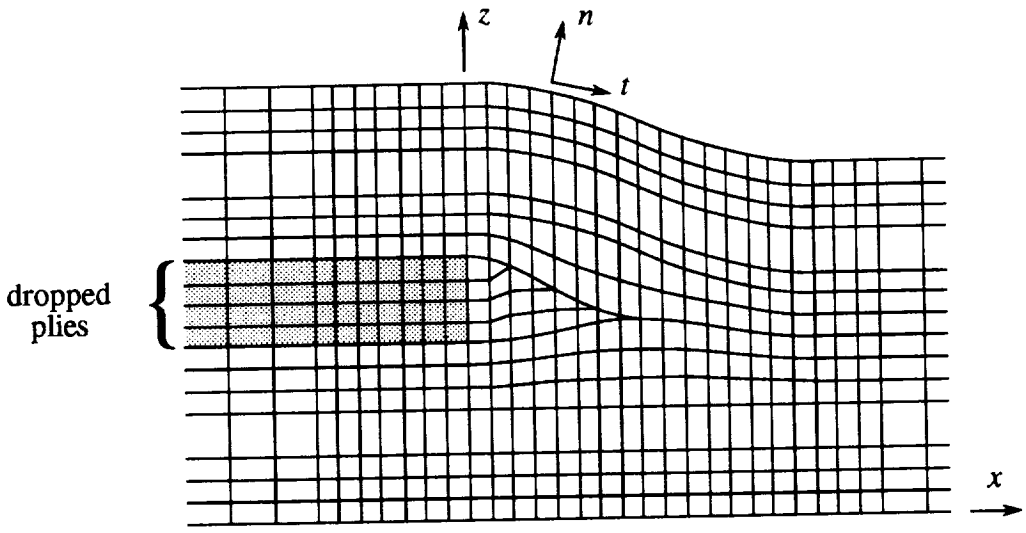

Fig. 5.20 Finite element mesh for the dropped-ply laminate modeled in Ref. 21.

This laminate was modeled with six mathematical layers as shown in Fig. 5.21. The two middle layers are given the material properties of 0° plies up to the drop after which they are treated as resin. While the two outer sublaminates appear to rejoin in Fig. 5.21, they are actually separated by the two thin resin layers, each 6.35 μm (0.00025 in.) thick, still present in the model. Note that the layers closer to the stress concentration are thinner than the top and bottom layers. The layups for the four continuous layers are, from bottom to top, $[\pm 45/0/90_2/0]$, $[\mp 45]$, $[\pm 45]$ and $[0/90_2/0/\mp 45]$. These layers, being composed of multiple plies of different orientations, are replaced by a single layer with effective compliances found using the homogenization procedure described in Sec. 5.2.2 and Appendix A.

The finite element model contained 2,905 nodes with three degrees of freedom per node for a total of 8,715 degrees of freedom. The six layer model was solved with 58 finite difference mesh points for a total of 8,004 degrees of freedom. No comparison is made in computation time because the two models were solved on different machines. However, because of the high cost of computing the difference equations using the two-stage Gauss scheme and the use of a banded matrix solver rather than a more efficient skyline solver for the six layer model, it is estimated that the six layer model would require at least twice as much time.

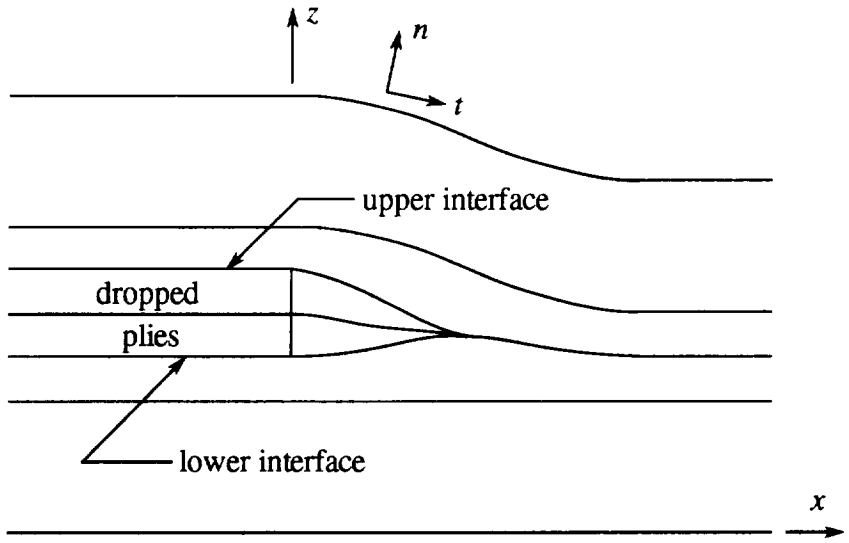

Fig. 5.21 Ply drop-off as modeled using present analysis.

The material properties for the individual plies are those of AS4/3502 graphite/epoxy:

$$E_{11} = 128\ \text{GPa} \quad (18.5\ \text{Msi}), \qquad E_{22} = E_{33} = 11.3\ \text{GPa} \quad (1.64\ \text{Msi})$$
$$G_{12} = G_{13} = 6.0\ \text{GPa} \quad (0.87\ \text{Msi}), \qquad G_{23} = 3.38\ \text{GPa} \quad (0.49\ \text{Msi})$$
$$\nu_{12} = \nu_{13} = 0.3, \quad \nu_{23} = 0.35$$

and for the neat resin:

$$E = 3.45\ \text{GPa} \quad (0.5\ \text{Msi})$$
$$\nu = 0.41$$

The loading for the case presented is uniaxial compression and the results are normalized by the average normal stress in the x-direction in the thin section of the laminate, denoted by σ_{app}. The boundary conditions at the ends are displacement prescribed conditions derived from a plate analysis of the test specimen.

The results of the analysis are shown in Figs. 5.22 through 5.25 and are taken along contours passing through the Gauss points of the finite element analysis. The terms lower and upper interface refer to the interfaces between the four 0° plies and the quasi-isotropic sublaminates. The stresses for the lower interface are taken along the contour passing through the Gauss points at the top of the elements modeling the 45° lamina just below the four 0° plies. The stresses for the upper interface are taken along the contour passing through the Gauss points at the bottom of the elements modeling the 45° lamina just above the four 0° plies. The stresses are taken at the Gauss points in order to obtain the most

accurate values from the finite element analysis. The *t–n* notation refers to contour following coordinates with *n* normal to the contour and *l* tangent to it. The positive senses for them are shown in Figs. 5.20 and 5.21. The longitudinal location in these plots is normalized by the thickness of the four dropped plies, denoted by t_d (t_d = 0.5588 mm in this example).

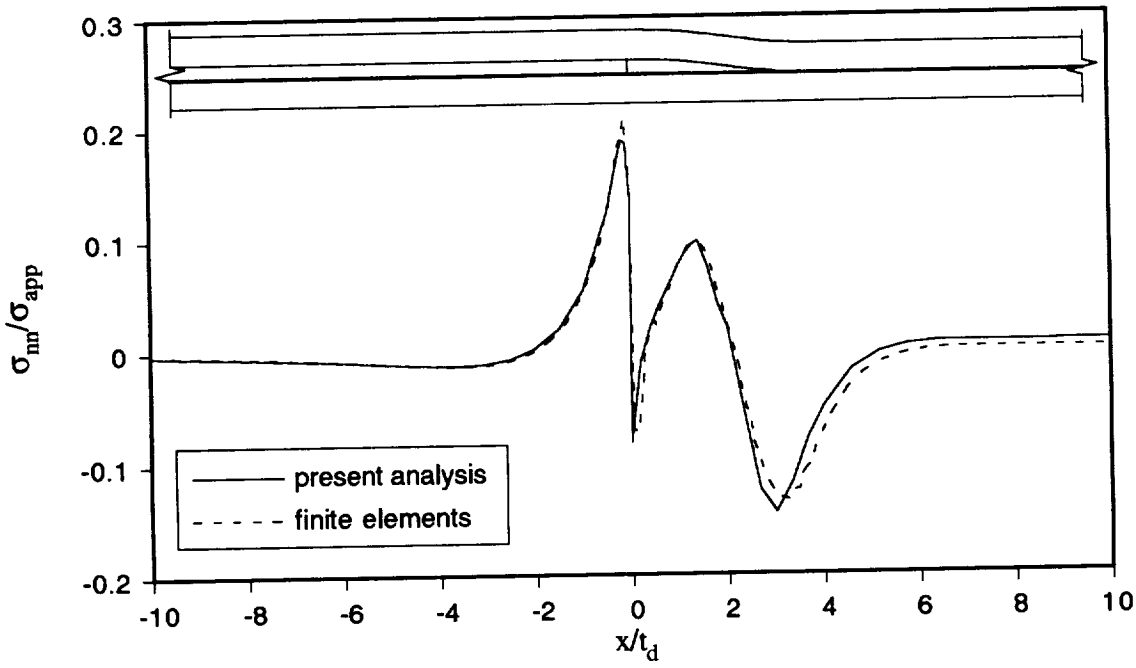

Fig. 5.22 Comparison to finite element model of Ref. 21 for σ_{nn} along lower interface.

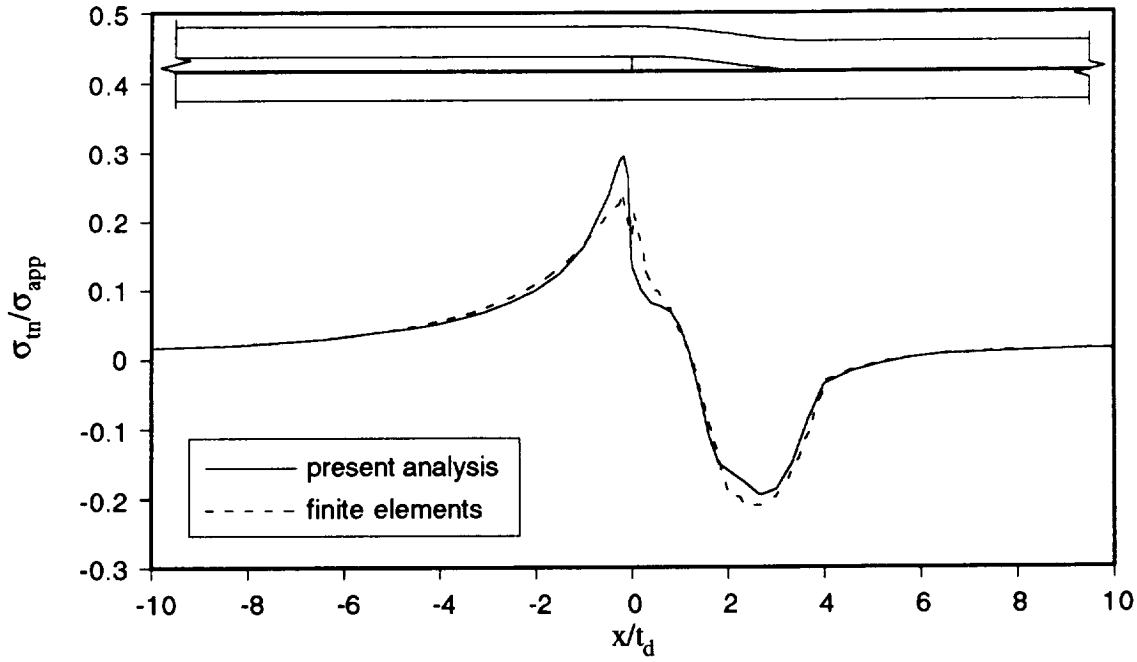

Fig. 5.23 Comparison to finite element model of Ref. 21 for σ_{tn} along lower interface.

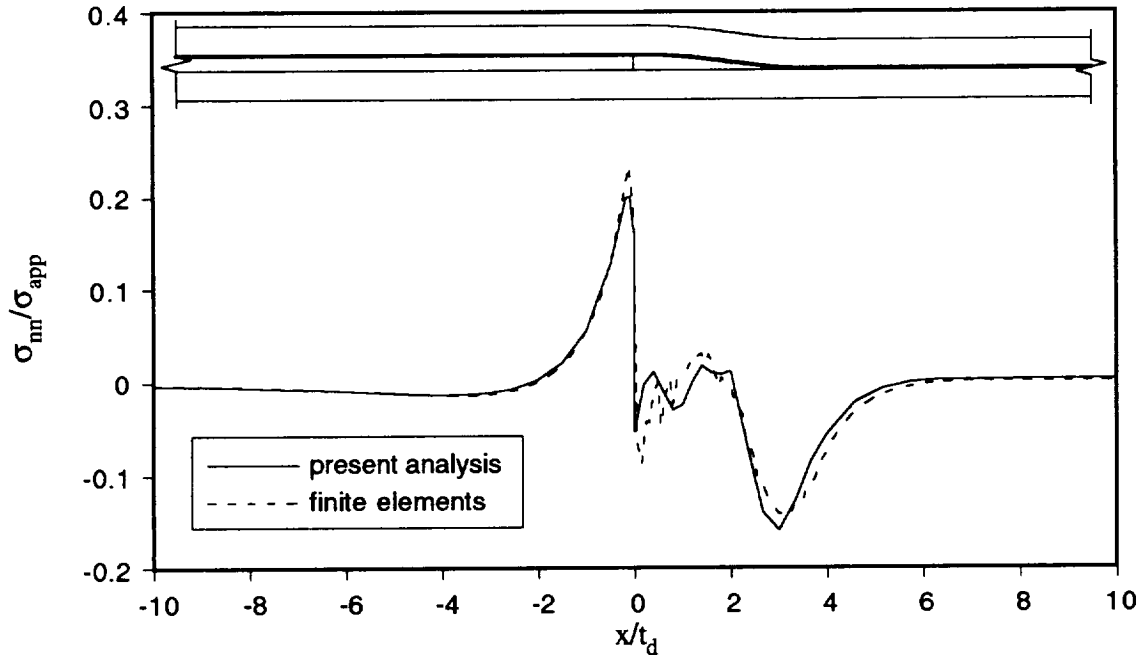

Fig. 5.24 Comparison to finite element model of Ref. 21 for σ_{nn} along upper interface.

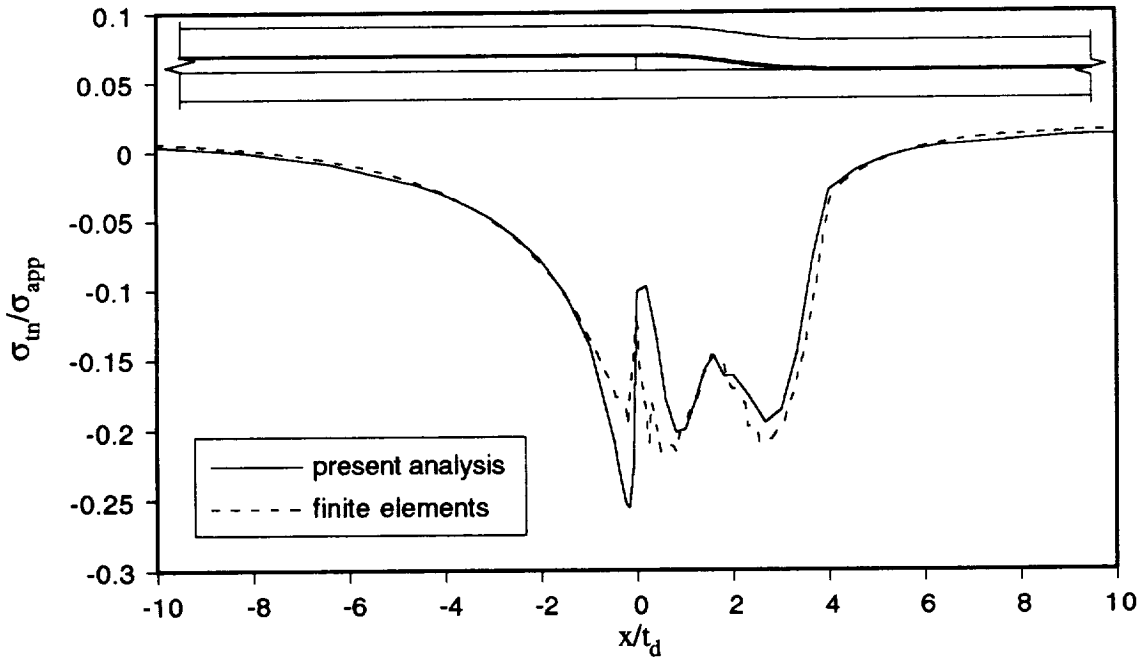

Fig. 5.25 Comparison to finite element model of Ref. 21 for σ_m along upper interface.

It is clear from Figs. 5.22–5.25 that the stresses predicted by the two approaches are in good agreement. While the two analyses do not agree as well as those in the previous section, this is understandable due to the coarseness of the finite element mesh used by Curry et al.[21]

Chapter 6: Parametric Studies

Having established the accuracy of the generalized plane deformation model, this chapter presents the results of parametric studies of dropped-ply laminates. A series of parametric studies were performed in order to examine the effects that various factors have on the stress concentration, and hence the potential for a reduction in strength, of laminates with dropped internal plies. The major factors that are felt to contribute to the stress concentration in an asymmetric dropped-ply laminate are the eccentricity of the middle surface through the ply drop-off and the magnitude of the stiffness discontinuity.

The effect of eccentricity is examined first as its effect on the stresses can easily be isolated by using the same layups for varying amounts of eccentricity. The magnitude of the stiffness discontinuity for a laminate composed of one fiber/matrix combination, on the other hand, cannot be changed without also changing the orientation of plies or the relative thickness between the continuous and dropped sublaminates. Rather than altering the geometry of the transition region by changing the number of dropped plies, the approach of altering the orientation of the dropped plies was chosen. Finally, the effect of the inclusion of a soft insert ahead of stiff dropped plies was evaluated.

6.1 Effect of Eccentricity of the Middle Surface

When a laminate contains an asymmetric ply drop-off, the middle surface is not a straight line (in the plane of the cross section) but instead contains an offset at the drop-off. This eccentricity in the middle surface would appear to be a factor in the strength degradation that a ply drop-off can cause in a laminate due to the bending or twisting

moment that may be induced. This study was done to determine the effect that this eccentricity has on the interlaminar stresses present at a ply drop-off.

Two geometries of ply drop-offs are compared, one that is asymmetric and therefore has an eccentric middle surface, and the other that is symmetric with no eccentricity (see Fig. 6.1). These two geometries were examined with three different layups for the dropped plies and under three different loadings for a total of eighteen different cases.

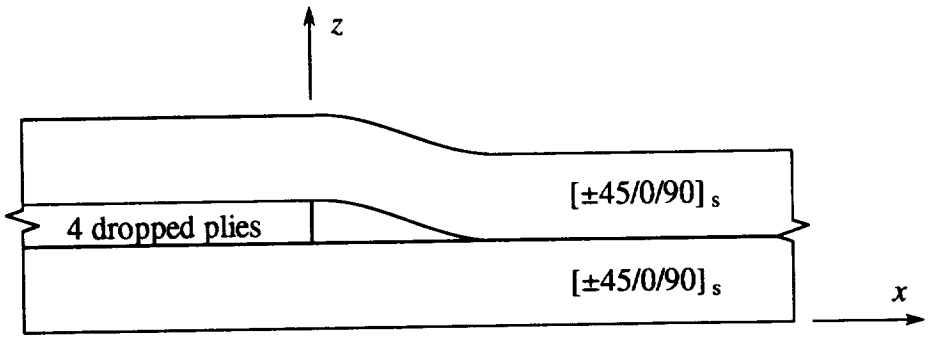

(a) With eccentricity.

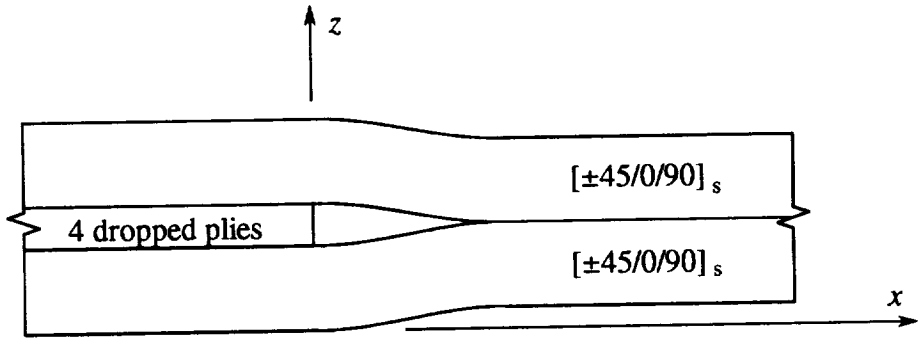

(b) Without eccentricity.

Fig. 6.1 Laminates with and without eccentricity in the middle surface.

In each case, the two continuous sublaminates have the same eight ply quasi-isotropic $[\pm 45 / 0 / 90]_s$ layup. The dropped sublaminate contains four plies with the layups $[0_4]_T$, $[90_4]_T$, or $[\pm 45]_s$. The material properties used are those for AS4/3502 graphite/epoxy and are given in Sec. 5.5.2. Each ply has thickness 0.1395 mm (0.0055 in.) giving a thickness of 0.558 mm (0.022 in.) for the dropped plies, 2.794 mm (0.110 in.) for the thick portion, and 2.248 mm (0.0885 in.) for the thin, which also contains a 0.0127 mm (0.0005 in.) thick resin layer between the continuous sublaminates. The eccentricity is, therefore, either zero or 0.273 mm (two ply thicknesses minus half the resin layer thickness). The length of

the thick and thin portions is 25.4 mm (1.0 in.) for each and the transition section is 2.24 mm (0.088 in.) long for a total laminate length of 53.04 mm (2.088 in.). The origin of the coordinate system for the study is located in the plane of the bottom of the thick portion of the laminate at the end of the dropped plies, i.e. the beginning of the thickness taper (see Fig. 6.1).

The model used in this analysis consists of six mathematical layers with the same distribution as those used in Sec. 5.5.2. That is, in moving from one surface to the other of the thick section, the layers are $[\pm 45 / 0 / 90_2 / 0]$, $[\mp 45]$, $[\pm\theta]$, $[\mp\theta]$, and $[0 / 90_2 / 0 / \mp 45]$. From the drop into the thin section, the central two layers are modeled as resin except for the 90° case. Experience in manufacturing specimens with 90° dropped plies has shown that these fibers tend to migrate into the area occupied by resin in the $[0_4]_T$ and $[\pm 45]_s$ layups. For this case, the triangular shaped resin region is modeled as 90° material with the origin remaining at the thick end of the taper.

The three loading cases are longitudinal compression (along the x-axis), transverse tension (along the y-axis), and shear in the x-y plane. The surfaces of the laminates are considered to be traction-free in all three cases. The boundary conditions at the left (thick) end ($x = -25.4$ mm) are also the same in all three cases, with $u = 0$, $v = 0$, and $\tau_z = 0$. These conditions were chosen to avoid a boundary layer at the end by simulating conditions at a far field location. Each laminate is constrained from rigid body translation in the z-direction through the prescription of $w = 0$ at the lower surface of a very short (0.254 mm) segment at the left end. The other rigid body modes are excluded through the displacement boundary conditions. The longitudinal compression and in-plane shear loads are applied through prescription of N_x and N_{xy} respectively at the right end ($x = 27.64$ mm), while restraining the u displacement to a uniform value through the thickness. The transverse tension load is applied through prescription of the uniform strain ε_y out of plane deformation allowed for by the generalized plane deformation formulation, i.e. C of Eqs. (3-1) and (3-2) is prescribed. The boundary conditions and out of plane deformations used for all three loading cases are presented fully in Table 6.1. It is worth noting that the conditions applied on the upper and lower surfaces of the laminates are not boundary conditions in that they are actually applied over the entire one dimensional mathematical domain and are therefore part of the field equations.

Table 6.1 Boundary conditions and out of plane deformations for eccentricity study.

Load Case	BCs at $x = -25.4$ mm	BCs at $x = 27.64$ mm	Out of Plane Defs.
longitudinal compression	$u = 0.0$ $v = 0.0$ $\tau_z = 0.0$	$N_x = -1$ kN / m u = uniform $v = 0.0$ $\tau_z = 0.0$	$A = 0.0$ $B = 0.0$ $C = 0.0$ $\theta = 0.0$
transverse tension	$u = 0.0$ $v = 0.0$ $\tau_z = 0.0$	$N_x = 0.0$ u = uniform $v = 0.0$ $\tau_z = 0.0$	$A = 0.0$ $B = 0.0$ $C = 0.001$ $\theta = 0.0$
in-plane shear	$u = 0.0$ $v = 0.0$ $\tau_z = 0.0$	$N_x = 0.0$ u = uniform $N_{xy} = 1$ kN / m v = uniform $\tau_z = 0.0$	$A = 0.0$ $B = 0.0$ $C = 0.0$ $\theta = 0.0$

A brief note is in order to explain the x-direction conditions at $x = 27.64$ mm for all three load cases as well as the y-direction condition for the shear loading case. The combination of a uniform u or v displacement and N_x or N_{xy} prescription was achieved as follows. The x-direction boundary conditions of Eq. (3-52) require $2N$ equations for the $\sigma_{11}^{(k)}$, $\sigma_{12}^{(k)}$, $\overline{U}^{(k)}$, and $\breve{U}^{(k)}$ unknowns. Constraining the u displacement to a uniform value through the thickness, $\tilde{U}$, gives the expressions for the weighted displacements

$$\begin{aligned} \overline{U}^{(k)} &= 1/2\,\tilde{U} \\ \breve{U}^{(k)} &= 1/2\,\tilde{U} \end{aligned} \qquad k = 1 \rightarrow N \tag{6-1}$$

from Eq. (3-14). Elimination of $\tilde{U}$ from these $2N$ equations leaves the $2N$–1 equations

$$\begin{aligned} \overline{U}^{(k)} &= \breve{U}^{(k)} && k = 1 \rightarrow N \\ \breve{U}^{(k)} &= \overline{U}^{(k+1)} && k = 1 \rightarrow N-1 \end{aligned} \tag{6-2}$$

The final equation is obtained through the definition for N_x,

$$N_x = \int_{z_0}^{z_N} \sigma_{xx}\, dz \tag{6-3}$$

which, when integrated through the thickness, leaves

$$1/2\sum_{k=1}^{N}\left(\sigma_{11}^{(k)}+\sigma_{12}^{(k)}\right)\left(z_k-z_{k-1}\right)=\tilde{N}_x \tag{6-4}$$

due to the linearity of σ_{xx} within layers. The tilde, as usual, indicates the prescribed value of N_x. The same procedure was used in the y-direction for $\bar{V}^{(k)}$, $\tilde{V}^{(k)}$, $\sigma_{61}^{(k)}$, and $\sigma_{62}^{(k)}$ in terms of $\tilde{N}_{xy}$.

Since the primary focus of this study is the effect of eccentricity on the tendency of laminates with dropped plies to delaminate, a measure of this tendency is necessary. Rather than looking at each interlaminar stress component separately, it is desirable to have an index that accounts for the combined effect of the different components. An index similar to the Quadratic Delamination Criterion proposed by Brewer and Lagace[29] was chosen. This delamination index is defined as

$$F=\left(\frac{\sigma_{zn}}{Z^{S1}}\right)^2+\left(\frac{\sigma_{yn}}{Z^{S2}}\right)^2+\left(\frac{\sigma_{nn}}{Z^{T}}\right)^2 \tag{6-5}$$

where Z^{S1}, Z^{S2}, and Z^T are the allowable interlaminar stresses. For AS4/3502, they are

$$Z^{S1}=Z^{S2}=93.08 \text{ MPa (13.5 ksi)}$$
$$Z^{T}=51.99 \text{ MPa (7.54 ksi)}$$

The onset of delamination is likely to occur when $F \geq 1$. However, $F = 0.5$ does not correspond to half of the delamination load for a linear analysis due to the quadratic nature of the index. Therefore, it was decided to examine the distribution of $\sqrt{F}$, which will be referred to as the delamination fraction. For a proportional loading, a base load resulting in a maximum value of $\sqrt{F}$ can be increased by the factor $1/\sqrt{F}$ before delamination initiates. Hence, the larger the value of $\sqrt{F}$, the more likely delamination is to occur.

The delamination fraction was examined along the two critical interfaces, i.e. the top of the lower continuous sublaminate and the bottom of the upper continuous sublaminate. These two interfaces will be referred to as the lower and upper interfaces respectively. For the non-eccentric cases, the distribution of $\sqrt{F}$ is the same for the two interfaces due to symmetry.

Results for the case of four 0° plies dropped from the laminate and subjected to longitudinal compression are presented here. Figs. 6.2 and 6.3 reveal that eccentricity has essentially no effect on the peak value of $\sqrt{F}$ along either interface for this case (t_d is once again the thickness of the dropped plies). There is a significant difference in the

interlaminar stresses in the transition region ($0 < x / t_d < 4$), however these stresses are well below the peak values at the end of the dropped plies and are therefore not considered critical.

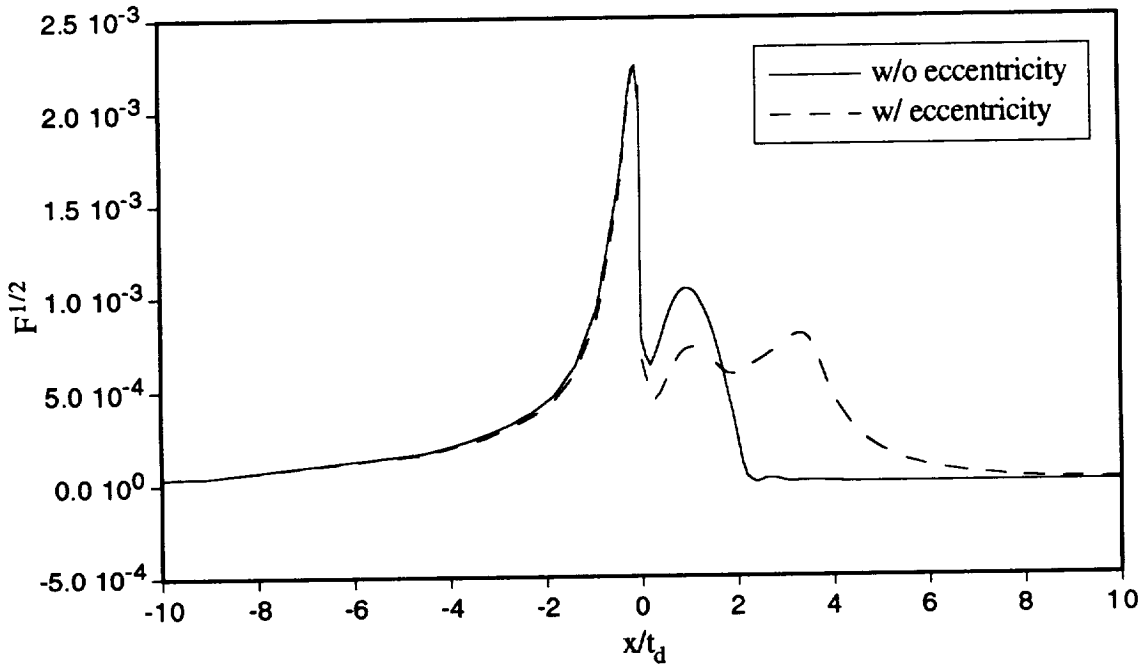

Fig. 6.2 Delamination fraction along the lower interface for four 0° plies dropped loaded in longitudinal compression.

It is informative to examine the interlaminar stress components separately to determine what each one is contributing to the delamination fraction. Figs. 6.4 and 6.5 show the distribution of σ_{nn} and σ_{tn} (σ_{yn} is approximately zero) along the upper interface (This loading represent an average compressive σ_{xx} stress in the thin section of the laminate of 445 kPa.) The maximum value of the delamination fraction coincides with the maximum values of both the interlaminar normal and shear stresses, which also are not significantly influenced by eccentricity. This indicates that for this layup and loading, the stiffness discontinuity influences the interlaminar stresses much more than the eccentricity. As for the relative contribution of the two stress components, the peak interlaminar normal tensile value of 97 kPa is 0.18% of Z^T while the peak interlaminar shear is –150 kPa, or 0.16% of Z^{SI}. This suggests that these components will have a comparable influence on the delamination of these laminates.

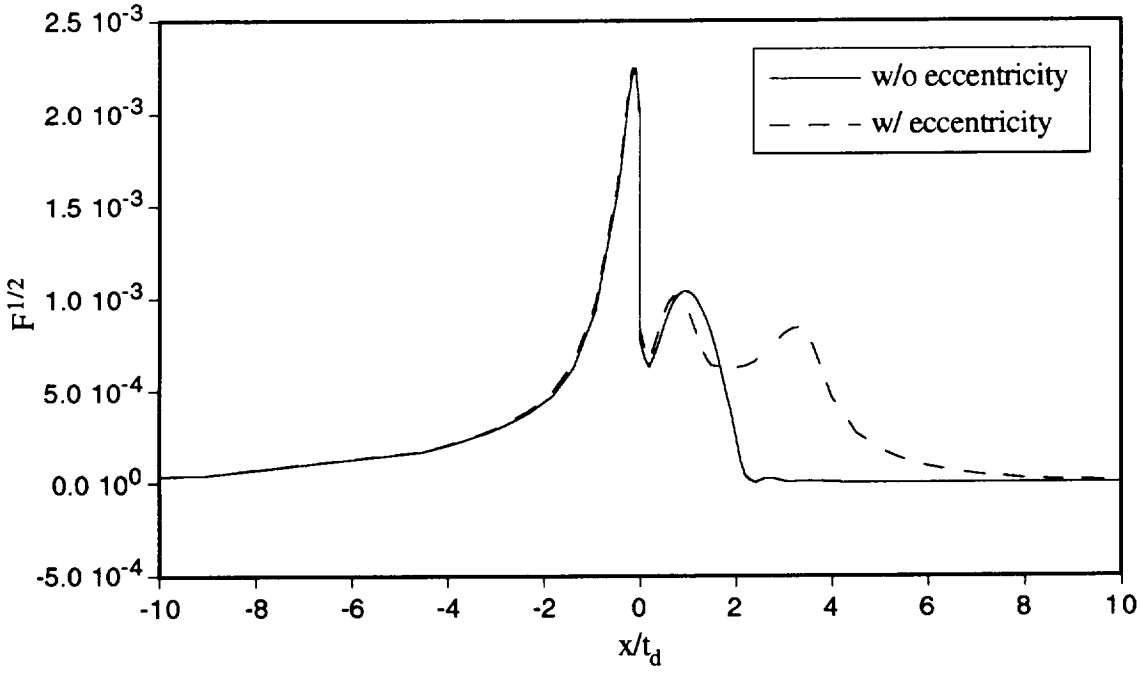

Fig. 6.3 Delamination fraction along the upper interface for four 0° plies dropped loaded in longitudinal compression.

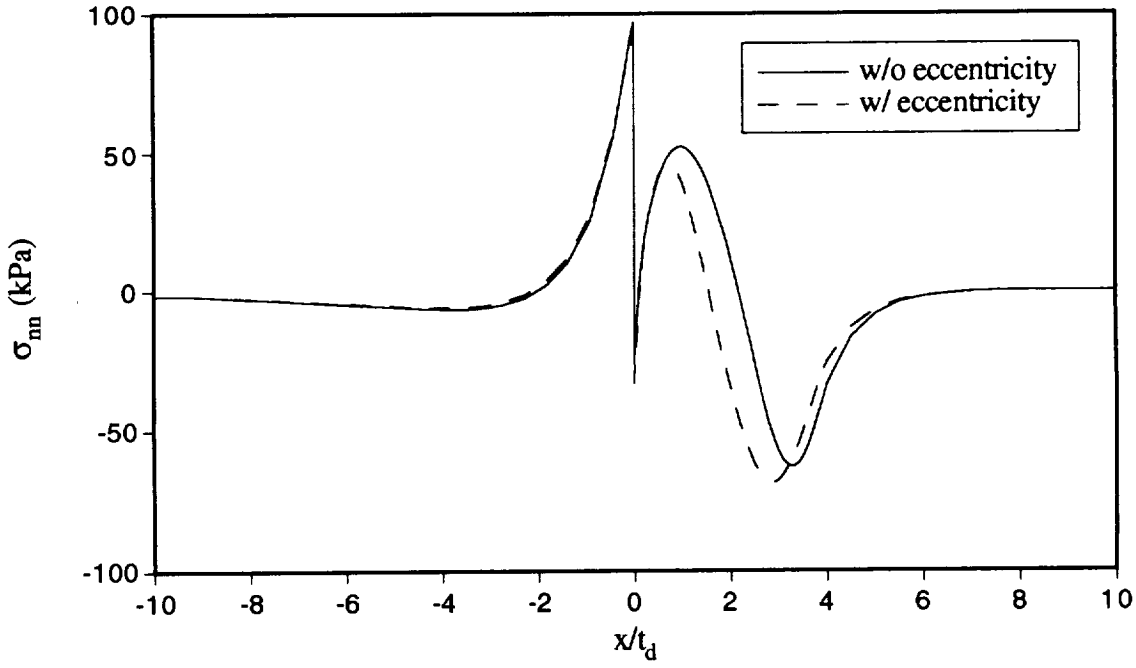

Fig. 6.4 σ_{nn} along the upper interface for four 0° plies dropped loaded in longitudinal compression.

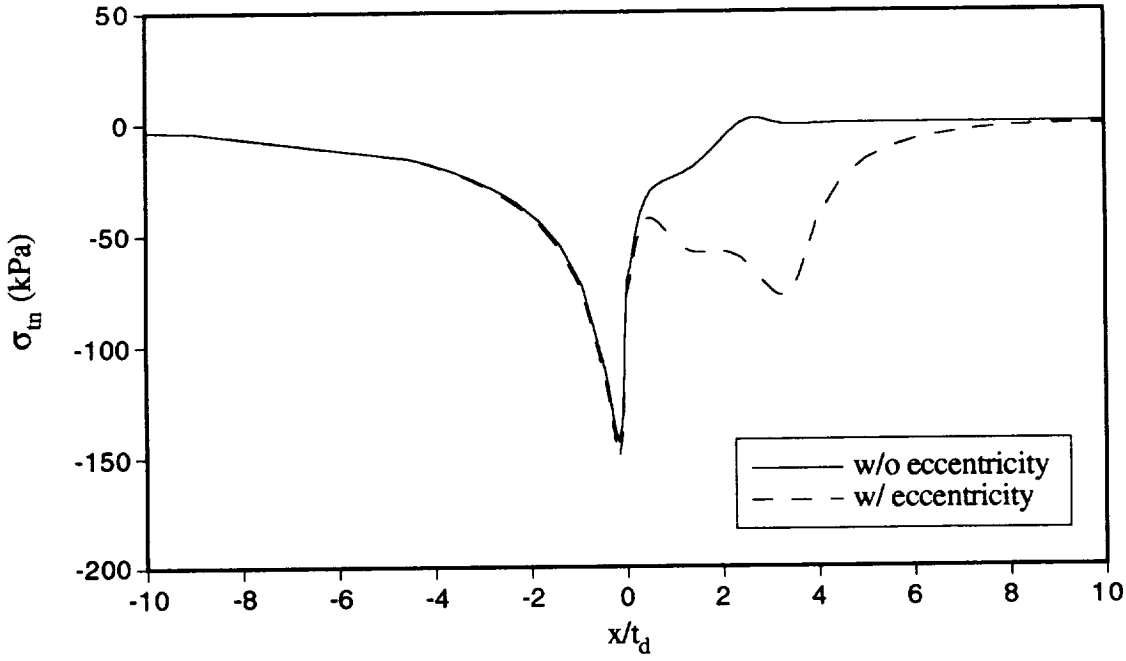

Fig. 6.5 σ_{tn} along the upper interface for four 0° plies dropped loaded in longitudinal compression.

Up until about $x = 2t_d$, the delamination fraction along the upper interface is very similar for the eccentric and non-eccentric cases. Each has a maximum at $x = 0$ with a second peak at about $x = t_d$ (the plots of the interlaminar stresses show that this second peak is caused by a second peak in the tensile interlaminar normal stress). The plots of the interlaminar stresses also closely agree up until about $x = t_d$. For $t_d < x < 2t_d$, the normal stress is less with eccentricity than without while the shear has a larger magnitude. These opposite trends tend to cancel leaving the failure fraction for the two cases in close agreement.

The delamination fraction is affected by the addition of eccentricity in the region $2t_d < x < 4t_d$ where an additional peak arises. Examination of Figs. 6.4 and 6.5 clearly reveals that this second peak is due to an increase in the interlaminar shear stress in that region. A plot of the bending moment resultant in Fig. 6.6 shows a reversal in the bending moment through the transition region for the case with eccentricity (there is no bending moment for the case without eccentricity). This reversal in bending moment introduces the additional negative shear that produces the additional peak in the delamination fraction. While this additional peak is an interesting consequence of the presence of eccentricity, its

magnitude is still slightly less than the peak in the transition region that occurs without eccentricity and much less than the maximum that is located at the end of the dropped plies.

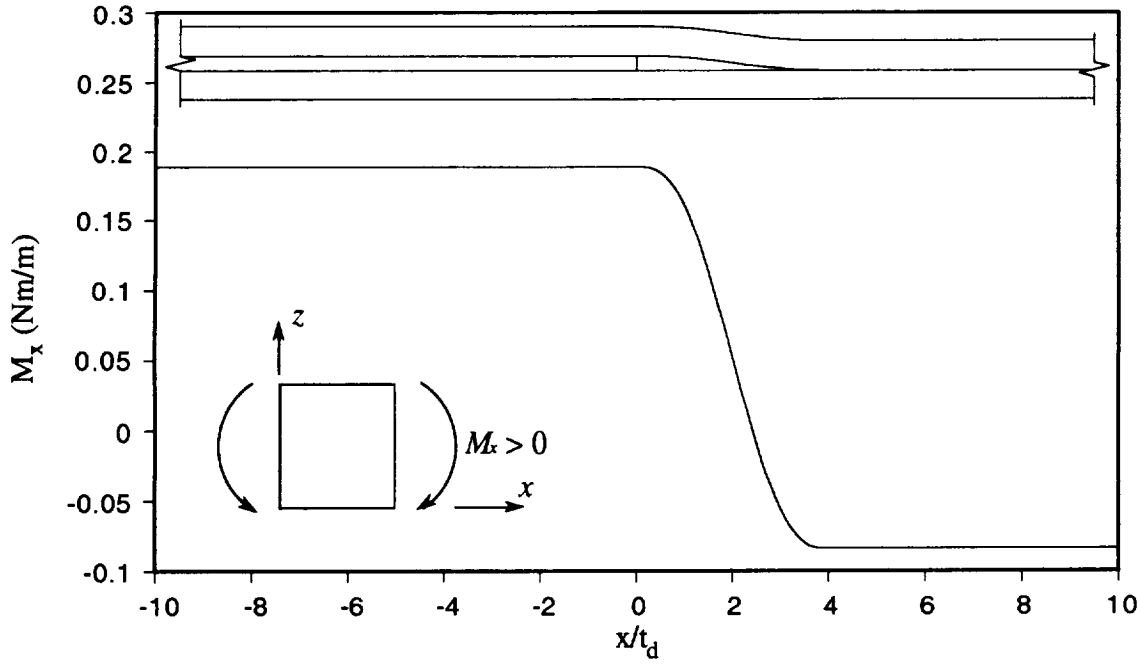

Fig. 6.6 M_x distribution for four 0° plies dropped loaded in longitudinal compression, with eccentricity.

The results for all of the load cases and layups are presented in Table 6.2. The values of $\sqrt{F}$ for load case b, transverse tension applied through prescription of ε_y, are scaled such that they correspond to $N_y = 1$ kN / m in the thin section. This was done in order to make the values of $\sqrt{F}$ correspond to comparable loads between the different load cases.

For the longitudinal compression loading, the $[90_4]_T$ dropped layup experiences the largest change in the delamination fraction due to eccentricity, a 15% increase from 1.22×10^{-3} to 1.4×10^{-3}. However, experimental results presented by Curry et al.[21] indicate that this configuration does not tend to fail by delamination under longitudinal compression. This layup having the smallest change in longitudinal stiffness and also the smallest values of $\sqrt{F}$ again indicates the larger role that the stiffness discontinuity plays in the delamination of dropped-ply laminates. The third layup ($[\pm45]_s$ dropped) loaded in longitudinal compression only experiences an increase of 3% in $\sqrt{F}$.

Table 6.2 Results for eccentricity study (t_{thin} is the thickness of the thin section).

Load Case	Layup	Eccentricity	Peak $\sqrt{F}$	x-location	Interface
$N_x = -1$ kN/m	$[0_4]_T$	0.0	2.25×10^{-3}	$-0.077t_d$	both
		$0.121t_{thin}$	2.25×10^{-3}	$-0.077t_d$	both
	$[90_4]_T$	0.0	1.22×10^{-3}	$0.80t_d$	both
		$0.121t_{thin}$	1.40×10^{-3}	$0.60t_d$	upper
	$[\pm45]_s$	0.0	1.63×10^{-3}	$-0.077t_d$	both
		$0.121t_{thin}$	1.68×10^{-3}	0.0	lower
$\varepsilon_y = 0.001$	$[0_4]_T$	0.0	0.54×10^{-3}	$-0.15t_d$	both
		$0.121t_{thin}$	0.56×10^{-3}	$-0.15t_d$	upper
	$[90_4]_T$	0.0	0.09×10^{-3}	$3.20t_d$	both
		$0.121t_{thin}$	0.10×10^{-3}	$3.20t_d$	upper
	$[\pm45]_s$	0.0	0.42×10^{-3}	0.0	both
		$0.121t_{thin}$	0.45×10^{-3}	0.0	lower
$N_{xy} = 1$ kN/m	$[0_4]_T$	0.0	1.14×10^{-3}	0.0	both
		$0.121t_{thin}$	1.21×10^{-3}	0.0	lower
	$[90_4]_T$	0.0	0.31×10^{-3}	$2.10t_d$	both
		$0.121t_{thin}$	0.51×10^{-3}	$2.30t_d$	upper
	$[\pm45]_s$	0.0	3.54×10^{-3}	0.0	both
		$0.121t_{thin}$	3.65×10^{-3}	0.0	lower

The values of $\sqrt{F}$ for the transverse tension loading are all well below the values for the $[90_4]_T$ dropped layup loaded in longitudinal compression, which again are below that required for a delamination failure at this level of load. Therefore, none of these three layups subjected to transverse tension would be expected to delaminate. Even so, eccentricity at most produces an increase in $\sqrt{F}$ of 11% for layup 2.

The shear loaded case also has its largest increase in $\sqrt{F}$ due to eccentricity occurring for the $[90_4]_T$ drop. This is also the case with the smallest value for the delamination fraction, too small to induce a delamination failure. The $[\pm45]_s$ drop layup, the stiffest with respect to shear, has the largest values of $\sqrt{F}$ for any of the cases, 3.65×10^{-3} for the eccentric laminate. However, this represents an increase of only 3% over the non-eccentric case.

Therefore, it appears that eccentricity does not significantly affect these laminates ability to resist delamination initiation when loaded by longitudinal compression, transverse tension, or in-plane shear. This does not imply that these laminates will not delaminate. Only that the presence of eccentricity of the middle surface does not appear to make this mode of failure more likely than for laminates without eccentricity.

6.2 Effect of the Magnitude of the Stiffness Discontinuity

Clearly, the results of the study examining the effect of the eccentricity of the ply drop-off indicate that the stiffness discontinuity has a much greater influence on the magnitude of the interlaminar stresses than the eccentricity of the dropoff. The purpose of the present study is to examine the relationship between the stiffness of the dropped plies and the resulting interlaminar stresses.

The geometry of the laminate examined is the same as the eccentric dropped-ply laminate of the eccentricity study and is shown in Fig. 6.7. Four plies are dropped from between two eight ply quasi-isotropic $[\pm 45 / 0 / 90]_s$ sublaminates with the bottom surface of the laminate flat. The stiffness of the four dropped plies is varied by altering the angle θ in the balanced angle-ply layup $[\pm\theta]_s$. Five orientations for the angle θ were examined: 0°, 30°, 45°, 60°, and 90°. These layups were subjected to longitudinal compression and in-plane shear loadings for a total of ten different cases. The transverse tension loading examined in the eccentricity study was not repeated here because of the relatively low interlaminar stresses found for that loading.

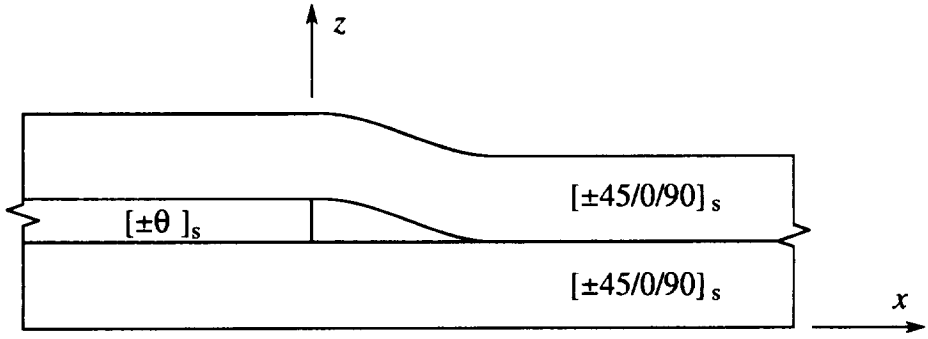

Fig. 6.7 Laminate used to examine effect of the stiffness of the dropped plies on the interlaminar stresses.

The material properties used are again those of AS4/3502 graphite/epoxy given in Sec. 5.5.2. The dimensions of the laminate and the discretization used in modeling it are the same as those of the eccentricity study. The modeling of the $\theta = 90^\circ$ case, however, does represent a change worth noting. In the eccentricity study, the 90° fibers were assumed to migrate into the region occupied by resin for the other orientations. The present study, being more interested in determining the effect of the magnitude of the stiffness discontinuity, uses the same location for the material discontinuity ($x = 0$) for $\theta = 90^\circ$ as the other layups for the sake of consistency and retains the triangular shaped resin region. The surface conditions are again traction free and the boundary conditions are the same as those given in Table 6.1 for the longitudinal compression and in-plane shear loadings of the eccentricity study.

The measure of the severity of the interlaminar stresses used in evaluating these layups remains the delamination fraction ($\sqrt{F}$). Figs. 6.8 through 6.11 are plots of the distribution of $\sqrt{F}$ for the two loading cases. As in the eccentricity study, the lower and upper interfaces referred to are the interfaces between the dropped plies and the lower and upper continuous sublaminates, respectively.

Figs. 6.8 and 6.9 show the distribution of the delamination fraction for the five different dropped-ply layups along the lower and upper interfaces for the longitudinal compression load case. Clearly, the peak value of the delamination fraction increases with increasing dropped sublaminate longitudinal stiffness, as expected. In addition, the decay length into the thick section required for the induced interlaminar stresses to vanish also increases. The interlaminar stresses within the transition region ($0 \le x/t_d \le 4$) do not vary significantly with the stiffness of the dropped plies.

Similar results are obtained for the in-plane shear loaded case shown in Figs. 6.10 and 6.11 with the in-plane shear stiffness of the dropped plies as the major factor influencing the magnitude of $\sqrt{F}$. That is, the $\theta = 45^\circ$ case has the largest peak in $\sqrt{F}$ as well as the greatest in-plane shear stiffness. As the value of θ increases or decreases from 45°, the in-plane stiffness of the dropped plies decreases as does the peak $\sqrt{F}$. An interesting difference between the response under in-plane shear and longitudinal compression loadings is that the decay length the interlaminar stresses is shorter for the shear loading.

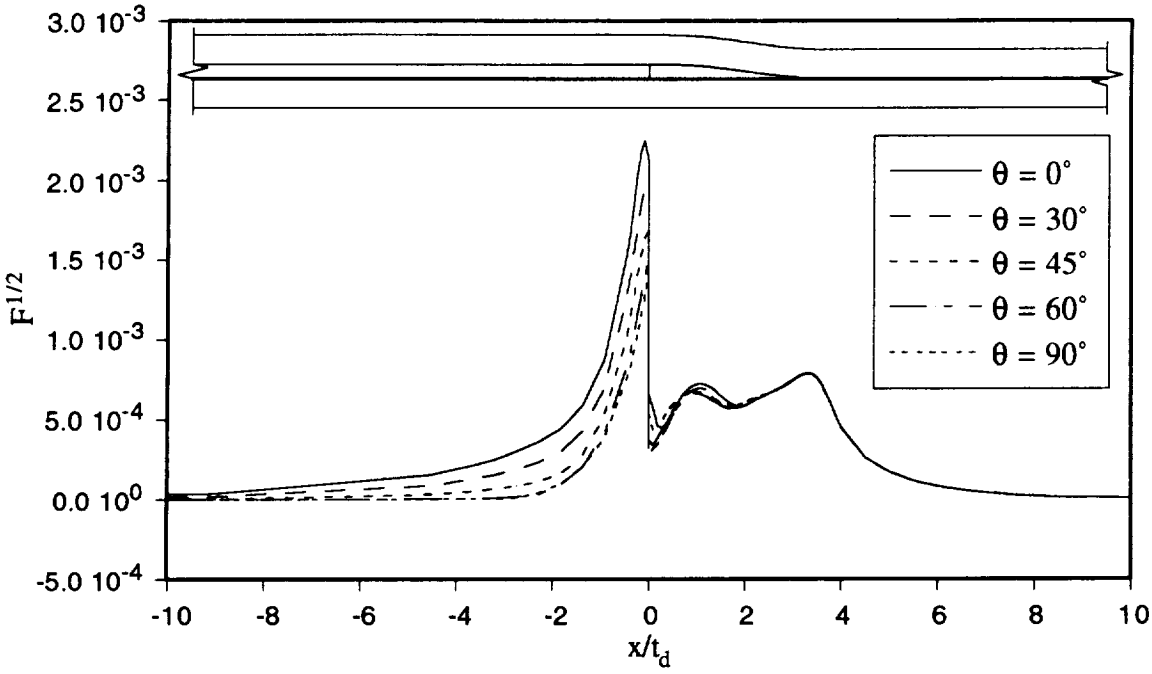

Fig. 6.8 Delamination fraction along the lower interface for different values of θ of the dropped sublaminate $[\pm\theta]_s$ (longitudinal compression loading).

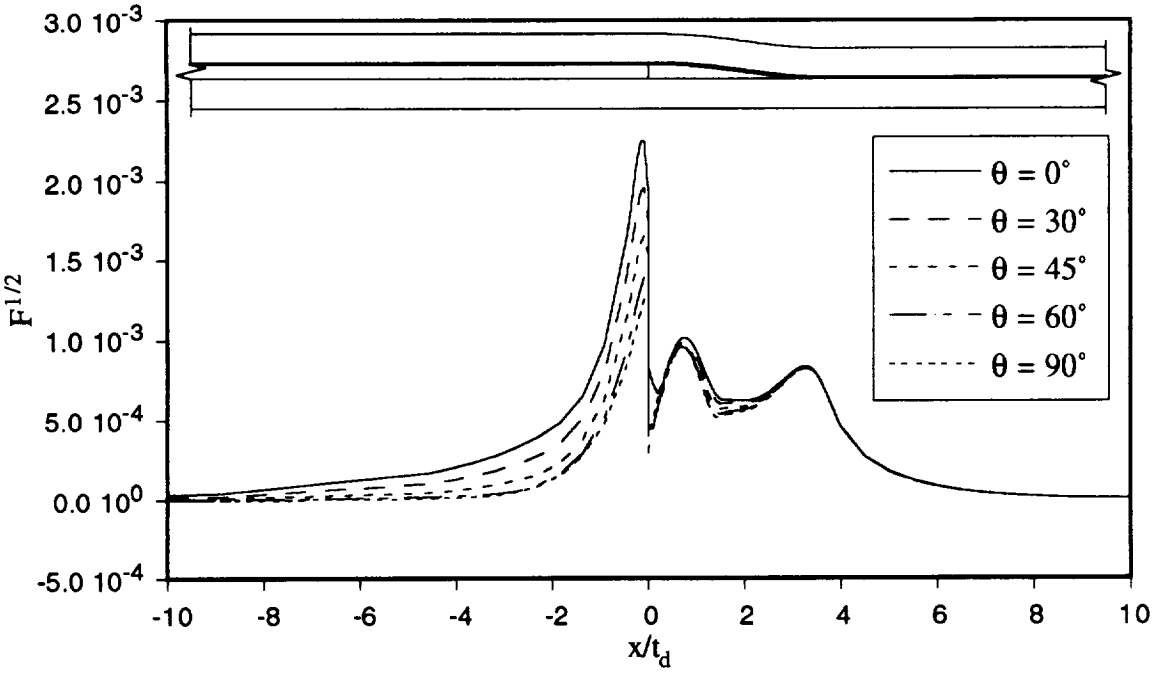

Fig. 6.9 Delamination fraction along the upper interface for different values of θ of the dropped sublaminate $[\pm\theta]_s$ (longitudinal compression loading).

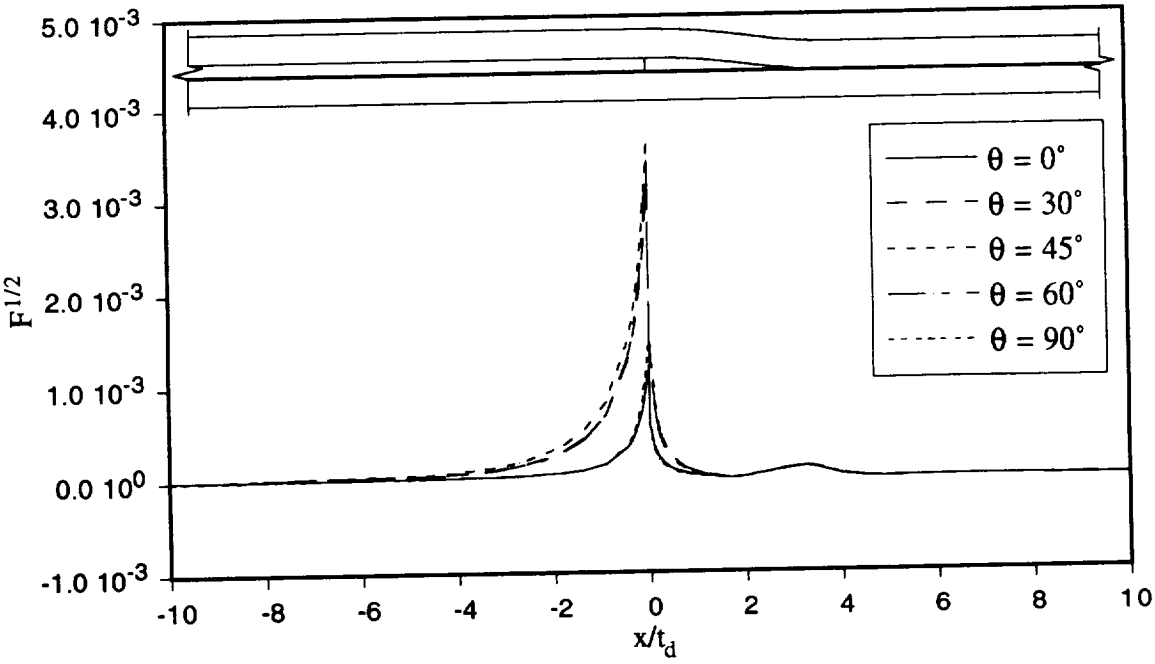

Fig. 6.10 Delamination fraction along the lower interface for different values of θ of the dropped sublaminate $[\pm\theta]_s$ (in-plane shear loading).

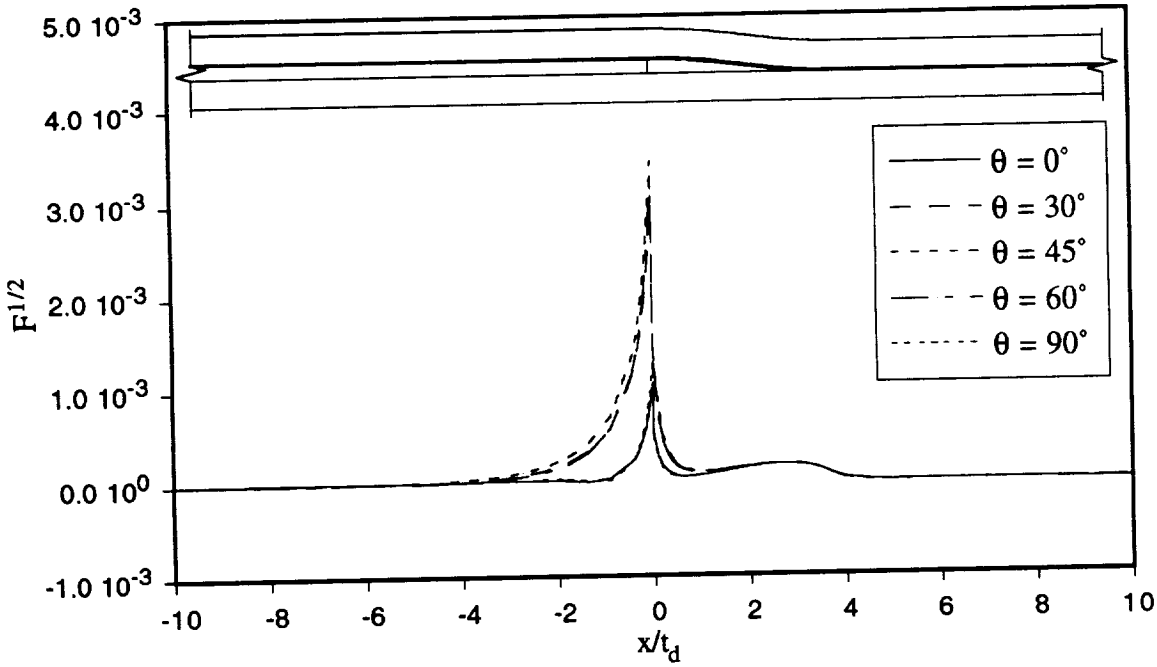

Fig. 6.11 Delamination fraction along the upper interface for different values of θ of the dropped sublaminate $[\pm\theta]_s$ (in-plane shear loading).

The numerical values for the peak delamination fraction in each of the cases as well as the x-location and the interface where the peak value occurs is presented in Table 6.3.

Table 6.3 Results for study of the effect of stiffness of the dropped plies $\pm\theta$ (t_{thin} is the thickness of the thin section).

Load Case	θ	Peak $\sqrt{F}$	x-location	Interface
$N_x = -1$ kN/m	0°	2.25×10^{-3}	$-0.077t_d$	both
	30°	1.96×10^{-3}	$-0.077t_d$	upper
	45°	1.68×10^{-3}	0.0	lower
	60°	1.52×10^{-3}	0.0	lower
	90°	1.43×10^{-3}	0.0	lower
$N_{xy} = 1$ kN/m	0°	1.21×10^{-3}	0.0	lower
	30°	3.14×10^{-3}	0.0	lower
	45°	3.64×10^{-3}	0.0	lower
	60°	3.44×10^{-3}	0.0	lower
	90°	1.48×10^{-3}	0.0	lower

In Curry et al.[21], a good experimental correlation was found between the ratio of the longitudinal stiffness of the thick to the thin sections of a dropped-ply laminate and the compressive strength ratio of the thin section to the dropped-ply laminate (tested independently). Despite the fact that this correlation neglects the change in failure mode from that of the thin section (compressive strength failure) to that of the dropped-ply laminate (delamination), the agreement was very good. A similar approach is now taken in looking for correlation between the magnitude of the stiffness change and the interlaminar stresses introduced.

In Curry's examination of the effect of stiffness change, strain gage measurements were used to determine the average stiffness of the thick and thin sections of the laminate and a ratio of the two values was computed. The present study, being purely analytical, will rely on an estimation of this ratio based on classical lamination theory (CLT), which has already been shown to be in close agreement with the homogenization scheme implemented in these analyses for flat laminates. Since the loading in the present study consists of an applied N_x with ε_y constrained to zero through the prescription of the out of plane deformations, the stiffness coefficient from CLT of interest is A_{11}. That is, this loading can be thought of as an applied strain field of ε_x prescribed with $\varepsilon_y = 0$. Because

both symmetric angle-ply and quasi-isotropic laminates have zero shear-extension coupling terms A_{16} and A_{26}, no γ_{xy}° is induced and the applied N_x is related to ε_x° through the relation $N_x = A_{11}\varepsilon_x^{\circ}$ in CLT.

Rather than correlating the stiffness change to a measured failure load as did Curry et al., the present study will use the peak value of the delamination fraction. The values of the longitudinal stiffness ratio for the five dropped-ply laminates examined are presented in Table 6.4, a plot of a linear least squares fit of these ratios vs. the peak $\sqrt{F}$ values presented in Table 6.3 are shown in Fig. 6.12. Although not compared to a baseline case of a uniform specimen as did Curry et al., since this would correspond to a zero $\sqrt{F}$, these results indicate that if failure is based on the magnitude of the peak $\sqrt{F}$, an increase in the longitudinal stiffness ratio will result in a proportional decrease in failure load of the dropped-ply laminate.

Table 6.4 Ratios of the longitudinal stiffness of the thick section to the thin section for different values of θ of the dropped sublaminate $[\pm\theta]_s$.

θ	$(A_{11})_{thick}/(A_{11})_{thin}$
0°	1.571
30°	1.350
45°	1.190
60°	1.090
90°	1.051

A similar examination of the in-plane shear loaded cases can be made by using the A_{66} stiffness coefficient instead of A_{11}. This choice is easily justified by the aforementioned decoupling of the shear and extension for symmetric angle-ply and quasi-isotropic laminates. That is, since A_{16} and A_{26} are zero, an applied N_{xy} induces no ε_x° or ε_y° in CLT, which is consistent with the out of plane normal deformation and x-direction boundary condition of the present analysis. Therefore the applied N_{xy} is related to γ_{xy}° through the relation $N_{xy} = A_{66}\gamma_{xy}^{\circ}$ in CLT.

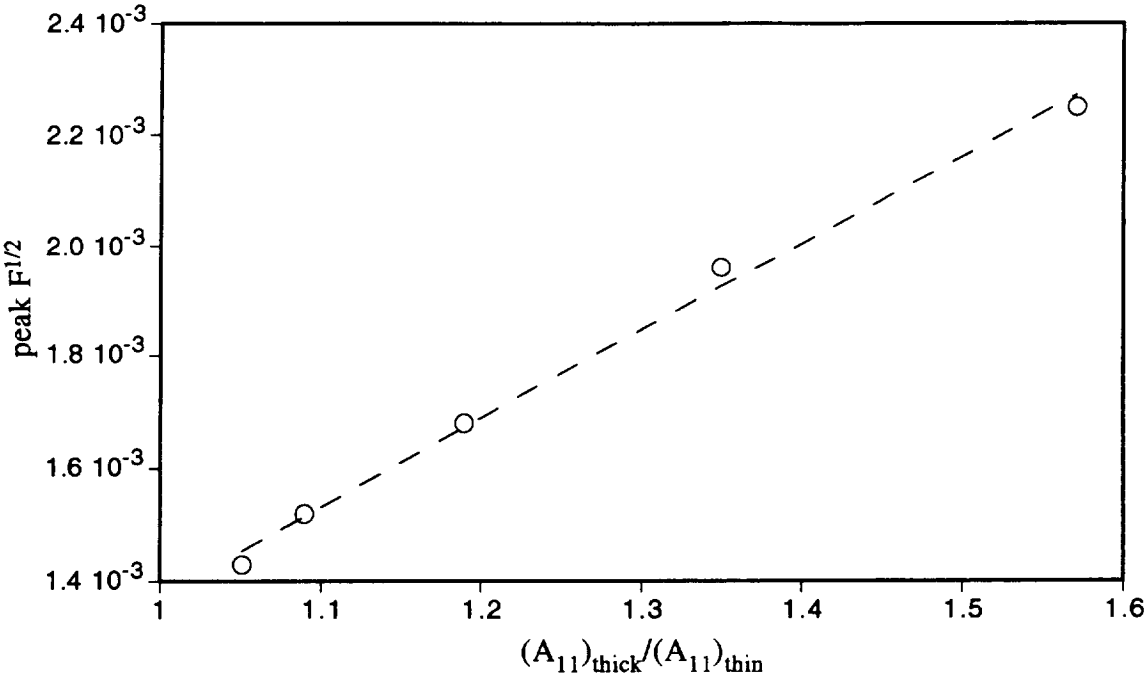

Fig. 6.12 Plot of the correlation between the stiffness ratio and the peak value of $\sqrt{F}$ (longitudinal compression loading).

The values of the shear stiffness ratio for the five dropped-ply laminates examined are presented in Table 6.5, a plot of a linear least squares fit of these ratios vs. the peak $\sqrt{F}$ values presented in Table 6.3 are shown in Fig. 6.13.

Table 6.5 Ratios of the shear stiffness of the thick section to the thin section for different values of θ of the dropped sublaminate $[\pm\theta]_s$.

θ	$(A_{66})_{thick}/(A_{66})_{thin}$
0°	1.076
30°	1.337
45°	1.425
60°	1.337
90°	1.076

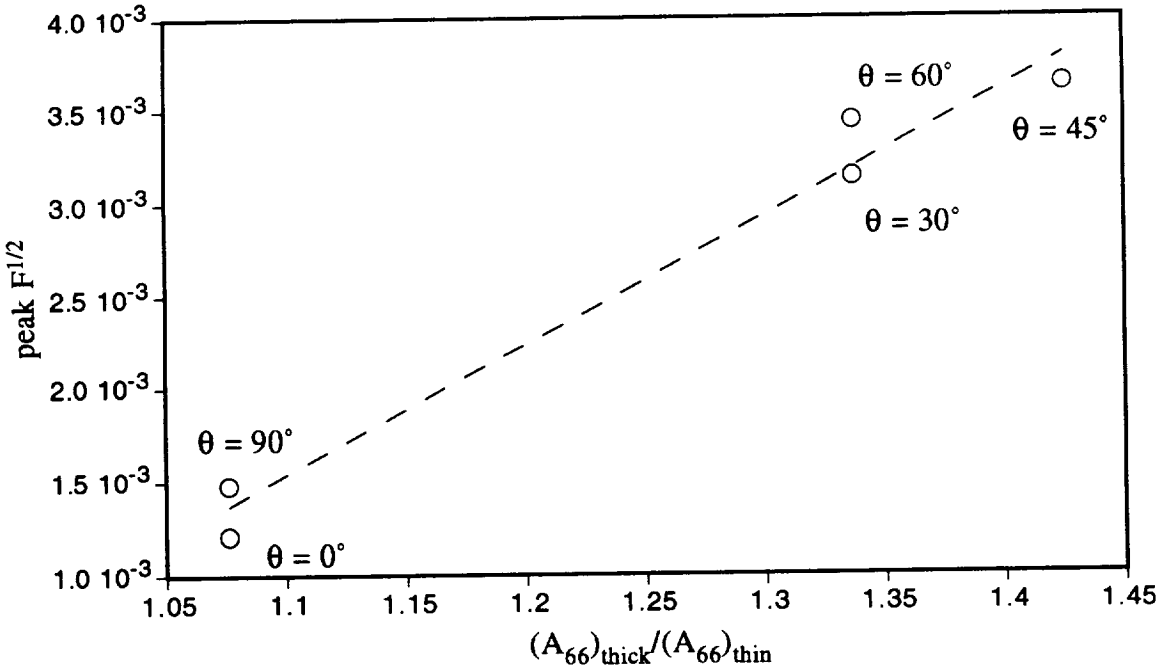

Fig. 6.13 Plot of the correlation between the stiffness ratio and the peak value of $\sqrt{F}$ (in-plane shear loading).

While the correlation here is not as good as for the longitudinal compression case, the trend is clearly represented. This is a somewhat curious result because unlike the longitudinal compression case, which has significant contribution from both σ_{nn} and σ_{tn}, the value of $\sqrt{F}$ for the in-plane shear loading is entirely due to one stress component, σ_{2n}. The most obvious deficiency here lies in the fact that A_{66} is symmetric with respect to θ about 45° for these layups while the peak values of $\sqrt{F}$ are not. The cause of this lack of symmetry lies in the difference in transverse shear stiffnesses G_{13} and G_{23} for a unidirectional ply, which do not enter into CLT. Because of the generalized plane deformation assumption of the present theory, the shear strain produced by the applied shear loading is due entirely to $\partial v/\partial x$ as $\partial u/\partial y$ is zero. As a consequence, the load is transferred to the dropped plies only through σ_{2n} as mentioned above. Therefore, a ply oriented such that it has a greater out-of-plane shear stiffness in the y-z plane will have larger interlaminar stresses for this shear loading. This would correspond to a θ closer to 90° rather than 0° and indeed these are the layups with the larger value of $\sqrt{F}$ in Fig. 6.13.

This difference in G_{13} and G_{23} also affects the load transfer for the longitudinal compression loading, however, in that case both σ_{nn} and σ_{tn} are major contributors to the peak value of the delamination fraction. Thus, the influence of the transverse shear

stiffnesses G_{13} and G_{23} on the delamination fraction in longitudinal compression is not as important as it is in the shear loading case.

A few other points regarding these correlations are worth noting. First, the fact that neither linear least squares fit passes through $\sqrt{F} = 0$ for a stiffness ratio of 1.0 indicates that other influences are contributing to the value of $\sqrt{F}$. These other influences are the geometry of the taper and the presence of the material discontinuity, neither of which need be accompanied by a stiffness change. For example, a laminate with the same taper geometry could be made with the dropped plies replaced by resin, leaving a laminate with a ratio of CLT stiffnesses of approximately one. A material discontinuity also need not be accompanied by a stiffness change as defined here. Wisnom's[17,18] work examining laminates with cut, but not discontinued, internal plies is an example of such a configuration. As stated in Sec. 1.1.1, he found this to be the greatest single factor contributing to delamination of unidirectional laminates containing dropped plies loaded longitudinally.

For the longitudinal compression loading, extrapolation of the linear curve fit to a value of one for the stiffness ratio would give a delamination fraction of about 1.4×10^{-3} while the range of values of $\sqrt{F}$ from $(A_{11})_{thick}/(A_{11})_{thin} = 1.0$ to its maximum of 1.57 is only about 0.8×10^{-3}. This indicates that these other influences are predominant in contributing to $\sqrt{F}$ for this load case. The shear loaded case, on the other hand, would have $\sqrt{F} \approx 1.2 \times 10^{-3}$ at a stiffness ratio of one while its range is approximately 2.5×10^{-3}, indicating that the stiffness change is the major influence. This difference between the longitudinal and shear loaded cases also likely contributes to the difference in the quality of the correlation.

In any event, while better in the longitudinal loading case, both of these correlations can be useful in rough estimates of a dropped-ply's likelihood of delamination. More accurate predictions, however, require more detailed analyses such as the ones developed in the present work.

6.3 Effect of a Soft Insert

This parametric study examines the effect of the inclusion of a soft insert ahead of stiff dropped plies. The baseline laminate chosen for this study is the same as the asymmetric cases with four 0° plies dropped analyzed in the previous two parametric studies and also in Sec. 5.5.2 where a comparison was made to the finite element results of Curry et al.[21] This

laminate is composed of a 20-ply $[(\pm 45 / 0 / 90)_s / 0_2]_s$ from which the center four 0° plies are dropped. The insert cases that are compared to the baseline contain four 90° plies between the four 0° plies and the thickness change (see Fig. 6.14). The dimension "a" in the figure is the distance from the original location of the end of the 0° plies ($x = 0$) to the new location. Manufacturing such laminates has shown a tendency for the 90° fibers to migrate into the area previously modeled as a resin region. Thus, the region which was occupied by the neat resin is assumed to be filled with 90° material.

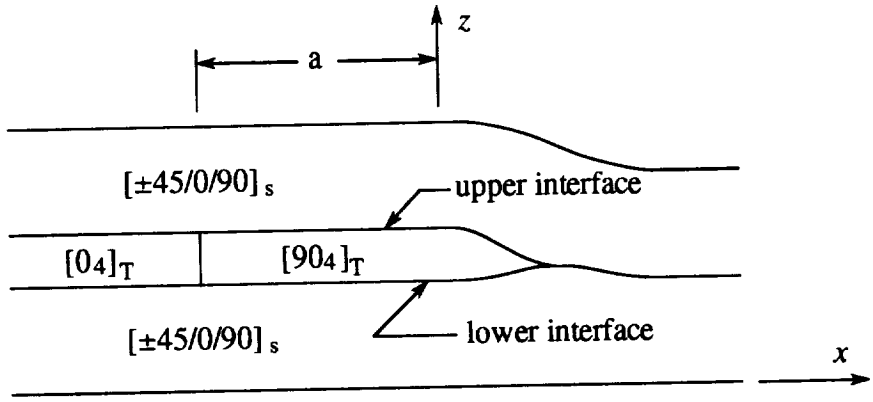

Fig. 6.14 Schematic of dropped ply laminate with soft insert.

The model used to analyze this problem has the same distribution of six mathematical layers as in the previous two studies and in Sec. 5.5.2. The boundary conditions employed are the same as those in Sec. 5.5.2 which were dictated by the test conditions used by Curry et al. The loading is uniaxial compression with the average normal applied stress in the thin section of the laminate designated σ_{app}. The dimensions are again normalized by the thickness of the dropped plies, t_d, which is 0.5588 mm for this laminate.

The experimental results obtained by Curry et al. for the baseline case show a strong tendency for delamination originating at $x = 0$ either along the top or the bottom of the dropped 0° plies. Therefore, the results presented here will be for the interlaminar stresses along these two contours, designated the upper and lower interfaces respectively. Figs. 6.15–6.18 are plots of the interlaminar normal and shear stresses in the contour following reference *t-n* for the baseline case and two soft insert cases. The first soft insert case, designated a = 0 (90s), simply replaces the triangular resin region of the baseline case with 90° material. The second soft insert case plotted is for a = $4.5t_d$ which is the longest insert analyzed. On a side note, the models with the soft insert produce a junction between the

migrated 90° fibers and the thin resin layer at $x / t_d = 2.5$ which causes small anomalies in the stresses.

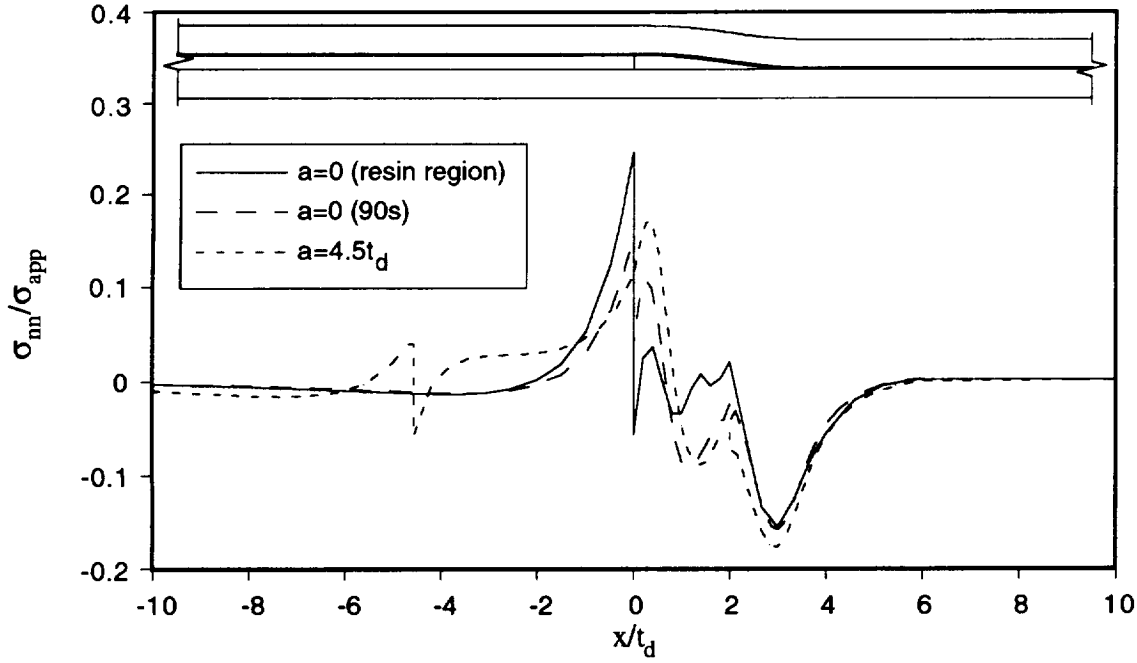

Fig. 6.15 Interlaminar normal stress along upper interface.

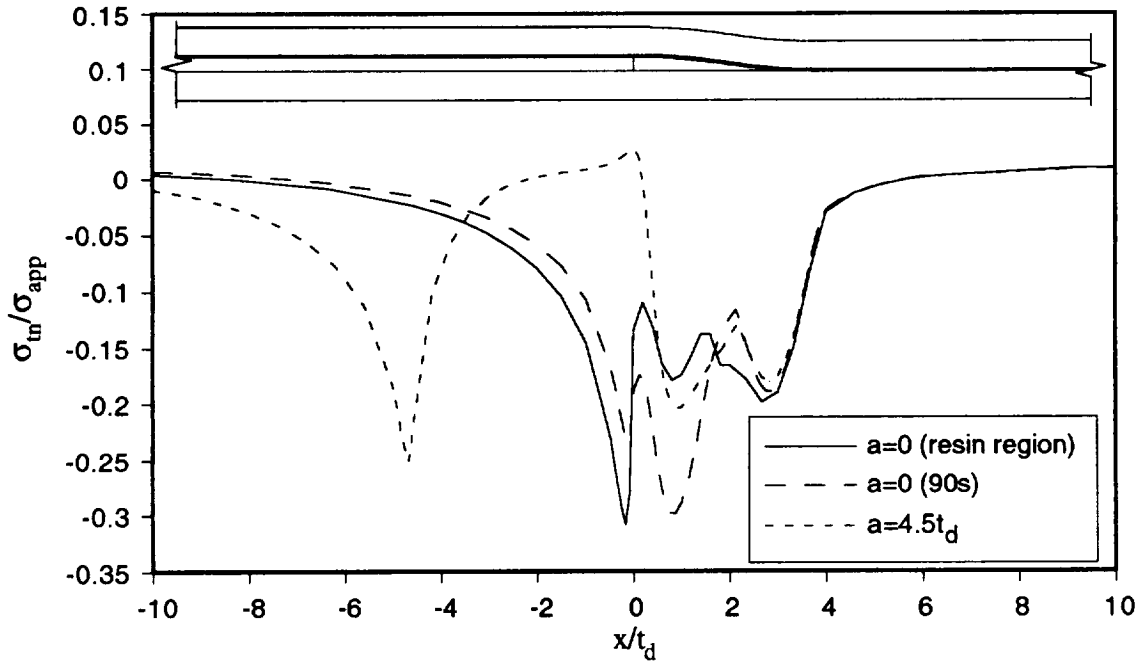

Fig. 6.16 Interlaminar shear stresses along upper interface.

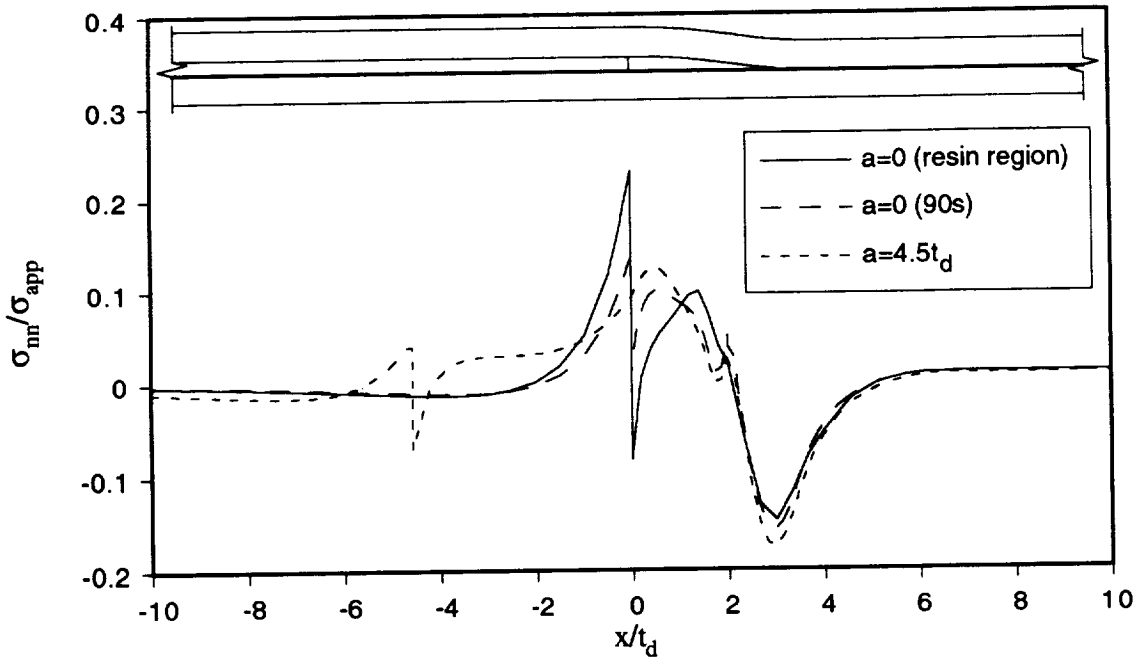

Fig. 6.17 Interlaminar normal stresses along lower interface.

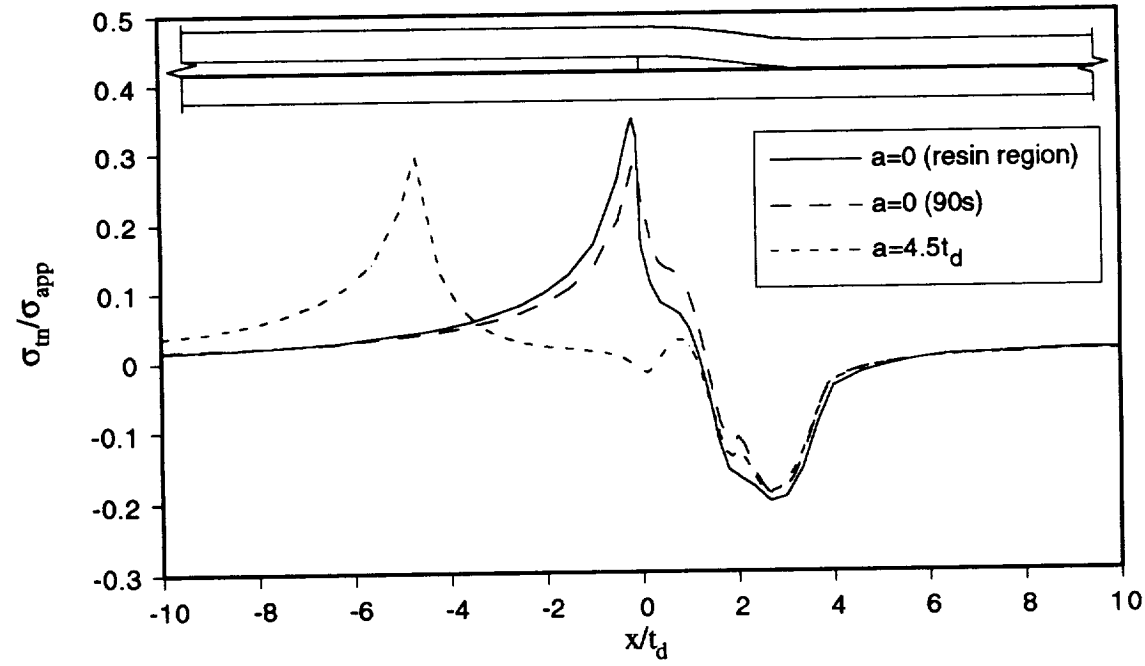

Fig. 6.18 Interlaminar shear stresses along lower interface.

From these plots it is clear that inclusion of a soft insert significantly reduces the peak interlaminar stresses for this particular laminate. This effect is consistent with what would

be expected when the magnitude of the stiffness change at the end of the four 0° plies is reduced. Fig. 6.19 shows the effect of the length of the 90° insert on the peak values of the tensile interlaminar normal stress and the absolute value of the shear stress. For the baseline case, designated w/o insert, the peak tensile interlaminar normal stress occurs at $x = 0$ on the upper interface and the largest interlaminar shear stress occurs at $x = 0$ on the lower interface.

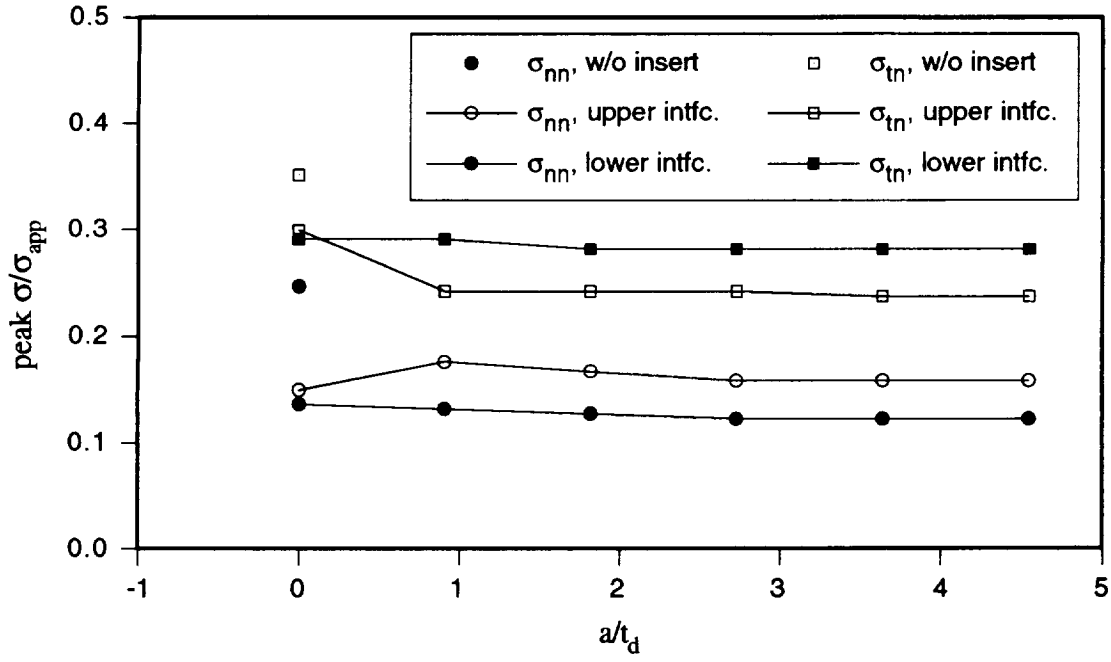

Fig. 6.19 Peak interlaminar stresses vs. length of 90° insert.

It is evident in Fig. 6.19 that the soft insert does not have to be very long to significantly reduce the likelihood of delamination initiating at this ply drop-off. Beyond filling the resin region with 90° material, which reduces the tensile interlaminar normal stress by 39%, the shear by 15%, and the delamination fraction $\sqrt{F}$ by 29%, little improvement is achieved by increasing the length of the soft insert. In fact, in going from a = 0 to a $\approx t_d$ the normal stress actually increases slightly.

Chapter 7: Concluding Remarks

7.1 Discussion and Conclusions

Summary of Approach

The objective of this research was to develop a stress-based method of approximation for the prediction of interlaminar stresses in the vicinity of a ply termination for a composite laminate. The aim was to accurately model the geometric and material properties of the dropped ply laminate such that interlaminar stresses predicted from the analysis could be employed with confidence in a delamination initiation criterion.

Based on Pagano's[45,48,49] approach for the analysis of axisymmetric involute bodies of revolution, the approach chosen modeled the laminate by a series of layers, which can have curved boundaries, with the stress field assumed within each layer. Developed for the two-dimensional problems of generalized plane deformation and axisymmetry, the stresses were assumed to be explicit functions of the thickness coordinate with "coefficients", or stress variables, that were functions only of the longitudinal coordinate x. The dependence of the stresses on the thickness coordinate was determined from the three-dimensional elasticity equations of equilibrium.

The assumed stress field was then substituted into the Hellinger-Reissner variational principle, which, after definition of weighted displacement variables in the thickness coordinate, was integrated through the thickness. Traction and displacement continuity conditions between layers were explicitly imposed on the dependent variables and their variations. Stationarity of the functional with respect to all admissible stress and

displacement variations consistent with these interlayer continuity conditions leads to the governing, or Euler, equations and boundary conditions for the model. Satisfaction of these governing equations by the stress and displacement variables, therefore, implies that the stress field satisfies equilibrium as well as traction reciprocity between layers and that the displacements satisfy continuity conditions between layers. The compatibility/constitutive conditions are satisfied in an integral sense within the layers.

Improvement in Solution Strategy

The governing equations resulting from the principle constitute a system of both differential and algebraic equations, or DAEs. Using Pagano's[48,49] two-step finite difference method of solution to this system of DAEs resulted in a solution exhibiting unacceptable oscillations when mixed boundary conditions were prescribed. (Pagano only solved prescribed traction boundary value problems in Refs. 45, 48, and 49). In the two-step finite difference solution, Pagano needed special treatment of the boundary points in developing what he called "end" conditions. This special treatment was based on assuming the integrand of the functional vanished at the end points, as well as in the open interval between the end points. A more detailed evaluation of the system of DAEs allowed a resolution of apparent inconsistencies in the number of differential equations and boundary conditions without resorting to the use of "end" conditions. This was done through a manipulation of some of the equilibrium equations and traction prescribed boundary conditions, and resulted in a system with an equal number of differential equations and boundary conditions (see Sec. 3.6). The combination of these manipulations and a switch to one-step finite differences was found to resolve the deficiency in the numerical solution following Pagano's approach. In addition to the elimination of the oscillations, these changes from Pagano's approach produce a more consistent system mathematically because the boundary conditions are distinctly separate from the field differential equations. This allows for their solution by other means besides one-step finite differences if desired, while Pagano's interpretation of "end" conditions is specifically tailored to solution by two-step finite differences.

Alleviation of Numerical Ill-Conditioning

Attempts to apply this new solution strategy to laminated shells of revolution revealed severe matrix conditioning difficulties for thin layers at even moderate radii. Development of a second model based on the assumption of generalized plane deformation in cartesian

coordinates was undertaken to determine the cause of the conditioning. Initially the model was developed using the same approach to deriving the governing equations as Pagano used, and conditioning problems were present for layers located at moderate values of the thickness coordinate. While providing some benefit, a series of changes to the stress assumptions including scaling of the bubble functions and imposing orthogonality on them were unsuccessful in overcoming the problem. The change that had the greatest positive impact on the conditioning difficulty was the modification of the displacement weighting functions from simple powers in the thickness coordinate to functions based on the shape functions used for the stresses. These modifications to the stress assumptions and weighted displacements are detailed in Secs. 3.2 and 3.3.

These changes allowed the generalized plane deformation model to handle problems with very thin layers, as would be encountered in modeling of laminates with dropped plies. However, when these remedies were applied to the axisymmetric model, the results were not as good. While the conditioning was greatly improved, patch test problems revealed that numerical conditioning was marginal even for layers that were thick relative to those that would need to be modeled in the analysis of cylindrical shells with axially dropped plies.

Sensitivity to Solution Accuracy

Attempts at solutions of these models by trapezoidal one-step finite differences revealed that they are very sensitive to the accuracy of the solution strategy employed. Unable to produce acceptable results for problems with rigid body displacements, the $O(h^2)$ accurate trapezoidal scheme was replaced with the $O(h^4)$ accurate two-stage Gauss implicit Runge-Kutta scheme. This improvement in accuracy did not come without cost, however. Implementation of the Gauss scheme required conversion of the algebraic equations to differential and the inversion of a $2n \times 2n$ matrix, n being the order of the system, at each finite difference step. In addition, this approach to solution was found to cause a degradation in solution matrix conditioning as compared to the application of the trapezoidal scheme to the DAEs. This degradation in conditioning was found to be caused mostly by the conversion of the DAEs to a fully differential system.

Reformulation of Axisymmetric Model

Along with the changes made to the axisymmetric model for the purpose of improving the reliability of the solutions obtained, a further modification was made to Pagano's

original approach. Through careful selection of the dependence of the "in-plane" stress components on the radial coordinate, the number of stress variables required to allow satisfaction of equilibrium was reduced by one per layer as was the number of displacement variables per layer. While this is a modest reduction in the number of unknowns per layer (from 25 to 23), it is significant and actually required less effort in the development of the model as compared to Pagano's. It also provided the added benefit of having a one-to-one correspondence in the stress and displacement unknowns to the generalized plane deformation model, allowing a simpler conversion in the coding of the two models. Unfortunately, the difficulties in obtaining accurate and reliable solutions with the axisymmetric model for problems subjected to internal pressure did not allow these advances to be utilized.

Modeling Multiple Plies in a Layer

A homogenization scheme was applied in order to allow multiple plies to be represented by a single layer in one of the models. This scheme used a combination of the Voigt and Reuss approximations in deriving compliance coefficients for a single homogeneous layer equivalent in a strain energy sense to the sublaminate comprising the actual layer. This approach to modeling multiple plies in a single layer was compared to piecewise evaluation of the weighted integrals of the compliances and was found to be superior due to a lack of in-plane displacement continuity enforcement in the latter approach (see Sec. 5.2.3).

Verification Studies

Patch test problems were used to evaluate the accuracy and limitations of the models and their solution by the finite difference approximation. The term patch test is used because of the similarity to tests of the same name used to verify the accuracy of finite elements. Essentially, a problem is chosen to which the exact elasticity solution is known, which is usually a state of uniform stress and strain. By geometrically distorting the layers subdividing the body, some limits on the accuracy of the numerical solution method can be determined. These patch tests revealed the difficulties with the axisymmetric model mentioned previously. They also helped establish the level of confidence in the generalized plane deformation model necessary to move on to the analysis of laminated composites.

Evaluation of the accuracy of the generalized plane deformation model for laminated composites was also done through comparing solutions obtained from it to established solutions. The first such comparison was to the tensile coupon free edge problem which

Pagano[44] compared to the highly refined finite element solution of Wang and Crossman.[57] The results for this case showed near perfect agreement for the interlaminar stresses. While this problem did not involve the geometric complexity of a dropped ply, the results indicated that the model was capable handling the stress gradients present in a region of stress concentration.

The second solution compared to was that of Curry et al.[21] and their finite element analysis of a compression loaded asymmetric dropped-ply test specimen. This extended the evaluation of the model to an examination of it's ability to model complex geometries with very thin layers as well as stress concentrations. While the interlaminar stresses predicted by the two approaches did not match as well as the free-edge problem, the correlation was good. This showed that the model had the ability to model complex problems such as dropped-ply laminates.

Effect of Dropped-Ply Laminate Eccentricity

Parametric studies were done to evaluate some of the factors affecting the stress concentration in dropped-ply laminates. Eccentricity of the middle surface was examined for a dropped-ply laminate composed of continuous quasi-isotropic sublaminates of $[\pm 45 / 0 / 90]_s$ layup, and with dropped sublaminates of either $[0_4]_T$, $[90_4]_T$, or $[\pm 45]_s$ layups. Material properties for AS4/3502 graphite/epoxy were used. Two geometries were evaluated for each of the three layups of the dropped sublaminates, one with eccentricity and one without. Each of these configurations was loaded in either longitudinal compression, transverse tension, or in-plane shear. The relative propensity of each case to delaminate was evaluated based on a quadratic delamination criterion using the interlaminar stresses. For the longitudinal compression and in-plane shear load cases, eccentricity was determined to have a minimal effect on the likelihood of delamination occurring. The transverse tension case was not considered likely to experience delamination failure at all due to the ply drop-off.

Effect of Stiffness Discontinuity

The eccentricity study clearly indicated that the stiffness discontinuity introduced by dropping plies had a much greater influence on the interlaminar stresses than did eccentricity. A second parametric study was performed to examine the correlation between the magnitude of the stiffness discontinuity and the likelihood of delamination for asymmetric dropped-ply laminates. The stiffness of the dropped sublaminate was varied

through changing the ply angle θ in a $[\pm\theta]_s$ sublaminate layup. The material used was again AS4/3502 graphite/epoxy, and the loadings examined were longitudinal compression and in-plane shear. For the longitudinal compression loading, a good correlation was found between the delamination criterion's prediction of the likelihood of delamination and the ratio of the longitudinal stiffness of the thick section of the laminate to that of the thin section. A similar correlation for the in-plane shear loaded cases using the shear stiffness discontinuity instead of the longitudinal stiffness was not quite as good, but did approximate the trend acceptably.

Influence of Soft Insert

A third study of dropped-ply laminates examined the effect of inserting "softer" 90° material ahead of four 0° dropped plies in an effort to reduce the peak interlaminar stresses under longitudinal compression. AS4/3502 graphite/epoxy material was used along with the same asymmetric geometry of taper as used in the eccentric case. The length of the soft insert was increased incrementally to determine an optimal length. It was found that simply filling the region ahead of the dropped plies previously occupied by resin had the most significant effect on the interlaminar stresses, reducing the interlaminar normal by nearly 40%. Beyond that, increasing the length of the insert provided only marginal benefit.

7.2 Suggestions for Future Work

At present, a major weakness of these models and their solution lies in the large computational burden in both storage and CPU time. This burden stems from three areas; the use of a banded matrix solver for a matrix with block structure, the large number of dependent variables, and the high degree of accuracy required of the solution method. Compounding this problem is the issue of conditioning of the solution matrix, which degraded with the application of the more accurate Gauss implicit Runge-Kutta scheme due mainly to the conversion of the DAEs to a fully differential system. Therefore, recommendations for future work on these models should begin with improvements in their solution with the easiest being the use of a block diagonal solver. This was not done in the present work because such a solver that also estimates condition numbers was not available. Elimination of variables that appear only algebraically in the governing equations through manipulation could reduce the number of unknowns per layer in the finite difference solution by nine. However, this procedure could likely only be done numerically

in a practical sense, and therefore would involve matrix inversions. The cost of these inversions, which would reduce the computational benefits of this approach, must be considered as well. Another approach worth consideration is adapting a higher order accurate one-step finite difference scheme, such as the Gauss scheme used here, to the solution of the original DAE form of the governing equations. This would avoid the conversion to a fully differential system, which was found to degrade the numerical solution conditioning significantly. Finally, some form of finite element solution such as the one developed by Sandhu et al.[50] deserves more attention than was possible in the present study.

These improved solution strategies should be implemented first for the generalized plane deformation model. Those that are most successful could then be applied to the axisymmetric model in an attempt to arrive at accurate solutions for laminated cylindrical shells subjected to internal pressure.

Other improvements to the models worth considering include the development of a more refined homogenization scheme (see Sec. 5.2 and Appendix A) that would provide compliance coefficients that vary through the thickness of a layer. This would account for some of the effect of the stacking sequence within a layer on the compliances and may produce more accurate results with fewer layers. Finally, developing continuity conditions that would allow two layers to be joined to form a single layer would provide the dual benefit of reducing the number of layers where they are not needed and minimizing the number of very thin layers in a model of such features as ply drop-offs.

References

[1]Madsen, C.B., Nuismer, R.J., and Bianca, C.J., "Space Shuttle Filament Wound Case Compressive Strength Study: Part I - Testing," *Proceedings of the AIAA/ASME/SAE/ASEE 22nd Joint Propulsion Conference*, (Huntsville, Alabama), AIAA, New York, NY, AIAA Paper No. 86-1580, June 1986.

[2]Messick, M.J., Nuismer, R.J., Jamison, G.T., and Graves, S.R., "Space Shuttle Filament Wound Case Compressive Strength Study: Part II - Analysis," *Proceedings of the AIAA/ASME/SAE/ASEE 22nd Joint Propulsion Conference*, (Huntsville, Alabama), AIAA, New York, NY, AIAA Paper No. 86-1417, June 1986.

[3]Daoust, J. and Hoa, S.V., "Parameters Affecting Interlaminar Stresses in Tapered Laminates Under Static Loading Conditions," *Polymer Composites*, Vol. 10, No. 5, October 1989, pp. 374-383.

[4]Fish, J.C. and Lee, S.W., "Edge Effects in Tapered Composite Structures," *Proceedings of the National Technical Specialists' Meeting on Advanced Rotorcraft Structures*, (Hampton, VA), October 1988.

[5]Fish, J.C. and Vizzini, A.J., "Tailoring Concepts for Improved Structural Performance of Rotorcraft Flexbeams," *Proceedings of the American Helicopter Society Rotorcraft Structures Specialists' Meeting*, (Williamsburg, VA), October 1991.

[6]Kulkarny, S.V., Stone, R.G., and Toland, R.H., "Prototype Development of an Optimized, Tapered-Thickness, Graphite/Epoxy Composite Flywheel," Report No. UCRL-52623, Lawrence Livermore Laboratory, University of California 1978.

[7]Kubr, T.J., *Stress Near a Change of Thickness in a Continuous-Fiber-Composite Plate*, Thesis, California Institute of Technology, Pasadena, CA, June 1990.

[8]Wu, C.M.L. and Webber, J.P.H., "Analysis of Tapered (in Steps) Laminated Plates Under Uniform Inplane Load," *Composite Structures*, Vol. 5, 1986, pp. 87-100.

[9]Wu, C.M.L., "Non-linear Analysis of Tapered (in Steps) Laminated Plates under Uniform Inplane Load," *Composite Structures*, Vol. 7, 1987, pp. 205-223.

[10]Chan, W.S. and Ochoa, O.O., "Suppression of Edge Delamination in Composite Laminates by Terminating a Critical Ply Near the Edges," *Proceedings of the 29th AIAA/ASME/ASCE/AHS Structures, Structural Dynamics and Materials Conference*, (Williamsburg, VA), AIAA, Washington, DC, April 1988, pp. 359-364.

[11]Ochoa, O.O. and Chan, W.S., "Tapered Laminates: A Study on Delamination Characterization," *Proceedings of the American Society for Composites Third Technical Conference*, (Seattle, WA), Technomic, Lancaster, PA, September 1988, pp. 633-641.

[12]Pogue, III, W.R. and Vizzini, A.J., "The Effect of Structural Tailoring by Edge Alteration on Free-Edge Delamination," *AHS Annual Forum Proceedings*, (Washington D.C.), American Helicopter Society, Washington, D.C., June 1988, pp. 445-452.

[13]Vizzini, A.J., "Strength of Laminated Composites with Longitudinal Discontinuities," *Proceedings of the 31st AIAA/ASME/ASCE/AHS Structures, Structural Dynamics and Materials Conference*, (Long Beach, CA), AIAA, Washington, DC, AIAA Paper No. 90-1065, April 1990, pp. 1260-1269.

[14]Kemp, B.L. and Johnson, E.R., "Response and Failure Analysis of a Graphite-Epoxy Laminate Containing Terminating Internal Plies," *Proceedings of the 26th AIAA/ASME/ASCE/AHS Structures, Structural Dynamics and Materials Conference*, (Orlando, FL), AIAA, New York, NY, AIAA Paper No. 85-0608, April 1985, pp. 13-24.

[15]Cannon, R.K., "The Effects of Ply Dropoffs on the Tensile Behavior of Graphite/Epoxy Laminates," TELAC Report, 87-12, Massachusetts Institute of Technology, Cambridge, MA, May 1987.

[16]Lagace, P.A. and Cannon, R.K., "Effects of Ply Dropoffs on the Tensile Behavior of Graphite/Epoxy Laminates," *Proceedings of the Fourth Japan-U.S. Conference on Composite Materials*, (Washington, DC), Technomic, Lancaster, PA, June 1988, pp. 1-11.

[17]Wisnom, M.R., "Delamination in Tapered Unidirectional Glass Fibre-Epoxy Under Static Tension Loading," *Proceedings of the 32nd AIAA/ASME/ASCE/AHS/ASC Structures, Structural Dynamics and Materials Conference*, (Baltimore, MD), AIAA, Washington, DC, AIAA Paper No. 91-1142-CP, April 1991, pp. 1162-1172.

[18]Wisnom, M.R., "Prediction of Delamination in Tapered Unidirectional Glass Fibre Epoxy with Dropped Plies Under Static Tension and Compression," *AGARD CP530, Specialists Meeting on Debonding/Delamination of Composites*, (Patras, Greece), May 1992, pp. 25-1 to 25-7.

[19]Botting, A.D., Vizzini, A.J., and Lee, S.W., "The Effect of Ply-Drop Configuration on the Delamination Strength of Tapered Composite Structures," *Proceedings of the 33rd AIAA/ASME/ASCE/AHS/ASC Structures, Strucural Dynamics and Materials Conference*, (Dallas, TX), AIAA, Washington, DC, AIAA Paper No. 92-2227-CP, April 1992, pp. 40-47.

[20]Curry, J.M. *Effect of Ply Drop-offs on the Strength of Graphite-Epoxy Laminates*, Master's thesis, Aerospace Engineering, Virginia Polytechnic Institute and State University, Blacksburg, VA, 1986.

[21]Curry, J.M., Johnson, E.R., and Starnes, Jr., J.H., "Effect of Dropped Plies on the Strength of Grahite-Epoxy Laminates," *Proceedings of the 28th AIAA/ASME/ASCE/AHS Structures, Structural Dynamics and Materials Conference*, (Monterey, CA), AIAA, New York, NY, AIAA Paper No. 87-0874, April 1987, pp. 737-747.

[22]Trethewey, Jr., B.R., Gillespie, Jr., J.W., and Wilkins, D.J., "Interlaminar Performance of Tapered Composite Laminates," *Proceedings of the American Society for Composites Fifth Technical Conference*, (E. Lansing, MI), Technomic, Lancaster, PA, June 1990, pp. 361-372.

[23]Grimes, G.C. and Dusablon, E.G., "Study of Compression Properties of Graphite/Epoxy Composites with Discontinuities," *Composite Materials: Testing and Design (Sixth Conference), ASTM STP 787*, (Pheonix, AZ), Daniel, I.M. (Ed), American Society for Testing and Materials, 1982, pp. 513-538.

[24]Adams, D.F., Ramkumar, R.L., and Walrath, D.E., "Analysis of Porous Laminates in the Presence of Ply Drop-Offs and Fastener Holes," Northrop Technical Report NOR 84-113, Northrop Corporation, Hawthorne, CA and the University of Wyoming, Laramie, WY, May 1984.

[25]Hoa, S.V., Daoust, J., Du, B.L., and Vu-Khanh, T., "Interlaminar Stresses in Tapered Laminates," *Polymer Composites*, Vol. 9, No. 5, October 1988, pp. 337-344.

[26]Fish, J.C. and Lee, S.W., "Tensile Strength of Tapered Composite Structures," *Proceedings of the 29th AIAA/ASME/ASCE/AHS Structures, Structural Dynamics and Materials Conference*, (Williamsburg, VA), AIAA, Washington, DC, AIAA Paper No. 88-2252, April 1988, pp. 324-333.

[27]Fish, J.C. and Lee, S.W., "Delamination of Tapered Composite Structures," *Engineering Fracture Mechanics*, Vol. 34, No. 1, 1989, pp. 43-54.

[28]Salpekar, S.A., Raju, I.S., and O'Brien, T.K., "Strain Energy Release Rate Analysis of Delamination in a Tapered Laminate Subjected to Tension Load," *Proceedings of the American Society for Composites Third Technical Conference*, (Seattle, WA), September 1988, pp. 642-654.

[29]Brewer, J.C. and Lagace, P.A., "Quadratic Stress Criterion for Initiation of Delamination," *Journal of Composite Materials*, Vol. 22, December 1988, pp. 1141-1155.

[30]O'Brien, T.K., "Mixed-Mode Strain-Energy-Release Rate Effects on Edge Delamination of Composites," *Effects of Defects in Composite Materials, ASTM STP 836*, (San Francisco, CA), American Society for Testing and Materials, Philadelphia, PA, 1984, pp. 125-142.

[31]Reddy, J.N., *An Introduction to the Finite Element Method*, McGraw-Hill, 1984, pp. 1-2.

[32]Reddy, J.N., *Energy and Variational Methods in Applied Mechanics*, John Wiley & Sons, 1984, pp. 211-217.

[33]Pian, T.H.H. and Tong, P., "Basis of Finite Element Methods for Solid Continua," *International Journal for Numerical Methods in Engineering*, Vol. 1, 1969, pp. 3-28.

[34]Pian, T.H.H., "Finite Element Methods by Variational Principles with Relaxed Continuity Requirement," *Variational Methods in Engineering; Proceedings of an International Conference held at the University of Southampton*, Brebbia, C.A. and Tottenham, H. (Eds), September 1972, pp. 3/1-3/24.

[35]Pian, T.H.H., "A Historical Note About 'Hybrid Elements'," *International Journal for Numerical Methods in Engineering*, Vol. 12, 1978, pp. 891-892.

[36]Atluri, S.N., "On 'Hybrid' Finite-Element Models in Solid Mechanics," *Advances in Computer Methods for Partial Differential Equations; Proceedings of the AICA International Symposium on Computer Methods for Partial Differential Equations*, (Lehigh University - Bethlehem, PA), Vichnevetsky, R. (Ed), AICA, June 1975, pp. 346-355.

[37]Xue, W.M., Karlovitz, L.A., and Atluri, S.N., "On the Existence and Stability Conditions for Mixed-Hybrid Finite Element Solutions Based on Reissner's Variational Principle," *International Journal of Solids and Structures*, Vol. 21, No. 1, 1985, pp. 97-116.

[38]Pian, T.H.H., "Hybrid Models," *Numerical and Computer Methods in Structural Mechanics*, Academic Press, 1973, pp. 59-78.

[39]Pian, T.H.H., "Derivation of Element Stiffness Matrices by Assumed Stress Distributions," *AIAA Journal*, Vol. 2, No. 7, July 1964, pp. 1333-1336.

[40]Spilker, R.L., "A Hybrid-Stress Finite-Element Formulation for Thick Multilayer Laminates," *Computers and Structures*, Vol. 11, 1980, pp. 507-514.

[41]Spilker, R.L., "Hybrid-Stress Eight-Node Elements for Thin and Thick Multilayer Laminated Plates," *International Journal for Numerical Methods in Engineering*, Vol. 18, 1982, pp. 801-828.

[42]Cook, R.D., "Two Hybrid Elements for Analysis of Thick, Thin and Sandwich Plates," *International Journal for Numerical Methods in Engineering*, Vol. 5, 1972, pp. 277-288.

[43]Shi, Y.B. and Chen, H.R., "A Mixed Finite Element for Interlaminar Stress Computation," *Composite Structures*, Vol. 20, 1992, pp. 127-136.

[44]Pagano, N.J., "Stress Fields in Composite Laminates," *International Journal of Solids and Structures*, Vol. 14, 1978, pp. 385-400.

[45]Pagano, N.J., "Axisymmetric Stress Fields in Involute Bodies of Revolution," *Advances in Aerospace Structures, Materials and Dynamics; A Symposium on Composites, AD-06*, (Boston, MA), Yuceoglu, U., Sierakowski, R.L., and Glasgow, D.A. (Eds), American Society of Mechanical Engineers, New York, NY, 1983, pp. 57-64.

[46]Lekhnitskii, S.G., *Theory of Elasticity of an Anisotropic Body*, Mir Publishers, Moscow, 1981, (p. 104).

[47]Mura, T., *Micromechanics of Defects in Solids,* Martinus Nijhoff Publishers: Dordrecht, The Netherlands, 2nd edition, 1987, pp. 421-428.

[48]Pagano, N.J. and Whitford, L.E., "On the Solution for the Elastic Response of Involute Bodies," *Composites Science and Technology*, Vol. 22, 1985, pp. 295-317.

[49]Pagano, N.J., "Refined Solutions for the Elastic Response of Involute Bodies," *Composites Science and Technology*, Vol. 25, 1986, pp. 251-270.

[50]Sandhu, R.S., Wolfe, W.E., and Chyou, H.H., "Variational Formulation and Finite Element Implementationof Pagano's Theory of Laminated Plates," Final Report to Air Force Systems Command, WL-TR-91-3016, NASA #N92-29594, Dept. of Civil Engineering, The Ohio State University, July 1991.

[51]Brenan, K.E., Campbell, S.L., and Petzold, L.R., *Numerical Solution of Initial-Value Problems in Differential-Algebraic Equations,* Elsevier Science Publishing Co., Inc.: New York, New York, 1989, pp. 9-10.

[52]Ascher, U.M., Mattheij, R.M.M., and Russell, R.D., *Numerical Solution of Boundary Value Problems for Ordinary Differential Equations*, Prentice Hall, 1988.

[53]*Math/Library: IMSL Fortran Subroutines for Mathematical Applications*, International Mathematical and Statistical Library, 1.1.

[54]Cline, A.K., Moler, C.B., Stewart, G.W., and Wilkinson, J.H., "An Estimate for the Condition Number of a Matrix," *SIAM Journal on Numerical Analysis*, Vol. 16, No. 2, April 1979, pp. 368-375.

[55]Golub, G.H. and Van Loan, C.F., *Matrix Computations*, The Johns Hopkins University Press, 1983.

[56]Timoshenko, S.P. and Goodier, J.N., *Theory of Elasticity*, 3rd, McGraw-Hill Book Company, 1970, pp. 68-71.

[57]Wang, A.S.D. and Crossman, F.W., "Some New Results on Edge Effect in Symmetric Composite Laminates," *Journal of Composite Materials*, Vol. 11, 1977, pp. 92-106.

[58]Voigt, W., "Über die Beziehung zwischen den beiden Elastizitätskonstanten isotroper Körper," *Wied. Ann.*, Vol. 38, 1889, pp. 573-587.

[59]Reuss, A., "Berechnung der Fliessgrenze von Mischkristallen auf Grund der Plastizitätsbedingung für Einkristalle," *Z. angew. Math. Mech.*, Vol. 9, 1929, pp. 49-58.

[60]Hill, R., "The Elastic Behavior of a Crystalline Aggregate," *Proc. Phys. Soc.*, Vol. A65, 1952, pp. 349-354.

[61]Sun, C.T. and Li, S., "Three Dimensional Effective Elastic Constants for Thick Laminates," *Journal of Composite Materials*, Vol. 22, July 1988, pp. 629-639.

Appendix A: Homogenization Procedure

This appendix presents the homogenization procedure applied to the mathematically modeled layers that contain multiple plies (a sub-laminate). It is based on the equivalence of the strain energy between a representative volume of the heterogeneous sub-laminate, for which the material properties are known on a constituent basis, and a representative volume of homogeneous solid, for which the material properties are desired. In equating the strain energies, a combination of the Voigt[58] and Reuss[59] approximations are applied such that in-plane compatibility and out-of-plane equilibrium are enforced between plies.

A.1 Equating Strain Energy

A schematic of representative volumes of the heterogeneous and the homogeneous materials is shown in Fig. A.1. Both elements have in-plane dimensions Δx and Δy and total thickness t. The heterogeneous element may be composed of any number of plies, n, with each ply having arbitrary thickness t_i within the restriction that $\Sigma t_i = t$. Therefore, the volume fraction of each constituent ply is $v_i = t_i/t$. In-plane dimensions Δx and Δy are assumed to be infinitesimal, and the stresses and strains within a ply are assumed spatially uniform. Each ply is assumed linear elastic, homogeneous, and anisotropic.

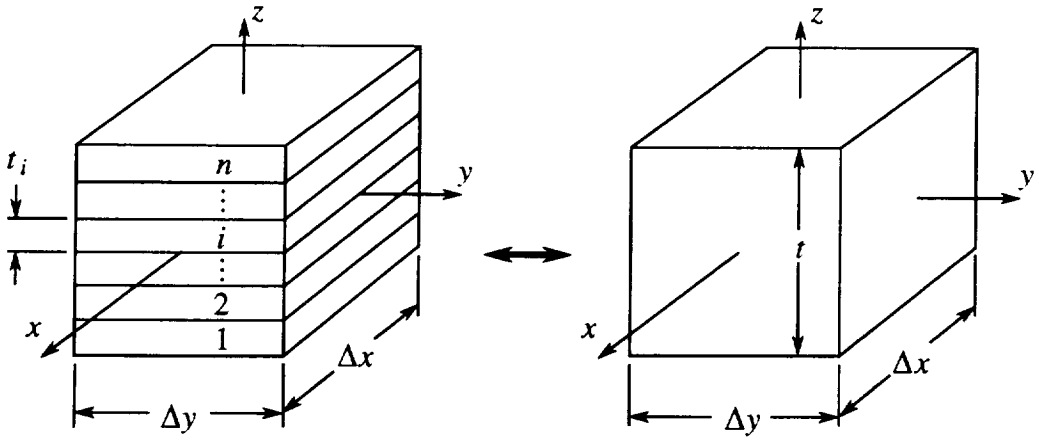

Fig. A.1 Heterogeneous sub-laminate and equivalent homogeneous solid.

The linear-elastic strain energy for the two volume elements are, for the heterogeneous sub-laminate:

$$\frac{1}{2}\sum_{i=1}^{n}\sigma_k^{(i)}\varepsilon_k^{(i)}t_i\Delta x\Delta y \tag{A-1}$$

and for the equivalent homogeneous solid:

$$\frac{1}{2}\sigma_k\varepsilon_k t\Delta x\Delta y \tag{A-2}$$

where σ_k and ε_k are the stresses and engineering strains in contracted notation, i.e. $[\sigma_x,\sigma_y,\sigma_z,\sigma_{yz},\sigma_{xz},\sigma_{xy}]^T=[\sigma_1,\sigma_2,\sigma_3,\sigma_4,\sigma_5,\sigma_6]^T$ with the same order for the engineering strains. Repeated subscripts on stress and strain components are summed out from one to six in the usual indicial notation. In Eq. (A-1), the superscript in parentheses denotes the layer that the stress or strain component is associated with. The stresses and strains for the homogeneous solid have no superscripts. Equating these expressions, eliminating like terms and employing the definition of the volume fraction leaves

$$\sigma_k\varepsilon_k=\sum_{i=1}^{n}v_i\sigma_k^{(i)}\varepsilon_k^{(i)} \tag{A-3}$$

Substituting Hooke's Law, expressed as

$$\sigma_k=C_{kl}\varepsilon_l \qquad or \qquad \varepsilon_k=S_{kl}\sigma_l \tag{A-4}$$

where **C** and **S** are the stiffness and compliance matrices respectively, the equivalence of

strain energy, Eq. (A-3), can be written in the following forms:

$$C_{kl}\varepsilon_k\varepsilon_l = \sum_{i=1}^{n} v_i C_{kl}^{(i)} \varepsilon_k^{(i)} \varepsilon_l^{(i)} \tag{A-5a}$$

$$S_{kl}\sigma_k\sigma_l = \sum_{i=1}^{n} v_i S_{kl}^{(i)} \sigma_k^{(i)} \sigma_l^{(i)} \tag{A-5b}$$

in which $\mathbf{C}^{(i)}$ and $\mathbf{S}^{(i)}$ denote the known stiffness and compliance matrices for the ith ply. The goal of the remaining derivation, therefore, is to determine the **C** and **S** matrices occurring on the left sides of Eqs. (A-5), i.e. the homogenized stiffness and compliance matrices.

A stress concentration matrix $\mathbf{K}^{(i)}$ for the ith ply, which relates the stress in the homogenized composite to the stresses in the individual constituent plies, is defined by:

$$\sigma_k^{(i)} = K_{kl}^{(i)} \sigma_l \tag{A-6}$$

Substituting into Eq. (A-5b) yields

$$S_{kl}\sigma_k\sigma_l = \sum_{i=1}^{n} v_i S_{kl}^{(i)} K_{km}^{(i)} K_{\ln}^{(i)} \sigma_m \sigma_n \tag{A-7}$$

for every state of stress in the homogeneous solid. Therefore,

$$S_{mn} = \sum_{i=1}^{n} v_i K_{km}^{(i)} K_{\ln}^{(i)} S_{kl}^{(i)} \tag{A-8}$$

and determining the homogenized compliance matrix **S** reduces to the determination of the stress concentration matrices $\mathbf{K}^{(i)}$ and the application of Eq. (A-8).

Similarly, a strain concentration matrix $\mathbf{L}^{(i)}$ is defined by

$$\varepsilon_k^{(i)} = L_{kl}^{(i)} \varepsilon_l \tag{A-9}$$

Substituting into Eq. (A-5a) leads to

$$C_{mn} = \sum_{i=1}^{n} v_i L_{km}^{(i)} L_{\ln}^{(i)} C_{kl}^{(i)} \tag{A-10}$$

So determination of **C** reduces to the determination of the strain concentration matrices $\mathbf{L}^{(i)}$.

A.2 Voigt and Reuss Approximations

The stress concentration matrix is determined through application of a combination of the Voigt[58] and Reuss[59] approximations. These approximations were developed for the micromechanical evaluation of average elastic moduli of materials with multiple constituents such as polycrystals. The Voigt approximation assumes that the strain in each constituent is uniform and equal to an average strain. The Reuss approximation assumes that the stress in each constituent is uniform and equal to an average stress. It has been proven by Hill[60] that the Voigt approximation gives upper bounds and the Reuss approximation gives lower bounds for determination of effective elastic moduli for a composite.

The Voigt approximation is applied to the in-plane strains and serves to enforce in-plane displacement compatibility between plies. The Reuss approximation is applied to the out-of-plane stresses and serves to enforce out-of-plane equilibrium between plies. These conditions are stated as

$$\begin{aligned} \varepsilon_1 &= \varepsilon_1^{(i)} \\ \varepsilon_2 &= \varepsilon_2^{(i)} \qquad i = 1,2,\ldots,n \\ \varepsilon_6 &= \varepsilon_6^{(i)} \end{aligned} \tag{A-11}$$

and

$$\begin{aligned} \sigma_3 &= \sigma_3^{(i)} \\ \sigma_4 &= \sigma_4^{(i)} \qquad i = 1,2,\ldots,n \\ \sigma_5 &= \sigma_5^{(i)} \end{aligned} \tag{A-12}$$

In addition, conditions are placed on the out-of-plane strains and the in-plane stresses. The conditions on the out-of-plane strains are stated as

$$\begin{aligned} t\varepsilon_3 &= \sum t_i \varepsilon_3^{(i)} \\ t\varepsilon_4 &= \sum t_i \varepsilon_4^{(i)} \\ t\varepsilon_5 &= \sum t_i \varepsilon_5^{(i)} \end{aligned} \tag{A-13}$$

and are imposed in order to equate the relative displacements between the lower and upper surfaces of the volume elements due to the out-of-plane strains. The conditions on the in-plane stresses are stated as

$$
\begin{aligned}
t\sigma_1 &= \sum t_i \sigma_1^{(i)} \\
t\sigma_2 &= \sum t_i \sigma_2^{(i)} \\
t\sigma_6 &= \sum t_i \sigma_6^{(i)}
\end{aligned}
\tag{A-14}
$$

and are imposed in order to equate the in-plane forces on the vertical faces between the volume elements. Division through by the thickness t gives the form for Eq. (A-13) of

$$
\begin{aligned}
\varepsilon_3 &= \sum v_i \varepsilon_3^{(i)} \\
\varepsilon_4 &= \sum v_i \varepsilon_4^{(i)} \\
\varepsilon_5 &= \sum v_i \varepsilon_5^{(i)}
\end{aligned}
\tag{A-15}
$$

and for Eq. (A-14)

$$
\begin{aligned}
\sigma_1 &= \sum v_i \sigma_1^{(i)} \\
\sigma_2 &= \sum v_i \sigma_2^{(i)} \\
\sigma_6 &= \sum v_i \sigma_6^{(i)}
\end{aligned}
\tag{A-16}
$$

A.3 Homogenized Compliances

Based on Eqs. (A-6), (A-12), and (A-16), the structure of the stress concentration matrix for layer i has the form

$$
\mathbf{K}^{(i)} = \begin{bmatrix}
K_{11} & K_{12} & K_{13} & K_{14} & K_{15} & K_{16} \\
K_{21} & K_{22} & K_{23} & K_{24} & K_{25} & K_{26} \\
0 & 0 & 1 & 0 & 0 & 0 \\
0 & 0 & 0 & 1 & 0 & 0 \\
0 & 0 & 0 & 0 & 1 & 0 \\
K_{61} & K_{62} & K_{63} & K_{64} & K_{65} & K_{66}
\end{bmatrix}^{(i)}
\tag{A-17}
$$

Determination of the 18 terms that are unknown is accomplished through the application of the conditions of Eq. (A-11) along with Hooke's law, the in-plane equilibrium conditions of Eq. (A-16) and the out-of-plane equilibrium conditions of Eq. (A-12).

Because the three in-plane strains for the homogeneous composite do not enter into the determination of the stress concentration matrix, they are eliminated from Eq. (A-11)

leaving $3(n-1)$ conditions:

$$\begin{aligned} \varepsilon_1^{(i)} &= \varepsilon_1^{(i+1)} \\ \varepsilon_2^{(i)} &= \varepsilon_2^{(i+1)} \qquad i = 1,2,\ldots,n-1 \\ \varepsilon_6^{(i)} &= \varepsilon_6^{(i+1)} \end{aligned} \tag{A-18}$$

Substitution of the strain-stress form of Hooke's law into Eq. (A-18) and accounting for the out-of-plane equilibrium conditions of Eq. (A-12) yields

$$\begin{aligned} &S_{11}^{(i)}\sigma_1^{(i)} + S_{12}^{(i)}\sigma_2^{(i)} + S_{16}^{(i)}\sigma_6^{(i)} - S_{11}^{(i+1)}\sigma_1^{(i+1)} - S_{12}^{(i+1)}\sigma_2^{(i+1)} - S_{16}^{(i+1)}\sigma_6^{(i+1)} \\ &\quad = \left(S_{13}^{(i+1)} - S_{13}^{(i)}\right)\sigma_3 + \left(S_{14}^{(i+1)} - S_{14}^{(i)}\right)\sigma_4 + \left(S_{15}^{(i+1)} - S_{15}^{(i)}\right)\sigma_5 \\ &S_{21}^{(i)}\sigma_1^{(i)} + S_{22}^{(i)}\sigma_2^{(i)} + S_{26}^{(i)}\sigma_6^{(i)} - S_{21}^{(i+1)}\sigma_1^{(i+1)} - S_{22}^{(i+1)}\sigma_2^{(i+1)} - S_{26}^{(i+1)}\sigma_6^{(i+1)} \\ &\quad = \left(S_{23}^{(i+1)} - S_{23}^{(i)}\right)\sigma_3 + \left(S_{24}^{(i+1)} - S_{24}^{(i)}\right)\sigma_4 + \left(S_{25}^{(i+1)} - S_{25}^{(i)}\right)\sigma_5 \\ &S_{61}^{(i)}\sigma_1^{(i)} + S_{62}^{(i)}\sigma_2^{(i)} + S_{66}^{(i)}\sigma_6^{(i)} - S_{61}^{(i+1)}\sigma_1^{(i+1)} - S_{62}^{(i+1)}\sigma_2^{(i+1)} - S_{66}^{(i+1)}\sigma_6^{(i+1)} \\ &\quad = \left(S_{63}^{(i+1)} - S_{63}^{(i)}\right)\sigma_3 + \left(S_{64}^{(i+1)} - S_{64}^{(i)}\right)\sigma_4 + \left(S_{65}^{(i+1)} - S_{65}^{(i)}\right)\sigma_5 \end{aligned} \tag{A-19}$$

for $i = 1,2,\ldots,n-1$.

Defining the 3×3 matrix of in-plane compliances for the ith ply as

$$\overline{\mathbf{S}}^{(i)} = \begin{bmatrix} S_{11} & S_{12} & S_{16} \\ S_{21} & S_{22} & S_{26} \\ S_{61} & S_{62} & S_{66} \end{bmatrix}^{(i)} \tag{A-20}$$

as well as the 3×3 matrix of differences in the compliances that couple in-plane and out-of-plane response as

$$\tilde{\mathbf{S}}^{(i)} = \begin{bmatrix} S_{13}^{(i+1)} - S_{13}^{(i)} & S_{14}^{(i+1)} - S_{14}^{(i)} & S_{15}^{(i+1)} - S_{15}^{(i)} \\ S_{23}^{(i+1)} - S_{23}^{(i)} & S_{24}^{(i+1)} - S_{24}^{(i)} & S_{25}^{(i+1)} - S_{25}^{(i)} \\ S_{63}^{(i+1)} - S_{63}^{(i)} & S_{64}^{(i+1)} - S_{64}^{(i)} & S_{65}^{(i+1)} - S_{65}^{(i)} \end{bmatrix} \tag{A-21}$$

and the 3×1 vector of in-plane stresses as

$$\overline{\sigma}^{(i)} = \begin{Bmatrix} \sigma_1 \\ \sigma_2 \\ \sigma_6 \end{Bmatrix}^{(i)} \tag{A-22}$$

Eqs. (A-19) can be rewritten in matrix form as

$$\overline{\mathbf{S}}^{(i)}\overline{\sigma}^{(i)} - \overline{\mathbf{S}}^{(i+1)}\overline{\sigma}^{(i+1)} = \tilde{\mathbf{S}}^{(i)} \begin{Bmatrix} \sigma_3 \\ \sigma_4 \\ \sigma_5 \end{Bmatrix} \tag{A-23}$$

which again is for $i = 1, 2, \ldots, n-1$. By defining the 3×3 volume fraction matrix as

$$\mathbf{V}^{(i)} = \begin{bmatrix} v_i & 0 & 0 \\ 0 & v_i & 0 \\ 0 & 0 & v_i \end{bmatrix} \tag{A-24}$$

Eq. (A-16) can be rewritten in the form

$$\mathbf{V}^{(1)}\overline{\sigma}^{(1)} + \mathbf{V}^{(2)}\overline{\sigma}^{(2)} + \cdots + \mathbf{V}^{(n)}\overline{\sigma}^{(n)} = \begin{Bmatrix} \sigma_1 \\ \sigma_2 \\ \sigma_6 \end{Bmatrix} \tag{A-25}$$

Eqs. (A-23) and (A-25) can be combined into one matrix equation:

$$\mathbf{A} \begin{Bmatrix} \overline{\sigma}^{(1)} \\ \overline{\sigma}^{(2)} \\ \vdots \\ \overline{\sigma}^{(n)} \end{Bmatrix} = \mathbf{B} \begin{Bmatrix} \sigma_1 \\ \sigma_2 \\ \sigma_6 \\ \sigma_3 \\ \sigma_4 \\ \sigma_5 \end{Bmatrix} \tag{A-26}$$

The partitioned form of **A**, a $3n \times 3n$ matrix, is

$$\mathbf{A} = \begin{bmatrix} \mathbf{V}^{(1)} & \mathbf{V}^{(2)} & \mathbf{V}^{(3)} & \cdots & \mathbf{V}^{(n-1)} & \mathbf{V}^{(n)} \\ \overline{\mathbf{S}}^{(1)} & -\overline{\mathbf{S}}^{(2)} & 0 & \cdots & 0 & 0 \\ 0 & \overline{\mathbf{S}}^{(2)} & -\overline{\mathbf{S}}^{(3)} & \cdots & 0 & 0 \\ 0 & 0 & \overline{\mathbf{S}}^{(3)} & \cdots & 0 & 0 \\ \vdots & \vdots & \vdots & \ddots & \vdots & \vdots \\ 0 & 0 & 0 & \cdots & \overline{\mathbf{S}}^{(n-1)} & -\overline{\mathbf{S}}^{(n)} \end{bmatrix} \tag{A-27}$$

and the partitioned form of the $3n \times 6$ matrix $\mathbf{B}$ is

$$\mathbf{B} = \begin{bmatrix} \mathbf{I} & 0 \\ 0 & \tilde{\mathbf{S}}^{(1)} \\ 0 & \tilde{\mathbf{S}}^{(2)} \\ \vdots & \vdots \\ 0 & \tilde{\mathbf{S}}^{(n-1)} \end{bmatrix} \tag{A-28}$$

In order to simplify the partitioned nature of the $\mathbf{A}$ and $\mathbf{B}$ matrices, the vector of homogenized stresses on the right hand side of Eq. (A-26) was reordered. In defining the stress concentration matrices $\mathbf{K}^{(i)}$ in Eq. (A-17), the conventional order was used. Therefore, a transformation matrix $\mathbf{T}$ is defined as

$$\mathbf{T} = \begin{bmatrix} 1 & 0 & 0 & 0 & 0 & 0 \\ 0 & 1 & 0 & 0 & 0 & 0 \\ 0 & 0 & 0 & 0 & 0 & 1 \\ 0 & 0 & 1 & 0 & 0 & 0 \\ 0 & 0 & 0 & 1 & 0 & 0 \\ 0 & 0 & 0 & 0 & 1 & 0 \end{bmatrix} \tag{A-29}$$

and solving for the heterogeneous in-plane stresses in Eq. (A-26) yields

$$\begin{Bmatrix} \overline{\sigma}^{(1)} \\ \overline{\sigma}^{(2)} \\ \vdots \\ \overline{\sigma}^{(n)} \end{Bmatrix} = \mathbf{A}^{-1}\mathbf{B}\mathbf{T} \begin{Bmatrix} \sigma_1 \\ \sigma_2 \\ \sigma_3 \\ \sigma_4 \\ \sigma_5 \\ \sigma_6 \end{Bmatrix} \tag{A-30}$$

Therefore, the undetermined portion of the stress concentration matrices, defined by

$$\overline{\mathbf{K}}^{(i)} = \begin{bmatrix} K_{11} & K_{12} & K_{13} & K_{14} & K_{15} & K_{16} \\ K_{21} & K_{22} & K_{23} & K_{24} & K_{25} & K_{26} \\ K_{61} & K_{62} & K_{63} & K_{64} & K_{65} & K_{66} \end{bmatrix}^{(i)} \tag{A-31}$$

are determined by

$$\begin{bmatrix} \overline{\mathbf{K}}^{(1)} \\ \overline{\mathbf{K}}^{(2)} \\ \vdots \\ \overline{\mathbf{K}}^{(n)} \end{bmatrix} = \mathbf{A}^{-1}\mathbf{B}\mathbf{T} \tag{A-32}$$

and the homogenized compliance matrix is defined by Eq. (A-8).

A.4 Homogenized Stiffnesses

Eqs. (A-9), (A-11), and (A-15) imply the structure of the strain concentration matrix in the *i*th ply is

$$\mathbf{L}^{(i)} = \begin{bmatrix} 1 & 0 & 0 & 0 & 0 & 0 \\ 0 & 1 & 0 & 0 & 0 & 0 \\ L_{31} & L_{32} & L_{33} & L_{34} & L_{35} & L_{36} \\ L_{41} & L_{42} & L_{43} & L_{44} & L_{45} & L_{46} \\ L_{51} & L_{52} & L_{53} & L_{54} & L_{55} & L_{56} \\ 0 & 0 & 0 & 0 & 0 & 1 \end{bmatrix}^{(i)} \tag{A-33}$$

Eqs. (A-12) imply

$$\begin{aligned} \sigma_3^{(i)} &= \sigma_3^{(i+1)} \\ \sigma_4^{(i)} &= \sigma_4^{(i+1)} \qquad i = 1,2,\ldots,n-1 \\ \sigma_5^{(i)} &= \sigma_5^{(i+1)} \end{aligned} \tag{A-34}$$

Substitution of the stress-strain form of Hooke's law into Eq. (A-34) and using Eqs. (A-11) leads to

$$\overline{\mathbf{C}}^{(i)}\overline{\boldsymbol{\varepsilon}}^{(i)} - \overline{\mathbf{C}}^{(i+1)}\overline{\boldsymbol{\varepsilon}}^{(i+1)} = \tilde{\mathbf{C}}^{(i)}\begin{Bmatrix}\varepsilon_1\\ \varepsilon_2\\ \varepsilon_6\end{Bmatrix} \qquad i = 1,2,\ldots,n-1 \tag{A-35}$$

in which

$$\overline{\mathbf{C}}^{(i)} = \begin{bmatrix} C_{33} & C_{34} & C_{35} \\ C_{43} & C_{44} & C_{45} \\ C_{53} & C_{54} & C_{55} \end{bmatrix}^{(i)} \tag{A-36}$$

$$\overline{\boldsymbol{\varepsilon}}^{(i)} = \begin{Bmatrix}\varepsilon_3\\ \varepsilon_4\\ \varepsilon_5\end{Bmatrix}^{(i)} \tag{A-37}$$

and

$$\tilde{\mathbf{C}}^{(i)} = \begin{bmatrix} C_{31}^{(i+1)} - C_{31}^{(i)} & C_{32}^{(i+1)} - C_{32}^{(i)} & C_{36}^{(i+1)} - C_{36}^{(i)} \\ C_{41}^{(i+1)} - C_{41}^{(i)} & C_{42}^{(i+1)} - C_{42}^{(i)} & C_{46}^{(i+1)} - C_{46}^{(i)} \\ C_{51}^{(i+1)} - C_{51}^{(i)} & C_{52}^{(i+1)} - C_{52}^{(i)} & C_{56}^{(i+1)} - C_{56}^{(i)} \end{bmatrix} \tag{A-38}$$

In matrix form Eq. (A-15) is

$$\mathbf{V}^{(1)}\overline{\boldsymbol{\varepsilon}}^{(1)} + \mathbf{V}^{(2)}\overline{\boldsymbol{\varepsilon}}^{(2)} + \cdots + \mathbf{V}^{(n)}\overline{\boldsymbol{\varepsilon}}^{(n)} = \begin{Bmatrix}\varepsilon_3\\ \varepsilon_4\\ \varepsilon_5\end{Bmatrix} \tag{A-39}$$

where matrices $\mathbf{V}^{(i)}$ are given by Eq. (A-24). Eqs. (A-35) and (A-39) form a $3n \times 3n$ system of equations for $\overline{\boldsymbol{\varepsilon}}^{(i)}$ given by

$$\mathbf{A}'\begin{Bmatrix}\overline{\boldsymbol{\varepsilon}}^{(1)}\\ \overline{\boldsymbol{\varepsilon}}^{(2)}\\ \vdots\\ \overline{\boldsymbol{\varepsilon}}^{(n)}\end{Bmatrix} = \mathbf{B}'\begin{Bmatrix}\varepsilon_3\\ \varepsilon_4\\ \varepsilon_5\\ \varepsilon_1\\ \varepsilon_2\\ \varepsilon_6\end{Bmatrix} \tag{A-40}$$

in which matrix $\mathbf{A}'$ is the same form as $\mathbf{A}$ in Eq. (A-27) with submatrices $\overline{\mathbf{S}}^{(i)}$ replaced by

$\overline{\mathbf{C}}^{(i)}$, and matrix $\mathbf{B}'$ is the same form as $\mathbf{B}$ in Eq. (A-28) with $\tilde{\mathbf{S}}^{(i)}$ replaced by $\tilde{\mathbf{C}}^{(i)}$. Let the nontrivial three rows of $\mathbf{L}^{(i)}$ be denoted by

$$\overline{\mathbf{L}}^{(i)} = \begin{bmatrix} L_{31} & L_{32} & L_{33} & L_{34} & L_{35} & L_{36} \\ L_{41} & L_{42} & L_{43} & L_{44} & L_{45} & L_{46} \\ L_{51} & L_{52} & L_{53} & L_{54} & L_{55} & L_{56} \end{bmatrix}^{(i)} \tag{A-41}$$

Then it can be shown that

$$\begin{bmatrix} \overline{\mathbf{L}}^{(1)} \\ \overline{\mathbf{L}}^{(2)} \\ \vdots \\ \overline{\mathbf{L}}^{(n)} \end{bmatrix} = (\mathbf{A}')^{-1}\mathbf{B}'\mathbf{T}' \tag{A-42}$$

where

$$\mathbf{T}' = \begin{bmatrix} 0 & 0 & 1 & 0 & 0 & 0 \\ 0 & 0 & 0 & 1 & 0 & 0 \\ 0 & 0 & 0 & 0 & 1 & 0 \\ 1 & 0 & 0 & 0 & 0 & 0 \\ 0 & 1 & 0 & 0 & 0 & 0 \\ 0 & 0 & 0 & 0 & 0 & 1 \end{bmatrix} \tag{A-43}$$

Recently, Sun and Li[61] have presented explicit formulas for the homogenized elastic moduli of a sub-laminate. Their formulation also uses Eqs. (A-11), (A-12), (A-15), (A-16) and Hooke's law as presented here, but they do not use the stress and strain concentration matrices, Eqs. (A-6) and (A-9), and equivalence of the strain energy as represented by Eq. (A-3).

Appendix B: Two-Stage Gauss Implicit Runge-Kutta Finite Difference Scheme

This appendix presents the two-stage Gauss implicit Runge-Kutta finite difference scheme. This is a finite difference adaptation of a subclass of the Runge-Kutta schemes for implicit integration of differential equations as presented on pp. 210-216 of Ref. 52 and summarized here. It should be noted that the notation used here is the same as that of Ref. 52 and that indicies or variables that coincide with previous chapters do not imply any relationship between the two.

B.1 Implicit Runge-Kutta Schemes

The k-stage Runge-Kutta scheme for the system $\mathbf{y}' = \mathbf{f}(x,\mathbf{y})$ over N intervals is given by

$$\mathbf{y}_{i+1} = \mathbf{y}_i + h_i \sum_{j=1}^{k} \beta_j \mathbf{f}_{ij} \qquad 1 \le i \le N \tag{B-1}$$

where

$$\mathbf{f}_{ij} = \mathbf{f}\left(x_{ij}, \mathbf{y}_i + h_i \sum_{l=1}^{k} \alpha_{jl} \mathbf{f}_{il}\right) \quad 1 \le j \le k \tag{B-2}$$

are the evaluations of the function $\mathbf{f}$ at the points

$$x_{ij} = x_i + h_i \rho_j \qquad 1 \le j \le k, \quad 1 \le i \le N \tag{B-3}$$

which are located by the values of ρ_j, with

$$0 \le \rho_1 \le \rho_2 \le \cdots \le \rho_k \le 1 \tag{B-4}$$

Subscript i denotes a mesh interval, while subscripts j and l are stage counters within a particular interval. Points x_{ij} are sometimes called collocation points.

The choice of the values of the parameters ρ_j, β_i, and α_{jl}, $j,l = 1,\ldots,k$ defines the specific Runge-Kutta scheme. If $\rho_1 = 0$ and $\alpha_{jl} = 0$ for $j \le l$, then the scheme is explicit, while if either condition does not hold, the scheme is implicit. Runge-Kutta schemes are typically represented in tableau form as shown in Eq. B-5.

$$\begin{array}{c|ccc} \rho_1 & \alpha_{11} & \cdots & \alpha_{1k} \\ \vdots & \vdots & \ddots & \vdots \\ \rho_k & \alpha_{k1} & \cdots & \alpha_{kk} \\ \hline & \beta_1 & \cdots & \beta_k \end{array} \tag{B-5}$$

B.2 Development of Finite Difference Scheme: Parameter Condensation

In order for the Runge-Kutta schemes to be applied in one-step finite difference approximations, they must be written in the form

$$S_i \mathbf{y}_i + R_i \mathbf{y}_{i+1} = \mathbf{q}_i \qquad 1 \le i \le N \tag{B-6}$$

where $\mathbf{y}_i$ and $\mathbf{y}_{i+1}$ are the mesh values of what are referred to as global unknowns because they are determined through solution over the entire domain. For the Runge-Kutta schemes, however, there are also variables local to the interval $[x_i, x_{i+1}]$ for each i, $1 \le i \le N$. The local unknowns for the ith interval are

$$\mathbf{f}_i^T \equiv \left(\mathbf{f}_{i1}^T, \ldots, \mathbf{f}_{ik}^T\right) \tag{B-7}$$

Elimination of these local unknowns, referred to as parameter condensation from the analogous procedure in finite elements, leaves an expression in the form of Eq. (B-6).

For the case of a linear boundary value problem, given by

$$\mathbf{y}' = \mathbf{f}(x,\mathbf{y}) = A(x)\mathbf{y} + \mathbf{q}(x) \tag{B-8}$$

where $A(x)$ is an $n \times n$ matrix, eq. (B-2) becomes

$$\mathbf{f}_{ij} = A(x_{ij})\left[\mathbf{y}_i + h_i \sum_{l=1}^{k} \alpha_{jl}\mathbf{f}_{il}\right] + \mathbf{q}(x_{ij}) \quad 1 \le j \le k \tag{B-9}$$

Using the notation of Eq. (B-7), Eq. (B-9) can be rearranged and written in matrix form for interval i as

$$W_i \mathbf{f}_i = V_i \mathbf{y}_i + \mathbf{q}_i \tag{B-10}$$

where

$$W_i = I - h_i \begin{bmatrix} \alpha_{11}A(x_{i1}) & \cdots & \alpha_{1k}A(x_{i1}) \\ \vdots & \ddots & \vdots \\ \alpha_{k1}A(x_{ik}) & \cdots & \alpha_{kk}A(x_{ik}) \end{bmatrix}, \; V_i = \begin{bmatrix} A(x_{i1}) \\ \vdots \\ A(x_{ik}) \end{bmatrix}, \; \mathbf{q}_i = \begin{Bmatrix} \mathbf{q}(x_{i1}) \\ \vdots \\ \mathbf{q}(x_{ik}) \end{Bmatrix} \tag{B-11}$$

By defining the matrix D_i as

$$D_i \equiv (\beta_1 I, \ldots, \beta_k I) \tag{B-12}$$

Eq. (B-1) can be restated as

$$\mathbf{y}_{i+1} = \mathbf{y}_i + h_i D_i \mathbf{f}_i \tag{B-13}$$

which, through substitution of Eq. (B-10) solved for $\mathbf{f}_i$, can then be expressed as

$$\mathbf{y}_{i+1} = \Gamma_i \mathbf{y}_i + \mathbf{r}_i \tag{B-14}$$

through the definition of Γ_i and $\mathbf{r}_i$ as

$$\Gamma_i \equiv I + h_i D_i W_i^{-1} V_i, \quad \mathbf{r}_i \equiv h_i D_i W_i^{-1} \mathbf{q}_i \tag{B-15}$$

Eq. (B-14) is now in the form of Eq. (B-6) with $S_i = \Gamma_i$, $R_i = I$ and $\mathbf{q}_i = \mathbf{r}_i$.

B.3 Gauss Schemes

Gauss schemes are characterized by the choice of points $\rho_1, \ldots, \rho_k$ as the zeroes of a Legendre polynomial. The 2-stage ($k = 2$) Gauss scheme used in the present study has the tableau

$$\begin{array}{c|cc} \frac{1}{2}-\frac{\sqrt{3}}{6} & \frac{1}{4} & \frac{1}{4}-\frac{\sqrt{3}}{6} \\ \frac{1}{2}+\frac{\sqrt{3}}{6} & \frac{1}{4}+\frac{\sqrt{3}}{6} & \frac{1}{4} \\ \hline & 1/2 & 1/2 \end{array} \qquad \text{(B-16)}$$

Since $\rho_1 \neq 0$, this scheme is implicit and the parameter condensation approach of the previous section was used. This particular scheme was chosen because of its implicitness, which produces better stability, its high order of accuracy, $O(h^4)$, and its efficiency in obtaining this accuracy.

The major drawback of this approach lies in the potential computational burden of inverting the $kn \times kn$ matrix W_i for each interval in the finite difference mesh. This expense was reduced in the present work by using a uniform mesh spacing h_i as much as possible in regions of constant coefficient governing equations, allowing the repeated use of the same computed W_i^{-1}.

BIBLIOGRAPHIC DATA SHEET	1. Report No. CCMS-94-04, VPI-E-94-04	2.	3. Recipient's Accession No.

4. Title and Subtitle
Interlaminar Stress Analysis of Dropped-Ply Laminated Plates and Shells by a Mixed Method

5. Report Date
May 1994

6.

7. Author(s)
Peter N. Harrison, Eric R. Johnson, James H. Starnes, Jr.

8. Performing Organization Rept. No.
VPI-E-94-04, CCMS-94-04

9. Performing Organization Name and Address
Virginia Polytechnic Institute and State University
Department of Engineering Science and Mechanics
Blacksburg, VA 24061-0219

10. Project/Task/Work Unit No.

11. Contract/Grant No.
NAG-1-343

12. Sponsoring Organization Name and Address
Polymeric Materials Branch
National Aeronautics and Space Administration
Langley Research Center
Hampton, VA 23681-0001

13. Type of Report & Period Covered
Interim Report 96
July 1986 - April 1994

14.

15. Supplementary Notes
This report constitutes the Ph.D. thesis in Aerospace Engineering of the first author. The second author is on the faculty of Virginia Polytechnic Institute and State University, while the third author is the Head of the Aircraft Structures Branch of the NASA Langley Research Center.

16. Abstract

A mixed method of approximation based on Reissner's variational principle is developed for the linear analysis of interlaminar stresses in laminated composites, with special interest in laminates that contain terminated internal plies (dropped-ply laminates). Two models are derived, one for problems of generalized plane deformation and the other for the axisymmetric response of shells of revolution. A layerwise approach is taken in which the stress field is assumed with an explicit dependence on the thickness coordinate in each layer. The dependence of the stress field on the thickness coordinate is determined such that the three-dimensional equilibrium equations are satisfied by the approximation. The solution domain is reduced to one dimension by integration through the thickness. Continuity of tractions and displacements between layers is imposed.

The governing two-point boundary value problem is composed of a system of both differential and algebraic equations (DAEs) and their associated boundary conditions. Careful evaluation of the system of DAEs was required to arrive at a form that allowed application of a one-step finite difference approximation. A two-stage Gauss implicit Runge-Kutta finite difference scheme was used for the solution because of its relatively high degree of accuracy. Patch tests of the two models revealed problems with solution accuracy for the axisymmetric model of a cylindrical shell loaded by internal pressure.

Parametric studies of dropped-ply laminate characteristics and their influence on the interlaminar stresses were performed using the generalized plane deformation model. Eccentricity of the middle surface of the laminate through the ply drop-off was found to have a minimal effect on the interlaminar stresses under longitudinal compression, transverse tension, and in-plane shear. A second study found the stiffness change across the ply termination to have a much greater influence on the interlaminar stresses. Correlations between the stiffness ratio of the thick to the thin sections of the laminates and the magnitude of a parameter based on a quadratic delamination criterion were found to be surprisingly good for longitudinal compression and in-plane shear loadings. For laminates with very stiff terminated plies loaded in longitudinal compression, inclusion of a short insert of softer composite material at the end of the dropped plies was found to significantly reduce the interlaminar stresses produced.

17. Key Words and Document Analysis. **17a. Descriptors**
Composite materials, ply drop-offs, interlaminar stresses, delamination, mixed method, assumed stress approach

17b. Identifiers/Open-Ended Terms

17c. COSATI Field/Group

18. Availability Statement	19. Security Class (This Report) UNCLASSIFIED	21. No. of Pages 171
	20. Security Class (This Page) UNCLASSIFIED	22. Price